ON THE RELATIONSHIP BETWEEN AEROSOL DYNAMICS AND THE RATE OF GAS-TO-PARTICLE CONVERSION

Thesis by

Peter Howard McMurry

In Partial Fulfillment of the Requirements

for the degree of

Doctor of Philosophy

California Institute of Technology

Pasadena, California

May 2, 1977

"...the sun produces certain kinds of fogs, yet it is by no means ...contended that it is to be censured for their appearance. It would rather appear that it is doing its best to show us the state of pollution into which our modern civilisation has brought our atmosphere, as it only inflicts these fogs on the areas upon which man has thrown the waste products of his industries and converted the atmosphere into a vast sewer, as a penalty for something wrong in his methods."

John Aitken (1912)

ACKNOWLEDGEMENTS

I particularly appreciate the help of my advisor, Professor S. K. Friedlander, during the course of this research. He suggested the topic, and made many key suggestions which directly influenced the results presented here.

Paul Roberts and Steve Heisler were the first graduate students in this group to use the large teflon reactor for smog chamber experiments; procedures which they worked out were used in this project. In addition, Paul's technique for analyzing the sulfur content of aerosols and Steve's work on particle growth laws were both applied directly in this thesis.

Susanne Hering participated in several experiments and her work with the low pressure impactor helped confirm the measurements of the electrical aerosol analyzer, on which many of the conclusions presented in this thesis are based.

Discussions with other students and faculty members at Caltech have been enjoyable and fruitful. These colleagues include Rick Flagan, Daniel Grosjean, Warren White, Patrick Delattre, John Brock, Antonio Miguel, George Jackson, Glen Cass, Steve Wright, Daryl Roberts, Don Kuehne, Alan Moskowitz, Stan Sander, Tom Peterson, Ken Bencala, Greg McRae, Fred Gelbard, and Lisa Anderson. I have particularly appreciated the helpful suggestions and good humor of Cliff Davidson, with whom I shared an office during my stay at Caltech.

This thesis was expertly typed by Pat Hofmann. Peace of mind is knowing that the original copy is in the hands of one more organized than I. The prompt and cheerful assistance of Helen Fabel and Elaine Granger during the earlier phases of this research is also greatly appreciated. In addition, the contributions of Elton Daly, Larry McClellan, Joe Fontana and Dave Byrum were invaluable.

This research was financially supported by the National Institute of Environmental Health Sciences (Grant No. 5 TO1-ES-00004) and the U.S. Environmental Protection Agency (Grant No. R-802/60).

The support and patience of my wife, Pam, through the ups and downs of my graduate study has been invariant. This I appreciate most of all.

ABSTRACT

A theoretical and experimental study of the dynamic behavior of secondary aerosols generated by homogeneous gas phase reactions is presented. The relationship between the rate at which new aerosol is formed by chemical reaction and the development of the aerosol is emphasized. The effect of an initial aerosol, present at the start of gas-to-particle conversion, on aerosol dynamics is also investigated.

Aerosol dynamics in such systems are typically separated into two stages. During the early stage, new particles are often formed by homogeneous nucleation. Particle concentrations rise to a maximum value after timescales of 10-60 minutes, then decrease continually as the coagulation rate exceeds the rate at which new particles are formed. A new theory which predicts the rate at which new particles of a given size are formed during the early stages of aerosol growth is presented. This rate is shown to be a known function of a single parameter which depends on the rate at which condensable molecules are produced and on the amount of pre-existing aerosol surface area per volume of gas. This parameter can be calculated from experimental data.

Theoretical predictions are compared with experimentally observed rates of particle formation in the SO_2-NO_x-propylene-hν system. Experiments were performed in a large (65 m^3) teflon reactor which was exposed to solar radiation. Agreement between theory and experiment is fair.

After the aerosol number concentration begins to decrease, the aerosol surface area per volume of gas typically reaches a nearly constant value dependent only on the rate of gas-to-particle conversion. During this stage, condensation on preexisting particles dominates, and the rate at which new particles are formed is small. An analytical expression relating these aerosol surface areas, A, to the rate of gas-to-particle conversion, dV/dt, and time, t, has been derived. It is shown that $A \sim (dV/dt)^{3/5} t^{1/5}$, in good agreement with the data of a number of investigators. For a given rate of aerosol formation, this result is essentially independent of the chemical and physical nature of the secondary aerosol. Preliminary evidence suggests that aerosol surface areas in the Los Angeles atmsophere may be regulated by the rate of gas-to-particle conversion.

The formation of new particles by gas phase reactions is believed to be an important source of condensation nuclei on the global scale. Evidence is presented in this thesis which indicates that formation of new sulfur containing particles occurs to a limited extent after sunup in the Los Angeles atmosphere. The results of this thesis can be applied to the formation of secondary aerosols in the atmosphere, both for the early dynamic stages when new particles are formed, and for the later stages when condensation on preexisting nuclei is dominant.

TABLE OF CONTENTS

TABLE OF CONTENTS (continued)

TABLE OF CONTENTS (continued)

LIST OF FIGURES

LIST OF FIGURES (continued)

LIST OF FIGURES (continued)

LIST OF TABLES

CHAPTER 1
INTRODUCTION

Aerosols in ambient air are either primary or secondary in nature. Secondary aerosols are formed by gas-to-particle conversion in the air, while primary aerosols are emitted directly from sources. Some of the unpleasant effects of air pollution are associated with secondary aerosol material; visibility reduction (White, 1976) and health effects (Amdur, 1971) are examples of such effects.

Health effects resulting from particle deposition in the lungs and light scattering by aerosols are functions of the chemical composition of the aerosol with respect to size. The size dependent chemical composition of secondary aerosols, in turn, is regulated by the mechanisms of gas-to-particle conversion; studies of such mechanisms give insight into possible benefits from air pollution control strategies.

Secondary aerosols can be produced by a number of mechanisms. Condensation of low vapor pressure products formed by homogeneous gas phase reactions is known to be important. Heterogeneous reactions such as might occur on the surface of a particle or within a liquid droplet are also possible. The subject of this thesis is the dynamics of secondary aerosols formed by homogeneous gas phase reactions.

Condensable molecules formed by homogeneous gas phase reactions can either combine with one another to form new particles, or condense on surrounding particles (heterogeneous condensation). In experiments

reported by Heisler and Friedlander (1976) and Roberts and Friedlander (1976b) in which secondary aerosol was formed by photochemical reactions in a volume of ambient air, extensive new particle formation was observed despite the fact that the air was unfiltered. Formation of new particles has also been reported to occur at sunup in rural areas (Went, 1966; Hogan, 1968), and is believed to be an important source of particles on a global scale (e.g. Lopex, et al., 1974; Flyger, et al., 1976).

Most previous studies of aerosol formation in smog chambers (Clark, 1972; Husar and Whitby, 1973; McNelis, 1974; Kocmond, et al., 1975) have been done with air which is initially particle free. In these studies, soon after the start of gas-to-particle conversion, the aerosol number concentration increased to a maximum value on timescales of about 10-60 minutes, and decreased continuously thereafter. After the aerosol number concentration began to decrease, the aerosol surface area per volume of gas leveled off at a fairly constant value which depended primarily on the rate of gas-to-particle conversion. These general trends have also been observed in the experiments reported in this thesis, where an initial aerosol was present.

The problem of aerosol formation in a system with a preexisting aerosol has been studied theoretically (e.g. Middleton and Kiang, 1977). The general approach in these studies has been to couple the classical theory of homogeneous nucleation for the prediction of new particle formation rates with numerical calculations to describe the growth and coagulation of both new and preexisting particles. While this approach can be very powerful, there has been little success at linking chemical

kinetics with observed aerosol behavior. The form of the classical theory of homogeneous nucleation used by these investigators has not been verified experimentally. In addition, this theory does not take account of scavenging of small molecular clusters by surrounding aerosol, which is an important effect.

These scavenging effects are taken into consideration in the theory developed in this thesis, and agreement between predicted and observed rates of particle formation is encouraging. The primary limitation of the new theory is that it only applies in the limit that the vapor pressure of the condensing species is small compared to partial pressures of interest; evaporation from molecular clusters is assumed to be slow compared with rates of condensation.

The development of new instrumentation capable of measuring aerosol size distributions in the small particle range between 0.01 μm and 0.3 μm has made the experimental phase of this research possible. The electrical aerosol analyzer (Liu, et al., 1974) and the low pressure cascade impactor (Hering, et al., 1977) have been particularly useful in this regard. Size distributions of molecular clusters and the tiniest aerosol particles remain inaccessible; conclusions about their effects on aerosol dynamics must be based on indirect evidence.

1.1 Thesis Organization

The main body of this thesis is divided into three primary chapters. Each chapter covers a different aspect of research on the central topic

of the thesis, and was written so as to stand by itself as a separate paper. Appropriate literature reviews were included with each chapter. Details of experimental error and analysis judged inappropriate for the main body of the thesis were put in the appendices.

Chapter 2 deals with the formation of new particles by gas phase reactions in ambient air. The results of a search for the formation of new particles by homogeneous nucleation in Los Angeles air are reported; some new particle formation appears to occur at sunup in Los Angeles, although this does not appear to be a major source of particles in local air. Experiments which showed that sulfur containing species probably participate in the formation of new particles in unfiltered ambient Los Angeles air are also reported.

In Chapter 3, a study of the relationship between aerosol surface area per volume of gas and the rate of aerosol formation for the later stages of aerosol development is presented. During this stage, condensation on preexisting nuclei is dominant, and the rate at which new particles are formed is slow. An analytical expression is obtained which shows that for constant rates of aerosol production, dV/dt, the aerosol surface area per volume of gas is proportional to $(dV/dt)^{3/5}t^{1/5}$, where t is time. This result is essentially independent of the chemical and physical properties of the new secondary aerosol. Agreement between theory and experiment for a variety of chemical systems is good.

Chapter 4 deals with the early dynamic stage of aerosol development when the formation of new particles is important. Procedures for and results of most of the experimental work discussed in this thesis are

presented in this chapter. A theory which predicts the rate at which new particles are formed as a function of experimentally measured parameters is presented, and predictions of the theory are compared with experimental results.

In Chapter 5, the results of this work are summarized, and recommendations for future research are made.

Appendix A presents an approximate numerical model which was developed to predict the dynamic behavior of aerosol systems from the early phase when new particle formation is important, through the later stages when condensation on preexisting particles is dominant. The model is presented since it was reasonably successful at predicting trends which were observed experimentally. In its current form, the model overestimates the importance of new particle formation relative to heterogeneous condensation. By incorporating some of the ideas developed in Chapter 4, it is likely that the model could be significantly improved.

Appendix B discusses the influence of particle losses on experimental results. Particles are lost on the reactor walls during the course of an experiment as well as in the sample line leading to the instrumentation in the laboratory. Wall loss rates and sample line losses were measured as a function of particle size, and results of these measurements are reported. The effect of these losses on experimental data was significant. All data presented in the main body of the thesis were corrected for sample line losses. Data for the rate of aerosol formation were corrected for wall losses as well.

In Appendix C, the growth of the initial aerosol is studied. It is shown that if the aerosol present in the chamber at the start of gas-to-particle formation is assumed to grow by a zero vapor pressure diffusional growth law, calculated results for the evolution of this aerosol agree well with observed results. Both calculated and observed results show that the aerosol volume distribution peaks between 0.1 μm and 0.2 μm, which is significantly below the peak of 0.4-0.5 μm observed for aerosol sulfur distributions in ambient Los Angeles air. This suggests that some mechanism other than homogeneous gas phase reactions may be important in shaping the aerosol sulfur distribution in Los Angeles air.

Experimental data from all experiments reported in this thesis are presented in Appendix D. These data have not been corrected for particle losses of any sort.

CHAPTER 2
HOMOGENEOUS NUCLEATION IN AMBIENT AIR

In this chapter the evidence for the formation of new particles by homogeneous nucleation in ambient air is reviewed and results of a search for homogeneous nucleation in the Los Angeles atmosphere are reported. Results of other investigations indicate that homogeneous nucleation is probably an important source of nuclei on the global scale. For the Los Angeles atmosphere, it appears that homogeneous nucleation probably occurs to a limited extent after sunrise, but that local nuclei concentrations are dominated by direct emissions from sources. Measurements of the sulfur distribution were made before and after homogeneous nucleation in a batch of Los Angeles air collected before sunup; small particles were enriched in sulfur after homogeneous nucleation indicating that sulfur containing species are involved in homogeneous nucleation in the Los Angeles atmosphere.

2.1 Introduction

Particles are both emitted directly into the air from sources and formed in the air by homogeneous nucleation of condensable vapors. Sufficient cooling of a gas containing a condensable vapor, or production of a vapor in the gas phase can cause homogeneous nucleation. Formation of condensable vapors by homogeneous gas phase reactions is probably the only important cause of new particle formation in ambient air. The rate

at which new particles of a given size and species are formed by homogeneous nucleation depends on the rate of production of condensable molecules by chemical reaction and the amount of aerosol present to scavenge condensable molecules. These factors are discussed in more detail in Chapters 3 and 4.

Concentrations of ambient aerosols are most commonly measured with a condensation nuclei monitor (Skala, 1963). This instrument measures the total number concentration, N, of particles larger than some minimum size, typically estimated to be 2.5 nm (25 Å). The equation which gives the time rate of change of condensation nuclei measured at a point in ambient air is approximately

$$\frac{\partial N}{\partial t} + \vec{u} \cdot \nabla N = - KN^2 + G \qquad (2.1)$$

where

t = time
$\vec{u}$ = velocity of air parcel with respect to monitoring station
K = effective aerosol coagulation constant
G = rate at which new particles grow past the minimum size detected by the condensation nuclei monitor
$N = \int_{v_{min}}^{\infty} n(v,t,\vec{r})dv$
v_{min} = minimum size detected by the condensation nuclei monitor
$\vec{r}$ = position vector

The first term on the right side of (2.1) is the rate at which particles are lost by coagulation, and the second term the rate at which particles formed by homogeneous nucleation reach a size detectable to the condensation nuclei monitor (an expression for G is derived in Chapter 4). Contributions of Brownian diffusion and gravitational settling to $\partial N/\partial t$ are generally small compared with the other terms, and have been omitted in Eq. 2.1.

The transport term is important if nuclei concentrations are not uniform. A system with transport from local sources of high concentration would result in fluctuating nuclei concentrations measured at a point. In the absence of local sources, homogeneous nucleation can be detected when $G > KN^2$, as indicated by an increase in the condensation nuclei concentration. If $G < KN^2$, it is difficult to make a definitive statement about whether or not homogeneous nucleation is occurring by monitoring nuclei concentrations.

Studies of photochemical aerosol formation in smog chambers show that nuclei concentrations generally increase dramatically soon after the start of the experiment, reach a peak concentration after timescales typically of 10 - 60 min., and decrease continuously thereafter. Homogeneous nucleation may continue indefinitely but will only be unambiguously observed at the beginning of the experiment. By analogy, homogeneous nucleation in ambient air can most easily be detected after a perturbation such as sunrise or the addition of fresh aerosol precursors from a source.

Homogeneous nucleation in rural atmospheres has been well documented. In the absence of local sources, nuclei concentrations tend to be uniform over large areas so that the second term on the left side of (2.1) is unimportant, and an increase in nuclei concentrations can often be unambiguously associated with homogeneous nucleation. Nuclei profiles in urban atmospheres are more difficult to analyze due to the influence of local sources. There has been no consensus among investigators about the occurrence of homogeneous nucleation in urban atmospheres with typically heavy aerosol loadings.

2.2 Previous Studies

Went (1964) studied formation of condensation nuclei from several terpene vapors known to be emitted from plants. He concluded that α-pinene and turpentine vapors quickly produce new nuclei when released with NO_2 in the presence of sunlight in ambient air, although the release of the terpene and NO_2 separately produced no detectable nuclei formation. In subsequent experiments, Went (1966) monitored ground level condensation nuclei concentrations as well as their variation with height at several rural sites. He concluded that concentrations consistently decrease during the night and increase after sunrise. Ground level concentrations were generally higher than elevated concentrations, although this gradient was less well defined at night. Emissions from nearby combustion sources such as campfires or combustion engines tended to dominate local condensation nuclei concentrations. Rasmussen and Went (1964) measured concentrations of terpene vapors ranging from 2-40 ppb in vegetated areas. Results of these studies led Went (1966) to conclude that homogeneous nucleation induced by the action of sunlight on volatile plant emissions occurs over vegetated areas. NO_2 was hypothesized to serve as a light absorbing catalyst for aerosol formation from the terpenes, which do not absorb in the visible or near ultraviolet bands.

Hogan (1968) monitored condensation nuclei profiles for a 20-day period surrounding the time change from Eastern Daylight Time to Eastern Standard Time in the fall of 1967. The rural sampling site was 8 miles NW of Schenectady, New York. By comparing profiles before and after the

time change it was possible to separate anthropogenic from solar influences on the condensation nuclei profiles. The results of the experiment showed conclusively that the profiles at this site were correlated with solar radiation and not anthropogenic activity from distant sources. It was concluded that homogeneous nucleation resulting from gas phase photochemistry occurred after sunrise during these experiments.

Lopez (1974) made a study of condensation nuclei concentrations by aircraft above both rural and urban sites in southwest France; he concluded that homogeneous nucleation occurs during daytime above rural areas. The Landes forest was shown to be an intense source of particles during daytime, while land covered with cereal crops also produced new nuclei, but at a considerably lower rate. In the entire region of his study, 75% of the particles were natural, and 25% man-made.

Hogan (1975) observed that nuclei concentrations rose from 50 cm^{-3} to 1000 cm^{-3} during a lowering of the tropopause in the Anarctic. He hypothesized that particles were formed when ozone from the lower stratosphere reacted with terpenes in the tropospheric air.

White, et al. (1976) used aircraft to measure condensation nuclei concentrations in the Labadie Power Plant plume in St. Louis. Vertical as well as horizontal profiles through the plume were measured at various downstream locations. Peaks in nuclei count were observed at the edges of the plume on one profile. Nuclei concentrations increased with distance downstream on another occasion. It was concluded that photochemical reactions in the plume resulted in the production of new particles by homogeneous nucleation.

Flyger, et al. (1976) used a condensation nuclei monitor coupled with a diffusion denuder to measure aerosol size distributions over Greenland and surrounding seas. The size spectra consistently showed the existence of significant numbers of small particles with diameters of about 0.005 μm. Air trajectory analyses along with the short expected lifetimes of such small particles indicated that they could not be of anthropogenic origin. They concluded that homogeneous nucleation by products of photochemical reactions occurs in the summer tropospheric air above Greenland and the surrounding seas.

2.3 A Search for Homogeneous Nucleation in Urban Air

A study was conducted to determine whether or not formation of new particles by homogeneous nucleation occurs in the urban air surrounding Caltech's Air Quality Laboratory on the roof of the Keck Laboratory in Pasadena. The primary difficulty in such a study is distinguishing increases in condensation nuclei concentrations caused by homogeneous nucleation from those resulting directly from sources. Two techniques were used to make this distinction.

Following Hogan (1968), ambient concentrations of condensation nuclei were monitored before and after changes to daylight and standard time. The extent to which diurnal variations in condensation nuclei profiles are dominated by anthropogenic activity (assumed to shift by one hour after a time change) and the sun can be qualitatively observed by this technique. Ambient air was sampled through a 6.1 meter TFE teflon tube with inside diameter of 2.5 cm. The inlet to the tube was located near the roof of the laboratory, about 12 m above the ground.

Condensation nuclei concentrations were monitored with an Environment One, Model Rich 100 condensation nuclei monitor; factory calibration of the instrument was assumed to give an accurate indication of trends in nuclei concentrations. Monitoring was restricted to weekends to eliminate the strong influence of source contributions by weekday rush hour traffic. A typical comparison between weekday and weekend traffic patterns is shown in Figure 2.1.

Comparisons between condensation nuclei profiles before and after time changes for the fall of 1975 and spring of 1976 are shown in Figures 2.2 and 2.3. All profiles had the same general features. Concentrations tended to decrease fairly steadily after midnight until approximately sunrise when they began to increase. One or two peaks were generally observed before 8:00 a.m. Peaks associated with late afternoon and evening traffic were observed (not shown) followed by an increase in concentration during the evening as the mixing height decreased due to the lowering of the inversion layer. Ideally one would compare average condensation nuclei profiles for several days before and after the time change. In fact, weather patterns for the periods studied were so variable as to make this impossible. Profiles observed on foggy days as shown, for example, in Figure 2.4, did not have many of the interesting features of the sunny day profiles. Therefore the time change comparison is restricted to pairs of days with qualitatively similar meteorological conditions.

The profiles for sunny days presented in Figures 2.2 and 2.3 all show two early morning peaks, consisting of a small peak near sunrise

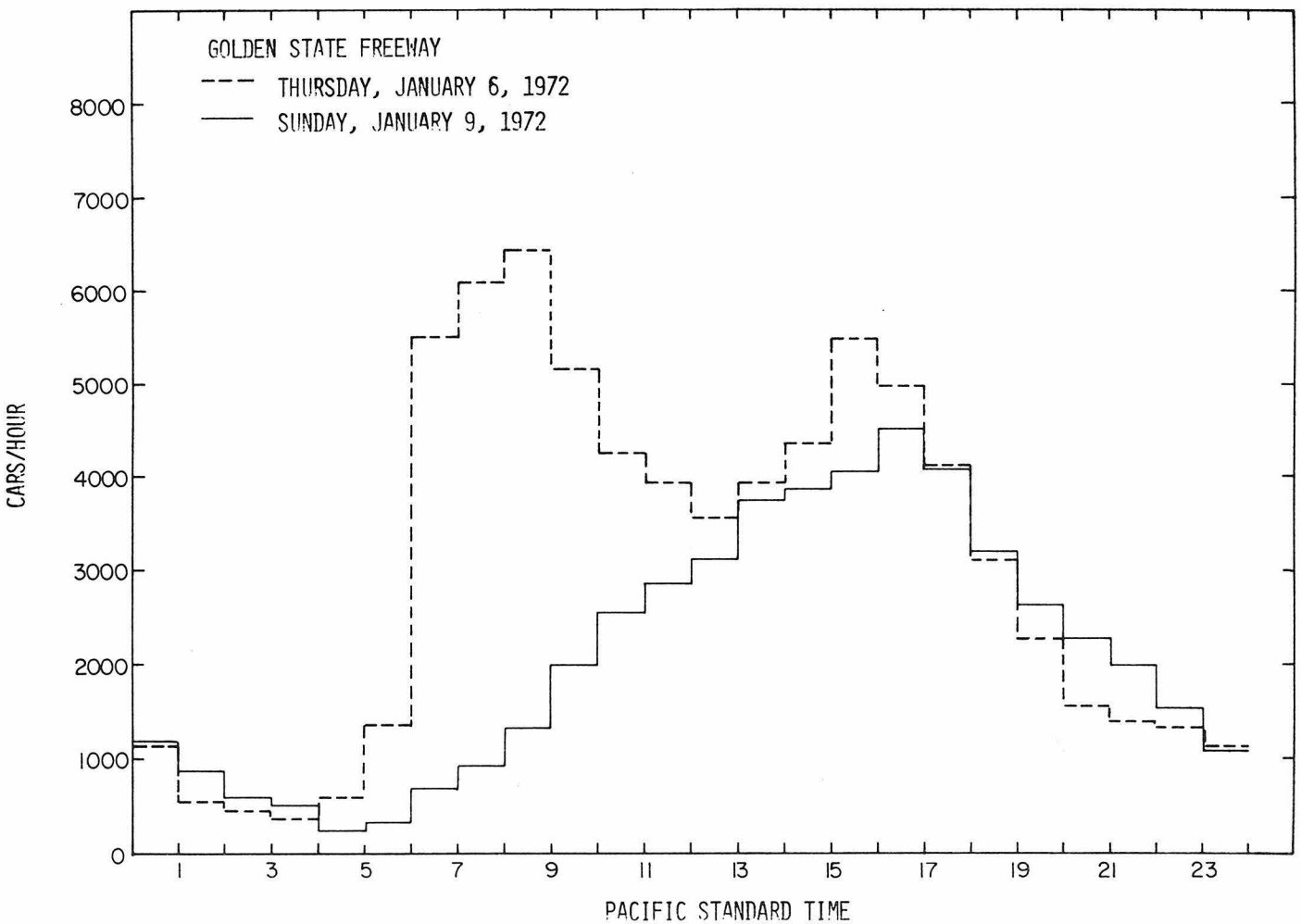

FIGURE 2.1

A comparison of freeway traffic patterns on weekdays and weekends in Los Angeles. Note the absence of rush hour traffic on Sunday morning. (California, State of, 1972)

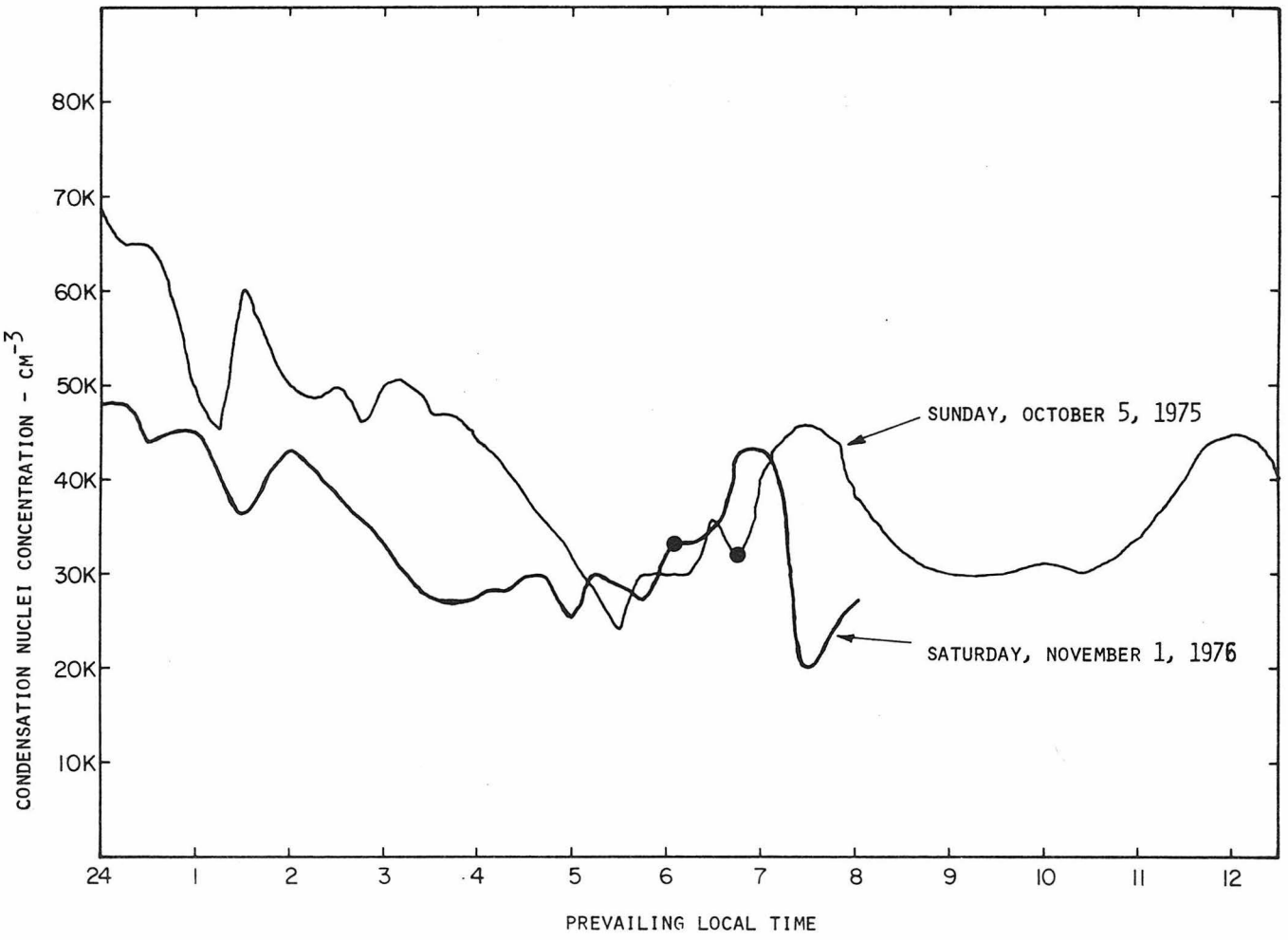

FIGURE 2.2

Comparison of condensation nuclei profiles for 2 sunny days before and after changes to Pacific Standard time in the fall of 1975. The black circles show the time of sunrise. Note that the predominant early morning features of the profiles appear to shift with the sun.

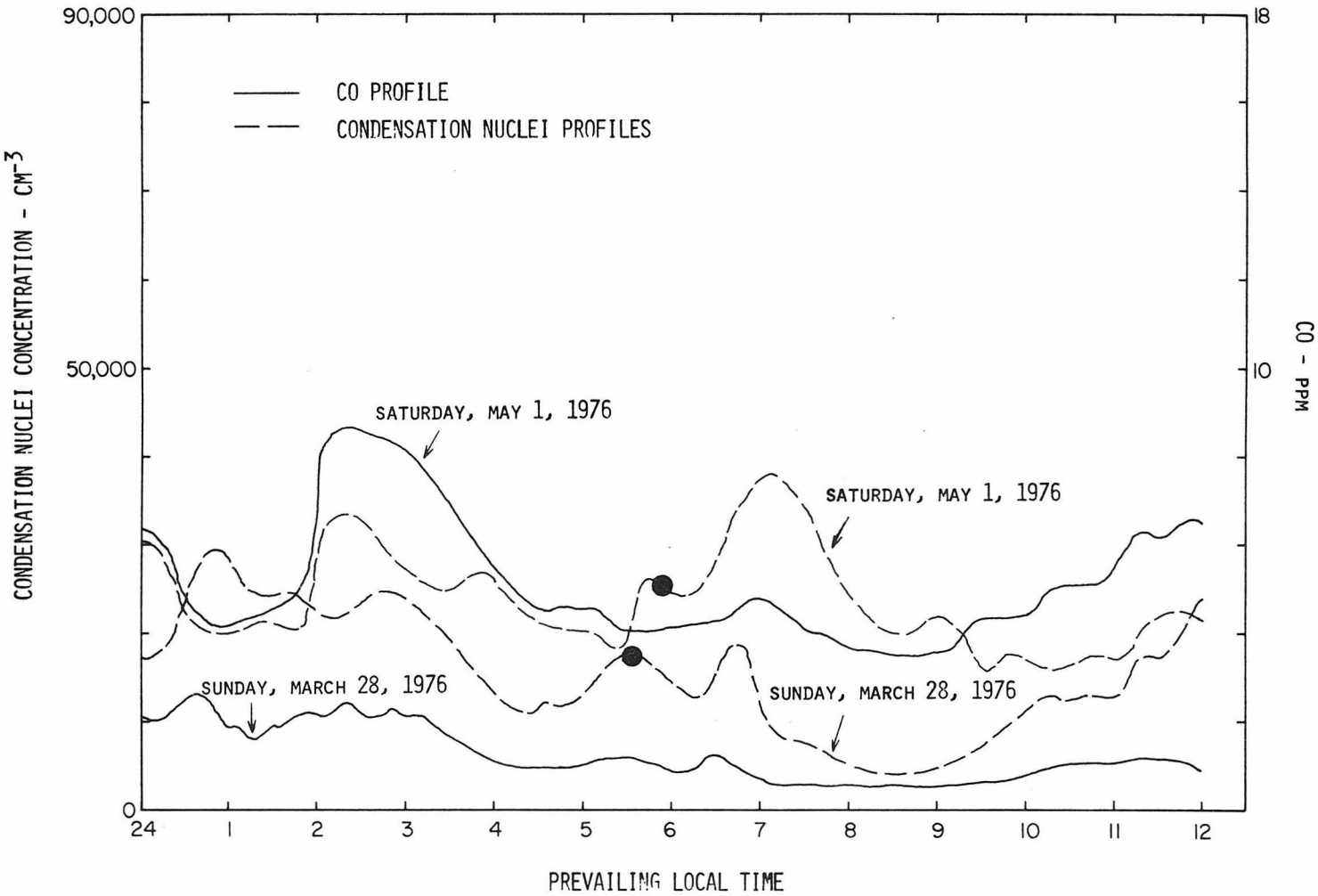

FIGURE 2.3

A comparison of condensation nuclei and carbon monoxide profiles for two sunny days before and after changes to Pacific Daylight Time in the spring of 1976. The black circles show the time of sunrise. Note that the peaks near sunrise are not obviously correlated with CO, unlike many other features of the profiles. Also, these peaks appear to shift with the sun unlike the second peak after sunrise which appears to occur at the same local time in both cases.

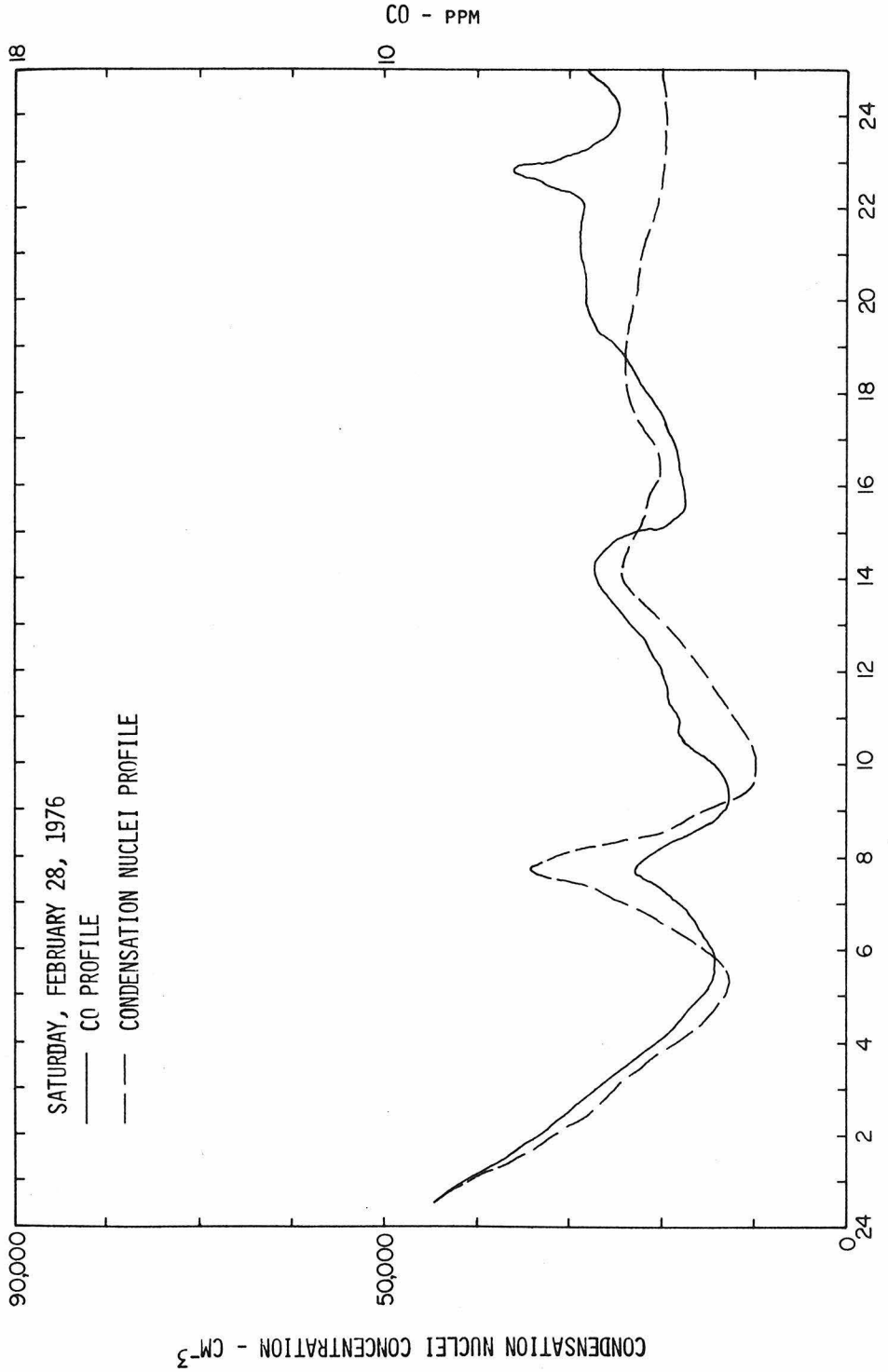

FIGURE 2.4

Comparison of condensation nuclei and carbon monoxide profiles on a foggy day.

(indicated by the black circles) and a second larger one between 6:30 and 7:30 a.m. In all cases the earlier of these two peaks shifted with the time of sunrise, indicating that it may well result from homogeneous nucleation induced by photochemical activity. This hypothesis is supported by the fact that this early peak is not present in the foggy day profile shown in Figure 2.4, when homogeneous nucleation would not be expected. The later peak shifts with the time of sunrise in Figure 2.2, but not in Figure 2.3 indicating that it may result partly from homogeneous nucleation, and partly from aerosols put directly into the air by early morning traffic.

To further test these hypotheses, carbon monoxide and condensation nuclei profiles were simultaneously monitored. Carbon monoxide was measured with an Ecolyzer model 2104 CO monitor; calibration of the instrument was checked routinely with span gas. By assuming that the automobile is the only important anthropogenic source of condensation nuclei and that CO is a good tracer for nuclei emissions from the automobile, one can conclude that an increase in condensation nuclei concentrations in the absence of a corresponding increase in CO results from homogeneous nucleation. Note that CO and condensation nuclei profiles for the foggy day profiles in Figure 2.4 trace one another well as one might expect in the absence of strong photochemical activity. Sunny day comparisons presented in Figure 2.3 show a much poorer correlation between CO and nuclei profiles, particularly for the early nuclei peak which occurs at sunrise. This is a second indication that the early peak is probably due to homogeneous nucleation. In addition, the increase in condensation nuclei concentration relative to the increase in carbon monoxide concentrations for the sunny day profiles shown in Figure 2.3

is much greater than that for the foggy day profile shown in Figure 2.4 for the later of the two early morning condensation nuclei peaks. This is a further indication that the second peak may result both from source contributions and homogeneous nucleation.

A final piece of evidence suggesting that homogeneous nucleation occurs in Los Angeles air is presented in Figure 2.5. CO and condensation nuclei profiles were simultaneously monitored on a day with intermittent periods of intense sunlight followed by decreases due to obstruction by clouds. The condensation nuclei concentrations exhibited striking peaks followed by rapid decreases, presumably as homogeneous nucleation was turned on and off by the sun. There is no proof that these increases are associated with sunlight intensity. The constancy of CO, however, is a strong indication that the new nuclei do not result from local traffic. The 25 second rise time of the carbon monoxide analyzer was short compared to the 5-10 minute widths of the condensation nuclei peaks; corresponding peaks in carbon monoxide concentrations should have been observed if the peaks resulted from local traffic.

2.4 Early Morning Experiments

A series of experiments was conducted to study homogeneous nucleation in a batch of unfiltered Los Angeles air collected before sunup. The air was trapped in a 65 cubic meter teflon reactor and aerosol dynamics were observed as a function of time. No gases other than ambient air were introduced into this reactor, eliminating the possibility of contamination. In all cases, homogeneous nucleation as indicated by an increase in the total number of particles detected by the condensation nucleus counter was observed several hours after sunrise. The results of the final experiment of this series are reported here.

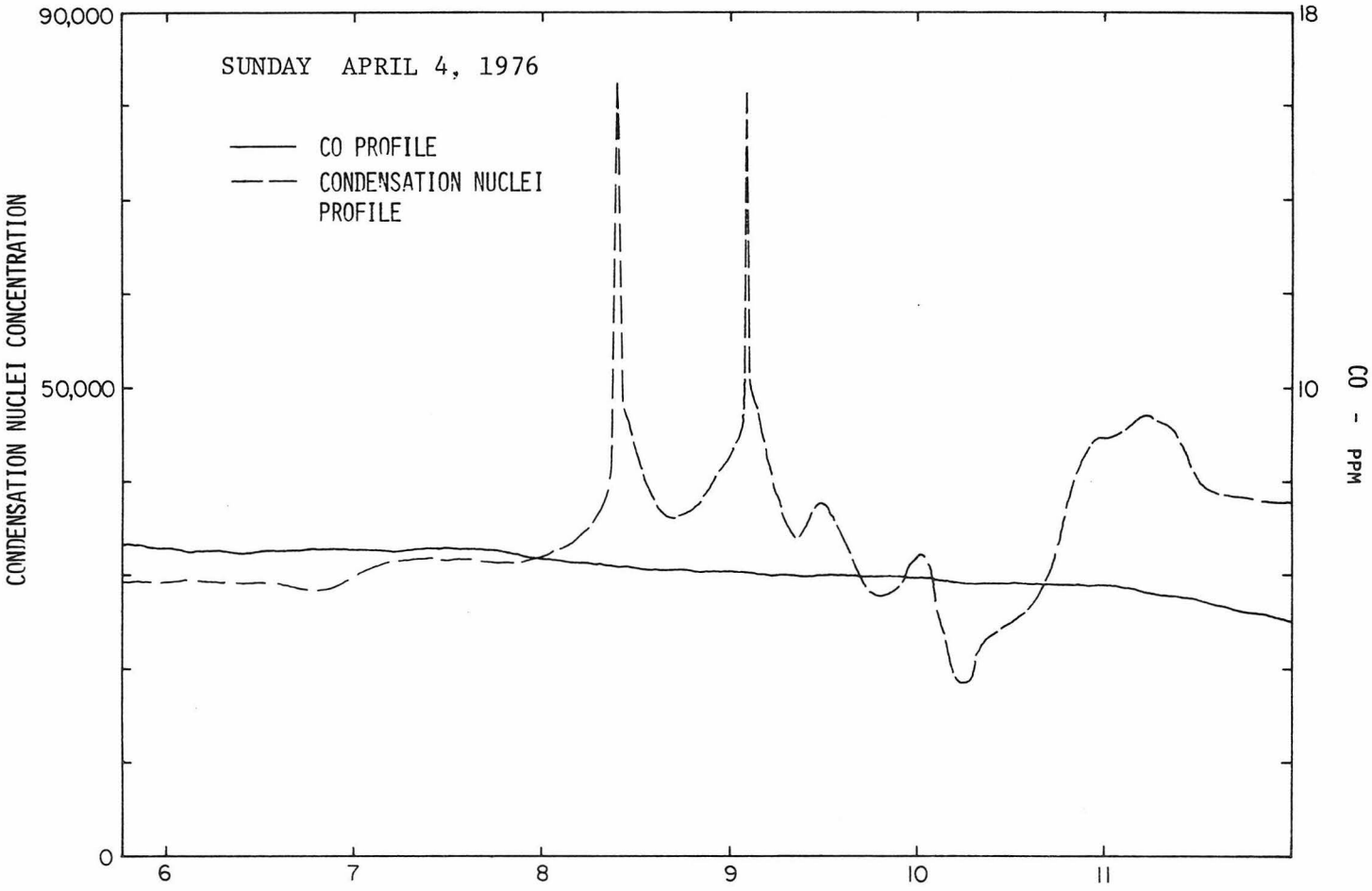

FIGURE 2.5

Comparison of condensation nuclei and carbon monoxide profiles on a day with intermittent cloud cover. The striking condensation nuclei peaks are hypothesized to result from homogeneous nucleation.

The reactor was filled with unfiltered ambient air at 600 Pacific Standard Time on November 9, 1976. Figure 2.6 shows the time evolution of the condensation nuclei concentration, total number concentration greater than 0.01 μm as measured by the electrical aerosol analyzer and optical particle counter, and sunlight intensity measured with an Eppley Pyrheliometer. (See Chapter 4 for details of instrumentation.) Note that homogeneous nucleation started at 830 PST, soon after the sunlight intensity became significant, and continued for at least two hours. The total number concentration measured by the size distribution instrumentation began to increase one hour after the condensation nuclei profile, presumably because extra time was required to grow the new particles to the 0.01 μm minimum detected by the electrical aerosol analyzer. The discrepancy between total number concentration measured by the condensation nuclei monitor and electrical aerosol analyzer is consistent with the results of Liu and Pui (1973).

The aerosol sulfur distribution with respect to size was measured before and after homogeneous nucleation occurred. Samples were collected on stainless steel strips with a five stage single jet low pressure impactor designed and calibrated by Hering, et al. (1977). The stainless steel impaction surfaces were coated with thin films of Vaseline petroleum jelly to minimize bounceoff. The aerosol sulfur collected on each stage was analyzed by the aerosol volatilization technique developed by Roberts and Friedlander (1976a). The first sample was collected between 719 PST and 950 PST, and the second between 1032 PST and 1300 PST. The uncertainties of the sulfur content on any stage are about 20%. The aerosol sulfur distributions before and after homogeneous

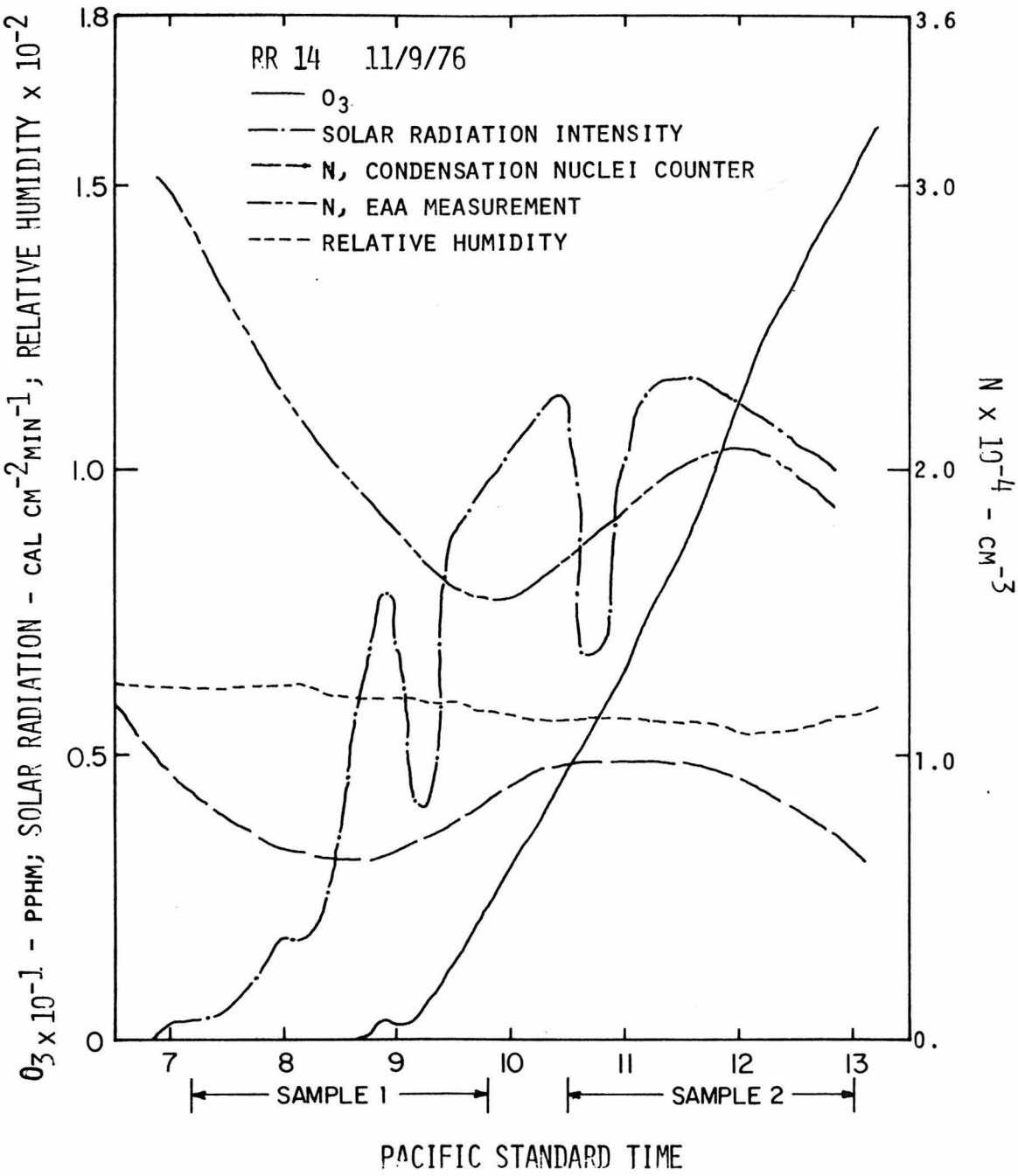

FIGURE 2.6

Time profiles of O_3, solar radiation, relative humidity and aerosol number concentrations for experiment RR14. The air was collected before sunrise and observed as sunlight intensity increased. Aerosol sulfur samples were collected with a low pressure cascade impactor during the indicated time periods.

nucleation, each normalized with respect to the total aerosol sulfur concentration during that measurement, are presented in Figure 2.7. Note that although most of the sulfur containing aerosol was lost to the reactor walls during the experiment, the relative amount of sulfur associated with small particles increased after homogeneous nucleation. This is a strong indication that sulfur containing species participate in homogeneous nucleation in ambient Los Angeles air, since particles in the small size range are lost preferentially due to their high mobilities. Likely candidates are H_2SO_4 (Mirabel and Katz, 1974; Cox, 1974; Stauffer, et al., 1973; Castleman, et al., 1975) and $(NH_4)_2SO_4$ (Friend, et al., 1973). H_2SO_4 is known to be a condensable product of several photochemical reactions involving SO_2 (Cox and Penkett, 1972; Endow, et al, 1963). The presence of NH_3 is known to augment rates of particle formation in photochemical systems involving SO_2 (Friend, et al., 1973).

2.5 Summary and Conclusions

Results of the study described in this chapter provide evidence that homogeneous nucleation occurs in the Los Angeles atmosphere at sunrise on sunny mornings. This conclusion is stated with some reservations. The condensation nuclei increase believed to be strictly associated with homogeneous nucleation starts before sunrise. In contrast, Hogan (1968) found that homogeneous nucleation in rural areas began about two hours after sunrise. Homogeneous nucleation in a batch of Los Angeles air collected before sunrise (see, e.g. Figure 2.6) typically begins about 2 hours after sunrise when ozone concentrations and sunlight intensities become significant. These discrepancies do not invalidate the conclusions of the study. Photochemistry above forested

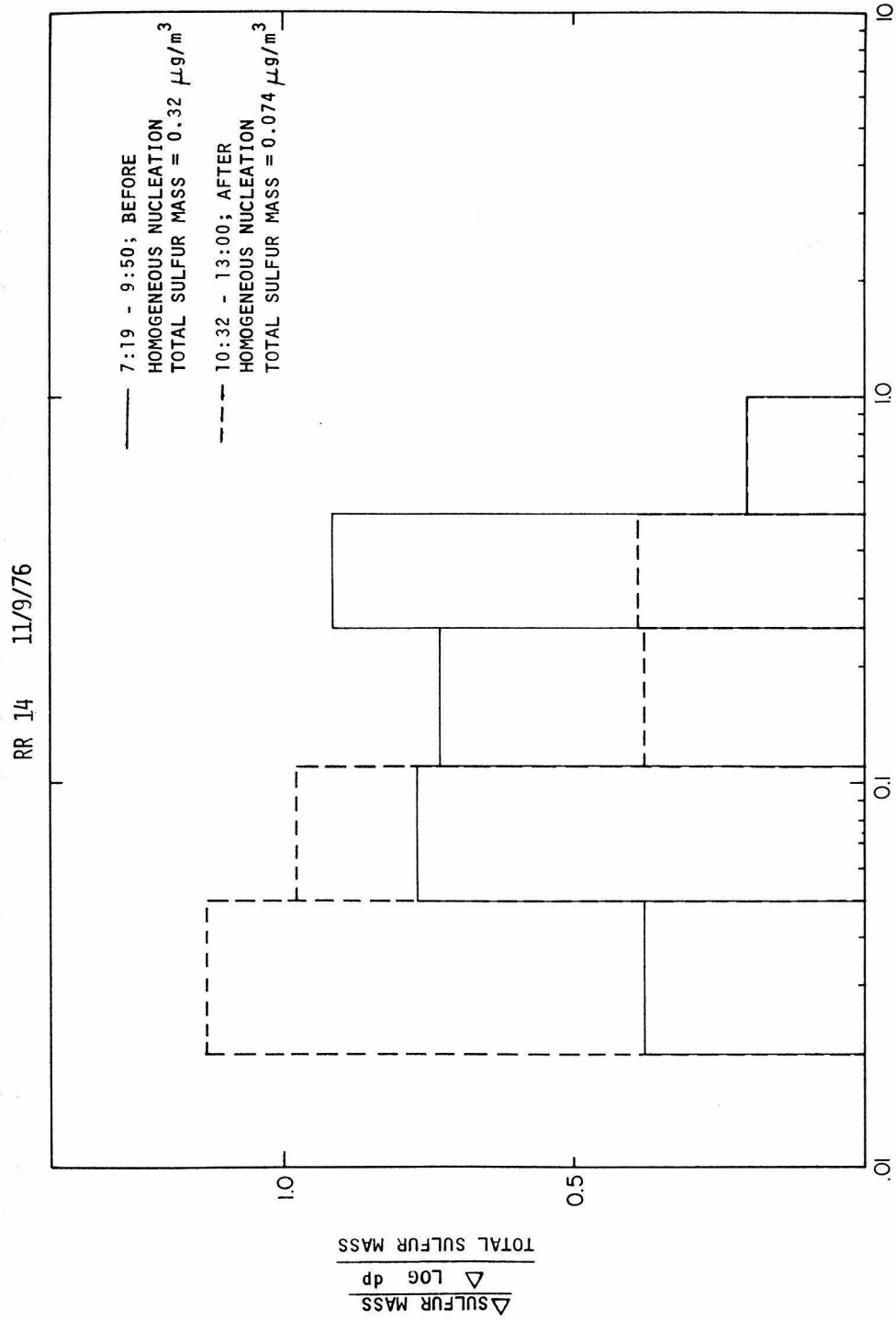

FIGURE 2.7

Aerosol sulfur distributions normalized with respect to total aerosol sulfur before and after homogeneous nucleation for experiment RR14. Note the enrichment in sulfur contained in small particles after homogeneous nucleation. The decrease in total aerosol concentration is due to wall losses.

areas in upstate New York is likely to be quite different from that which takes place in Los Angeles, and the spectrum of sunlight penetrating through the walls of a teflon reactor (Dupont, 1966) is likely to be different from that in the atmosphere. Nevertheless, it must be noted that if the early condensation nuclei peak is indeed a result of homogeneous nucleation, it occurs sooner than would be expected on the basis of other evidence.

The fact that homogeneous nucleation occurs in unperturbed ambient air confirms that formation of condensable products by homogeneous gas phase reactions is a mechanism of gas-to-particle conversion. Heterogeneous mechanisms of gas-to-particle conversion take place on or within preexisting particles. Evidence was presented to show that sulfur containing species participate in the homogeneous nucleation which occurs in Los Angeles air. Homogeneous nucleation in rural areas, in contrast, appears to originate with organic aerosol precursors (Went, 1964).

It is unlikely that homogeneous nucleation is an important source of condensation nuclei in the Los Angeles atmosphere. A casual glance at Figures 3 and 4 shows that the nuclei peak believed to be associated with homogeneous nucleation is small compared with peaks associated with direct input by sources. On a global scale, however, it is likely that homogeneous nucleation plays an important role in shaping aerosol size distributions.

CHAPTER 3
RELATION OF SURFACE AREA TO RATE OF GAS-TO-PARTICLE CONVERSION

During the growth of a photochemically generated aerosol, both condensation and coagulation occur simultaneously. The dynamics of the aerosol size distribution and its integral moments are linked to the rate of the chemical reaction generating aerosol material through the term dV/dt, representing the volumetric rate of gas-to-particle conversion. For monodisperse aerosols and aerosols whose size distributions are self-preserving, the surface area per volume of gas can be expressed as a function of the rate of gas-to-particle conversion, dV/dt, and time, t. For the special case of constant aerosol formation rate, these surface areas vary as $(dV/dt)^{3/5}t^{1/5}$ and are essentially independent of the chemical properties of the new secondary aerosol. Several investigators have reported that chemically formed aerosols establish constant surface areas which depend only on the rate of gas-to-particle conversion. The values and functional dependences of these measured surface areas are in good agreement with the theory given in this chapter. Thus by carrying out photochemical reactions under controlled conditions, aerosols of controlled surface area can be generated.

3.1 Introduction

Chemical reactions in the gas phase may result in the formation of condensable products. These molecules will either deposit on preexisting particles, or form new particles by homogeneous nucleation.

Low vapor pressure products such as sulfuric acid are particularly likely to undergo homogeneous nucleation.

Particles generated by homogeneous nucleation are initially much smaller than the mean free path of the gas. They continue growing both by coagulation and condensation as long as production of condensable products continues. Eventually sufficient aerosol surface area is generated either to suppress homogeneous nucleation or to scavenge newly formed molecular clusters before they have the opportunity to grow to an observable size, depending on the chemical nature of the condensing species.

This sequence of processes occurs frequently in air pollution. Aerosol formation by the photooxidation of SO_2 to sulfate probably takes place this way. Homogeneous nucleation, probably of condensable organic vapors, has been well documented over forested areas (Went, 1966; Hogan, 1968; Flyger, et al., 1976; Lopez, et al., 1974). Related processes may occur following coal combustion during the cooling of combustion gases (Flagan and Friedlander, 1976). The mechanism of gas-to-particle conversion has an important effect on the chemical properties of the secondary aerosol. When homogeneous nucleation occurs, the condensing vapors initially accumulate in the very small particle size range and later grow into the larger sizes.

A complete characterization of these systems would require information on the particle size distribution as a function of time and the chemical composition as a function of particle size. Such data are difficult to obtain and to handle. Integral functions or

moments of the size distribution such as the total number and volume concentrations and overall chemical composition of the particulate phase are easier to obtain experimentally and require less data handling. Their relation to the rate of gas-to-particle conversion is of particular interest.

When the size distribution is self-preserving, certain simple relationships exist among the moments. As shown in this paper, such relationships can be used to correlate data and to test them for self-consistency. They should also prove useful in testing the results of numerical calculations, especially for the later stages of coagulation when the similarity theory is best applied.

An analysis of this kind was carried out for particles much larger then the mean free path (Pich, Friedlander, and Lai, 1970). They found that when the rate of gas-to-particle conversion is constant, the surface area reaches a constant, steady-state value such that the rate of formation of surface area by condensation is equal to the rate of loss by coagulation. Subsequently, experimental data for a coagulating free molecule aerosol with simultaneous gas-to-particle conversion have become available (Clark, 1972; Husar and Whitby, 1973; McNelis, 1974; Kocmond, et al., 1975; this thesis, Chapter 4). Results of these investigators show that for constant rates of aerosol volume production, aerosol surface areas per volume of gas reach a constant value dependent only on the rate of aerosol production. They refer to this value as the "equilibrium" surface area, although the term "steady state" would be more appropriate. As shown in this chapter, theory indicates that the

surface area increases slowly with time in the free molecule range.

The data of the various investigators are analyzed in this paper in terms of a new theory for the free molecule range where particles are much smaller than the mean free path of the gas ($d_p << \ell$). An analytical expression relating aerosol surface area per volume of gas to the rate of aerosol production and time is derived. The predicted magnitude of aerosol surface area as well as its functional dependences are in excellent agreement with the data.

Aerosol surface area is a key aerosol property linking interactions between gases and aerosols. Adsorption of gaseous species on particles is a function of available surface area. Transport limited processes, such as condensation and free radical scavenging by aerosol surfaces, occur at rates proportional to surface area for free molecule aerosols ($d_p << \ell$). Ambient urban aerosols fall largely in the transition regime ($d_p \simeq \ell$) where transport limited processes occur at rates proportional to d_p^x where $1 \lesssim x \lesssim 2$. Fuchs and Sutugin (1971) have proposed an interpolation expression based on the work of Sahni (1966) for molecular transport to transition regime aerosols. It is not, in general, correct to assume that the transport of diffusing species is proportional to the surface area of such aerosols, although this is often a good approximation. The total molecular collision rate (molecules/cm^3/sec) with the average Los Angeles aerosol size distribution measured by Whitby, et al. (1972) was calculated by using the interpolation expression from Fuchs and Sutugin (1971) and also by assuming that transport was proportional to total aerosol surface area per volume of gas. Results agreed to within 10%.

Interactions between aerosol surfaces and gaseous species have received scant attention in the literature. Experimental studies of surface reactions of the OH radical on H_3PO_4 and graphite surfaces were reported by Mulcahy and Young (1975). The collision efficiency for loss of OH on these surfaces varies between 0.01 and 0.05. Despite these high efficiencies, calculations for typical aerosol loadings and rates of OH production and consumption in the atmosphere indicated that aerosol surfaces are a minor sink for the OH radical. It was hypothesized that aerosol scavenging of radicals less reactive in the gas phase, for example HO_2, may be important. Graedel, et al. (1975) considered interactions between aerosol surfaces and free radicals in modeling tropospheric chemistry in northern New Jersey. As a first-order approximation it was assumed that all radicals were lost on collision with particles. Agreement between calculated and observed O_3, NO, and NO_2 profiles was improved by including these heterogeneous effects. Judeikis and Siegel (1973) established criteria for the importance of heterogeneous interactions between CO, NO, SO_2, NO_2 and olefins and aerosol surface area in reacting systems. They concluded that surface catalyzed reactions can, in some cases, compete with homogeneous gas phase reactions. Liberti (1970) reported adsorption of CO_2, CO, CH_4, NH_3, NO and C_2H_4 on ambient aerosol surfaces. Novakov, et al. (1974) studied the oxidation of SO_2 on surfaces of graphite particles. It was concluded that similar surface reactions may be important mechanisms of sulfate aerosol formation in ambient air. The importance of gas-surface interactions undoubtedly is strongly dependent on the chemical characteristics of the aerosol surface.

In Chapter 4 a new theory is presented which predicts rates at which particles of a given size are formed in the presence of a given aerosol surface area for systems in which condensable molecules are produced in the gas phase by chemical reaction at a known rate. It is shown that for typical ambient aerosol production rates, the self-preserving surface area falls between the dynamic regimes in which new particle formation can be important and in which heterogeneous condensation dominates. Predicted rates of new particle formation in the presence of the self-preserving surface area are small compared with expected coagulation rates. Thus, the self-preserving surface area is sufficient to scavenge most of the clusters formed by homogeneous nucleation before they grow to a detectable size.

3.2 Aerosol Surface Area per Volume of Gas - Self-Preserving Distribution

The surface area per volume of gas of an aerosol consisting of spherical particles is

$$A(t) = \int_0^\infty \pi d_p^2 \, n(v,t) dv \tag{3.1}$$

where d_p is particle diameter.

The aerosol size distribution function, $n(v,t)$, is defined so that the number of particles with volume between v and v + dv is

$$dN = n(v,t)dv \tag{3.2}$$

Previous studies (Swift and Friedlander, 1964; Friedlander and Wang, 1966; Wang and Friedlander, 1967; Pich, et al., 1970; Lai, et al., 1972; Graham and Homer, 1973) have shown that knowledge of the total aerosol number concentration, N, and aerosol volume fraction, V, is often sufficient to predict asymptotic size distributions of coagulating aerosols. These asymptotic size distributions are related to the

dimensionless self-preserving distributions, $\Psi(\eta)$, through the self-preserving transformation defined by

$$n(v,t) = \frac{N^2}{V} \Psi(\eta) \tag{3.3}$$

where the dimensionless volume, η, is

$$\eta = \frac{Nv}{V} \tag{3.4}$$

The self-preserving size distribution, $\Psi(\eta)$, is independent of time, but does depend on the mechanism of particle interactions. The above investigators have evaluated $\Psi(\eta)$ for several different cases. For self-preserving distributions, Equation (3.1) reduces to

$$A = (36\pi)^{1/3} \mu N^{1/3} V^{2/3} \tag{3.5}$$

where

$$\mu = \int_0^\infty \eta^{2/3} \Psi(\eta) d\eta \tag{3.6}$$

In the absence of condensation, $\mu = 0.90$ (Lai, et al., 1972) and $\frac{A}{N^{1/3}V^{2/3}} = 4.35$. We do not expect the dimensionless moments to vary much from unity even when condensation is occurring. In Figure 3.1 this theoretical prediction is compared with data for an aerosol generated photochemically in filtered ambient air. After an initial period during which homogeneous nucleation takes place, the ratio $A/N^{1/3}V^{2/3}$ closely approaches the asymptotic value 4.35 characteristic of the self-preserving distribution.

Aerosol number and volume concentrations can be related to the rate of aerosol formation, dV/dt, for self-preserving aerosols. If production of condensable material in a particle free system is initiated

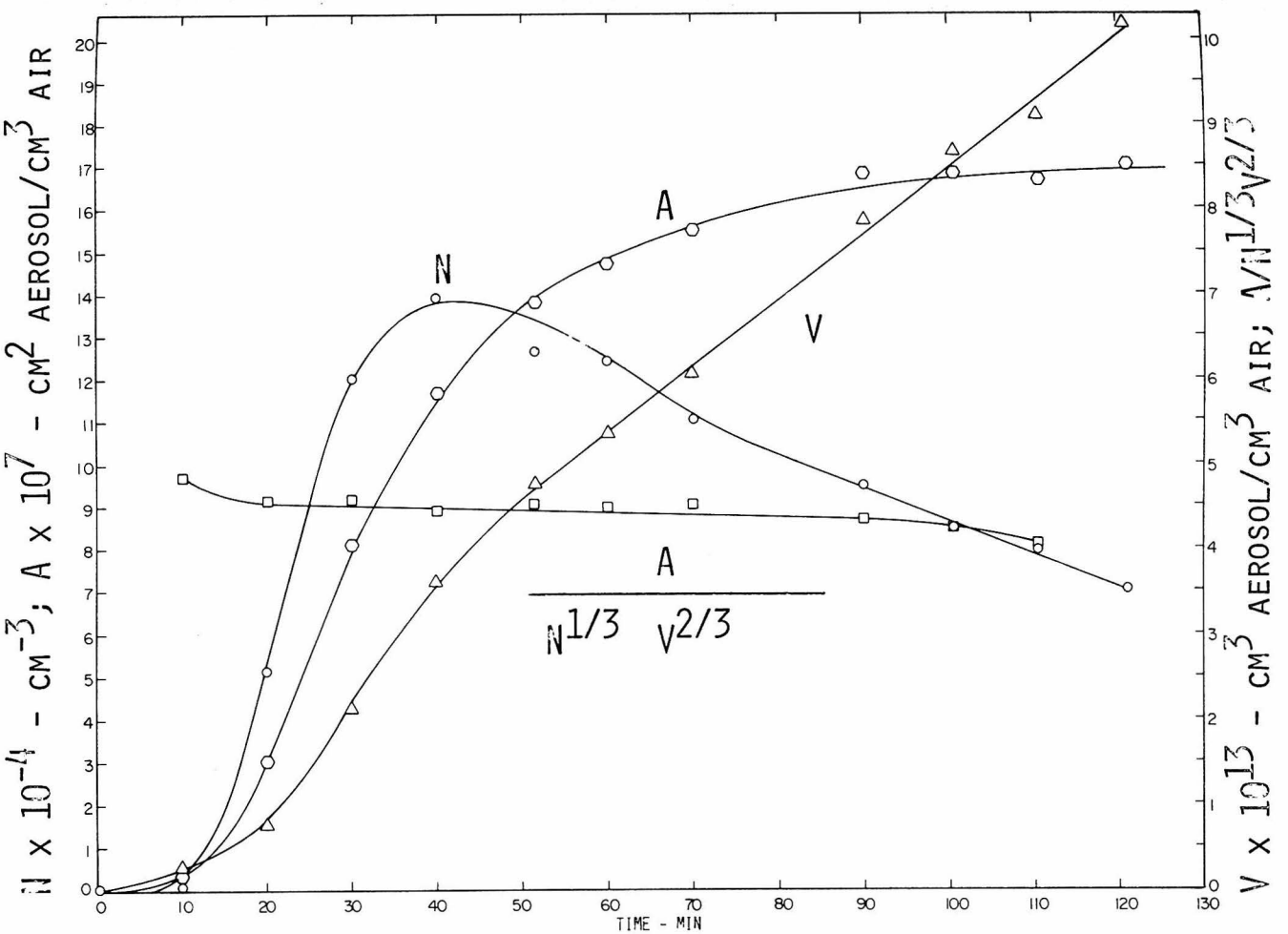

FIGURE 3.1

Evolution of N, V, and A and the ratio $A/V^{2/3}N^{1/3}$ with time for a photochemical aerosol (experiment RR15, Appendix D) measured with an electric aerosol analyzer. Air in a $65m^3$ teflon reactor was exposed to sunlight at time zero. Note that although the aerosol volume fraction, V, increased at a relatively constant rate, the aerosol surface area concentration, A, increased very slowly after about 70 minutes. The ratio $A/N^{1/3}V^{2/3}$ approached the value of 4.35 predicted by theory.

at a constant rate, F, at time zero, then at time t the aerosol volume fraction is

$$V = Ft \tag{3.7}$$

During the later stages of aerosol development when homogeneous nucleation is no longer important, the decay in aerosol number concentration, dN/dt results only from coagulation and is given by

$$\frac{dN}{dt} = \frac{1}{2}\int_0^\infty\int_0^\infty \beta(v,\tilde{v})n(v,t)n(\tilde{v},t)dvd\tilde{v} \tag{3.8}$$

The collision frequency function, $\beta(v,\tilde{v})$, for spherical particles much smaller than the mean free path of air is

$$\beta(v,\tilde{v}) = \left(\frac{3}{4\pi}\right)^{1/6}\left(\frac{6kT}{\rho}\right)^{1/2}\left(\frac{1}{v}+\frac{1}{\tilde{v}}\right)^{1/2}(v^{1/3}+\tilde{v}^{1/3})^2 \tag{3.9}$$

where ρ is the density of the aerosol particles. Graham and Homer (1973) have discussed modifications of this expression to account for interparticle dispersion forces which tend to increase coagulation rates by about a factor of two. Substituting (3.3) and (3.9) in (3.8) gives

$$\frac{dN}{dt} = -\frac{\alpha_1}{2}\left(\frac{3}{4\pi}\right)^{1/6}\left(\frac{6kT}{\rho}\right)^{1/2} V^{1/6}\, N^{11/6} \tag{3.10}$$

where

$$\alpha_1 = \int_0^\infty\int_0^\infty (\eta^{1/3}+\tilde{\eta}^{1/3})^2\left(\frac{1}{\eta}+\frac{1}{\tilde{\eta}}\right)^{1/2}\Psi(\eta)\Psi(\tilde{\eta})d\eta d\tilde{\eta} \tag{3.11}$$

By assuming that as a result of coagulation the number concentration at time t is much smaller than the concentration soon after the start of aerosol production, Equation (3.10) with (3.7) can be solved for N(t) to give

$$N = \left(\frac{14}{5\alpha_1}\right)^{6/5}\left(\frac{4\pi}{3}\right)^{1/5}\left(\frac{\rho}{6kT}\right)^{3/5}\frac{1}{F^{1/5}\,t^{7/5}} \tag{3.12}$$

Substituting (3.7) and (3.12) in (3.5), the result is

$$A = \left(\frac{2}{\alpha_1}\right)^{2/5} \mu \left[\left(\frac{7}{5}\right)^{2/5} (36\pi)^{1/3} \left(\frac{4\pi}{3}\right)^{1/15} \left(\frac{\rho}{6kT}\right)^{1/5}\right] F^{3/5} t^{1/5} \qquad (3.13)$$

The self-preserving surface area, A, is a weak function of time, and increases as the 3/5 power of the rate of aerosol formation. The only aerosol property on which A depends is density, and this dependence is relatively weak. In general, α_1 and μ depend on the form of the self-preserving size distribution which, in turn, depends on the rate and mechanism of gas-to-particle conversion. In the absence of condensation α_1 and μ approximately equal 6.67 and 0.9 respectively (Lai, et al., 1972; Graham and Robinson, 1976). Assuming these values, and taking time to be one hour, density 1.46 g/cm^3 and temperature 300°K, (3.13) reduces to

$$A = 6.23 \times 10^3 F^{3/5} \qquad (3.14)$$

A full treatment of the effects of dispersion forces on these results is not within the scope of this paper. A first order estimate of their effect on (3.13) and (3.14) was made, however. Following Graham and Homer (1973) it was assumed that the form of the distribution function is unaffected by interparticle dispersion forces, but that the rate of decrease in total number concentration was enhanced by a factor of between 2.0 and 2.5. This range of values was determined by choosing a reasonable range of Hamaker constants for the coagulating aerosol. Based on these approximations, dispersion forces would be expected to decrease the self-preserving surface areas predicted in Equation (3.13) by 24-31%.

3.3 Surface Area per Volume of Gas for Monodisperse Aerosols

An expression similar to (3.13) can be derived for monodisperse aerosols which are simultaneously coagulating and growing by gas-to-particle conversion. In this case, the aerosol surface area per volume of gas is given by

$$A = \pi d_p^2 N = (36\pi)^{1/3} N^{1/3} V^{2/3} \tag{3.15}$$

The second equality was obtained by noting that particle volumes are given by

$$v = \frac{\pi d_p^3}{6} = \frac{V}{N} = \frac{Ft}{N} \tag{3.16}$$

The rate of decrease in number concentration by coagulation is

$$\frac{dN}{dt} = - \beta(v,v) N^2 \tag{3.17}$$

Substituting (3.9) and (3.16) in (3.17) and solving for N we obtain

$$N(t) = \left(\frac{1}{4\sqrt{2}}\right)^{6/5} \left(\frac{7}{5}\right)^{6/5} \left(\frac{4\pi}{3}\right)^{1/5} \left(\frac{\rho}{6kT}\right)^{3/5} \frac{1}{F^{1/5} t^{7/5}} \tag{3.18}$$

By substituting (3.16) and (3.18) in (3.15), the surface area of a monodisperse aerosol simultaneously growing by coagulation and gas-to-particle conversion can be expressed as

$$A = \frac{1}{2} \left[\left(\frac{7}{5}\right)^{2/5} (36\pi)^{1/3} \left(\frac{4\pi}{3}\right)^{1/15} \left(\frac{\rho}{6kT}\right)^{1/5} \right] F^{3/5} t^{1/5} \tag{3.19}$$

This expression for monodisperse aerosol surface areas is nearly identical to the self-preserving surface area given by Equation (3.13). The ratio of (3.13) to (3.19) is $2(2/\alpha_1)^{2/5}\mu$, and depends on the form of the self-preserving distribution. For distributions similar in

shape to the self-preserving distribution for free molecule aerosols growing only by coagulation (without gas-to-particle conversion) this ratio equals 1.11.

3.4 Experimental Measurements of Aerosol Surface Area in Reactive Systems

Several investigators (Clark, 1972; Husar and Whitby, 1973; Kocmond, et al., 1975; this thesis, Chapter 4) have used the electrical aerosol analyzer (Liu, et al., 1974) to study the evolution of photochemically generated aerosols in chambers of various types. McNelis (1974) studied aerosols generated by thermal reactions in the SO_2-O_3-propylene system. The experimental procedures and apparatus used by these investigators are summarized in Table 3.1. In all cases, aerosol formation was initiated in a volume of air containing trace amounts of aerosol precursors. Aerosol size distributions were measured as a function of time with the electrical aerosol analyzer and integrated to obtain integral moments such as aerosol number and volume concentrations, and aerosol surface area per unit volume of gas. Uncertainties in the data result from the finite resolution of the electrical aerosol analyzer (Liu and Pui, 1975), and changes in the aerosol by growth and coagulation during the course of a measurement.

Several minutes are required to measure an aerosol size distribution with the electrical aerosol analyzer. The above investigators measured new distributions at intervals of 8 to 20 minutes. For each experiment the rate of aerosol formation, F, was obtained by measuring

TABLE 3.1

Studies on Aerosol Dynamics in Smog Chambers

Investigators	Chamber Volume	Light Source	Chamber Material	Chemical System	Range of Initial Reactant Concentrations (ppm)	Relative Humidity Range
Clark (1972)	17.7 m^3	artificial	Teflon	SO_2	0.05 - 2.9	10 - 25%
Husar and Whitby (1973)	90. m^3	sun	Polyethylene	Filtered Ambient Air	-	unknown
Kocmond, et al. (1975)*				SO_2	0.03 - 0.62	12 - 48%
Calspan Chamber	589. m^3	artificial	Fluoroepoxy Coating	toluene	0.35 - 1.17	20 - 47%
				+ NO	0.15 - 0.53	
University of Minnesota Chamber	17. m^3	artificial	Teflon	toluene	0.35 - 0.38	24 - 57%
				+ NO	0.15 - 0.30	
				+ SO_2	0.04 - 0.11	
				hexene	0.33 - 0.35	33 - 40%
				+ NO	0.12 - 0.18	
				hexene	0.35 - 0.37	28 - 55%
				+ NO	0.12 - 0.18	
				+ SO_2	0.03 - 0.07	
				m-xylene	0.34 - 0.35	26 - 75%
				+ NO	0.13 - 0.16	
				m-xylene	0.34 - 0.35	26 - 54%
				+ NO	0.12 - 0.15	
				+ SO_2	0.04 - 0.06	
				cyclohexene	0.33 - 0.35	29 - 51%
				+ NO	0.10 - 0.14	
				cyclohexene	0.33 - 0.35	38 - 33%
				+ NO	0.13 - 0.22	
				+ SO_2	0.04 - 0.05	
McNelis (1974)	0.437 m^3	none thermal reaction	Teflon	propylene	1. - 8.6	19 - 39%
				+ O_3	0.27 - 3.	
				+ SO_2	0. - 0.65	
This Thesis, Chapter 4	65. m^3	sun	Teflon			13 - 50%
				propylene	0.7 - 2.5	
				+ NO	0.3 - 1.3	
				+ NO_2	0.15 - 0.34	
				+ SO_2	0.01 - 0.51	

NOTE:

1. Temperature ranges are reported by McNelis (1974) (23°-28°C) and for experiments presented in this thesis (31°-49°C). Experiments were generally started at ambient or room temperature, but temperatures tend to increase with time due to radiative heating.

2. The effects of preexisting nuclei were extensively considered in Chapter 4 of this thesis. Kocmond, et al. (1975) report several experiments in which an initial NaCl aerosol was present.

3. A considerable amount of data for aerosol formation from photooxidation of SO_2 is presented by Kocmond (1973). These data are not reported here since it is redundant for our purposes.

* Data reported by Kocmond, et al. (1975) were obtained in the smog chambers at the Calspan Corporation and at the University of Minnesota. Measurements of aerosol formation in most of the chemical systems reported were done in both laboratories.

the slope of the volume versus time curve. Observed rates of volume increase typically increased from near zero early in the experiments to reasonably constant values which were maintained for timescales of about 60-100 minutes, although significant reductions in rates were observed after only 30 minutes in some cases. Aerosol formation rates reported by Clark (1972) were more nearly constant than those reported by the other investigators. Reported rates of aerosol formation are based on data over the time during which aerosol formation rates were constant.

3.5 Aerosol Chemical Composition

An important result of the theoretical analysis given above is that aerosol surface area per volume of gas should be essentially independent of the chemical nature of the condensing species. The investigators mentioned above have studied aerosol formation for a variety of chemical systems. The nature of the aerosol products produced by these systems is discussed below.

Husar and Whitby (1973), Clark (1972) and Kocmond, et al. (1975) did not measure the chemical composition of aerosols formed in the experiments described above. McNelis (1974) measured total aerosol sulfur with x-ray fluorescence and used liquid chromatography to identify water soluble sulfates. Results of the two techniques were comparable, and sulfur balances were good. For experiments reported in Chapter 4 of this thesis, aerosol samples were collected with a low pressure cascade impactor (Hering, Flagan, and Friedlander, 1977) and analyzed for elemental sulfur with the flash volatilization technique developed by Roberts and

Friedlander (1976a). The increase in aerosol sulfur was equal to the decrease in gas phase sulfur. Aerosol volume distributions were calculated from aerosol sulfur distributions based on the assumption that the sulfur was in the form of H_2SO_4 in equilibrium with ambient humidity; agreement with volume distributions measured by the electrical aerosol analyzer was good.

Aerosols formed by homogeneous gas phase reactions of SO_2 and various organics in the presence of O_3 or NO_x and ultraviolet light generally consist of a mixture of sulfur containing and organic species; the relative amounts of the two types of aerosol depend on the nature of the organic precursor. Irradiated mixtures of alkenes with fewer than seven carbon atoms (e.g. propylene and 1-hexene) and SO_2 produce aerosols containing much more sulfur than organics. Endow, et al., 1963, identified H_2SO_4 as the primary photochemical aerosol produced by the SO_2-NO_2-propylene system. Groblicki and Nebel (1971) found that the predominant aerosol formed by photochemically reacting SO_2, NO and propylene was $(NH_4)_2SO_4$; ammonia present in the chamber diluent air probably accounted for the ammonium ions. Praeger, et al. (1960), identified the sulfate ion as a product of photochemical reactions between olefins, SO_2, and NO_2; 1-Hexene was one of the olefins included in the study. Little additional aerosol is formed when SO_2 is added to systems containing aromatics (e.g. m-xylene and toluene) or cyclic olefins (e.g. cyclohexene). Any aerosol sulfur formed in such chemical systems is generally in the form of sulfate. Grosjean (1976) has reviewed the literature on aerosols formed by homogeneous gas phase reactions of mixtures of SO_2 and various organics.

Chemical compositions of the organic aerosol fractions are poorly documented. Grosjean (1976) and Schwartz, et al. (1974) used combined gas-chromatography and mass spectrometry to study aerosol products formed by the photochemical reaction of cyclohexene with NO_x. Grosjean (1976) found adipic acid to be the major aerosol constituent. Schwartz, et al. (1974) did not find adipic acid, but along with Grosjean (1976), found a number of other products, mostly difunctional compounds bearing in many cases a carboxylic acid group. Schwartz, et al. (1976) studied photochemical aerosol products from the NO_x-toluene system and found highly oxygenated polar products resembling several embalming fluids in composition (adding yet another dimension to the concept of self-preserving aerosols). Chu and Orr (1974) found approximately half of the reacted toluene carbon in this system in the aerosol phase. Lipeles, et al. (1973) reported the composition of aerosols formed in the 1-butene, ozone system was organic with highly oxygenated constituents. Heavier alkenes such as 1-hexene probably produce aerosols similar in composition. Chu and Orr (1974) studied photochemical aerosols produced in the o-xylene-NO_x system and found that more than half of the carbon in the reacted o-xylene molecules was in the aerosol phase. Aerosols produced by analogous reactions of m-xylene are probably similar in composition.

There is ample evidence to show that aerosols produced in the studies on aerosol dynamics reported above are varied in chemical composition. When sulfur is present, it is generally believed to be in the form of inorganic sulfate. The organic aerosol fraction is complex

and poorly understood. It is well documented, however, that organic aerosol consisting of a variety of species is produced in several of the chemical systems discussed.

3.6 Results of Experiments

The dynamics of the aerosols generated in the various studies was similar. Soon after illumination, a large number of particles is formed by homogeneous nucleation (Figure 3.1). The aerosol reaches a maximum number concentration follwed by a steady decrease due to coagulation. The aerosol volume fraction increases at a relatively constant rate for one to two hours, while the aerosol surface area increases rapidly at first but levels off at a relatively constant value after about one hour.

Size distributions of aerosols growing by gas-to-particle conversion apparently become self-preserving after the surface area levels off. Husar and Whitby (1973) found that aerosols growing by simultaneous condensation and coagulation fell on a single curve when plotted according to the self-preserving transformation, given by Equations (3.1) and (3.4). The shape of the dimensionless distribution varied with the rate of gas-to-particle conversion. Four size distributions from an experiment reported in Chapter 4, scaled according to the self-preserving transformation, are shown in Figure 3.2. Although a considerable amount of growth occurred during the course of these measurements, the dimensionless size distributions at different times fell on approximately the same curve, indicating that the aerosols were self-preserving in form. The dimensionless size distribution for coagulating

free molecule aerosols in the absence of condensation is also shown in Figure 3.2 (Lai, et al., 1972). Note that the experimental distribution for simultaneous coagulation and condensation is distinctly different from the theoretical distribution for coagulation alone. In general, different dimensionless size distributions will be obtained for different rates and mechanisms of gas-to-particle conversion.

Clark (1972) and McNelis (1974) found that the constant aerosol surface areas which were established during their experiments depended only on the rate of gas-to-particle conversion, F. The steady state ("equilibrium") aerosol surface areas measured by Clark (1972) after times of about one hour obeyed the empirical relation.

$$A = 2.79 \times 10^{3} F^{0.575} \tag{3.20}$$

Similarly, the steady state surface areas obtained by McNelis (1974) fit the relation

$$A = 2.90 \times 10^{3} F^{0.583} \tag{3.21}$$

Note that in both cases the functional dependence of A on F is very close to the 0.600 power predicted by the self-preserving theory (Equation 3.14). The expressions of Clark (1972) and McNelis (1974) agree with the theoretical prediction (3.14) to within ± 27% for aerosol formation rates between 10^{-18} and 10^{-12} cm^3 aerosol/cm^3 air/sec. In addition the nearly constant surface areas observed experimentally are consistent with the weak time dependence of the theory. The predicted increase in A during the second hour is 15%, an amount typical of wall losses and instrumental uncertainty for this type of experiment.

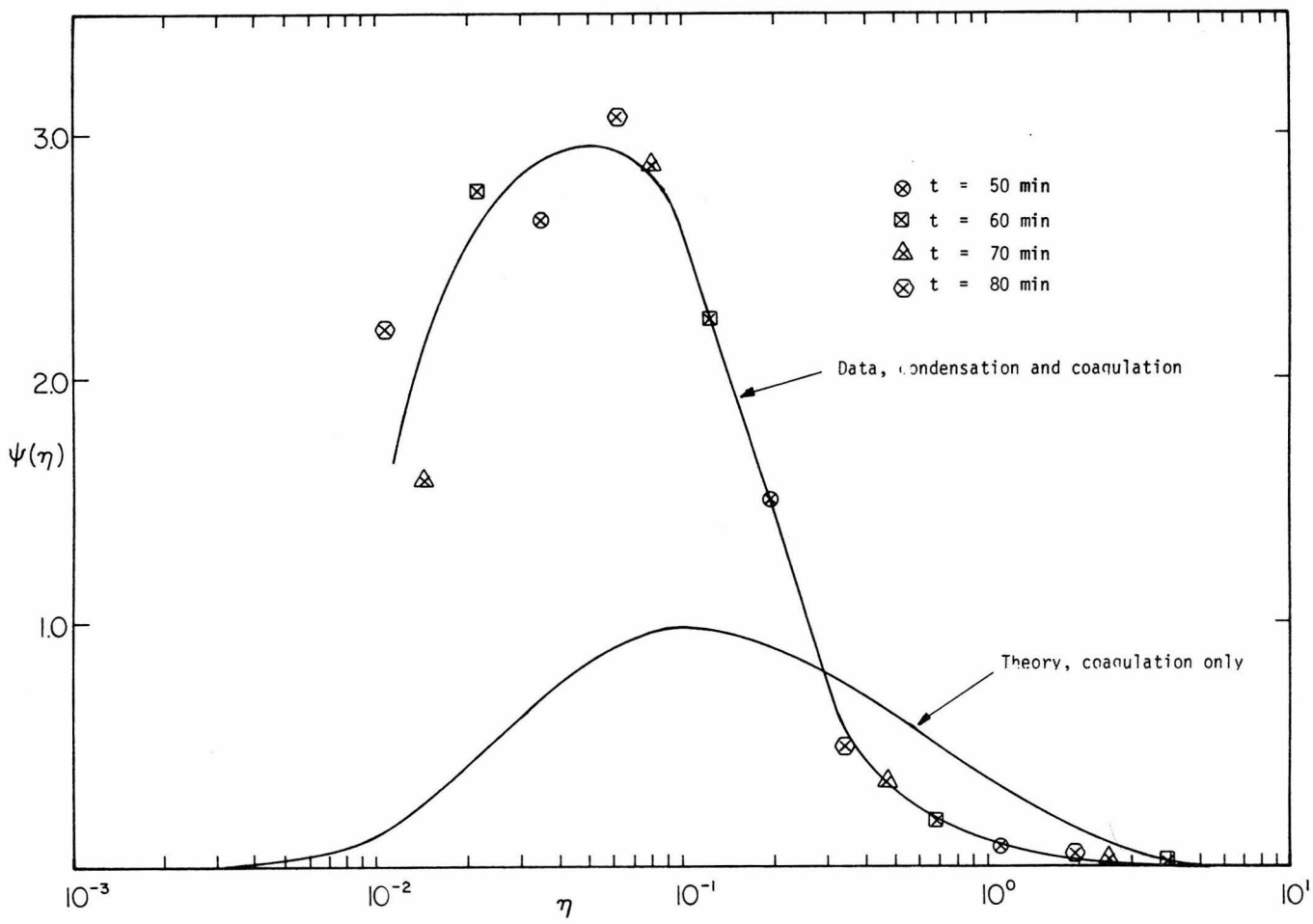

FIGURE 3.2

The dimensionless self-preserving size distribution $\psi(\eta)$, is shown as a function of dimensionless particle volume, η, for four aerosol size distributions during one experiment (experiment P22). Aerosol formation took place at the rate of 25.4 $\mu m^3/cm^3$/hour during the measurements. The self-preserving size distribution for free-molecule aerosols evolving only by coagulation (Lai, et al. 1972) is shown for comparison.

Figure 3.3 shows experimental results of Clark (1972), Husar and Whitby (1973), Kocmond, et al. (1975) and McNelis (1974), as well as some data by the author for surface areas as a function of rate of aerosol formation. Husar and Whitby (1973) also reported a range of values for the rate at which aerosol volume, measured at a point in Los Angeles, was observed to increase, along with the range of aerosol surface areas for corresponding times. These data are also presented in Figure 3.3. On the same graph is plotted the self-preserving surface area, Equation (3.14) where time was taken to be one hour in accordance with experimental results.

From Figure 3.3 it is clear that agreement between experiment and theory for the aerosol surface area generated by a given rate of aerosol formation is quite good for a variety of chemical systems. An exception is the cyclohexene + NO system where the experimental values are considerably less than those predicted by theory. With this system the maximum total number of particles formed generally ranges from 10^3 to 10^4 per $cm.^3$ Aerosol concentrations generated by other chemical systems typically are 10 to 1000 times larger. As a result the assumption that $N(t) << N(o)$ is comparatively poor for the cyclohexene system. Also, since the number of particles generated by the cyclohexene, NO system for a given rate of aerosol formation is small, the particles grow out of the free molecule regime more quickly than particles in systems with higher concentrations, thus invalidating the assumption of free molecule aerosol dynamics.

Data reported by Husar and Whitby (1973) for the Pasadena aerosol fall near the theoretical line indicating that surface areas of ambient

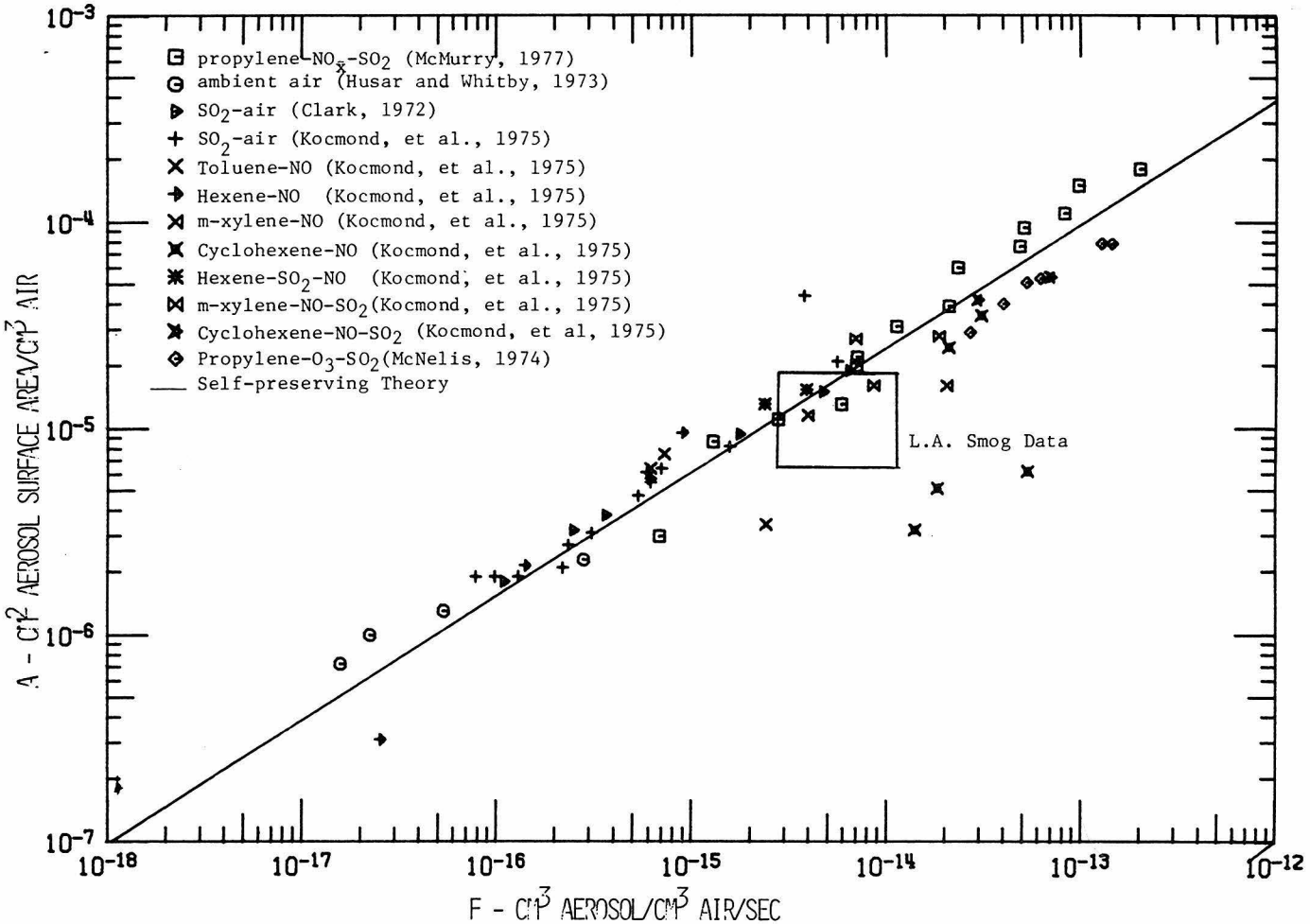

FIGURE 3.3

Comparison of experimental aerosol surface areas for a given rate of aerosol formation, F, with the surface areas predicted by self-preserving theory. A time of one hour was chosen for the theoretical line in accordance with laboratory time scales required to achieve constant surface areas. The range of values for Los Angeles smog was reported by Husar and Whitby (1973).

aerosols may be regulated by gas-to-particle conversion. However, this is not a firm conclusion since the measurements were made at a fixed point (Eulerian framework); both transport and gas-to-particle conversion affect the time rate of change of aerosol volume measured at a point in ambient air. It is necessary to distinguish between these two effects to obtain a true value for ambient aerosol formation rates.

Iron oxide aerosols have been generated by the irradiation of air containing $Fe(CO)_5$ vapor (Jander and Winkel, 1933; Whytlaw-Gray, Cawood, and Patterson, 1936). Under proper conditions, the theory developed in this chapter should also be applicable to the generation of such aerosols with controlled surface areas.

3.7 Summary

Several investigators have reported that constant aerosol surface areas per volume of gas are established when aerosols are generated by chemical reaction at a constant mass rate. A simple relationship between these surface areas and the rate of gas-to-particle conversion has been observed over a wide range of aerosol formation rates. In this chapter, a theory has been developed which explains these observations.

Aerosols simultaneously evolving by coagulation and gas-to-particle conversion establish self-preserving size distributions during the later stages of aerosol growth. For the special case of constant aerosol production rates, F, the theory predicts that self-preserving aerosol surface areas vary as $F^{3/5}t^{1/5}$, and are essentially independent of the chemical composition of the new secondary aerosol. The dependence of the

self-preserving surface area on F is in very good agreement with experimental data for aerosol formation rates varying from 10^{-17} to 2×10^{-13} cm^3 aerosol/cm^3 air/sec. The weak dependence of surface area on time, t, is consistent with the nearly constant observed surface areas. The magnitude of predicted surface areas is also in good agreement with data.

Data for aerosol formation rates and aerosol surface areas for the Los Angeles atmosphere are consistent with the theoretical prediction. This indicates that aerosol surface area in ambient air may be regulated by the rate of secondary aerosol formation. The results may also have application to the generation of metallic aerosols of controlled (and predictable) surface area by the irradiation of gases containing metallic carbonyls.

CHAPTER 4

NEW PARTICLE FORMATION IN THE PRESENCE OF A PREEXISTING AEROSOL

Condensable molecules generated in the gas phase by chemical reaction can either form new particles or condense on surrounding aerosol. A new theory which predicts the rate at which new particles of a given size are formed in such systems is presented. Scavenging of molecular clusters by surrounding aerosol is important, and is taken into account in the theory. Theoretical predictions are compared with experimentally observed rates for particle formation by photochemical reactions in the SO_2-NO_x-propylene system; agreement between theory and experiment is fair. During the later stages of aerosol development when the self-preserving surface area has been established (Chapter 3), predicted rates of homogeneous nucleation are small.

4.1 Introduction

Formation of secondary aerosols in the atmosphere can take place by a number of different mechanisms. Chemical reactions within droplets or on their surfaces can convert gas phase material to aerosols. It is also possible for homogeneous gas phase reactions to produce condensable products which eventually accumulate in the aerosol. The mechanism of gas-to-particle conversion probably varies with the nature of the aerosol precursor as well as with ambient conditions.

The mechanisms of gas-to-particle conversion are instrumental in determining the chemical and physical nature of an evolving secondary aerosol. Condensable products of homogeneous gas phase reactions, for example, tend to accumulate in smaller particle sizes than equal volumes of secondary aerosol formed by solution phase reactions (see, e.g. Appendix C). Health (Amdur, 1971) and visibility (White, 1976) effects of particulate pollution are linked to the chemical composition of the aerosol with respect to size. Studies of secondary aerosol formation, therefore, are useful in gaining insight into the effects of source control strategies on problems associated with pollutant aerosols.

Condensable products of homogeneous gas phase reactions can combine with other condensable molecules to form new particles or condense on preexisting particles (heterogeneous condensation). A pictorial representation of the problem is given in Figure 4.1. The relative importance of each mechanism depends on the thermodynamic properties of the condensing molecules, the rate at which they are being produced, and the amount of aerosol available for them to condense on. Species with low vapor pressures and high surface tensions such as sulfuric acid or many solid products are more likely to undergo homogeneous nucleation than substances with weaker molecular attractions. The evidence for new particle formation by homogeneous nucleation in ambient air is reviewed in Chapter 2.

A number of investigators (Clark, 1972; Husar and Whitby, 1973; McNelis, 1974; Kocmond, et al., 1975) have studied the formation of condensation aerosols in systems initially free of particles for a variety of chemical species. Goetz and Pueschel (1965) studied the effect of

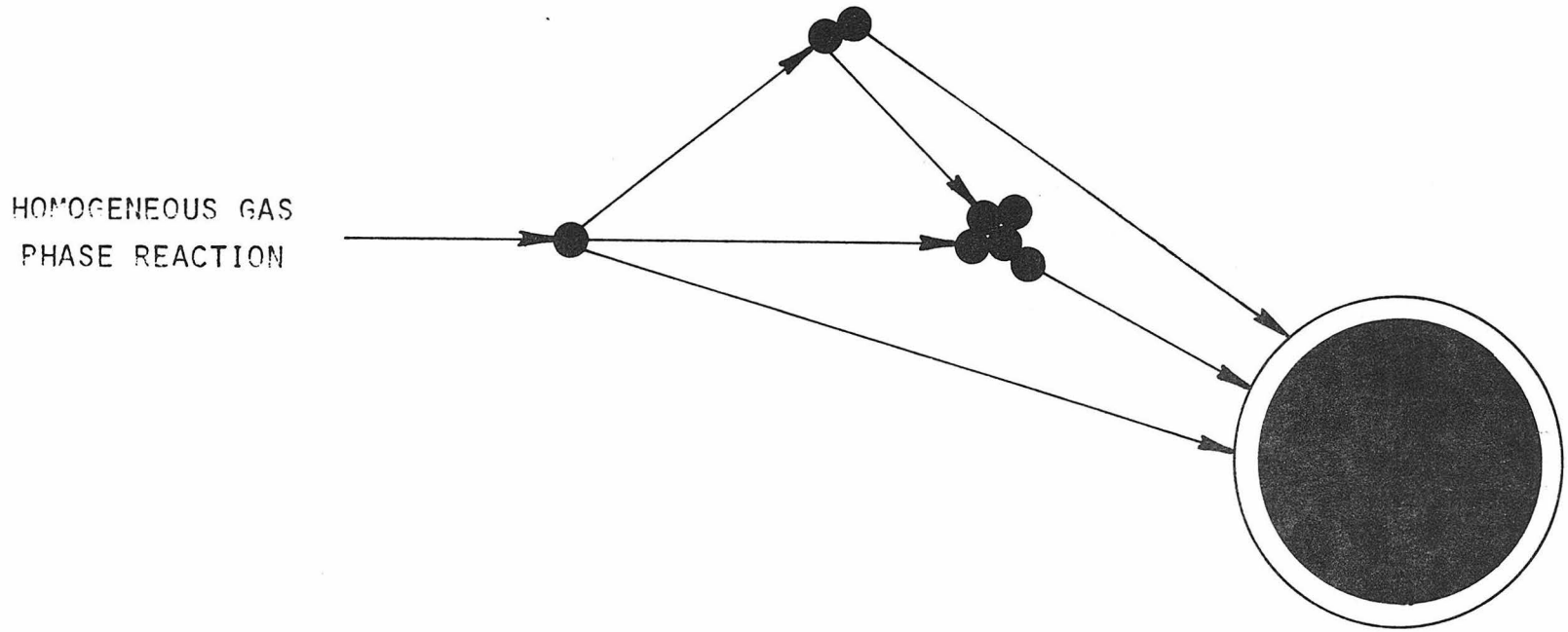

FIGURE 4.1

A pictorial representation of aerosol formation when homogeneous nucleation and heterogeneous condensation are occurring simultaneously. Condensable molecules (monomer) produced by a gas phase reaction can either produce new particles or condense on larger preexisting particles.

polystyrene latex particles on photochemical aerosol formation in the 1-octene-NO_2 system and found that the rate of aerosol formation was proportional to the concentration of preexisting particles. It was concluded that heterogeneous reactions dominate aerosol formation processes for this system; this has not been confirmed by other investigators. Heisler and Friedlander (1976) studied the growth of preexisting aerosols in the presence of reacting organic precursors in unfiltered ambient air and concluded the results were consistent with diffusional growth when the increased vapor pressure above smaller particles due to curvature was accounted for. Walter (1973) computed numerical solutions to the coagulation equation assuming a source of particles at a constant rate and size, as might be formed by gas phase reactions. He concluded that observed aerosol distributions in clean air where rates of gas-to-particle conversion are slow, are consistent with his results. His calculations also showed that the size distribution of new particles approached a steady state; the time required to reach steady state concentrations depended on the amount of preexisting aerosol. Husar and Whitby (1973) hypothesized that sufficient aerosol was present in ambient air to prevent homogeneous nucleation.

Urone and Schroeder (1969), Bufalini (1971), Calvert (1974), and Sander and Seinfeld (1976) have reviewed work on SO_2 photooxidation. The mechanisms of SO_2 photooxidation are not well understood for many chemical systems. It is known that the presence of an olefin speeds up SO_2 photooxidation, and Cox and Penkett (1972) found these high rates consistent with oxidation of SO_2 by a short lived intermediate of the

ozone-olefin reaction. It is generally conceded, however, that whatever the mechanism, SO_2 is oxidized to SO_3. Castleman, et al. (1975) have shown that SO_3 combines quickly with H_2O to form H_2SO_4 molecules. These findings are consistent with the work of Endow, et al. (1963) who found H_2SO_4 was the only important aerosol product formed by photochemical reactions of SO_2, NO_x and propylene.

The objective of this study has been to investigate experimentally and theoretically a system in which new particle formation and heterogeneous condensation occur simultaneously. Experiments were performed in unfiltered or partially filtered ambient air, and condensable material was produced by photochemical reactions in the SO_2-NO_x-propylene system. The details of the mechanism of SO_2 photooxidation were not considered. SO_2 concentrations were continuously measured as a function of time. It was assumed that SO_2 lost from the gas phase was immediately converted to H_2SO_4 molecules which could either form new particles by homogeneous nucleation or condense on existing aerosol.

4.2 Experimental Apparatus

Experiments were carried out in Caltech's Air Quality Laboratory on the roof of Keck Laboratory in Pasadena. The smog chamber facility has previously been described by Roberts and Friedlander (1976b) and Heisler and Friedlander (1976), and is shown schematically in Figure 4.2. A 65 cubic meter reactor constructed of 2 mil FEP Teflon film was filled with either unfiltered or partially filtered ambient air and exposed to solar radiation. Teflon film was chosen for the reactor walls

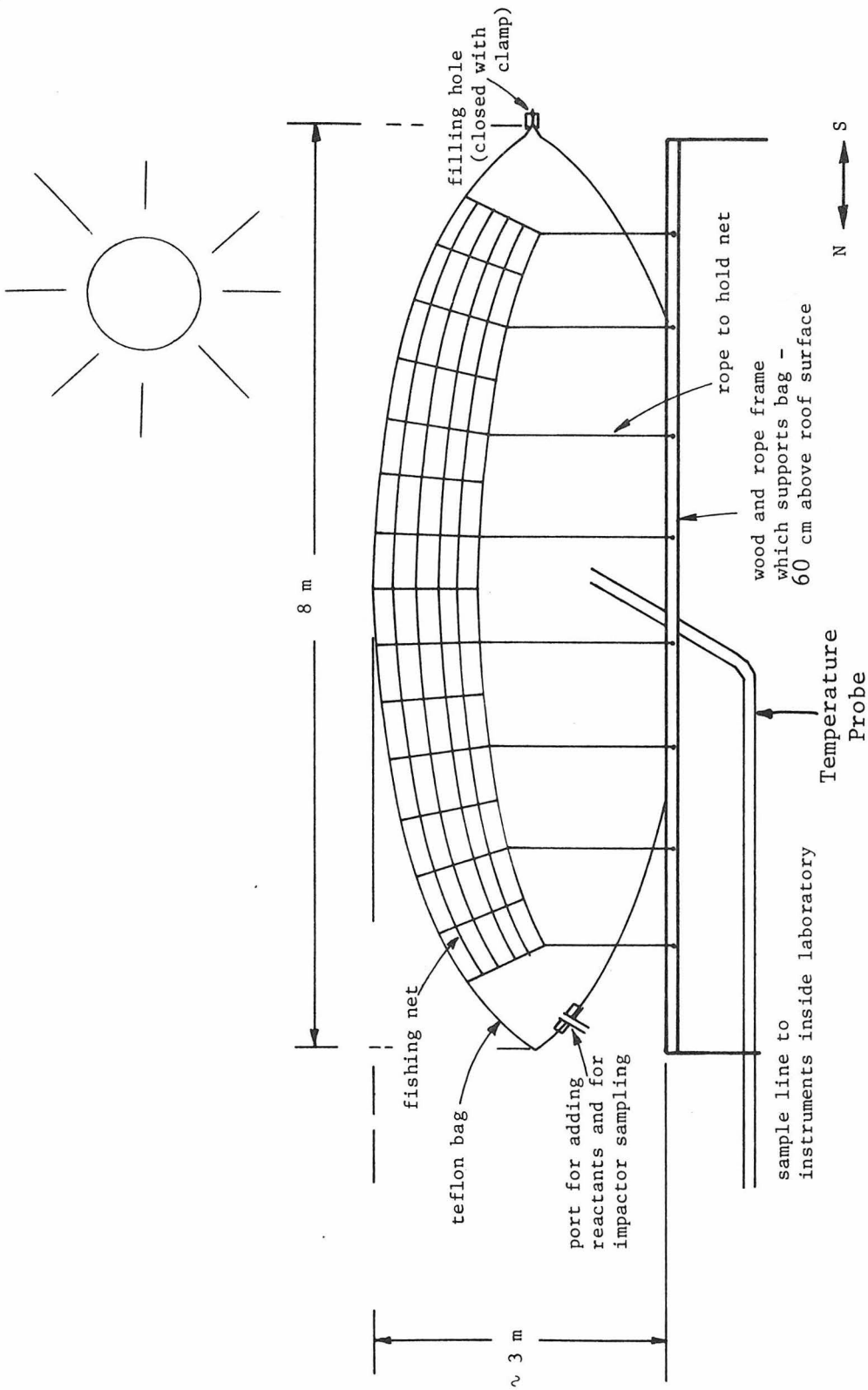

FIGURE 4.2

Diagram of a Smog Chamber

because it is reasonably transparent to ultraviolet radiation which is largely responsible for photochemical activity, and because it is relatively inert chemically (Dupont, 1966). The large volume of the reactor was necessary to provide adequate air to sample for the 2 to 3 hour duration of the experiments as well as to keep wall effects as small as was practicable.

Air from the reactor was continuously drawn through a flexible 6.1 meter TFE teflon sample line of 2.5 cm inside diameter to a sampling manifold inside the laboratory. The residence time in the sample line was approximately 6 seconds. Gas and aerosol phase instrumentation continuously sampled from the manifold. A summary of instrumentation and calibration procedures is provided in Table 4.1.

4.3 SO_2-NO_x-Propylene-Sunlight Experiments

4.3.1 Procedures

A series of experiments was carried out with the SO_2-NO_x-propylene-sunlight system. The teflon reactor was first filled with either unfiltered or partially filtered ambient air. The aerosol in the reactor was allowed to coagulate for approximately 30 to 60 minutes before the reactant gases were added. This delay permitted a more accurate measurement of the initial aerosol size distribution since particles with diameter less than 0.01 μm were lost by coagulation with larger particles. The response of the electrical aerosol analyzer (EAA) was felt to be unreliable below 0.01 μm.

TABLE 4.1

Instrumentation and Calibration Procedures

Measured Parameter	Instrument make, model, and measurement principle	Calibration method and frequency	Comments
SO_2	Meloy Labs Model SA 160-2, flame photometry	daily-electronic checks monthly-SO_2 permeation tube	stable between calibrations
O_3	Dasibi Model 1003-AH; UV absorption	not calibrated routinely	data used only as an indicator of photochemical activity
light scattering coefficient (b_{scat})	Meteorology Research Inc., Model 1550 Integrating Nephelometer	daily-electronic checks monthly-absolute calibration	
aerosol size distribution $0.01\mu m \leq d_p^{\dagger} \leq .32\mu m$	Thermo-Systems Model 3030 electrical aerosol analyzer (EAA)	use factory calibration	checked against recently calibrated instrument borrowed from the Univ. of Minnesota in Oct. 1976
aerosol size distribution $0.37\mu m \leq d_p^{\dagger} \leq 1.5\mu m$	Modified Climet Instruments Model CI-201-light scattering from single particles	daily-polystyrene latex spheres	see Husar, 1974 and Heisler, 1975 for discussion of modifications and calibrations
Temperature	YSI Tele-thermometer Model 43-TC, thermistor	Use factory calibration	
Relative Humidity	Hygrometrix, Inc. Model#8501-10 expansion of hygroscopic crystal	Use factory calibration checked with sling psychrometer	
Data Acquisition	Digital Equipment Corp. PDP 11/10 mini computer		

† d_p is particle diameter

The reactor was filled with one of two different fans. For unfiltered air a 23 cm diameter axial fan was used, and about 5 minutes were required to fill the reactor. For the partially filtered experiments, a centrifugal blower was used to force ambient air through a 20 cm diameter Gelman Type A glass fiber filter with a small hole in the center. Filling time in these experiments was about 30 minutes. The reactor was flushed with unfiltered ambient air twice between experiments to remove loosely bound gases or small pockets of high aerosol concentration.

Partial filtration of ambient air was found to be a sufficient perturbation to result in homogeneous nucleation. It was necessary to prevent homogeneous nucleation until after reactant gases were added in order to measure the initial aerosol size distribution and to have a definitive starting time for the initiation of gas-to-particle conversion. This was accomplished by covering the reactor with a black plastic sheet during the filling process and adding NO to consume ambient ozone as it entered the reactor. The reactor remained covered until after the reactant gases were added and had been allowed to mix uniformly throughout the reactor. Premature homogeneous nucleation of unfiltered ambient air was not a problem.

The reactant gases were added after a reliable measurement of the initial aerosol size distribution was made. Addition of NO while filling the reactor with partially filtered air was an exception to this procedure. The gases were blown through a teflon port in the side of the reactor by a centrifugal fan. The excess air carrying the reactant gases into the chamber was filtered and small in volume compared to the size of the reactor. An estimate of the time required for uniform mixing of these

reactant gases throughout the chamber was obtained by noting that fluctuations in SO_2 concentration were damped out about 15 minutes after adding the SO_2.

The quantity of each reactant gas added for a particular experiment was measured with a syringe. If the volume of the reactor were known exactly the initial concentration of each reactant could be computed. Because the reactor is collapsible, however, its volume varied approximately ± 20% about a mean of 49 cubic meters. Only SO_2 gas phase concentrations were measured. The initial reactor volume for each experiment was calculated by dividing the quantity of SO_2 added by the measured concentration. This calculated volume was used to estimate initial NO, NO_2, and propylene concentrations for each experiment. Initial conditions for the experiments discussed in this chapter are presented in Table 4.2.

Aerosol size distributions were measured at 10 minute intervals throughout the experiments; data analysis was done during the experiments by the data acquisition system. Ozone and the light scattering coefficient (b_{scat}) were monitored continuously with the data acquisition system, while temperature and SO_2 concentrations were recorded manually. The location of the temperature probe is shown in Figure 4.2. The temperature and relative humidity of ambient air were recorded while the reactor was being filled, and from this the water vapor content of the air was calculated. Relative humidity as a function of time during the experiments was calculated from the water vapor content and temperature of the air being withdrawn from the reactor.

TABLE 4.2

Initial Experimental Conditions[§]

Experiment	Date	Time(PDT)*	$[SO_2]_0$ (ppb)	$[Propylene]_0^{\dagger}$ (ppm)	$[NO]_0^{\dagger}$ (ppm)	$[NO_2]_0^{\dagger}$ (ppm)	Bag Volume[‡] (m^3)	Initial Aerosol Surface Area (cm^2/cm^3 Air)	Initial Aerosol Volume Fraction (cm^3/cm^3 Air)	Partially Filtered
P7	5.31.76	1200-1440	47.	0.9	0.31	0.15	69.	2.7×10^{-6}	8.9×10^{-12}	NO
P12	7.28.76	1415-1700	190.	1.2	0.39	0.19	55.	6.1×10^{-6}	1.4×10^{-11}	NO
P13	8.5.76	1330-1620	280.	1.2	0.39	0.19	54.	5.6×10^{-6}	1.2×10^{-11}	NO
P14	8.9.76	940-1225	360.	1.2	0.36	0.19	56.	5.0×10^{-6}	1.3×10^{-11}	NO
P15	8.9.76	1235-1545	420.	2.1	0.70	0.34	47.	5.5×10^{-6}	1.5×10^{-11}	NO
P16	8.11.76	958-1306	420.	2.5	0.55	0.27	60.	3.3×10^{-6}	1.0×10^{-11}	NO
P17	8.25.76	1345-1621	81.	1.0	0.42	0.21	49.	5.3×10^{-6}	1.3×10^{-11}	NO
P19	8.26.76	1430-1648	73.	0.54	0.36	0.18	56.	9.0×10^{-6}	2.7×10^{-11}	NO
P21	8.27.76	1300-1539	91.	0.93	0.47	0.23	43.	2.3×10^{-7}	3.7×10^{-12}	YES
P22	8.28.76	900-1240	67.	1.0	0.65	0.32	31.	5.7×10^{-6}	1.4×10^{-12}	YES
P23	8.28.76	1300-1628	43.	0.69	1.3	0.	29.	1.1×10^{-6}	2.4×10^{-12}	YES
P27	8.30.76	1205-1430	10.	u	u	u	u	2.6×10^{-6}	7.6×10^{-12}	NO
P28	8.31.76	835-1157	510.	1.5	0.51	0.26	39.	7.8×10^{-8}	1.1×10^{-13}	YES
P29	8.31.76	1225-1458	10.	u	u	u	u	3.8×10^{-6}	1.0×10^{-11}	NO

[§]Aerosol data is corrected for sample line losses as described in Appendix B.

*Starting time is time at which bag filling began.

[†]Based on bag volume and amount of reactant added. Ambient contributions are not included.

[u]Unknown

[‡]Calculated: Bag volume = amount of SO_2 added to reactant/initial SO_2 concentration.

Time profiles of aerosol number, surface area, and volume concentrations as well as of SO_2 and O_3 concentrations from experiment P23 are shown in Figure 4.3. These data are typical of the results of the other experiments, although the extent of new particle formation by homogeneous nucleation did vary depending on the initial aerosol loading and the rate of aerosol formation. In all cases, the decrease in SO_2 concentrations was small relative to the initial concentration. Results of all experiments reported in this chapter are summarized in Table 4.3.

4.3.2 Consistency of Data

The uncontrolled nature of the experiments and the uncertainties inherent in aerosol measurements made with the electrical aerosol analyzer required that extreme care be taken in interpreting the data. The dynamic behavior of an aerosol during gas-to-particle conversion depends both on the chemical and physical nature of the new aerosol and the mechanism of the conversion process. For each experiment it was necessary to ascertain whether aerosol formation was dominated by reactions of the SO_2-NO_x-propylene system; interference by other aerosol precursors present in the diluent air had to be minimized. SO_2 profiles and aerosol size distributions were measured during each experiment. Aerosol sulfur distributions were measured during several of the experiments. Consistency of the data was checked by comparing results of the three independent but related measurement.

Endow, et al. (1963) have shown that H_2SO_4 is the primary constituent of aerosols formed by the photochemical reaction of SO_2, NO_2, and propylene. The vapor pressure of H_2SO_4 at ambient humidities is negligible (Gmitro and Vermeulen, 1963), compared with the amount of H_2SO_4

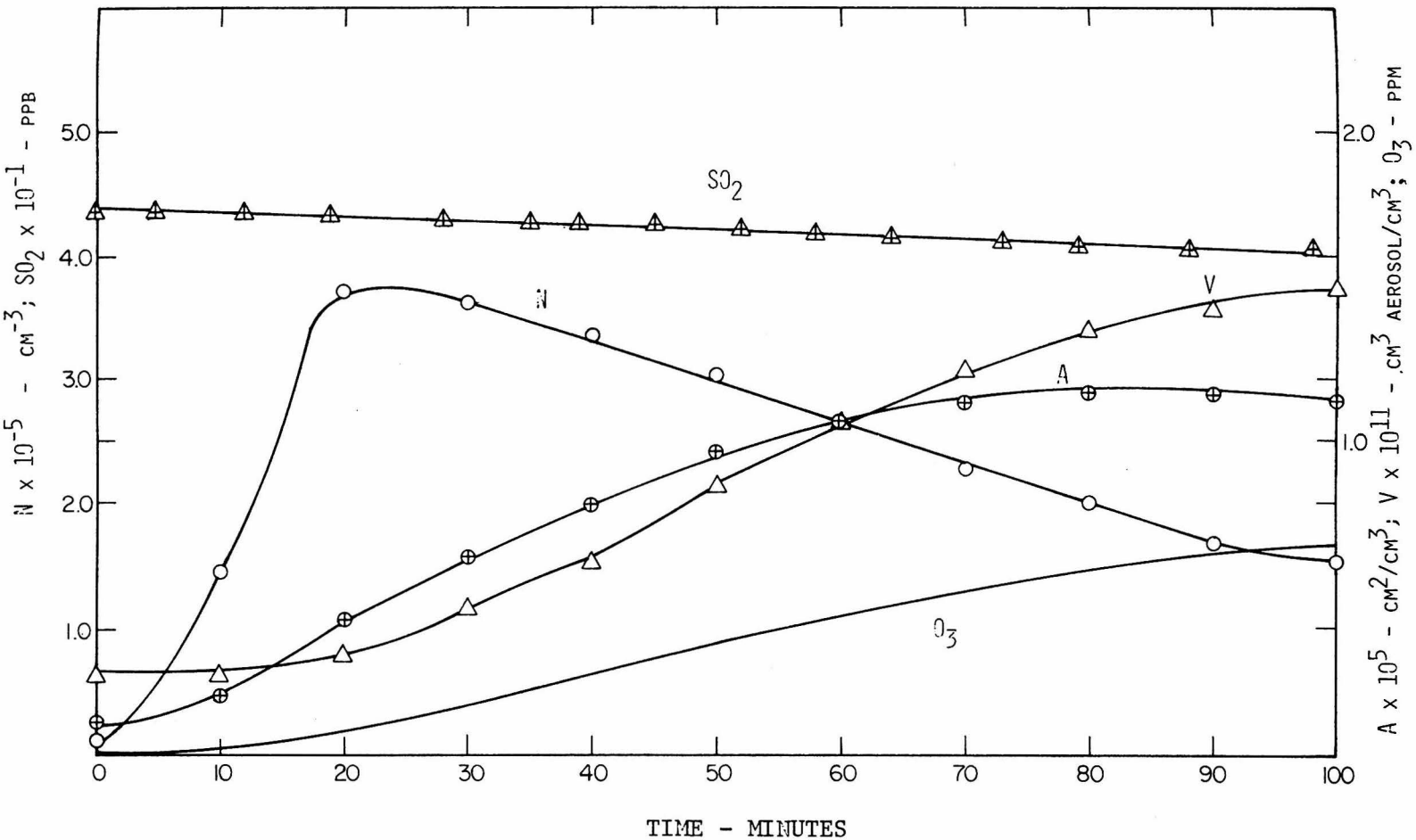

FIGURE 4.3

These data from experiment P23 are typical of results of all experiments reported in this chapter. Note that the rate of SO_2 decrease was fairly constant, and the decrease in SO_2 was small relative to the initial concentration. Aerosol volume fraction, V, increased throughout the experiment, while number concentration, N, reached a maximum early in the experiment and decreased continuously thereafter; the aerosol surface area, A, leveled off at a fairly constant value after about one hour. Gas-to-particle conversion started at about the same time that ozone concentrations started to increase.

TABLE 4.3

Summary of Experimental Results ǂ

Experiment	Relative Humidity Range(%)	Temp Range C°	$\frac{dV}{dt}$† ($cm^3/cm^3/sec$)	$\frac{dSO_2}{dt}$† (ppb/sec)	Initial Aerosol* Number Conc. (No/cm^3)	Maximum Aerosol* Number Conc. (No/cm^3)	Maximum O_3 (ppm)
P7	13-17	33-41	7.03×10^{-15}	-1.8×10^{-3}	2.4×10^{4}	2.8×10^{5}	1.36
P12	36-50	31-35	2.32×10^{-14}	-4.12×10^{-3}	6.2×10^{4}	7.5×10^{6}	1.00
P13	30-39	32-36	5.03×10^{-14}	-8.87×10^{-3}	4.3×10^{4}	1.0×10^{5}	1.00
P14	32-35	30-38	4.82×10^{-14}	-1.05×10^{-2}	4.0×10^{4}	9.9×10^{6}	1.03
P15	20-22	37-38	9.68×10^{-14}	-2.13×10^{-2}	3.2×10^{4}	1.1×10^{5}	1.14
P16	25-26	38-40	2.00×10^{-13}	-4.19×10^{-2}	2.8×10^{4}	9.2×10^{5}	1.20
P17	34-36	36-27	1.12×10^{-14}	-2.93×10^{-3}	4.4×10^{4}	5.5×10^{5}	1.05
P19	39-47	37-38	U	-9.52×10^{-4}	5.1×10^{4}	2.4×10^{5}	0.43
P21	29-35	35-28	2.08×10^{-14}	-4.30×10^{-3}	2.9×10^{3}	8.7×10^{5}	1.10
P22	29-26	38-42	7.07×10^{-15}	-1.85×10^{-3}	6.7×10^{4}	6.2×10^{5}	1.12
P23	28-37	40-46	2.77×10^{-15}	-7.33×10^{-4}	1.1×10^{4}	3.7×10^{4}	0.69
P27	27-36	44-49	U	-1.20×10^{-4}	2.2×10^{4}	9.4×10^{6}	0.67
P28	24-28	39-41	8.18×10^{-14}	-2.45×10^{-2}	4.4×10^{3}	1.1×10^{5}	1.25
P29	29-31	42-43	1.28×10^{-15}	-2.97×10^{-4}	3.8×10^{4}	2.8×10^{5}	1.31

ǂ Aerosol data is corrected for sample line losses as described in Appendix B.

† Least squares rates of change, dV/dt and dSO_2/dt were calculated for the same 30 to 60 minute portion of the experiment during which slopes were maximum. Aerosol volume was corrected for wall losses, as described in Appendix B.

* Based on size distribution data from electrical aerosol analyzer and optical particle counter

U Unknown; aerosol growth rate was small in comparison to rate of aerosol losses on reactor walls.

produced after several seconds of reaction for production rates reported in this thesis. By assuming that each sulfur-containing molecule lost from the gas phase became H_2SO_4 aerosol in equilibrium with the ambient relative humidity one can calculate the expected increase in aerosol volume. After correcting aerosol measurement for wall losses and sample line losses as described in Appendix B, the observed increase in aerosol volume as measured by the electrical aerosol analyzer and optical particle counter was, on the average, 6% (± 18%) greater than the expected increase. Experiments for which the expected increase differed from the measured increase by more than 35% were discarded.

The assumption that the new aerosol could be accounted for by SO_2 loss was given additional support by measurements of the aerosol sulfur distribution for several experiments. Samples were collected by means of a single jet low pressure impactor (Hering, Flagan, and Friedlander, 1977), and analyzed by the aerosol volatilization technique discussed by Roberts and Friedlander (1976a). The total increase of aerosol sulfur after the reaction had proceeded for about one hour was typically within 20% of the decrease in gas phase sulfur. Furthermore, the shape of the aerosol sulfur size distribution measured with the impactor agreed well with the shape of the aerosol size distribution. If the aerosol sulfur was assumed to be H_2SO_4 in equilibrium with ambient humidity, the impactor and size distribution data also agreed reasonably well in magnitude (Figure 4.4).

The electrical aerosol analyzer was not calibrated on a routine basis since no means of producing calibration aerosols of known size and concentration was available. It was found that monodisperse polystyrene latex particles with diameters of 0.088 μm were sized correctly by the analyzer.

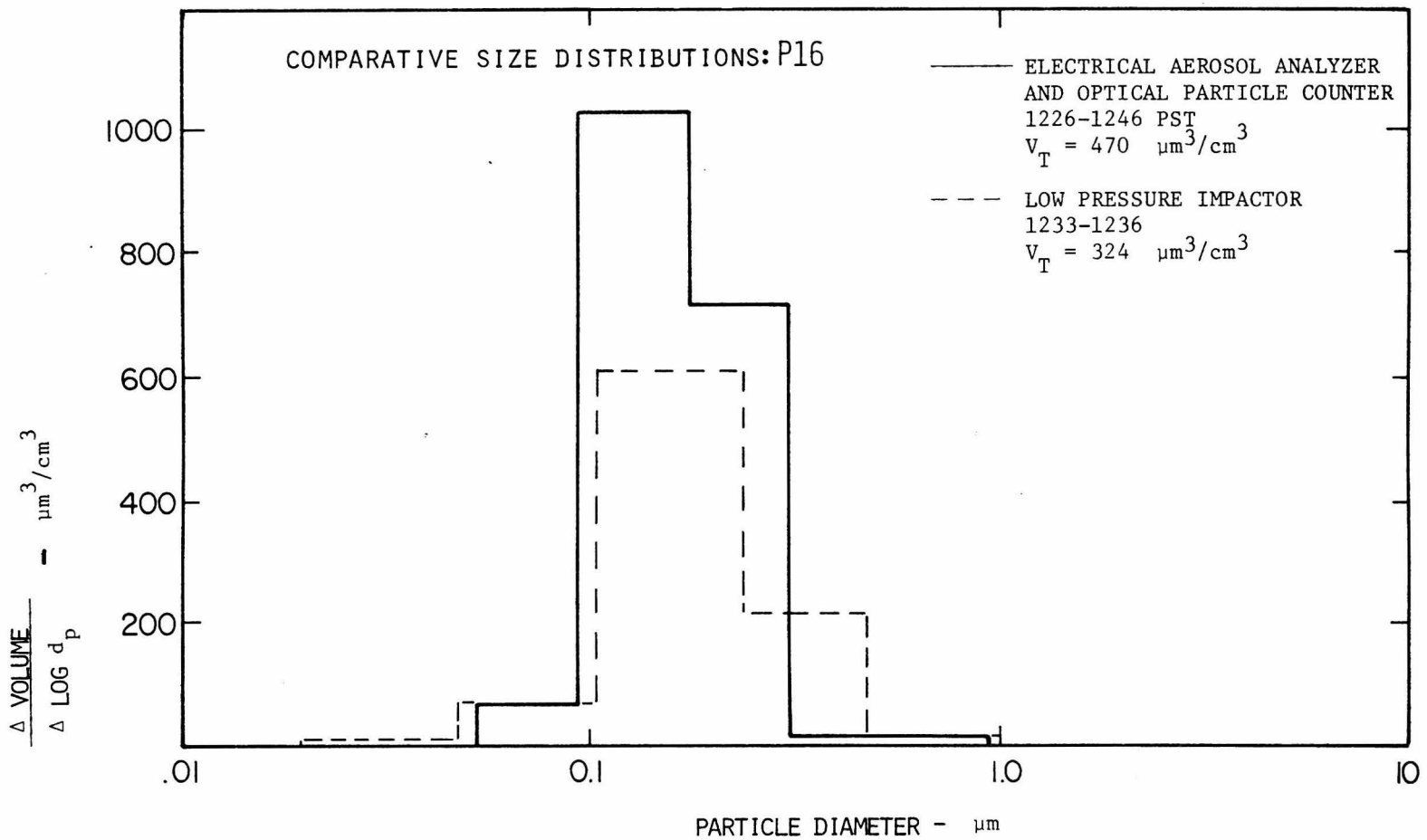

FIGURE 4.4

A comparison of the aerosol size distribution measured by the electrical aerosol analyzer and optical particle counter and the aerosol sulfur distribution measured by the low pressure cascade impactor for experiment P16. The assumption was made that the aerosol sulfur was in the form of sulfuric acid in equilibrium with ambient humidity.

Also, after completing the experiments reported in this chapter, measurements with the instrument used in this study agreed well with those from a new electrical aerosol analyzer which had recently been calibrated. The consistency of measurements made with the electrical aerosol analyzer, SO_2 detector, and low pressure cascade impactor give additional support for the data from the electrical aerosol analyzer. Most of the analysis presented in this chapter are based on integral moments of the aerosol size distributions which are less sensitive to instrumental error than the distribution itself. A conservative estimate for the maximum error for these measurements is ± 40%.

All aerosol data presented in this chapter have been corrected for sample line losses as discussed in Appendix B. All experimental data are included in Appendix D.

4.4 The Dynamics of New Particle Formation

If systems containing aerosol precursors such as SO_2 are irradiated, formation of new particles is often observed. Particle concentrations typically climb to a maximum after timescales of 10-60 minutes, and then decrease continually since coagulation exceeds the rate at which new particles are formed.

If condensable molecules are produced by chemical reaction in the gas phase, the rate at which new particles of a given size are formed depends on the rate at which the molecules are produced and the amount of aerosol available for them to condense on. These effects are shown qualitatively in Figures 4.5 and 4.6. In Figure 4.5, the total aerosol number concentration larger than 0.01 μm as a function of time is shown for experiments with different initial aerosol loadings; the SO_2 oxidation rate in each case was about the same. Note that the effect of increasing the initial aerosol loading for a fixed rate of SO_2 oxidation

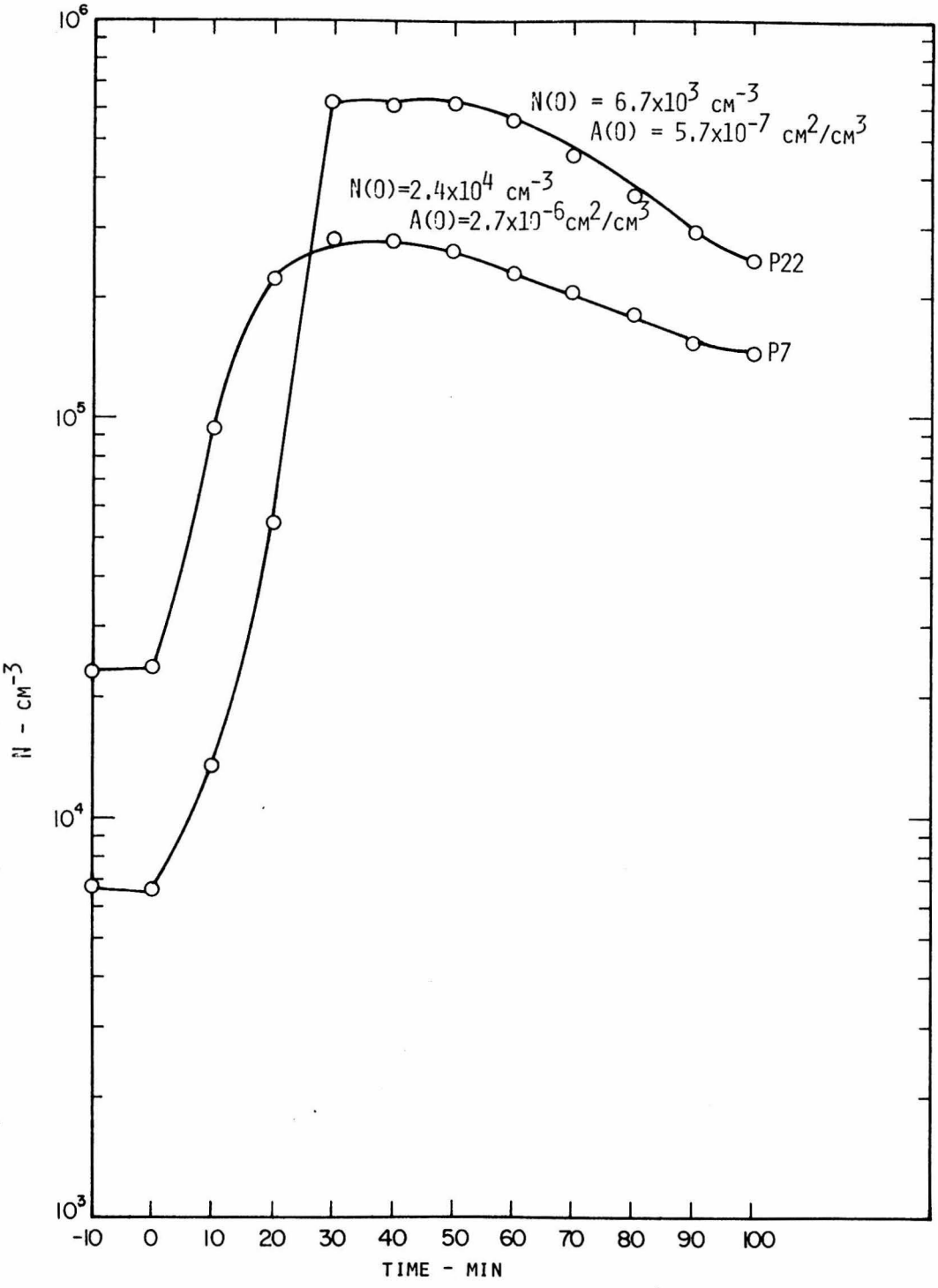

FIGURE 4.5

Aerosol number concentrations measured by the electrical aerosol analyzer as a function of time for experiments with similar rates of SO_2 oxidation ($1.8x10^{-3}$ ppb/sec) but different initial aerosol loadings. The initial aerosol number concentrations, N(0), and surface area concentrations, A(0), are shown. Gas-to-particle conversion started at time zero. Note that the effect of increasing the initial aerosol concentration is to suppress new particle formation.

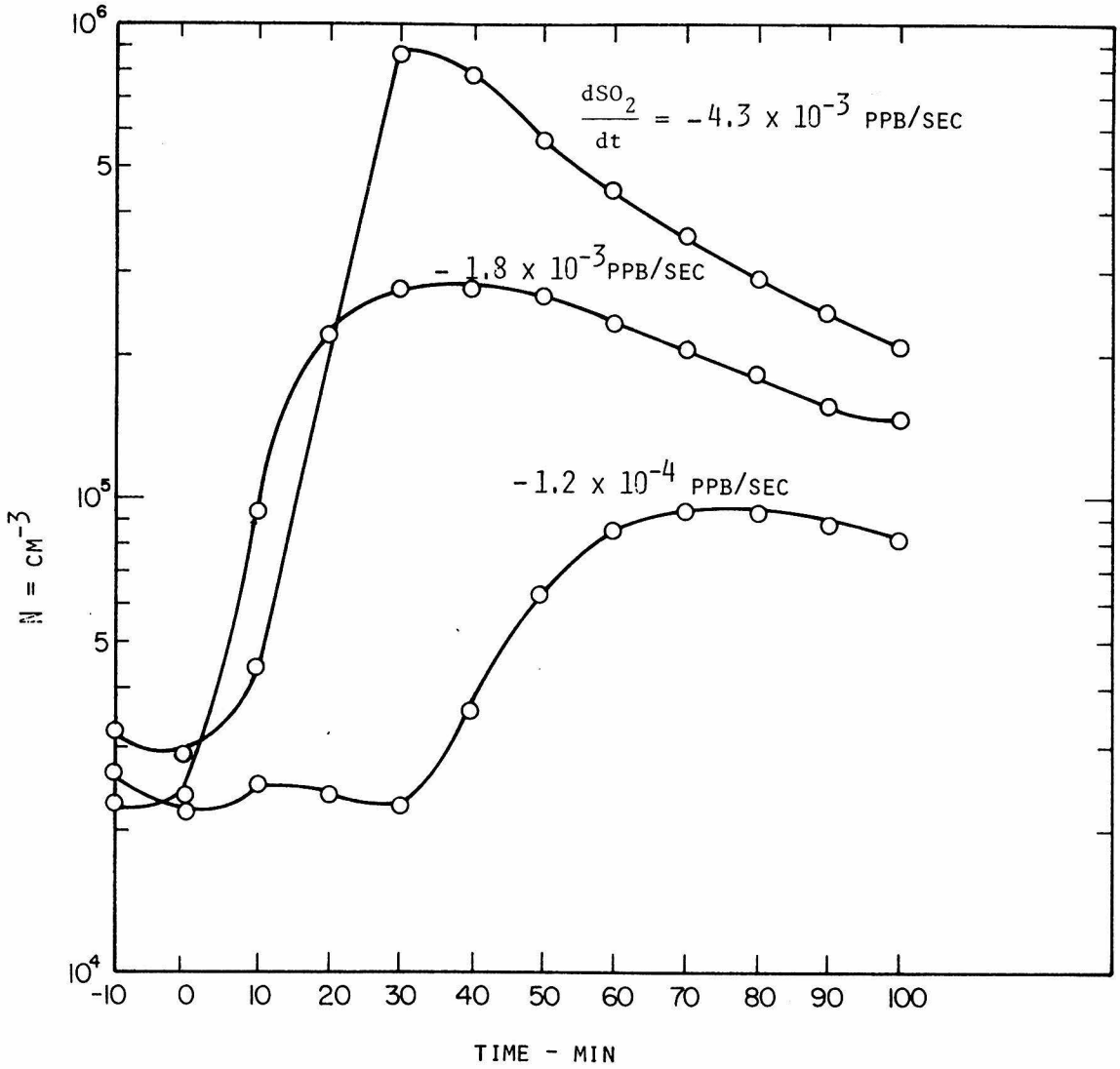

FIGURE 4.6

Aerosol number concentration as a function of time for experiments with similar initial aerosol loadings but different rates of SO_2 oxidation. Gas-to-particle conversion started at time zero. The initial aerosol number and surface area concentrations were about 2.5×10^4 cm^{-3} and 2.5×10^{-6} cm^2/cm^3 air respectively. Note that the effect of increasing SO_2 oxidation rates is to increase the number of particles formed.

is to suppress new particle formation. In Figure 4.6, aerosol number concentration as a function of time is shown for experiments with similar initial aerosol loadings but different rates of SO_2 oxidation. Note that the effect of increasing the rate of SO_2 photooxidation is to increase the number of new particles formed by homogeneous nucleation.

An analysis is presented in the following sections which leads to an expression for the rate at which new particles of a given size are formed for given rates of production of condensable molecules and aerosol loadings. Growth of molecular clusters by condensation and scavenging of clusters by surrounding aerosol are considered; reevaporation from and coagulation of clusters are assumed to be slow compared with condensation and scavenging. All collisions between condensable molecules and other condensable molecules or molecular clusters are assumed to be effective. This is analogous to the approaches of Ulrich (1971) for modeling the growth of silica aerosols formed by the combustion of silicon tetrachloride in hydrogen and air, and George, et al. (1973) for the development of titanium dioxide aerosols formed by high temperature oxidation of titanium tetrachloride. This approach is different from that of previous investigators (e.g. Middleton and Kiang, 1977), who have used the classical theory of homogeneous nucleation to calculate the rate at which stable clusters are formed. In the classical theory, scavenging of clusters smaller than those of the smallest stable size is ignored, and predicted rates of particle formation are likely to be too high for systems with preexisting aerosols. The classical theory does, however, account for evaporation from molecular clusters; this effect is ignored in the following sections.

4.4.1 Monomer Balance Equation

For sufficiently high concentrations of condensable molecules, rates of molecular collisions with clusters formed by homogeneous nuclea-

tion or with surrounding aerosol will greatly exceed rates of reevaporation. The theory which is developed below applies when concentrations of condensable molecules are large compared with the equilibrium vapor pressure over tiny molecular clusters, so that reevaporation can be neglected.

If condensable molecules (monomer) are being produced by gas phase chemical reaction at a rate R, the balance between monomer production and loss can be expressed as

$$\frac{dN_1}{dt} = R - \beta_{11}N_1^2 - \sum_{j=2}^{k-1} \beta_{1j}N_jN_1 - \alpha 2\pi DIN_1 \qquad (4.1)$$

where

N_1 = monomer concentration

N_j = concentration of molecular clusters formed by homogeneous nucleation which contain j monomer (i.e. of size j)

α = collision efficiency (assumed = 1)

I = diffusion integral of surrounding aerosol (defined below)

The collision frequency function, β_{ij}, for rates of coagulation between particles small compared to the mean free path of the surrounding gases is

$$\beta_{i,j} = \left(\frac{3}{4\pi}\right)^{1/6}\left(\frac{6kT}{\rho}\right)^{1/2}\left(\frac{1}{v_i} + \frac{1}{v_j}\right)^{1/2}\left(v_i^{1/3} + v_j^{1/3}\right)^2 \qquad (4.2)$$

This expression is derived from the kinetic theory of billiard ball gases. In keeping with the assumption that reevaporation is unimportant, the vapor pressure of the condensing species has been assumed small compared to monomer concentrations of interest. The second term on the right side of (4.1) is the rate at which monomer collide with themselves, and the third term the rate at which they collide with molecular clusters formed by homogeneous nucleation. The fourth term on the right side of (4.1) is the rate at which monomer are lost by condensation on particles larger than clusters of size k-1.

The diffusion integral, I, for rates of transport of condensing vapors to aerosols in the transition regime is (Sahni, 1966, Fuchs and Sutugin, 1971)

$$I = \int_{kv_1}^{\infty} d_p \left(\frac{1 + Kn}{1 + 1.71\ Kn + 1.33\ Kn^2} \right) n(v,t)dv \qquad (4.3)$$

where $Kn = \frac{2\lambda}{d_p}$ = Knudsen number

d_p = particle diameter

λ = effective mean free path of diffusing species

This expression has been verified experimentally for evaporation rates of transition regime particles by Chang and Davis (1976). For condensation on free molecule aerosols, I is proportional to aerosol surface area per unit volume of air, while for aerosols in the continuum regime, I is proportional to the 1/3 moment of the distribution function.

The deposition rate (molecules/cm^3 air/time), Q, of monomer on an average Los Angeles aerosol (Whitby, et al., 1972) was calculated from the expression

$$Q = 2\pi DIN_1 \qquad (4.4)$$

where I is the transition regime diffusion integral given in Equation (4.3). The effective mean free path of the diffusing molecules was based on the formula given by Jeans (1925) when evaluating Knudsen numbers. This deposition rate was compared with the rate for the same aerosol calculated from the expression

$$Q = \left(\frac{kT}{2\pi\rho v_1} \right)^{1/2} A\ N_1 \qquad (4.5)$$

where A is the aerosol surface area per volume of gas, ρ is the particle density, and v_1 the molecular volume of the condensing molecules.

Equation 4.5 represents the collision rate of molecules with an aerosol consisting of particles much smaller than the effective mean free path of the condensing molecules, and is derived from the kinetic theory of spherical molecules. The fluxes for the two calculations agreed to within 10% for unit density monomer with molecular weights between 20 and 200. Assuming therefore, that (4.5) can be substituted for (4.4) in Equation (4.1) we obtain

$$\frac{dN_1}{dt} = R - \beta_{1,1} N_1^2 - \sum_{j=2}^{k-1} \beta_{1,j} N_1 N_j - \gamma A N_1 \tag{4.6}$$

where

$$\gamma = \sqrt{\frac{kT}{2\pi\rho v_1}} \tag{4.7}$$

For typical ambient aerosol loadings, steady state monomer concentrations are established on a timescale of minutes. At steady state,

$$R = \beta_{1,1} N_1^2 + \sum_{j=2}^{k-1} \beta_{1,j} N_1 N_j + \gamma A N_1 \tag{4.8}$$

Dividing (4.8) by R and expressing cluster concentrations in terms of the characteristic concentration $\frac{\gamma A}{\beta_{1,1}}$, we obtain

$$1 = L \tilde{N}_1^2 + L \sum_{j=2}^{k-1} c_i \tilde{N}_1 \tilde{N}_j + L\tilde{N}_1 \tag{4.9}$$

where

$$L = \frac{\gamma^2 A^2}{\beta_{1,1} R} = \frac{1}{16\sqrt{3}\,\pi} \left(\frac{4\pi}{3}\right)^{1/6} \frac{(kT)^{1/2} A^2}{v_1^{7/6} \rho^{1/2} R} \tag{4.10}$$

$$C_j = \beta_{1,j}/\beta_{1,1} = \frac{1}{4\sqrt{2}} \left(1 + \frac{1}{j}\right)^{1/2} (1 + j^{1/3})^2 \tag{4.11}$$

and

$$\tilde{N}_i = \frac{\beta_{1,1}}{\gamma A} N_i \tag{4.12}$$

Note that $v_j = jv_1$.

Solving equation (4.9) for L gives

$$L = \frac{1}{\tilde{N}_1^2 + \tilde{N}_1 + \sum_{j=2}^{k-1} c_i \tilde{N}_1 \tilde{N}_j} \tag{4.13}$$

The parameter L is proportional to the ratio of the rate at which condensable molecules collide with the aerosol surface area, A, to the rate at which they collide with themselves. Rates of new particle formation should increase as L decreases.

4.4.2 Cluster Balance Equations

In the following analysis it is assumed that monomer concentrations are sufficiently high such that reevaporation from clusters is slow compared to condensational growth or scavenging by surrounding aerosol, but that cluster concentrations are low enough such that coagulation between clusters is unimportant. With these assumptions, a balance between production and removal rates for clusters of size j is

$$\frac{dN_j}{dt} = \beta_{1,j-1} N_1 N_{j-1} - \beta_{1,j} N_1 N_j - \frac{\gamma A}{\sqrt{j}} N_j \tag{4.14}$$

The coefficients γ and $\beta_{i,j}$ were defined above. Substituting (4.10), (4.11), and (4.12) and dividing through by RL, the dimensionless form of (4.14) at steady state is

$$0 = c_{j-1} \tilde{N}_{j-1} \tilde{N}_1 - c_j \tilde{N}_j \tilde{N}_1 - \frac{\tilde{N}_j}{\sqrt{j}} \tag{4.15}$$

The dimensionless cluster distribution can be obtained in terms of the dimensionless monomer concentration by noting that

$$\frac{\tilde{N}_j}{\tilde{N}_{j-1}} = \frac{c_{j-1}\,\tilde{N}_1}{c_j\tilde{N}_1 + \frac{1}{\sqrt{j}}} \tag{4.16}$$

Multiplying successive terms of this form together, we obtain

$$\frac{\tilde{N}_j}{\tilde{N}_1} = \frac{\tilde{N}_j}{\tilde{N}_{j-1}}\,\frac{\tilde{N}_{j-1}}{\tilde{N}_{j-2}} \cdots \frac{\tilde{N}_2}{\tilde{N}_1} = \prod_{i=2}^{j} \frac{c_{i-1}\tilde{N}_1}{c_i\tilde{N}_1 + \frac{1}{\sqrt{i}}} \tag{4.17}$$

The dimensionless cluster distribution depends only on the value of the monomer concentration, $\tilde{N}_1$. Substituting (4.17) in (4.13) for cluster concentrations, a relationship between the dimensionless variable, L, and the dimensionless monomer concentration, $\tilde{N}_1$ is obtained. The relationship between L and $\tilde{N}_1$ can be determined by choosing values of $\tilde{N}_1$ and computing corresponding values of L. The upper limit on the summation should correspond to the largest cluster size not included in the aerosol surface area, A.

4.4.3 Rates of Particle Formation

The rate per volume of gas at which particles of size k are formed by condensation on particles of size k-1 is

$$G(k) = \beta_{1,k-1}\, N_1\, N_{k-1} \tag{4.18}$$

Substituting (4.10), (4.11), and (4.12) this can be expressed in dimensionless form as

$$\frac{G(k,L)}{R} = c_{k-1}\, L\, \tilde{N}_{k-1}\, \tilde{N}_1 \tag{4.19}$$

The dimensionless cluster concentration, $\tilde{N}_{k-1}$, depends only on $\tilde{N}_1$, which in turn depends only on L. Therefore, G/R is a function only of L for a fixed value of k. This relationship can be computed with Equations (4.13) and (4.17), and is shown in Figure 4.7 for several values of k. For small values of L, the rate of monomer production $R \rightarrow kG(k)$. This is equivalent to saying that all monomer which is produced condenses on clusters of size k or smaller; rates of scavenging of monomer or clusters by preexisting aerosol is negligible compared with rates of condensational growth. In this limit, quasi-steady state cluster distributions do not exist since larger clusters are continuously being produced. Therefore, for $L \lesssim 10^{-2}$, a time dependent theory must be used to predict particle formation rates.

From Figure 4.7 it can be seen that for large values of L, the rate of particle formation is a very strong function of L. L is proportional to the ratio A^2/R (see Equation 4.10); therefore a definitive test of the theory requires accurate measurements of R and A.

In Figure 4.8 the calculated rate of particle formation as a function of particle size is shown; the rate of monomer production, R, was set equal to 1.43×10^7 cm^{-3} sec^{-1}, and the aerosol surface area, A, was 5×10^{-6} cm^2/cm^3 air. Aerosol density and monomer volume were set equal to 1.46 g/cm^3 and 2.1×10^{-22} cm^3 respectively, values corresponding to sulfuric acid aerosol at 30% relative humidity. Note that the predicted rate of particle formation is a strong function of particle size. An experimental test of the theory requires that the minimum size detected experimentally be well characterized. Figure 4.8

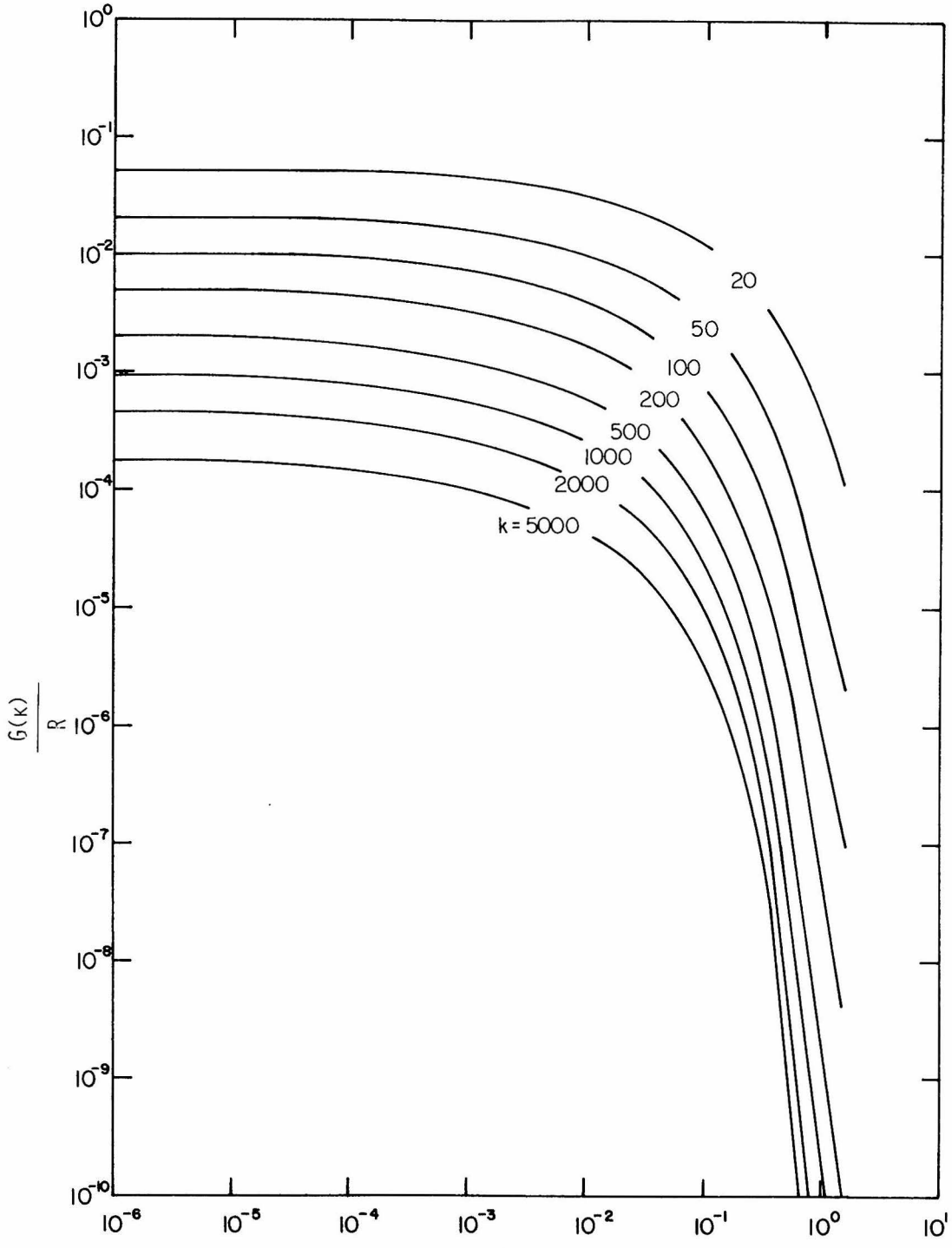

FIGURE 4.7

Rate of formation of particles containing k monomer, G(k), normalized with respect to the rate of monomer production, R, as a function of the parameter, L. For small values of L, the rate of formation of the monomer, R, approaches kG(k) since rates of scavenging of monomer or clusters by preexisting aerosol are negligible compared with rates of condensational growth. In this limit, a time dependent theory must be used to predict particle formation rates.

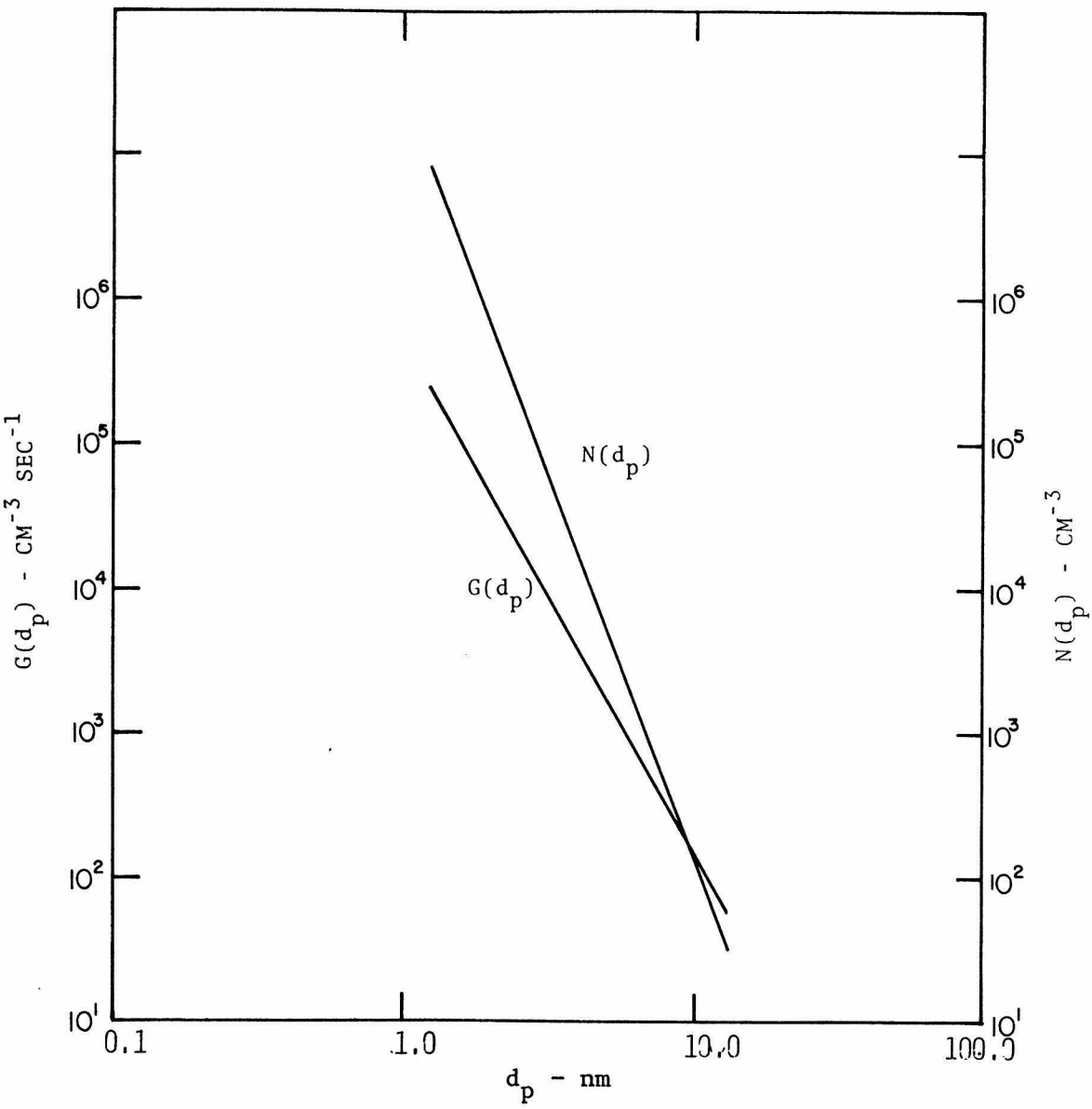

FIGURE 4.8

The rate of formation of particles as a function of particle size for $R = 1.43 \times 10^7$ cm^{-3} sec^{-1} and $A = 5 \times 10^{-6}$ cm^2 aerosol surface area/cm^3 air. The monomer volume was taken to be 2.1×10^{-22} cm^3 and aerosol density was 1.46 g/cm^3, values characteristic of H_2SO_4 at 30% relative humidity. Temperature was fixed at 300°K. Steady state cluster concentrations, $N(d_p)$, as a function of particle size for the same conditions are also shown. The calculated value of the monomer concentration was 6.25×10^7 cm^{-3}, and the volume fraction of clusters smaller than size 2500 was 10-12.

also shows the cluster distributions for these conditions, calculated from Equations 4.18 and 4.19.

4.5 Experimental Test of the Theory for Rates of Particle Formation

An attractive feature of the theory is that particle formation rates are obtained as a function of particle size. Rates of particle formation in aerosol systems are typically measured with instruments which measure particles larger than some minimum size. For the experiments reported in this thesis, for example, the electrical aerosol analyzer was used to detect particles with diameters larger than 0.01 μm corresponding roughly to k = 2500 for sulfuric acid droplets in equilibrium at ambient humidities. To compare experimental results with the theory, it is necessary to evaluate observed rates of particle formation as a function of the parameter L.

If v_{min} is the smallest particle size detected experimentally, the dynamic equation which describes the evolution of a measured aerosol distribution, n(v,t), assuming spatial homogeneity is (e.g. Friedlander, 1977)

$$\frac{\partial n}{\partial t} + \frac{\partial (n \frac{dv}{dt})}{\partial v} = G(\frac{v_{min}}{v_1}) \delta (v - v_{min}) + (\frac{\partial n}{\partial t})_{coagulation} \qquad (4.20)$$

where v_1 is the volume of condensable monomer. $(\frac{\partial n}{\partial t})_{coagulation}$ accounts for gain and loss of particles with volumes between v and v+dv by coagulation. The second term on the left side represents the change in the distribution due to growth by gas-to-particle conversion, and conceptually includes growth caused by monomer condensation and cluster scavenging. The product G times the Dirac delta function, $\delta(v-v_{min})$, specifies that there is a source of particles at the minimum detected size, v_{min}, which enter at a rate G.

Integrating from a volume infinitesimally smaller than v_{min} to infinity, we obtain

$$\frac{dN}{dt} = G_{experimental} + \frac{dN}{dt})_{coagulation} \tag{4.21}$$

The growth of preexisting aerosol by gas-to-particle conversion does not affect the total number concentration, and does not contribute to (4.21). The rate of homogeneous nucleation observed experimentally is

$$G_{experimental} = \frac{dN}{dt})_{observed} - \frac{dN}{dt})_{coagulation} \tag{4.22}$$

Aerosol size distributions were measured at 10 minute intervals throughout all experiments. The total number concentration was obtained by integrating over the distributions measured by the electrical aerosol analyzer and the optical particle counter. $dN/dt)_{observed}$ was calculated by dividing the change in number concentration between two consecutive size distributions by the time between measurements.

An estimate for coagulation rates of the aerosol larger than size k was made by using the expression for coagulation of a self-preserving free molecule aerosol derived by Lai, et al. (1972). They showed that

$$\frac{dN}{dt} = -\frac{\alpha_1}{2}\left(\frac{3}{4\pi}\right)^{1/6}\left(\frac{6kT}{\rho}\right)^{1/2} V^{1/6} N^{11/6} \tag{4.23}$$

where V is the aerosol volume fraction and α_1 a constant which is an integral over the dimensionless self-preserving distribution. For coagulating free molecule aerosols, $\alpha_1 = 6.67$; this should vary somewhat depending on the rate and mechanism of gas-to-particle conversion, since these factors alter the shape of the self-preserving distribution (Chapter 3). Equation 4.23 was used to calculate rates of coagulation for each of

the two consecutive distributions which were used to calculate $dN/dt)_{observed}$. $dN/dt)_{coagulation}$ was assumed to be given by the average of these rates.

The parameter L given by Equation (4.10) can also be evaluated from experimental data. The rate of monomer production, R, was assumed to be equal to the observed rate of decrease of gas phase sulfur molecules (Table 4.3). Sulfur molecules lost from the gas phase were assumed to be immediately available for condensation as molecules of $H_2SO_4 \cdot nH_2O$, where n is the ratio of H_2O to H_2SO_4 molecules in bulk solutions in equilibrium with surrounding relative humidities. Theory predicts that droplets smaller than 0.01 μm become enriched in H_2SO_4 relative to bulk solutions (Mirabel and Katz, 1974; Nair and Vohra, 1975); this effect has not been considered but should not significantly alter the results. From Table 4.3 it is seen that 30% is a representative value for the relative humidities in the experiments reported here. For the purpose of these calculations it was assumed that the monomer volume, v_1, was equal to 2.1×10^{-22} cm^3, its expected value at 30% relative humidity, for all experiments. Density was taken to be $1.46\ g/cm^3$ and temperature 300°K. L was calculated for each of the aerosol surface areas measured in the two successive size distributions which were used to evaluate $G_{experimental}$; these values were averaged to find corresponding values of $L_{experimental}$. Data used to calculate observed rates of particle formation is shown in Table 4.4.

In the experiments reported in this chapter, the rate of SO_2 consumption was not constant throughout the experiment. Rates increased from near zero early in the experiment to the fairly constant values

TABLE 4.4

Experimental Data Used to Calculate Rates of Particle Formation

Experiment	R[§] $cm^{-3}sec^{-1}$	Time Interval (min.)*	N[†] number/cm^3	A[†] cm^2/aerosol surface area/cm^3 air	V[†] cm^3 aerosol/ cm^3 air	$\left(\frac{dN}{dt}\right)^{\#}$ obser. number/cm^3/sec	$G_{experimental}$[#] number/cm^3/sec	$G_{theoretical}$ number/cm^3/sec
P7	3.99×10^{7}	10 - 20	9.4×10^{4}	3.3×10^{-6}	9.2×10^{-12}			
		20 - 30	2.2×10^{5}	6.0×10^{-6}	1.0×10^{-11}	210	270	2200
		30 - 40	2.8×10^{5}	9.2×10^{-6}	1.3×10^{-11}	97	230	320
P12	1.03×10^{8}	10 - 20	5.9×10^{5}	6.1×10^{-6}	1.6×10^{-11}			
		20 - 30	7.5×10^{5}	1.1×10^{-5}	2.4×10^{-11}	270	1200	35,000
P14	2.63×10^{8}	10 - 20	5.3×10^{4}	5.0×10^{-6}	1.3×10^{-11}			
		20 - 30	9.9×10^{5}	1.6×10^{-5}	1.7×10^{-11}	1700	2500	16,000
P15	5.32×10^{8}	10 - 20	1.6×10^{5}	6.3×10^{-6}	1.6×10^{-11}			
		20 - 30	1.1×10^{6}	3.6×10^{-5}	4.0×10^{-11}	1600	2800	27,000
P16	1.05×10^{9}	10 - 20	5.9×10^{5}	1.3×10^{-5}	2.0×10^{-11}			
		20 - 30	9.2×10^{5}	9.0×10^{-5}	1.3×10^{-10}	1400	2900	83,000
P17	7.34×10^{7}	10 - 20	5.1×10^{4}	5.3×10^{-6}	1.3×10^{-11}			
		20 - 30	4.1×10^{5}	9.0×10^{-6}	1.5×10^{-11}	600	770	37,000
		30 - 40	5.3×10^{5}	1.5×10^{-5}	1.9×10^{-11}	200	650	300
P19	2.38×10^{7}	10 - 20	9.9×10^{4}	8.7×10^{-6}	2.5×10^{-11}			
		20 - 30	1.7×10^{5}	9.3×10^{-6}	2.4×10^{-11}	130	180	1
		30 - 40	2.2×10^{5}	1.0×10^{-5}	2.3×10^{-11}	72	170	1
		40 - 50	2.4×10^{5}	1.1×10^{-5}	2.3×10^{-11}	33	160	1
P21	1.08×10^{8}	10 - 20	4.4×10^{4}	2.3×10^{-6}	3.4×10^{-12}			
		20 - 30	2.2×10^{5}	4.3×10^{-6}	4.3×10^{-12}	290	340	27,000
		30 - 40	8.7×10^{5}	1.5×10^{-5}	1.1×10^{-11}	1100	1800	14,000
P22	4.63×10^{7}	10 - 20	1.3×10^{4}	5.4×10^{-7}	1.2×10^{-12}			
		20 - 30	5.4×10^{5}	4.3×10^{-6}	2.2×10^{-12}	890	1100	3600
		30 - 40	6.1×10^{5}	8.0×10^{-6}	3.9×10^{-12}	100	590	2600
P23	1.83×10^{7}	10 - 20	1.5×10^{5}	1.9×10^{-6}	2.4×10^{-12}			
		20 - 30	3.7×10^{5}	4.3×10^{-6}	3.2×10^{-12}	380	500	2500
P27	3.01×10^{6}	30 - 40	2.2×10^{4}	1.7×10^{-6}	4.9×10^{-12}			
		40 - 50	3.5×10^{4}	2.2×10^{-6}	5.4×10^{-12}	22	25	45
		50 - 60	6.2×10^{4}	2.4×10^{-6}	5.2×10^{-12}	44	51	9
		60 - 70	8.6×10^{4}	2.6×10^{-6}	5.1×10^{-12}	40	52	30
		70 - 80	9.4×10^{4}	2.9×10^{-6}	5.1×10^{-12}	13	31	72
P28	6.12×10^{8}	20 - 30	3.5×10^{4}	4.2×10^{-7}	2.3×10^{-13}			
		30 - 40	1.1×10^{6}	1.7×10^{-5}	7.9×10^{-12}	1800	2800	290,000
P29	7.42×10^{6}	10 - 20	1.1×10^{5}	4.2×10^{-6}	9.6×10^{-12}			
		20 - 30	2.8×10^{5}	6.2×10^{-6}	1.0×10^{-11}	280	380	48

§ Rate of monomer production = rate of SO_2 decay

* Times shown are measured from the start of gas-to-particle conversion

† Aerosol data for particles larger than 0.01 μm; measured with the electrical aerosol analyzer and optical particle counter

Based on aerosol data shown on **preceding** and following lines

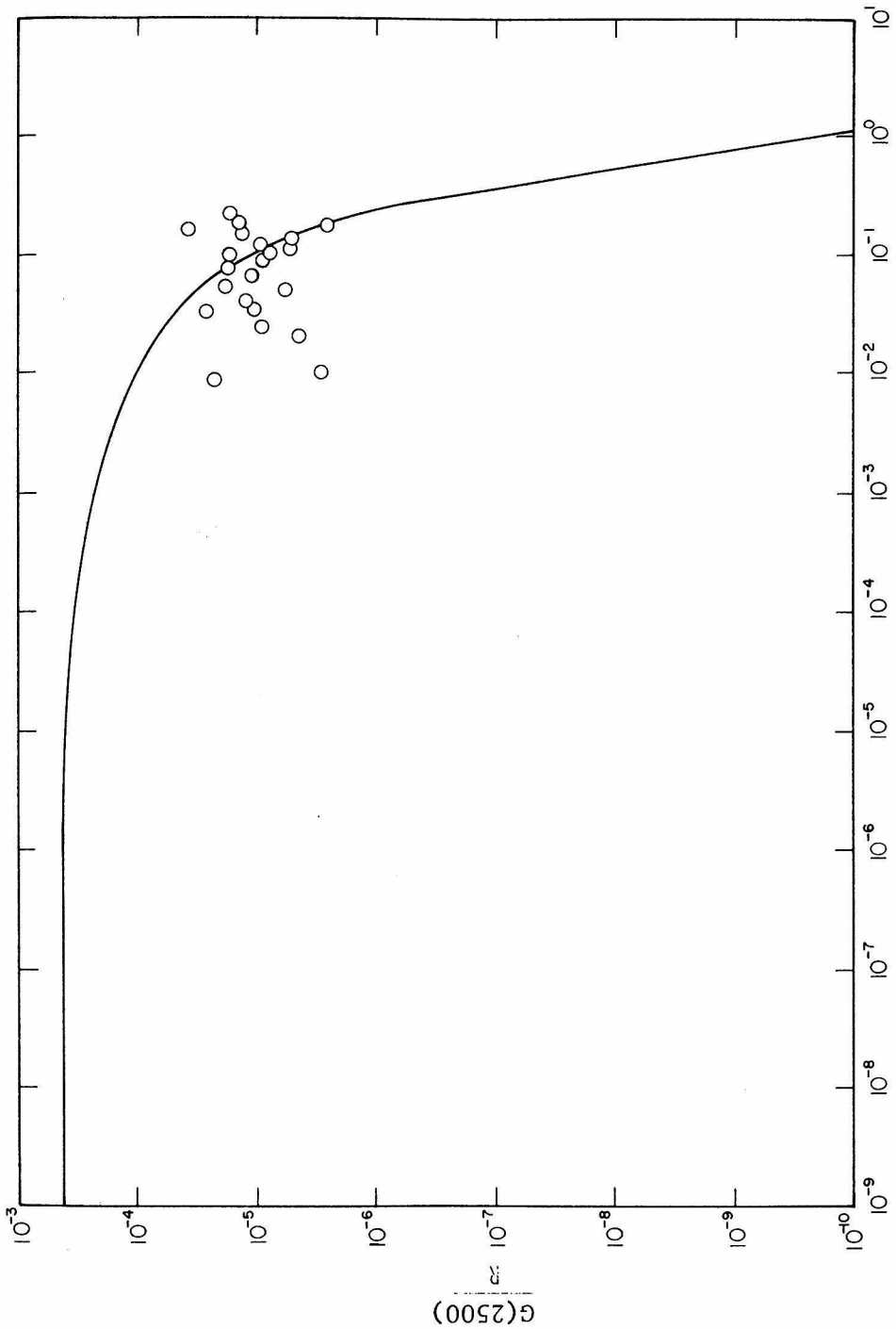

FIGURE 4.9

A comparison of predicted and measured rates of particle formation, normalized with respect to the rate of monomer production, R, as a function of the parameter L defined in Equation (4.10). The data were obtained for photochemically generated aerosols in the SO_2-NO_x-propylene system. The minimum size particle detected experimentally was 0.01 μm, corresponding to a particle containing 2500 sulfuric acid molecules at 30% relative humidity.

on L. For k = 2500, $\sum_{j=2}^{k-1} \tilde{N}_j/\tilde{N}_1 > 1$ for $L \leq 0.8$. All of the data reported fall in the range $L < 0.8$ for which cluster coagulation should have been important. The ratio $\sum_{j=2}^{k-1} \tilde{N}_j/\tilde{N}_1$ increases slowly as L decreases, however; the agreement between theory and experiment for values of L down to 0.1 may result because collisions between clusters are less frequent than collisions between a monomer and a cluster due to the higher mobilities of the monomer.

4.6 Predictions of the Theory of Binary Nucleation

The classical theory of homogeneous nucleation can be used to predict a critical concentration of condensable molecules below which homogeneous nucleation is unimportant. If the maximum expected monomer concentration is less than this critical concentration, homogeneous nucleation would not be expected.

In the absence of homogeneous nucleation, the monomer balance equation is

$$\frac{dN_1}{dt} = R - \alpha \gamma A(N_1 - N_{1\infty}) \tag{4.24}$$

where $N_{1\infty}$ is the H_2SO_4 vapor concentration in equilibrium with an aqueous sulfuric acid solution at ambient humidity (Gmitro and Vermeulen, 1963). Neglecting the Kelvin effect for particles larger than 0.01 μm in (4.24) should be a good assumption. The maximum expected monomer concentration is expected at steady state, and is given by

$$N_{1_{max}} = \frac{R}{\gamma A} + N_{1\infty} \tag{4.25}$$

where the accomodation coefficient, α, has been assumed equal to 1. These maximum concentrations have been compared to the critical concentrations required for nucleation rates of 1 cm^{-3} sec^{-1} in the H_2O-H_2SO_4 system which were reported by Kiang and Stauffer (1973) and Mirabel and Katz (1974). Homogeneous nucleation was predicted for all experiments according to the calculations of Kiang and Stauffer (1973) although it was expected only for experiments P16 and P28 according to Mirabel and Katz (1974). The primary difference between the two calculations is that the later investigators used more generally accepted thermodynamic properties for H_2SO_4 . It should also be emphasized that even though homogeneous nucleation is predicted to occur according to the classical theory, it will only be observed experimentally if these new stable particles grow to a detectable size before being scavenged by surrounding aerosol.

New particle formation resulting from homogeneous nucleation was observed in all experiments reported in this chapter indicating an inconsistency between experimental results and the predictions of Mirabel and Katz (1974). There are, however, uncertainties involved with applying such a test of the classical theory to the experiments reported here. If mixing was not complete at the start of gas-to-particle conversion, pockets of reactant gases high in concentration could have resulted in local high rates of monomer production resulting in homogeneous nucleation when it would not have been expected on the basis of average rates. The presence of trace amounts of other gases such as NH_3 would invalidate the assumption that H_2SO_4 and H_2O were the only species participating in the nucleation process. Also if the accomodation coefficient were significantly smaller than 1.0 in Eq. 4.24, monomer concentrations could have risen higher than was estimated here. These calculations serve to show the difficulty of applying the classical theory to atmospheric systems, however.

4.7 Scavenging Potential of the Self-Preserving Surface Area

In Chapter 3 the relationship between aerosol surface area and the rate of gas-to-particle conversion was investigated for the later stages of aerosol growth for photochemically generated aerosols. For a constant rate of aerosol formation, the relationship between aerosol surface area and the rate of aerosol formation was typically

$$A = 6.23 \times 10^{3} \; F^{3/5} \tag{4.26}$$

where time was taken to be 1 hour. The rate of aerosol formation can be expressed as

$$F = v_1 \, R \tag{4.27}$$

Substituting (4.26) and (4.27) in (4.10), the parameter L is

$$L \simeq 1.8 \times 10^{-2} \; R^{1/5} \tag{4.28}$$

where temperature = 300°K, $v_1 = 2.1 \times 10^{-22}$ cm^3, and $\rho = 1.46$ g/cm^3. Using Figure 4.7, the expected rate at which 0.01 μm particles are formed in the presence of a self-preserving aerosol is found to be less than 1.0 cm^{-3} sec^{-1} for rates of monomer production between 10^4 and 10^9 cm^{-3} sec^{-1}. This is small in comparison with coagulation rates typically expected for such systems, which can be estimated with Equation (4.23), and is consistent with the experimental observation that aerosol concentrations typically reach a maximum after timescales of 10 - 60 minutes, followed by a continual decrease in the total number concentration.

4.8 Summary and Conclusions

A new theory for predicting the rate at which new particles of an arbitrary size are formed as a result of homogeneous nucleation in chemically reacting systems has been presented. For quasi-steady state conditions, the rate of particle formation is shown to depend on a single parameter which can be calculated directly from experimental data; a

knowledge of aerosol surface area, the rate at which condensable molecules are formed and properties of the condensable molecules are required to evaluate this parameter. The theory applies when concentrations of condensing molecules are large compared to their saturation concentrations, so that condensation on clusters is fast compared to reevaporation. This eliminates the need of estimating the condensing species' thermodynamic properties, which are often not known. The theory is useful because formation rates are obtained as a function of particle size, and can be directly compared with experimental data.

Particle formation rates for photochemically generated aerosols in the SO_2-NO_x-propylene system have been compared with theoretical predictions. Agreement between predicted and observed rates is fairly good, but more carefully controlled experiments are required for a definitive comparison.

A substantial number of the particles in the earth's atmosphere are believed to have been generated by homogeneous nucleation resulting from gas phase reactions. This theory should be useful in estimating the rate at which such particles are formed for given rates of chemical reaction and aerosol loadings.

CHAPTER 5
SUMMARY AND RECOMMENDATIONS

This thesis discussed the behavior of aerosols generated by homogeneous gas phase reactions; the general features of aerosol dynamics observed in this study were qualitatively similar to those reported by previous investigators. Soon after the start of gas-to-particle conversion, the total aerosol number concentration often increases dramatically, reaching a maximum value after timescales of 10-60 minutes. After the aerosol number concentration begins to decrease, the aerosol surface area per volume of gas levels off at a nearly constant value even though the aerosol volume fraction continues to increase. New particle formation is not important during this later stage, and the aerosol number concentration decreases continuously since coagulation rates exceed the rates at which new particles are formed. The emphasis in this study has been to link the observed behavior of aerosol systems with the rate of gas-to-particle conversion. A new theory has been developed which predicts the rate at which new particles are formed for given rates of gas-to-particle conversion and aerosol loadings. An analytical expression relating the nearly constant aerosol surface area concentrations observed in the later stages of aerosol growth to rate of gas-to-particle conversion has also been presented.

The rate at which new particles of a given size are formed as a result of homogeneous nucleation of low vapor pressure substances formed by gas phase reactions was shown to be a known function of a single

parameter. This parameter can be calculated from experimental data and is proportional to A^2/R, where A is the aerosol surface area concentration which is contained in particles sufficiently large to be measured, and R the rate at which condensable molecules are being produced. This new theory for particle formation rates is based on the steady state balance equations for gain and loss of condensable molecules (monomer) and of clusters formed by collisions of condensable molecules. In the monomer balance equation, gain by chemical reaction and loss by collisions are considered; collisions include those with other monomer, with clusters formed by previous collisions and with aerosol surface area, A. In the cluster balance equations, gain and loss by condensation of monomer as well as scavenging by aerosol surface area, A, are considered. Collisions between clusters and reevaporation from clusters have been ignored.

Since the theory predicts particle formation rates as a function of particle size, predicted rates can be compared with experimental data for the rates at which particles of a known size are formed. In the experiments reported in this thesis, new particles were generated photochemically in the SO_2-NO_x-propylene system. A large (65 m^3) teflon reactor was filled with unfiltered or partially filtered ambient air and exposed to solar radiation. Aerosol size distributions, sulfur dioxide concentrations, and several other parameters were measured as functions of time. Agreement between observed and predicted rates of particle formation was fair. The theory tended to overpredict rates of particle formation.

The aerosol surface area per volume of gas typically reached a nearly constant value after about one hour of aerosol growth. After

this point, aerosol size distributions were found to be self-preserving; that is, when scaled according to the self-preserving transformation given by Equations (3.3) and (3.4), size distributions for the remainder of the experiment fell on a single curve. The shape of this dimensionless distribution was evidently a function of the rate of aerosol formation, but was independent of time for a fixed rate. Self-preserving size distribution theory was used to investigate the relationship between the rate of gas-to-particle conversion and the nearly constant surface areas observed experimentally during the later stages of aerosol growth. An analytical expression relating the aerosol surface area per volume of gas, A, to the rate of aerosol formation, dV/dt, and time, t, was obtained. It was shown that $A \sim (dV/dt)^{3/5} t^{1/5}$. Experimental data presented in this thesis as well as the data from a number of other investigators were compared with the self-preserving prediction for surface area. Both the magnitude and functional dependences of observed aerosol surface areas for chemically formed aerosols are in good agreement with the predictions of the theory for a variety of chemical systems. The aerosols formed by photochemically reacting NO_x and cyclohexene in air are an exception; considerably less aerosol surface area is produced than is predicted by the theory.

Rates of aerosol formation and aerosol surface area concentrations measured in ambient air appear to fall in the range predicted by self-preserving theory. If ambient aerosol surface area concentrations are indeed determined by the rate of gas-to-particle conversion rather than primary aerosol loadings, this result from self-preserving theory may have significant practical applications. In particular, it provides

a simple and key link between gas phase chemistry and aerosol dynamics. Adsorption of gaseous species and heterogeneous surface reactions on particles can be limited by available aerosol surface area. Transport of species to aerosols occurs at a rate nearly proportional to aerosol surface area for aerosols in urban air. Condensation and free-radical scavenging are examples of processes in which transport to particles is important.

New particle formation is a significant factor in the dynamics of chemically produced aerosols only soon after perturbations since aerosol systems eventually regulate themselves so as to stop the formation of detectable new particles. Examples of such perturbations are initiation of photochemical activity after sunup, and fresh input of aerosol precursors such as might occur near a source. On a global scale it appears that homogeneous nucleation may be an important source of atmospheric particles, although experiments reported in this thesis show that this is probably not the case for Los Angeles aerosols. Homogeneous nucleation is probably an important factor in shaping global aerosol size distributions even though formation of detectable new particles may only continue for short time periods. Subsequent growth of these abundant small particles by gas-to-particle conversion will cause secondary aerosol to accumulate in smaller average particle sizes than would be observed in the absence of new particle formation.

Recommendations

More work needs to be done on the new theory which was developed to predict rates of particle formation. The steady state assumption

should be investigated in more depth, and the theory should be generalized to include coagulation of and reevaporation from clusters. Experiments designed specifically to test the theory should also be carried out.

After further verification, the theory should be applied to model the time dependent behavior of an aerosol system during the early dynamic stages of aerosol behavior. It should be possible, for example, to predict the maximum number of particles generated for given initial conditions.

Solutions for the form of the self-preserving aerosol distribution growing by condensation and coagulation should be obtained. It would be worthwhile to find out how the rate of gas-to-particle conversion affects the shape of a self-preserving aerosol distribution. Solutions for the self-preserving distribution function would also enable one to rigorously evaluate the integral moments on which the self-preserving surface area depends.

REFERENCES

Aitken, J. 1911-1912. The sun as a fog producer. Proc. R. Soc. Edinburgh, 32: 32: 9-34.

Amdur, M.O. 1971. Aerosols formed by oxidation of sulfur dioxide - review of their toxicology. Arch. Environ. Health, 23: 459-468.

Bufalini, M. 1971. Oxidation of sulfur dioxide in polluted atmospheres-a review. Environ. Sci. Technol., 5: 685-700.

California, State of. 1972. Traffic volumes on California state highways. Business and Transportation Agency, Department of Public Works, Division of Highways.

Calvert, J.G. 1974. Modes of formation of the salts of sulfur and nitrogen in an NO_x-SO_2-hydrocarbon polluted atmosphere. Paper presented at the Conference of Atmospheric Salts and Gases of Sulfur and Nitrogen in Association with Photochemical Oxidant, University of California, Irivine, California (January).

Castleman, A.W., Davis, R.E., Munkelwitz, H.R., Tang, I.N., and Wood, W.P. 1975. Kinetics of association reactions pertaining to H_2SO_4 aerosol formation. Int. J. Chem. Kinet., Symp. No. 1: 629-640.

Chang, R. and Davis, E.J. 1976. Knudsen aerosol evaporation. J. Colloid Interface Sci. 54: 352-363.

Chu, R.R. and Orr, C. 1974. Particulate products from photochemical oxidation of organic vapors in the air. Paper #74-156, presented at the 67th annual meeting of the Air Pollution Control Association, Denver, Colorado, June 9-13.

Clark, W.E. 1972. Measurements of aerosols produced by the photochemical oxidation of SO_2 in air. Particle Laboratory Publication No. 181. University of Minnesota.

Cox, R.A. 1974. Particle formation from homogeneous reactions of sulfur dioxide and nitrogen dioxide. Tellus 26: 235-240.

Cox. R.A. and Penkett, S.A. 1972. Aerosol formation from sulfur dioxide in the presence of ozone and olefinic hydrocarbons. J. Chem. Soc., Faraday Trans. I, 68: 1735-1753.

Dupont. 1966. Technical information bulletins T-3E (chemical properties) and T-5A (optical properties) of teflon FEP hydrocarbon film.

Endow, N., Doyle, G.J. and Jones, J.L. 1963. The nature of some model photochemical aerosols. J. Air Pollut. Control Assoc. 13: 141-147.

Epstein, P.S. 1924. On the resistance experienced by spheres in their motion through gases. Phys. Rev. 23: 710-723.

Eskinazi, D. 1976. Unpublished data. California Institute of Technology.

Flagan, R.C. and Friedlander, S.K. 1976. Particle formation in pulverized coal combustion - a review. Presented at the Eighty-second national meeting of the American Institute of Chemical Engineers, Atlantic City, New Jersey, August 29- September 1.

Flyger, H., Heidam, N.Z., Hansen, K., Megaw, W.J., Walther, E.G., and Hogan, A.W. 1976. The background level of the summer tropospheric aerosol, sulfur dioxide, and ozone over Greenland and the North Atlantic Ocean. J. Aerosol Sci. 7: 103-140.

Friedlander, S.K. 1977. Smoke, Dust and Haze: Fundamentals of Aerosol Behavior. Wiley Interscience, New York.

Friedlander, S.K. and Wang, C.S. 1966. The self-preserving particle size distribution for coagulation by Brownian motion. J. Colloid Interface Sci. 22: 126-132.

Friend, J.P., Leifer, R., and Trichon, M. 1973. On the formation of stratospheric aerosols. J. Atmos. Sci. 30: 465-479.

Fuchs, N.A. and Sutugin, A.G. 1971. High-dispersed aerosols, in Topics in Current Aerosol Research, vol. 2, Ed. G.M. Hidy and J.R. Brock, Pergamon Press, Oxford.

George, A.P., Murley, R.D. and Place, E.R. 1973. Formation of TiO_2 aerosol. Faraday Symp. 7: 63-71.

Gmitro, J.I. and Vermeulen, T. 1963. University of California Lawrence Berkeley Radiation Laboratory. Contract No. W-7405-eng-48, Report No. UCRL-10886, TID 4500.

Goetz, A. and Pueschel, R.F. 1965. The effect of nucleating particles on photochemical aerosol formation. J. Air Pollut. Control Assoc. 15: 90-95.

Graedel, T.E., Farrow, L.A., and Weber, T.A. 1975. The influence of aerosols on the chemistry of the troposphere. Int. J. Chem. Kinet., Symp. No. 1: 581-594.

Graham, S.C. and Homer, J.B. 1973. Coagulation of molten lead aerosols. Faraday Symp. 7: 85-96.

Graham, S.C. and Robinson, A. 1976. A comparison of numerical solutions to the self-preserving size distribution for aerosol coagulation in the free molecule regime. J. Aerosol Sci. 7: 261-273.

Groblicki, P.J. and Nebel, G.J. 1971. The photochemical formation of aerosols in urban atmospheres, pp. 241-263. In C.S. Tuesday, Ed. Chemical Reactions in Urban Atmospheres. Proceedings of the symposium held at General Motors Research Laboratories, Warren, Michigan, 1969. New York: American Elsevier Publishing Co., Inc.

Grosjean, D. 1976. Chapter 3 in Ozone and Other Photochemical Oxidants, report to the National Academy of Sciences, Washington, D.C.

Heisler, S.L. 1975. Gas-to-Particle conversion in photochemical smog: growth laws and mechanisms for organics. Ph.D. Thesis, California Institute of Technology, Pasadena, California.

Heisler, S.L. and Friedlander, S.K. 1976. Gas-to-particle conversion in photochemical smog: growth laws and mechanisms for organics. Atmos. Environ. (in press).

Hering, S.V., Flagan, R.C., and Friedlander, S.K. 1977. A new low pressure impactor: determination of the size distribution of aerosol sulfur compounds. Paper presented at the American Chemical Society Conference, New Orleans, March 20-25.

Hogan, A.W. 1968. An experiment illustrating that gas conversion by solar radiation is a major influence in the diurnal variation of Aitken nucleus concentrations. Atmos. Environ. 2: 599-601.

Hogan, A.W. 1975. Antarctic aerosols. J. Appl. Meteorol. 14: 550-559

Husar, R.B. and Whitby, K.T. 1973. Growth mechanisms and size spectra of photochemical aerosols. Environ. Sci. Technol. 7: 241-247.

Husar, R.B., Whitby, K.T., and Liu, B.Y. H. 1972. Physical mechanisms governing the dynamics of Los Angeles smog aerosols. J. Colloid Interface Sci. 39: 211-224.

Husar, R.B. 1974. Recent developments in insitu size spectrum measurements of submicron aerosols. ASTM Special Publication 555.

Jander, V.G. and Winkel, A. 1933. Über aerosol in Sonderheit die das Eisenoxyds. Kolloid Z. 63: 5-12.

Jeans, J.H. 1925. The Dynamical Theory of Gases. Cambridge University Press.

Judeikis, H.S. and Siegel, S. 1973. Particle catalyzed oxidation of atmospheric pollutants. Atmos. Environ. 7: 619-631.

Kiang, C.S. and Stauffer, D. 1973. Chemical nucleation theory for various humidities and pollutants. Faraday Symposia of the Chemical Society, No. 7.

Kocmond, W. C., Kittelson, D.B., Yang, J.Y., and Demerjian, K.L. 1973. Determination of the formation mechanisms and composition of photochemical aerosols. Calspan Report No. NA5365-M-1, Calspan Corp. Buffalo, New York.

Kocmond, W.C., Kittelson, D.B., Yang, J.Y., and Demerjian, K.L. 1975. Study of aerosol formation in photochemical air pollution. EPA-650/3-75-007. Calspan Corporation.

Lai, F.S., Friedlander, S.K., Pich, J., and Hidy, G.M. 1972. The self-preserving particle size distribution for Brownian coagulation in the free-molecule regime. J. Colloid Interface Sci. 39: 395-405.

Liberti, A. 1970. The nature of particulate matter. Pure and Appl. Chem. 24: 631-642.

Lipeles, M., Burton, C.S., Wang, H.H., Parry, E.P., and Hidy, G.M. 1973. Mechanisms of formation and composition of photochemical aerosols. EPA-R3-73-036. Rockwell International Corporation, Thousand Oaks, California.

Liu, B.Y.H. and Pui, D.Y.H. 1973. A submictron aerosol standard and the primary, absolute calibration of the condensation nuclei counter. J. Colloid Interface Sci. 47: 155-171.

Liu, B.Y.H. and Pui, D.Y.H. 1975. On the performance of the electrical aerosol analyzer. J. Aerosol Sci. 6: 249-264.

Liu, B.Y.H., Whitby, K.T., and Pui, D.Y.H. 1974. A portable electrical analyzer for the size distribution measurement of submicron aerosols. J. Air Pollut. Control Assoc. 24: 1067-1072.

Lopez, A., Servant, J. et Fontan. 1974. Methodes de mesure de l'intensite des sources de noyaus d'Aitken dans l'atmosphere. Atmos. Environ. 8: 733-754.

McNelis, D.N. 1974. Aerosol formation from gas-phase reactions of ozone and olefin in the presence of sulfur dioxide. EPA-650/4-74-034.

Middleton, P. and Kiang, C.S. 1977. A kinetic aerosol model for the formation and growth of secondary sulfuric acid particles. Submitted to J. Aerosol Sci., March 1977.

Mirabel, P. and Katz, J.L. 1974. Binary homogeneous nucleation as a mechanism for the formation of aerosols. J. Chem. Phys. 60: 1138-1144.

Mulcahy, M.F.R. and Young, B.C. 1975. Heterogeneous reactions of OH radicals. Int. J. Chem. Kinet. Symp. No. 1: 595-609.

Nair, P.V.N. and Vohra, K.G. 1975. Growth of aqueous sulfuric acid droplets as a function of relative humidity. J. Aerosol Sci. 6: 265-271.

Novakov, T., Chang, C.S., and Harker, A.B. 1974. Sulfates as pollution particles: catalytic formation on carbon (soot) particles. Science 186: 259-261.

Pich, J., Friedlander, S.K., and Lai, F.S. 1970. The self-preserving particle size distribution for coagulation by Brownian motion-III. Smoluchowski coagulation and simultaneous Maxwellian condensation. J. Aerosol Sci. 1: 115-126.

Praeger, M.J., Stephens, E.R., and Scott, W.E. 1960. Aerosol formation from gaseous air pollutants. Ind. Eng. Chem. 52: 521-524.

Rasmussen, R.A. and Went, F.W. 1964. Volatile organic material of plant origin in the atmosphere. Proc. Nat. Acad. Sci. 53: 215-220.

Roberts, P.T. and Friedlander, S.K. 1976a. Analysis of sulfur in deposited aerosol particles by vaporization and flame photometric detection. Atmos. Environ. 10: 403-408.

Roberts, P.T. and Friedlander, S.K. 1976b. Photochemical aerosol formation - SO_2, 1-heptene, and NO_x in ambient air. Environ. Sci. Technol. 10: 573-580.

Sahni, D. 1966. The effect of a black sphere on the flux distribution in an infinite moderator. J. Nucl. Energy 20: 915-920.

Sander, S.P. and Seinfeld, J.H. 1976. Chemical kinetics of homogeneous atmospheric oxidation of sulfur dioxide. Environ. Sci. Technol. 10: 1114-1123.

Schwartz, W.E., Jones, P.W., Riggle, C.J., and Miller, D.F. 1974. Chemical characterization of model aerosols. EPA 650/3-74-011. Columbus, Ohio: Battelle Memorial Institute.

Schwartz, W.E., Mendenhall, G.D., Jones, P.W., Riggle, C.J., Graffeo, A.P., and Miller, D.F. 1976. Chemical characterization of model aerosols. EPA 600/3-76-085. Columbus, Ohio: Battelle Memorial Institute.

Sitarski, M. and Seinfeld, J.H. 1977. Coagulation of transition regime aerosols. J. Colloid Interface Sci. (in press).

Skala, G.F. 1963. A new instrument for the continuous measurement of condensation nuclei. Anal. Chem. 35: 702-706.

Stauffer, D., Mohnen, V.A. and Kiang, C.S. 1973. Heteromolecular condensation theory applied to particle growth. J. Aerosol Sci. 4: 461-471.

Swift, D.L. and Friedlander, S.K. 1964. The coagulation of hydrosols by Brownian motion and laminar shear flow. J. Colloid Sci. 19: 621-647.

Thomson, W. 1869. On the equilibrium of vapour at a curved surface of liquid. Proc. R. Soc. Edinburgh. 7: 63-69.

Ulrich, G.D. 1971. Theory of particle formation and growth in oxide synthesis flames. Combust. Sci. Technol. 4: 47-57.

Urone, P. and Schroeder, W.H. 1969. SO_2 in the atmosphere: a wealth of monitoring data but few reaction rate studies. Environ. Sci. Technol. 3: 436-445.

Walter, H. 1973. Coagulation and size distribution of condensation aerosols. J. Aerosol Sci. 4: 1-15.

Wang, C.S. and Friedlander, S.K. 1967. The self-preserving particle size distribution for coagulation by Brownian motion II. Small particle slip correction and simultaneous shear flow. J. Colloid. Interface Sci. 24: 170-179.

Went, F.W. 1964. The nature of Aitken condensation nuclei in the atmosphere. Proc. Nat. Acad. Sci. 51: 1259-1267.

Went, F.W. 1966. On the nature of Aitken condensation nuclei. Tellus 18: 549-556.

Whitby, K.T., Husar, R.B. and Lui, B.Y.H. 1972. The aerosol size distribution of the Los Angeles smog. J. Colloid Interface Sci. 39: 177-204.

White, W.H., Anderson, J.A., Knuth, W.R., Blumenthal, D.L. Hsuing, J.C., and Husar, R.B. 1976. Mapping large pollutant plumes by instrumented aircraft: support for project MISTT, 1974. Meteorology Research Inc. report MRI 76 FR-1414 to EPA, Contract 68-02-1919, Altadena, California.

White, W.H. 1976. Reduction of visibility by sulfates in photochemical smog. Nature 264: 735-736.

Whytlaw-Gray, R., Cawood, W., and Patterson, H.S. 1936. The influence of pressure on the coagulation of ferric oxide smokes in Disperse systems in gases; dust, smoke and fog, (reprinted from Trans. Faraday Soc.) Gurney and Jackson, London.

APPENDIX A
NUMERICAL MODELING

An approximate numerical model for evaluating aerosol dynamics when the formation of new particles by homogeneous nucleation and heterogeneous condensation are occurring simultaneously is developed. The emphasis of the model is to calculate the percent of new volume associated with old and new particles as a function of time, since this can be compared with experimental data. The model tends to overpredict the importance of homogeneous nucleation. The functional dependences of the percent of new volume associated with preexisting particles on the rate of aerosol production for a given initial loading as well as on time are in reasonably good agreement with experimental results.

A.1 Physical Model

As in previous chapters, the problem of new particle formation by homogeneous nucleation is treated as a coagulation phenomenon. Homogeneous gas phase reactions produce condensable molecules (monomer) which can collide with themselves to form new particles by homogeneous nucleation, or can condense on surrounding aerosol. Monomer which collide with themselves or other particles are assumed to stick, and subsequent reevaporation is not considered. Implicit in the above assumptions are the assumptions that the vapor pressure of the condensing species is negligible compared with its steady state partial pressure, and that variation of vapor pressure (Thomson, 1869) or droplet composition (e.g. Mirabel and Katz, 1974) with particle size can be ignored.

Calculated results (Mirabel and Katz, 1974; Nair and Vohra, 1975) for droplets consisting of H_2SO_4-H_2O solutions indicate that these approximations are not rigorously justifiable for this system. Thus, the model should overpredict the importance of homogeneous nucleation for the experiments presented in this thesis, where H_2SO_4 droplets were the primary aerosol product.

The dynamic equation describing aerosol dynamics in a coagulating system with a source of particles of volume v_1 is

$$\frac{\partial n}{\partial t} = R\delta(v-v_1) + 1/2 \int_{v_1}^{v} \beta(\tilde{v},v-\tilde{v})\, n(\tilde{v},t)\, n(v-\tilde{v},t)\, d\tilde{v}$$

$$- \int_{v_1}^{\infty} \beta(v,\tilde{v})\, n(\tilde{v},t)\, n(v,t)\, d\tilde{v} \qquad \text{(A.1)}$$

where

$n(v,t)$	=	aerosol size distribution function
v	=	particle volume
t	=	time
R	=	rate of monomer production (No./vol/time)
δ	=	Dirac delta function
$\beta(v,\tilde{v})$	=	collision frequency function

It is assumed that v_1 is the smallest particle size in the system. An initial condition corresponding to an initial aerosol size distribution is assumed to be known.

A general solution to A.1 for $n(v,t)$ can be obtained only with sophisticated numerical computations. In order to further simplify the problem mathematically, additional approximations are introduced.

A.2 Mathematical Model

Consider a system consisting of an initial aerosol with particles large in volume compared to molecular dimensions (e.g. particle diameters greater than 0.01 μm). At time zero, production of particles of volume v_1 (particle diameters typically less than 0.001 μm) is initiated by chemical reaction. These particles can collide with one another to produce clusters of volume $2v_1$ and larger, or can condense on the pre-existing aerosol causing it to grow.

A pictorial representation of the mathematical model used in this appendix is shown in Figure A.1. The aerosol is split into three distinct types of particles. Monomer of volume v_1 and concentration N_1 make up the smallest particles. Clusters of minimum volume $2v_1$ make up the central mode, and transport to the preexisting aerosol in the upper mode is proportional to the diffusion integral I(t) given by (Fuchs and Sutugin, 1971)

$$I(t) = \int \left(\frac{d_p (1 + Kn)}{1 + 1.71Kn + 1.333\ Kn^2} \right) n(v,t)dv \qquad (A.2)$$

where $Kn = 2\ell/d_p$ = Knudsen Number, and ℓ is the effective mean free path of the diffusing species, taking account of persistence (Jeans, 1925). The upper two modes are assumed not to overlap. With these approximations the total distribution function can be expressed as the sum of the three separate contributions

$$n(v,t) = N_1(t)\delta(v-v_1)+n_c(v,t)+n_u(v,t) \qquad (A.3)$$

where

n_c = distribution function for central mode
n_u = distribution function for upper mode

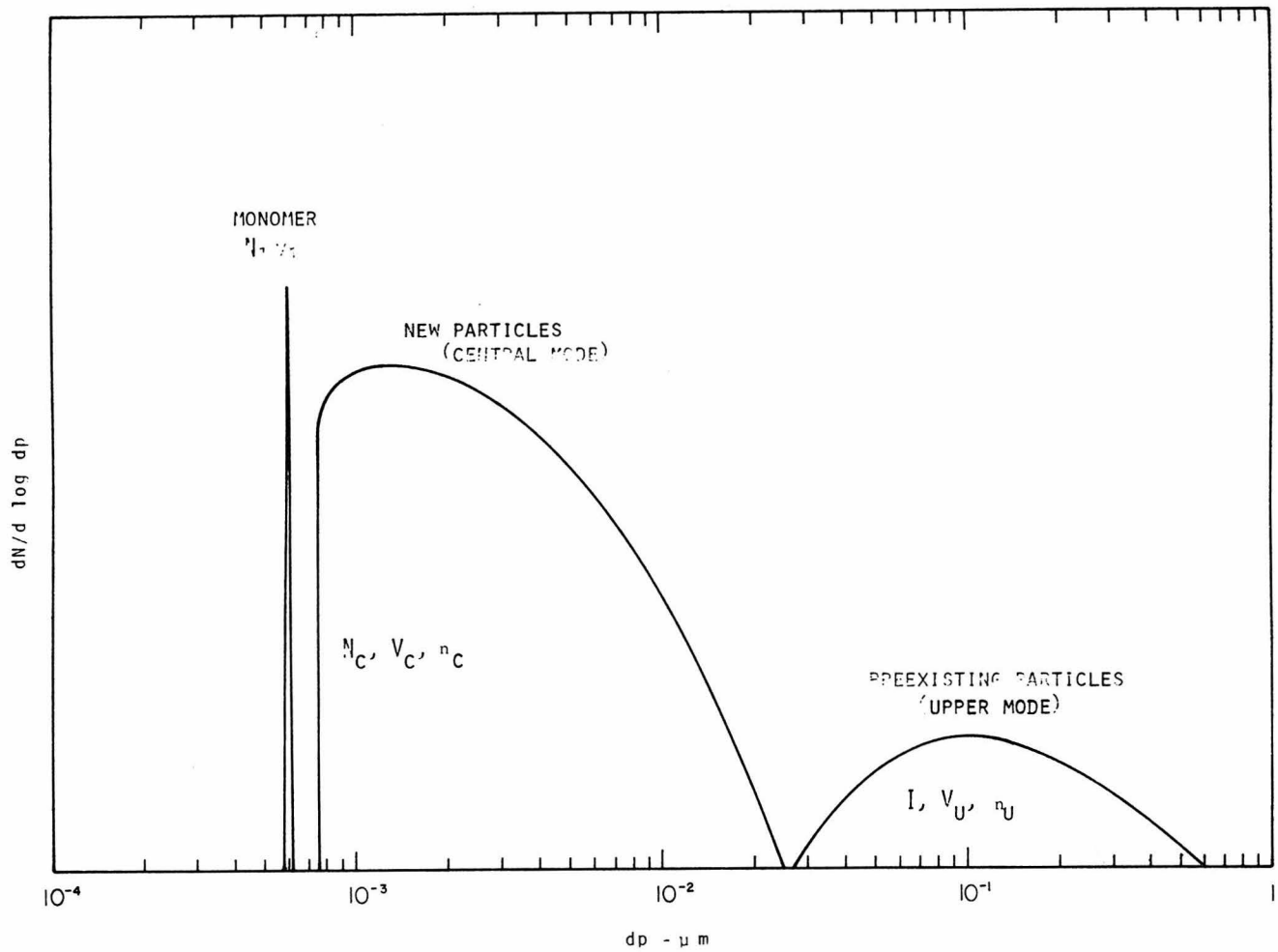

FIGURE A.1

A schematic representation of the assumed aerosol distribution used for the numerical modeling discussed in this appendix. The smallest particles are condensable monomer formed by gas phase reactions. Molecular clusters in the central mode are new particles formed by homogeneous nucleation, while the largest particles are preexisting particles which grow by gas-to-particle conversion. The particle sizes shown are for illustrative purposes only.

The most serious mathematical difficulties arise from treatment of the central mode. The approach of this section is to assume that the central mode has a self-preserving form (Eqns. 3.3 and 3.4) characterized by total number concentration N_c and volume concentration V_c. The form of the dimensionless distribution function, $\psi(\eta)$, is not assumed or calculated, however, it is assumed that the -2/3, 1/3, and 2/3 moments of the dimensionless distribution equal unity, as is rigorously correct for the 0^{th} and 1^{st} moments. It is further assumed that the particles in this mode are in the free molecule regime. With these approximations, Equation A.1 can be reduced to several first order differential equations for the time rate of change of integral moments for the three aerosol modes.

The analysis begins by deriving an expression for the monomer balance. Substituting A.3 into A.1 and integrating from v_1- to v_1+ gives:

$$\frac{dN_1}{dt} = R - \left(\frac{3}{4\pi}\right)^{1/6} \left(\frac{6kT}{\rho}\right)^{1/2} \left(\frac{2}{v_1}\right)^{1/2} (2v_1^{1/3})^2 \; N_1^2$$

$$- N_1 \int_{v_1}^{\infty} \beta(\tilde{v},v) \; \{n_c(\tilde{v},t) + n_u(\tilde{v},t)\} \; d\tilde{v} \qquad (A.4)$$

The expressions v_1- and v_1+ represent volumes slightly less than and slightly more than v_1 respectively. All other cross terms vanish since $n_c(v,t)$ and $n_u(v,t)$ equal zero in the interval v_1- to v_1+. The second term on the right is the rate at which monomer collide with themselves, and the third term the rate at which monomer collide with particles in the central and upper modes. If it is assumed that monomer is much smaller than most of the particles in the other two modes, coagulation of monomer with particles can be treated as condensation. This is equivalent

to assuming that the diffusivity of monomer is much greater than that of the other particles. With these assumptions, and by introducing the self-preserving assumption for the central mode, Equation A.4 reduces to

$$\frac{dN_1}{dt} = R - \left(\frac{3}{4\pi}\right)^{1/6}\left(\frac{6kT}{\rho}\right)^{1/2}\left(\frac{2}{v_1}\right)^{1/2}(2v_1^{1/3})^2 N_1^2$$

$$- N_1\left(\frac{kT}{2\pi\rho\, v_1}\right)^{1/2}(36\pi)^{1/3} V_c^{2/3} N_c^{1/3}$$

$$- 2\pi I D_1 N_1 \qquad (A.5)$$

where ρ is the aerosol density, D_1 the monomer diffusion coefficient, and I(t) the diffusion integral for the preexisting particles. So far there are one equation and four unknowns (N_1, N_c, V_c, and I(t)). Two more equations can similarly be obtained for the number concentration and volume concentration of the central mode. Assume there exists a particle volume, v_u, which separates particles in the upper and lower modes; expressed mathematically, $n_u(v,t) = 0$ for $v < v_u$ and $n_c(v,t) = 0$ for $v > v_u$. Substituting A.3 into A.1, and integrating from v_1 to v_u we obtain

$$\frac{dN_c}{dt} = \frac{1}{2}\left(\frac{3}{4\pi}\right)^{1/6}\left(\frac{6kT}{\rho}\right)^{1/2}\left(\frac{2}{v_1}\right)^{1/2}(2v_1^{1/3})^2 N_1^2 - \frac{\alpha_1}{2}\left(\frac{3}{4\pi}\right)^{1/6}\left(\frac{6kT}{\rho}\right)^{1/2} V_c^{1/6} N_c^{11/6}$$

$$- 2\pi I \int_{v_1^+}^{v_u} D_c\, n_c\, dv \qquad (A.6)$$

where

$$\alpha_1 = \int_0^\infty\int_0^\infty \left(\frac{1}{\eta} + \frac{1}{\tilde{\eta}}\right)^{1/2}(\eta^{1/3} + \tilde{\eta}^{1/3})^2\, \psi(\eta)\, \psi(\tilde{\eta})\, d\eta d\tilde{\eta} \simeq 6.67$$

$D_c(v)$ = diffusion coefficient of particles in the central mode

The first term on the right side of A.6 is the rate at which new particles are put into the central mode by monomer condensation, and the second term the rate of coagulation of the self-preserving free molecule cluster distribution. The constant α_1 was assumed to have the same value as it has for coagulation in the absence of condensation (Lai, et al., 1972). The third term is the rate at which clusters are lost by coagulation with aerosol in the upper mode. The cluster diffusion coefficient is given by

$$D_c = \frac{kT}{f} \tag{A.7}$$

where (Epstein,1924)

$$f = \left(\frac{2}{3}\right)\left(\frac{6}{\pi}\right)^{2/3} v^{2/3} \rho_a \left(\frac{2\pi kT}{m_a}\right)^{1/2}\left[1 + \frac{\pi\alpha}{8}\right] \equiv \nu\, v^{2/3}$$

and

ρ_a = density of air

m_a = molecular mass of air

$\alpha \simeq 0.9$

Substituting A.7 into A.6 we obtain

$$\frac{dN_c}{dt} = \frac{1}{2}\left(\frac{3}{4\pi}\right)^{1/6}\left(\frac{6kT}{\rho}\right)^{1/2}\left(\frac{2}{v_1}\right)^{1/2}(2v_1)^2 N_1^2$$

$$- \frac{\alpha_1}{2}\left(\frac{3}{4\pi}\right)^{1/6}\left(\frac{6kT}{\rho}\right)^{1/2} V_c^{1/6} N_c^{11/6}$$

$$- \frac{2\pi I kT}{\nu} N_c^{5/3} V_c^{-2/3} \tag{A.8}$$

An equation for the volume concentration of the central mode is obtained by multiplying A.1 by v and integrating from v_1+ to v_u. Using the same assumptions described above, the following result is obtained:

$$\frac{dV_c}{dt} = \left(\frac{3}{4\pi}\right)^{1/6} \left(\frac{6kT}{\rho}\right)^{1/2} \left(\frac{2}{v_1}\right)^{1/2} (2v_1)^2 v_1 N_1^2 + v_1 N_1 \left(\frac{kT}{2\pi\rho v_1}\right)^{1/2} (36\pi)^{1/3} V_c^{2/3} N_c^{1/3}$$

$$- \frac{2\pi I k T}{\nu} N_c^{2/3} V_c^{1/3} \qquad (A.9)$$

If coagulation is unimportant, the growth of the aerosol in the upper mode can be described by the equation

$$\frac{\partial n_u(v,t)}{\partial t} = - \frac{\partial n_u (dv/dt)}{\partial v} \qquad (A.10)$$

where

$\frac{dv}{dt}$ = growth rate of single particles by gas-to-particle conversion

The approximation that coagulation of particles in the upper mode can be ignored is not unreasonable for initial aerosol concentrations and time scales of the experiments discussed in this thesis.

The growth law for condensational growth of preexisting particles can be expressed as (e.g., Heisler, 1975; Fuchs and Sutugin, 1971)

$$\frac{dv}{dt} = \underbrace{2\pi d_p \left\{ \frac{1 + Kn}{1+1.71\ Kn+1.333\ Kn^2} \right\}}_{G(v)} \left\{ \sum_i D_i v_i N_i \right\}$$

$$= G(v) \left\{ \underbrace{D_1 v_1 N_1 + \int_{v_1+}^{v_u} D_c v n_c(v,t) dv}_{H(t)} \right\} \qquad (A.11)$$

$$\simeq G(v)\ H(t)$$

where the sum in the first expression is over all condensing species, and vapor pressures have been assumed negligible. The term $G(v)D_1 v_1 N_1$ on the right side of A.11 represents the rate of

growth of particles in the upper mode by monomer condensation, and the integral term the rate of growth resulting from scavenging of particles in the central mode. Heisler (1975) has shown that the solution to A.10 is

$$n_u(v,t) = n_u(v,\xi) = \frac{G(\xi)}{G(v)} \quad n_u(\xi,\xi) \tag{A.12}$$

where ξ is the initial size of particles which have grown to size v at time t.

Multiplying A.11 by n_u and integrating over volume from v_u to ∞ gives

$$\frac{dV_u}{dt} = 2\pi I \{D_1 v_1 N_1 + \frac{kT}{\nu} N_c^{2/3} V_c^{1/3}\} \tag{A.13}$$

where

$$V_u = \int_{v_u}^{\infty} v\, n_u(v,t)\, dv$$

and the diffusion integral I is given by Equation A.2.

Equations A.5, A.8, A.9, and A.13 were solved simultaneously for various rates of monomer production, R, and initial aerosol distributions $n_u(v,0)$ by using a fourth order Runge-Kutta technique. After each iteration, the diffusion integral, I, was updated by substituting A.12 into A.2 and performing the integration. All computations were performed on a PDP-11/10 mini computer. Temperature was set at 300°K. Monomer was assumed to consist of one H_2SO_4 molecule associated with several water molecules; the ratio of H_2O to H_2SO_4 molecules was assumed equal to that in bulk solutions in equilibrium at the same humidity. Monomer volumes were assumed equal to m_1/ρ, where ρ is density of H_2SO_4

solutions at the appropriate humidity and m_1 monomer mass. The mean free path was calculated to be 0.11 μm, and variation with particle size was ignored.

No absolute check on computational accuracy was performed. Time intervals were shortened to the point that no change in calculated results was observed. In addition, the total volume produced by reaction was found to equal the computed sum $V_c+V_u+ v_1N_1$, as it should.

Data from experiments P27 and P16 and computed values for the time dependence of the percent of new volume associated with preexisting particles are compared in Figure A.2. The criterion which was used to distinguish preexisting from new aerosol is discussed in Appendix C, section C.1. For these calculations, the rate of monomer production, R(t), was assumed equal to the observed rates at which SO_2 was removed from the gas phase, and was calculated from SO_2 data presented in Appendix D. Note that the trends with time are similar, but that the importance of homogeneous nucleation is overestimated by the model. Note also that after about one hour, the distribution of new volume between new and preexisting particles changes relatively slowly. The poor agreement between theory and data early in the experiments is probably due to instrumental limitations; a good deal of new aerosol was probably associated with new particles which were smaller than 0.01 μm, the lower limit of resolution of our instrumentation.

The dependence of the percent of new aerosol associated with preexisting particles on the rate of monomer production, R, for given initial aerosol loadings was also investigated using the above numerical model. Table A.1 shows that the SO_2-NO_x-propylene experiments described in this thesis basically group themselves into four categories corresponding to very light, light, moderate and heavy initial aerosol loadings. The

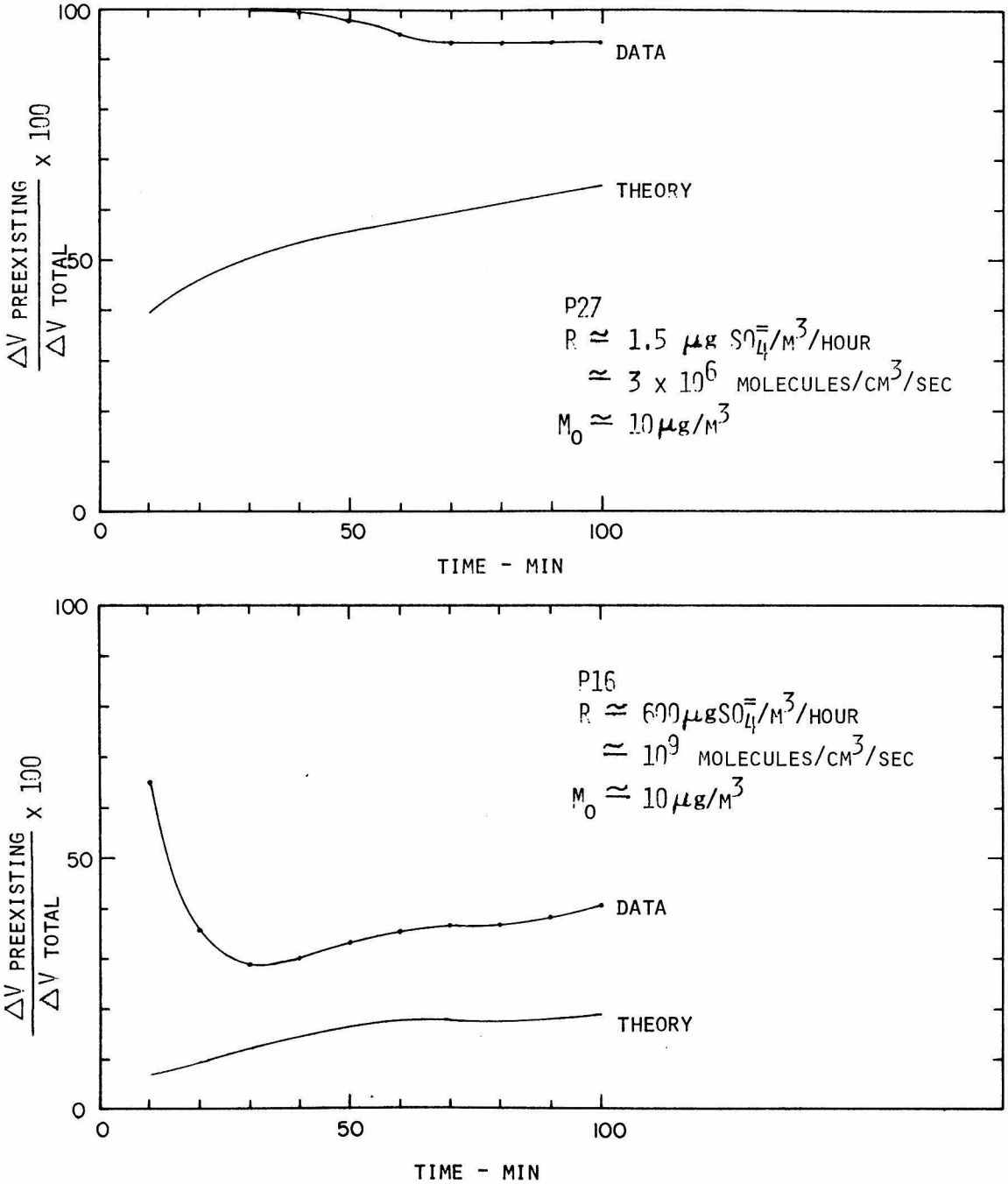

FIGURE A.2

Percent of new aerosol associated with preexisting particles as a function of time for experiments P27 and P16. Data and results of the numerical calculations described in this appendix are compared. Note that the model tends to overpredict the importance of new particle formation.

TABLE A.1
Initial Loadings for Smog Chamber Experiments*

Loading	Experiment	Initial Aerosol Surface Area ($\mu m^2/cm^3$)	Initial Aerosol Volume Fraction ($\mu m^3/cm^3$)	Initial Distribution Used When Calculating Results Presented In Figure A.3
very light	P22	42.	1.0	Initial distribution from P22
	P23	76.	1.8	
	P28	5.4	0.085	
light	P7	200.	6.6	Initial distribution from P7
	P16	250.	7.6	
	P21	170.	2.8	
	P27	190.	5.8	
	P29	280.	7.6	
moderate	P12	490.	11.	Initial distribution from P13
	P13	410.	9.	
	P14	370.	10.	
	P15	410.	11.	
	P17	390.	9.9	
heavy	P19	680.	20.	1338 on 8/26/76

*Data not corrected for sample line losses

percentage of new aerosol associated with preexisting aerosol as a function of time was calculated for four initial aerosol loadings for a range of constant monomer production rates, R. The initial distributions from experiments P7, P13, P22 and a heavy aerosol loading measured in ambient air on 8/26/76 at 1338 were used as the initial aerosol loadings in the computations; these data are presented in Appendix D. Data from the SO_2-NO_x-propylene experiments listed in Table A.1 and results of these computations are compared in Figure A.3; a time of 40 minutes after the start of aerosol production was chosen for the comparison. Note that the numerical model again overpredicts the importance of homogeneous nucleation; the trend of the percentage of new aerosol associated with preexisting particles as a function of the reaction rate was qualitatively correct for these calculations.

The emphasis in these calculations has been to deal with aerosol volume fraction rather than aerosol number concentration. Volume accumulates primarily in larger particle sizes where data is more reliable; it is possible that there is a high number concentration of particles below the detection limits of the instrumentation used in these experiments. The data presented in Figure A.2 suggest also that a considerable amount of the volume associated with new particles is not detected early in an experiment.

A.3 Summary

A numerical model which describes the dynamics of aerosol growth resulting from the production of condensable molecules in the gas phase by homogeneous gas phase reactions has been presented. Homogeneous

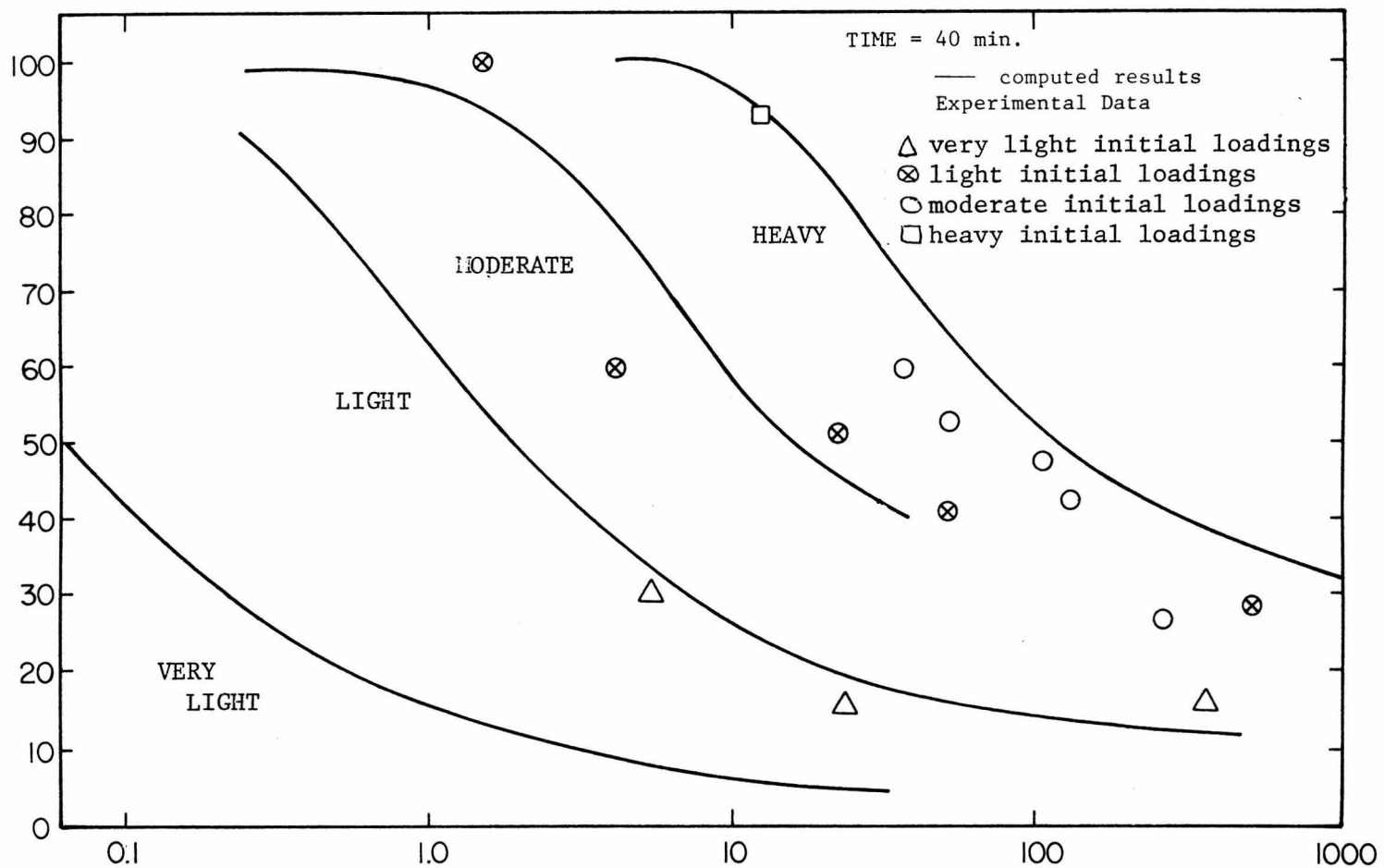

FIGURE A.3

Percent of new aerosol associated with preexisting particles as a function of rate of monomer production, R. Data for the SO_2-NO_x-propylene experiments are grouped into four different initial loadings, and results of these experiments are compared with computed results for four initial loadings corresponding to those of the experiments. Note that the model tends to overestimate the importance of new particle formation.

nucleation and heterogeneous condensation were allowed to occur simultaneously. Homogeneous nucleation was treated as a coagulation process, and evaporation from clusters was not considered. The model was reasonably successful at predicting trends in the percent of new volume associated with preexisting particles as a function of time and rate of monomer production. In all cases, the importance of homogeneous nucleation was overestimated. The qualitative agreement over a wide range of reaction rates and initial aerosol loadings is encouraging.

The advantage of the model presented in this appendix is that a difficult numerical problem is reduced to one which is easy to deal with numerically, and that most mechanisms of particle interactions can be considered. There are, of course, several serious objections to the model. Two types of approximations were made in deriving the equations. The first was that the physics of particle interactions could be treated as a coagulation process, and that no reevaporation would be considered after a collision. The effect of this assumption is to overemphasize the importance of homogeneous nucleation. The error imposed by this assumption when modeling aerosol dynamics depends on the nature of the condensing species. The approximation becomes more acceptable as the saturation ratio for the condensing species becomes large. The second uncertainty concerns the mathematical treatment of the problem. The errors induced by splitting the aerosol size distribution into three distinct but interacting parts are unknown as are the errors imposed by treating the central mode as self-preserving in form. An understanding of the extent to which the computed results resemble the physical model proposed can only be obtained by comparing results with a rigorous solution to Equation A.1.

The model could be improved considerably by introducing some of the concepts introduced in Chapter 4. Calculated results should be defined in terms of quantitites which are measured experimentally. The weak link is the treatment of the central mode. The assumption that this is self-preserving in form may be incorrect, and alternate representations should be explored.

APPENDIX B
PARTICLE LOSSES

Particle losses on the walls of the 65 m^3 teflon reaction chamber during experiments as well as losses in the teflon sample line leading to the instrumentation in the laboratory caused errors in the smog chamber data reported in this thesis. Experiments were performed to measure the extent of these losses. Results of these particle loss experiments as well as their effect on aerosol dynamics are presented in this appendix.

B.1 Wall Losses

The teflon reactor was filled with unfiltered air in experiment T2. No reactants were added to the chamber, so no significant aerosol formation was observed. Aerosol distributions were measured at 10 minute intervals during a 3 hour period. The data was averaged into 3 one hour intervals, and rates of concentration decrease from one hour to the next were obtained for particles in each size interval of the electrical aerosol analyzer and optical particle counter. The average of the two rates is presented as a function of particle diameter in Figure B.1. Data obtained by Eskinazi (1976) for loss rates of monodisperse particles in the same system are also shown. The decrease in removal rates for particle diameters between 0.03 μm and 0.2 μm is consistent with filtration data; larger particles are removed by inertial and gravitational mechanisms while smaller particles are removed by Brownian diffusion to surfaces.

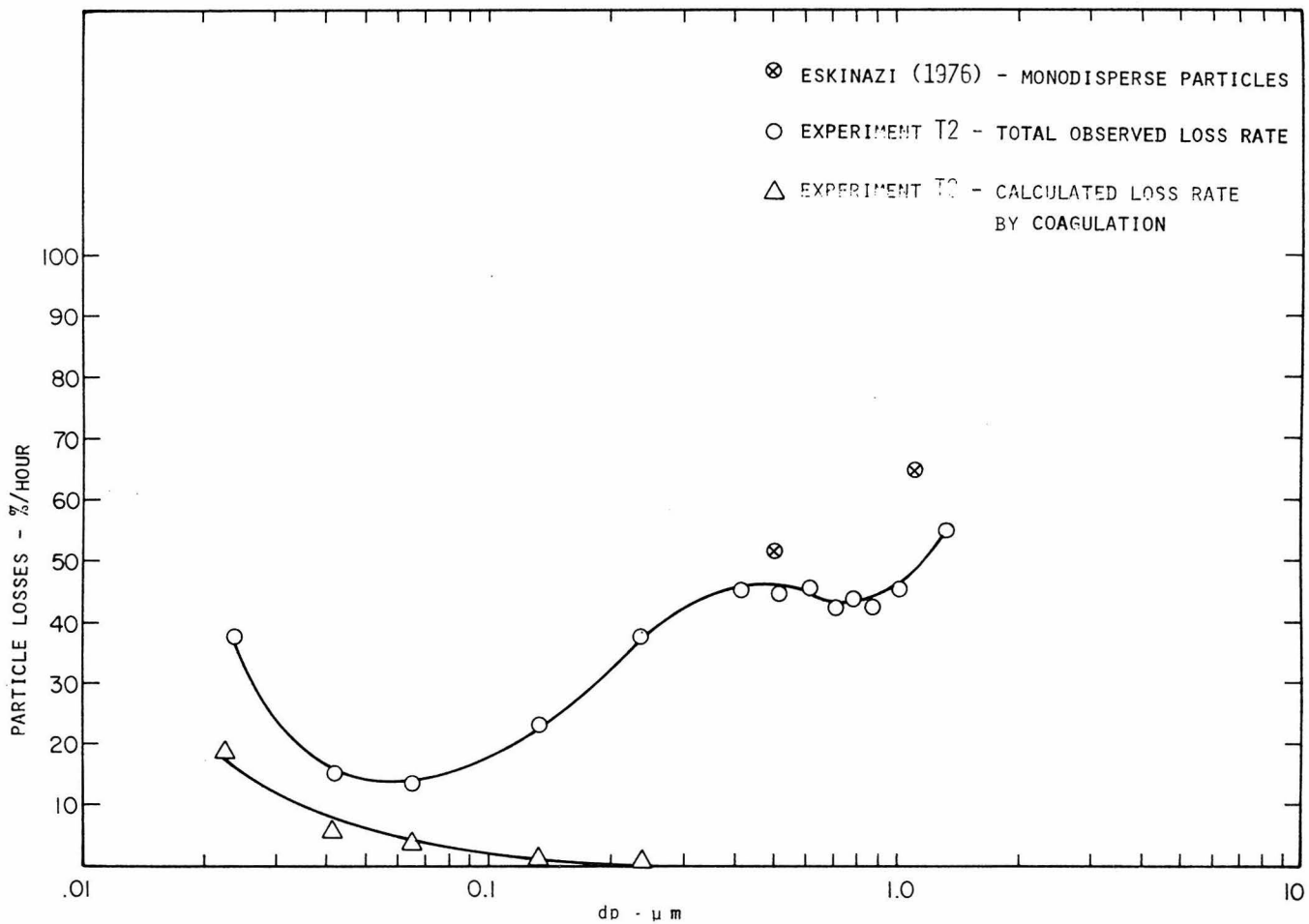

FIGURE B.1

Rate of particle losses in the 65 m^3 teflon reactor as a function of particle size. The circles represent measured total loss rates, and the triangles calculated rates of loss by coagulation for the same aerosol.

Particle concentration in any arbitrary size range decreased as a result of coagulation as well as wall losses. Both of these effects are included in the measured rate of loss presented in Figure B.1. Total aerosol volume decreased at an average rate of 30%/hour during the experiment. Since coagulation does not affect the aerosol volume fraction, it is clear that wall losses were an important effect. An estimate of coagulation effects was made by using the transition regime coagulation collision frequency function discussed by Sitarski and Seinfeld (1976). The rates of particle losses by coagulation are also shown in Figure B.1. Note that coagulation was significant in comparison to wall losses only for the smallest particles.

B.2 Sample Line Losses

Loss of particles in the sampling system during transport from the teflon reactor to the instrumentation caused observed particle concentrations to be lower than those in the reactor. The extent of these losses is difficult to calculate; effects of the corrugated surface of the sample line and the circuitous path between the reactor and instrumentation cannot easily be evaluated. Instead, particle losses were measured, and results of these experiments are presented in this section.

The penetration efficiency of five sizes of monodisperse particles and of room air through the sampling system was measured. The monodisperse aerosols were generated by nebulizing dilute solutions of polystyrene latex particles; these aerosols were passed through a Kr 85 decharger before entering the sampling system in order to minimize charge effects on deposition in the sample line. Losses of particles smaller

than 0.3 μm were measured by the electrical aerosol analyzer, while losses of larger particles were measured by the optical particle counter. The sampling system was operated under the same conditions as it was for the other experiments reported in this thesis. The nephelometer pump was the primary pump (Figure B.2), and the transit time between the entrance to the sample line and the instruments was about 6 seconds. Particles were alternately sent to the instrumentation directly and through the sampling system. For each particle size, the percent lost in the sampling system was measured at least three times. Average results and standard deviations of the percent of particles of various sizes lost in the sampling system are presented in Figure B.3. Again, note the characteristic dip in removal efficiency for particles with diameters near 0.3 μm.

In order to minimize data manipulation, data were not corrected to account for sample line losses. For the smog chamber experiments reported, aerosol volume accumulated mostly in particle sizes between 0.075 μm and 0.2 μm where losses fall between about 30% and 20%. This is a substantial source of error, since most of the data on which conclusions are based is subject to an instrumental error of about 20%. These sample line losses must be kept in mind when analyzing experimental data.

B.3 Wall Loss Corrections to Rate of Aerosol Formation

Wall loss corrections were made when calculating the rate of aerosol formation, F. These corrections were necessary since the rate of volume decrease due to wall losses could be substantial compared to the rate of volume increase by gas-to-particle conversion. This effect was

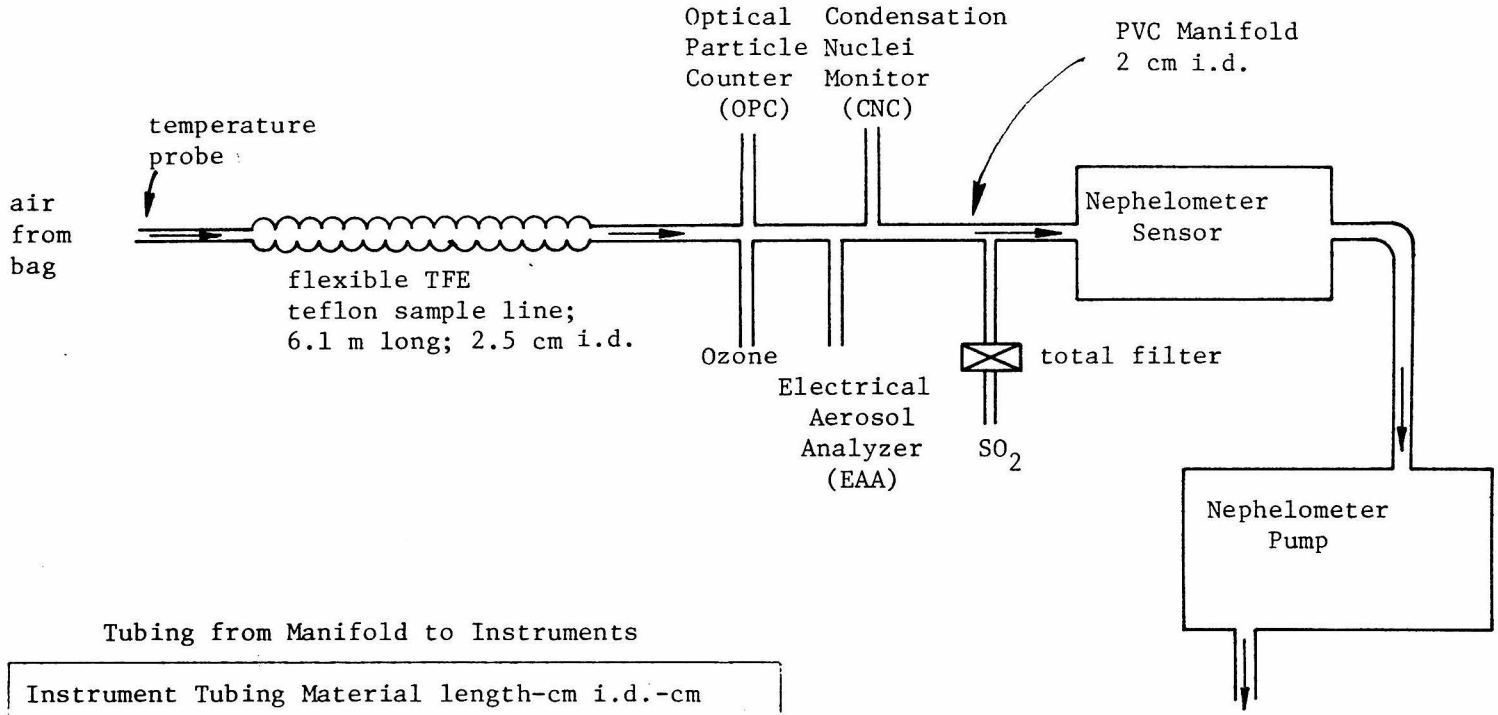

Tubing from Manifold to Instruments

Instrument	Tubing Material	length-cm	i.d.-cm
OPC	Tygon	90	0.7
CNC	Tygon	90	0.7
O_3	Teflon	30	0.2
EAA	Tygon	130	0.8
SO_2	Teflon	300	0.4

FIGURE B.2

Diagram of the sampling system used to take air from the 65 m^3 teflon reactor to the instruments in the laboratory.

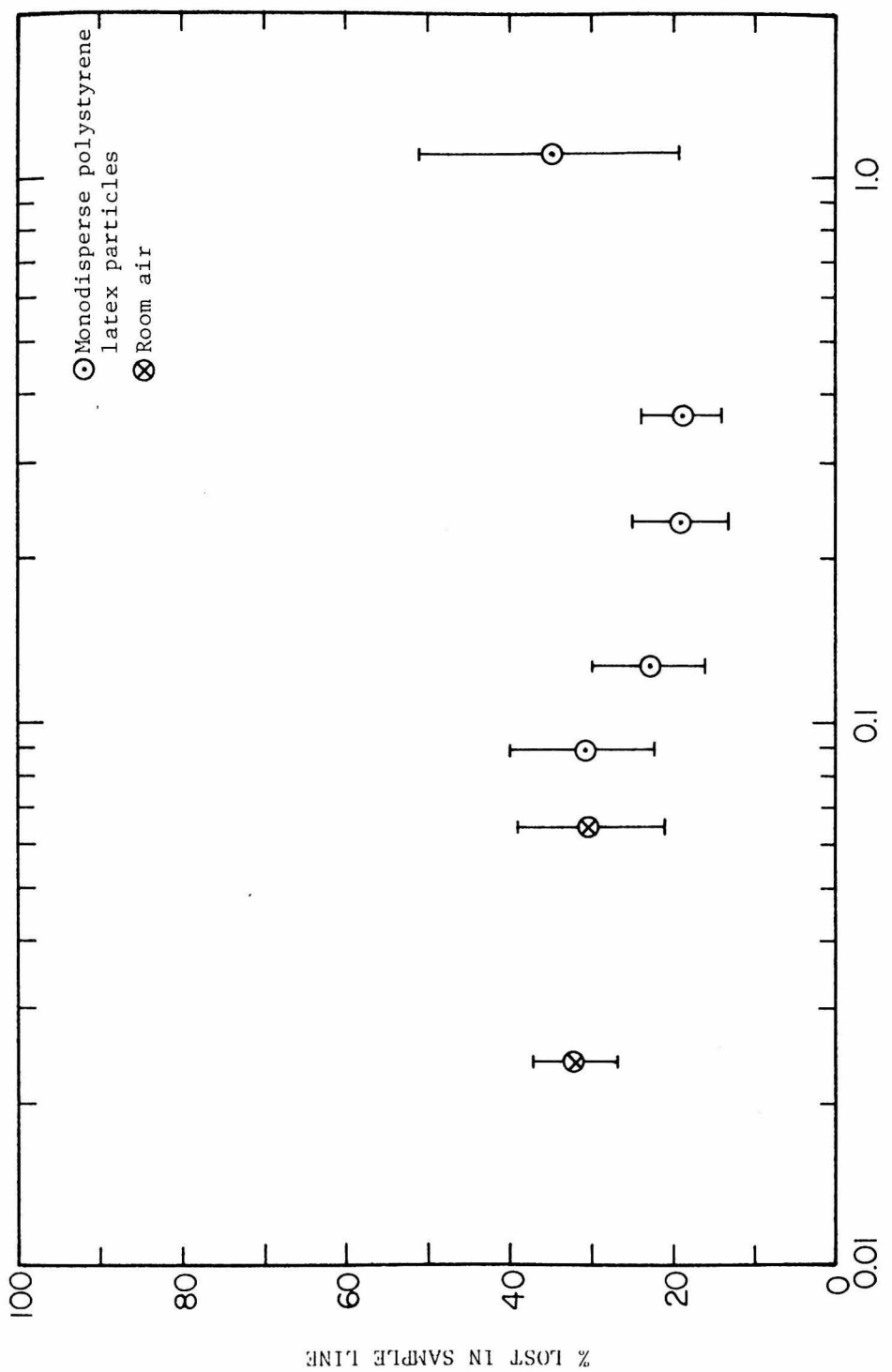

FIGURE B.3

Percent of particles lost in the sampling system as a function of particle size. The error bars represent standard deviations of at least three separate measurements.

particularly important for experiments with high initial aerosol loadings where, on occasion, the total aerosol volume decreased during early stages of the experiments despite evidence of gas-to-particle conversion (e.g. SO_2 decrease, homogeneous nucleation). This effect was so pronounced for experiments P19 and P27 that no determination of F was made.

In order to correct the rate of aerosol formation, F, for wall losses, the measured aerosol volumes were corrected to account for wall losses since the beginning of the experiment. Aerosol size distributions were measured at 10 minute intervals during each experiment. The amount of aerosol loss, δV_j, expected during the j^{th} interval, Δt_j, was calculated from the expression

$$\delta V_j = \Delta t_j \sum_{i=1}^{\ell} a(v_i)\, DV_{ij} \qquad \text{(B.1)}$$

where

δV_j = total aerosol volume fraction lost during the j^{th} time interval
$a(v_i)$ = fractional loss rate per unit time for particles with volume v_i
DV_{ij} = aerosol volume fraction associated with particles of size i at the beginning of the j^{th} time interval
ℓ = number of size intervals

The aerosol volume fraction at the end of the k^{th} time interval, corrected for wall losses since the beginning of the experiment, was taken to be

$$V = V_{measured} + \sum_{j=1}^{k} \delta V_j \qquad \text{(B.2)}$$

This calculation was done for all size distributions measured in the smog chamber experiments.

B.4 Correction of Aerosol Data for Sample Line Losses

All aerosol data presented in Chapters 3 and 4 have been corrected for sample line losses. Let DX_{ij} be the observed quantity of an aerosol property in size range i at time j. X could refer, for example, to aerosol number, surface area or volume concentrations. After correcting for sample line losses, the amount of this property, DX_{ij}, is

$$DX_{ij}' = \left(\frac{1}{1-\varepsilon_i}\right) DX_{ij} \tag{B.3}$$

where ε_i is the fraction of size i aerosol lost in the sample line, and is obtained from Figure (B.3). The total amount of X at time j, corrected for sample losses is

$$X_j' = \sum_{i=1}^{\ell} DX'_{ij}. \tag{B.4}$$

B.5 Rate of Aerosol Formation

The rate of aerosol formation, F, was obtained by calculating the slope of the volume versus time curve for that portion of the experiment during which dV/dt was constant. The aerosol volume fractions used in obtaining these slopes were corrected both for sample line and wall losses; the effects of the two processes were assumed to be additive. Thus, the aerosol volume at time k, corrected for particle losses is

$$\underset{\substack{\text{corrected for}\\ \text{particle losses}}}{V_k} = V'_k + \sum_{j=1}^{K} \delta V_i$$

where V_k' is given by (B.4), and δV_i by (B.1).

Table B.1 shows the importance of this correction for each of the SO_2-NO_x-propylene experiments reported in this thesis. Also shown is the time interval over which F was calculated, and the number of pairs of points (V,t). The rate of aerosol formation, F, is the least square slope of these points.

B.6 Summary and Conclusions

Particle losses on the walls of the 65 m^3 teflon balloon used in the smog chamber studies discussed in this thesis are significant despite the large size of the reactor. Loss rates depend on particle size, and vary between 15%/hour and 60%/hour for the range of particle sizes measured. Most of the aerosol formed in these experiments accumulated near 0.1 μm where rates of particle losses were relatively low.

Losses of particles in the sample line were shown to be on the order of 20% to 30%, which is comparable to other experimental uncertainties. All aerosol data presented in Chapters 3 and 4 were corrected for sample line losses.

Corrections to the rate of aerosol formation, F, varied between 32% and 300% when particle losses were taken into account; most corrections were less than 45% however.

TABLE B.1

Effect of Particle Losses on Calculated
Rates of Aerosol Formation

Experiment	$F = \frac{dV}{dt}$ * cm^3 Aerosol/cm^3 Air/sec	F uncorrected / F corrected for particle losses	Time interval over which F was evaluated (PDT)	Number of pairs (V,t) used for least square slope dV/dt
P7	8.85×10^{-15}	0.63	1340-1420	4
P12	3.01×10^{-14}	0.68	1540-1630	5
P13	6.52×10^{-14}	0.72	1450-1530	4
P14	6.62×10^{-14}	0.71	1115-1156	4
P15	1.20×10^{-13}	0.72	1425-1507	4
P16	2.48×10^{-13}	0.76	1138-1204	3
P17	1.52×10^{-14}	0.62	1505-1550	5
P19	A	---	---	---
P21	2.82×10^{-14}	0.71	1425-1445	3
P22	9.28×10^{-15}	0.68	1130-1225	6
P23	3.52×10^{-15}	0.69	1510-1610	6
P27	A	---	---	---
P28	1.01×10^{-13}	0.74	1105-1135	3
P29	1.58×10^{-15}	0.34	1320-1410	5

*Includes particle loss corrections

A. Was not calculated since rates of wall losses were too large compared to rates of aerosol formation.

APPENDIX C
GROWTH OF PREEXISTING AEROSOL

During the smog chamber experiments reported in Chapter 4, the preexisting particles grew as a result of gas-to-particle conversion. It is shown in this appendix that the growth of the preexisting particles is consistent with a zero vapor pressure diffusional growth law. Calculated and observed aerosol volume distributions for these sulfate aerosols tend to peak at about 0.1 μm, which is smaller than sulfate distributions measured in ambient air. This suggests that in ambient air, secondary sulfate aerosols may be formed by mechanisms other than homogeneous gas phase reactions.

The equation which describes the evolution of a non-coagulating aerosol growing as a result of gas-to-particle conversion is (Friedlander, 1977)

$$\frac{\partial n}{\partial t} = - \frac{\partial n(dv/dt)}{\partial v} \qquad (C.1)$$

where

t = time
v = particle volume

The aerosol size distribution function, n(v,t), is defined such that the number of particles with volume between v and v + dv is

$$dN = n(v,t)dv \qquad (C.2)$$

The solution to Equation C.1 by the method of characteristics has been discussed by Heisler (1975).

Equation C.1 has been used to calculate the evolution of experimentally measured initial aerosols for various particle growth laws. A summary of the various growth laws which have been considered is given in Table C.1. Figure C.1 shows the initial aerosol volume distribution and the measured distribution after 50 minutes of aerosol production for experiment P13. During this experiment a large number of new particles was produced by homogeneous nucleation. The number of particles initially was 30,000 per cm^3. The vertical dashed line separates the largest 30,000 particles per cm^3 from the remainder. If volume to the right of this line is assumed to be associated with the initial aerosol which has grown, calculated results for the diffusional growth of the initial aerosol, also shown in Figure C.1, agree reasonably well with experimental results. The effective mean free path of the condensing molecules, λ, was estimated to be 0.11 μm (Jeans, 1925). Results of calculations for other growth laws presented in Figure C.2 show that if the initial aerosol had grown to the same volume by solution phase reaction, or if curvature effects had been important as found by Heisler and Friedlander (1976) for condensable products of several organic precursors, the measured result would have been strikingly different.

The results of Figure C.1 show that condensational growth with no curvature effects is plausible for aerosol larger than 0.01 μm growing by products of the SO_2-NO_x-propylene system. The unimportance of curvature effects for particles of these sizes is consistent with calculations of Mirabel and Katz (1974) and Nair and Vohra (1975) for

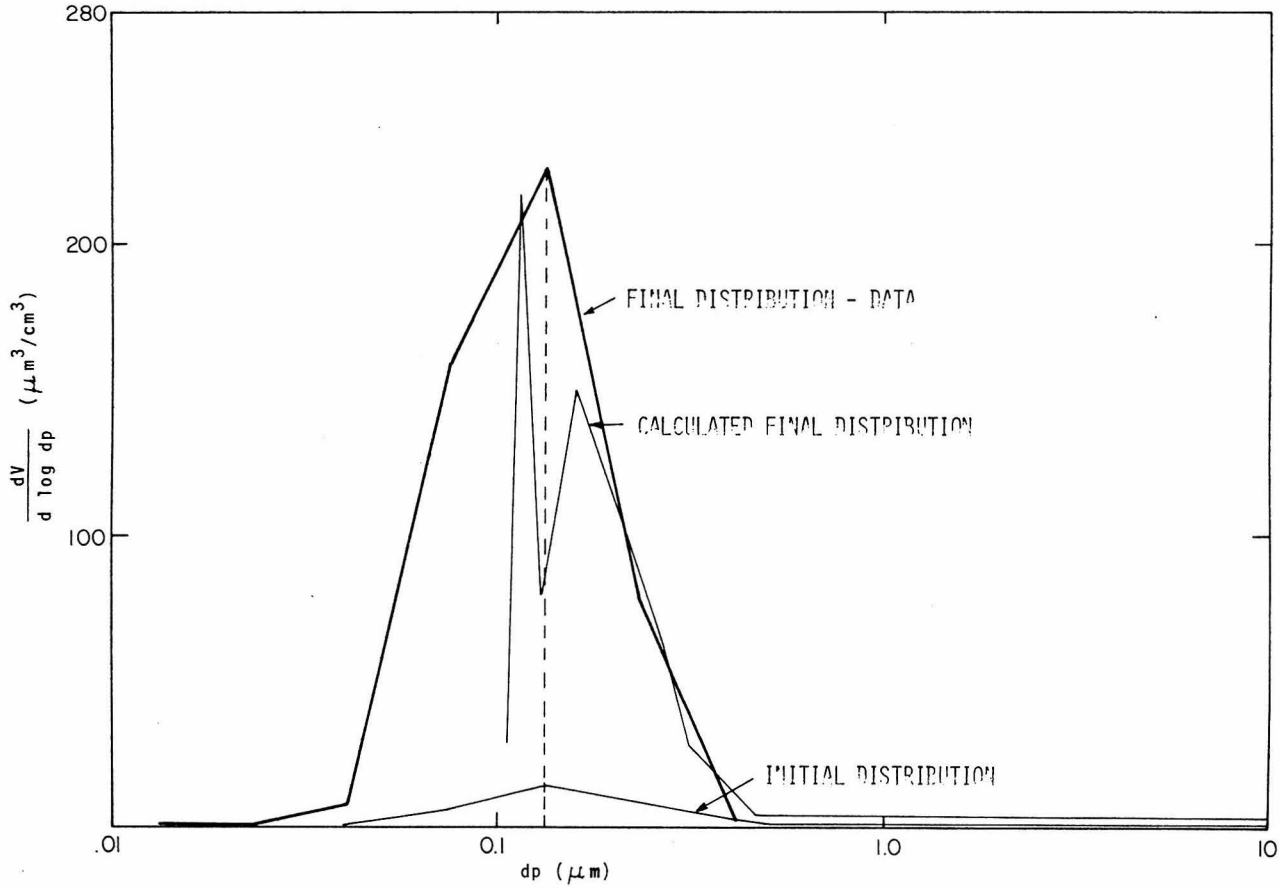

FIGURE C.1

A comparison between observed and calculated volume distributions for growth of the initial aerosol in experiment P13. A transition regime expression for condensational growth of the preexisting aerosol was assumed in obtaining the final calculated distribution. Calculated results should be compared with the data to the right of the vertical dashed line which is assumed to be associated with preexisting particles which have grown.

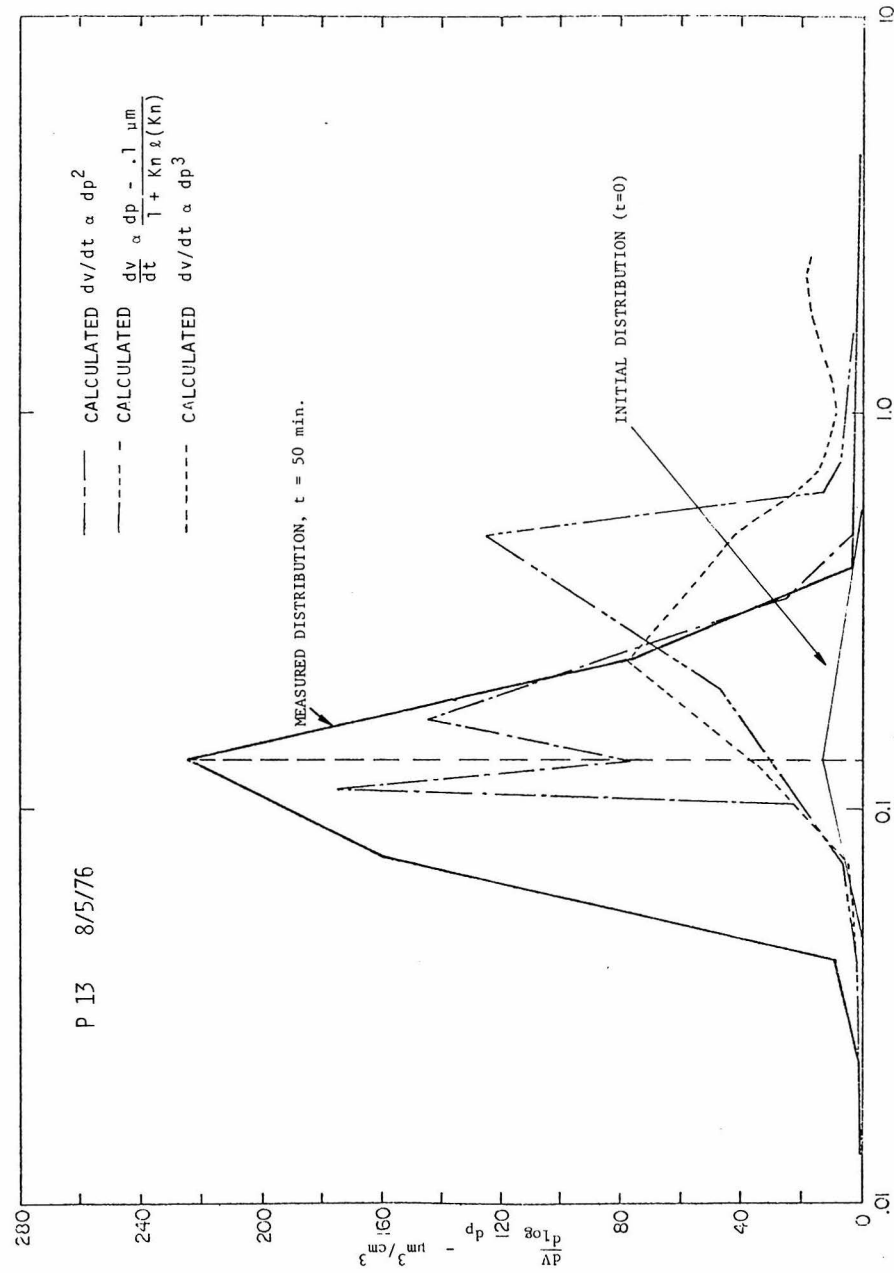

FIGURE C.2

A comparison between observed and several calculated distributions for growth of the initial aerosol in experiment P13. Calculated distributions should be compared with data to the right of the vertical dashed line. The growth laws are described more completely in Table C.4.

TABLE C.1

Examples of Particle Growth Laws

Growth Mechanism	Growth Law†	Reference
Condensation on transition regime aerosols	$\frac{dv}{dt} = \frac{2\pi D v_1}{kT}\left(\frac{d_p}{1+K_n\ 1(K_n)}\right)(P_1 - P_s)$	Fuchs and Sutugin (1971)
Condensation on free molecule aerosols	$\frac{dv}{dt} = \left(\frac{v_1}{2\pi\rho kT}\right)^{1/2} \pi d_p^2 (P_1 - P_s)$	e.g. Friedlander (1977)
Condensation on transition regime aerosols; curvature effects included to first order	$\frac{dv}{dt} = \frac{2\pi\ D\ v_1 P_1}{kT}\left(\frac{d_p - d_p^*}{1+K_n\ 1(K_n)}\right)$	Heisler and Friedlander (1976)
Solution phase reaction	$\frac{dv}{dt} = K\ d_p^{\ 3}$	e.g. Friedlander (1977)

† nomenclature

v = particle volume
v_1 = molecular volume of condensing species
p_1 = partial pressure of condensing species
P_s = vapor pressure of condensing species
d_p = particle diameter
k = Boltzman constant
T = temperature
ρ = particle density
K_n = Knudsen numbers = $2\lambda/d_p$
$1(K_n) = \frac{1.33\ K_n + 0.71}{1.0 + K_n}$
d_p^* = critical size; particles smaller than this won't grow
λ = effective mean path of diffusing species

sulfuric acid droplets. The striking differences between size distributions calculated for various particle growth laws shows that a knowledge of the size distribution of a secondary aerosol as well as the initial size distribution from which it grew can be useful in inferring mechanisms of gas-to-particle conversion. Heisler and Friedlander (1976) have discussed such calculations for aerosol in the Los Angeles atmosphere.

C.1 Effect of Particle Losses on Growth of Preexisting Nuclei

When calculating the growth of preexisting nuclei with Equation C.1, it was assumed that the number of preexisting nuclei remained constant. In fact, this number decreased due to coagulation and wall losses. There was no way to distinguish preexisting particles from new particles formed by homogeneous nucleation, so there was no way to determine the extent of this decrease experimentally. Estimates of the importance of this effect have been made by using the loss rates presented in Figure B.1. Coagulation and wall losses were not treated separately; the upper curve in Figure B.1 was assumed to give a reasonable estimate of the combined effect for the two processes. The calculation presented here was done for experiment P13 where total aerosol number concentration was comparable to that in wall loss experiment T2 so that coagulation effects may be assumed to be comparable.

In the absence of particle losses, the growth of a preexisting aerosol can be calculated by solving Equation C.1. The shape of the evolving aerosol size distribution depends only on the amount of aerosol added for a given particle growth law, dv/dt, (Heisler, 1975). The distribution only depends on time to the extent that the amount of

aerosol added by gas-to-particle conversion depends on time. If particle losses are important, the dynamic equation of an aerosol growing by gas-to-particle conversion is

$$\frac{\partial n}{\partial t} = \frac{\partial n \quad dv/dt}{\partial v} - a(v)n \qquad (C.3)$$

where a(v) is the fractional loss rate for particles of volume v. In this case, the shape of the evolving aerosol distribution depends independently on time and on the amount of aerosol added. A solution to C.3 requires a dynamic model which includes a time dependent expression for dv/dt. Because homogeneous nucleation occurred in all of the experiments reported here, contributions of monomer condensation as well as scavenging of clusters had to be included when evaluating the growth rates of preexisting particles through the growth law dv/dt.

Equation C.3 was solved numerically in real time for several experiments. Equation A.11 was used to evaluate dv/dt. The numerical approach was nearly identical to the approach outlined in Appendix A for aerosol dynamics in the absence of losses of preexisting nuclei. After each iteration, however, particles were subtracted off at a rate consistent with experimentally measured loss rates, a(v), shown in Figure B.1. A Lagrangian interpolation technique was used to estimate a(v) from data presented in Figure B.1.

In order to compare these calculated distributions with experimental data, it is necessary to establish a criteria for distinguishing preexisting particles from new particles formed by homogeneous nucleation. This cannot be done experimentally since new and preexisting particles tended to grow together into a single distribution. Instead,

the remaining number of preexisting particles at a given time is calculated by considering particle loss rates, and it is assumed that these particles form the largest particles in the measured distributions.

Calculating the number of preexisting nuclei is analogous to calculating volume loss rates. The number of preexisting particles, δN_j, lost during the j^{th} time interval, Δt_j, is

$$\delta N_j = \Delta t_j \sum_{i=1}^{\ell} a(v)\ DN_{ij} \qquad (C.4)$$

where DN_{ij} is the number of preexisting particles in the i^{th} size interval at the beginning of the j^{th} time increment. Size distribution data were taken at 10 minute increments during all experiments, and the number of preexisting nuclei after the k^{th} time interval was

$$N = N_{i=0} - \sum_{j=1}^{k} \delta N_j \qquad (C.5)$$

Figure C.3 compares calculated distributions for growth of preexisting particles and experimental data for experiment P13. Calculated results should be compared to the data to the right of the vertical dashed line which is assumed to be the volume associated with the remaining preexisting particles. The initial number of particles for this experiment was 29,610 cm^{-3}. The number of remaining particles after 60 minutes was calculated with Equation C.5 to be 23,900 cm^{-3}. The remaining number calculated in the numerical solution to Equation C.3 was 24,800 cm^{-3}.

Figure C.3 can be compared with Figure C.1, where losses of preexisting particles were not considered when calculating the growth of

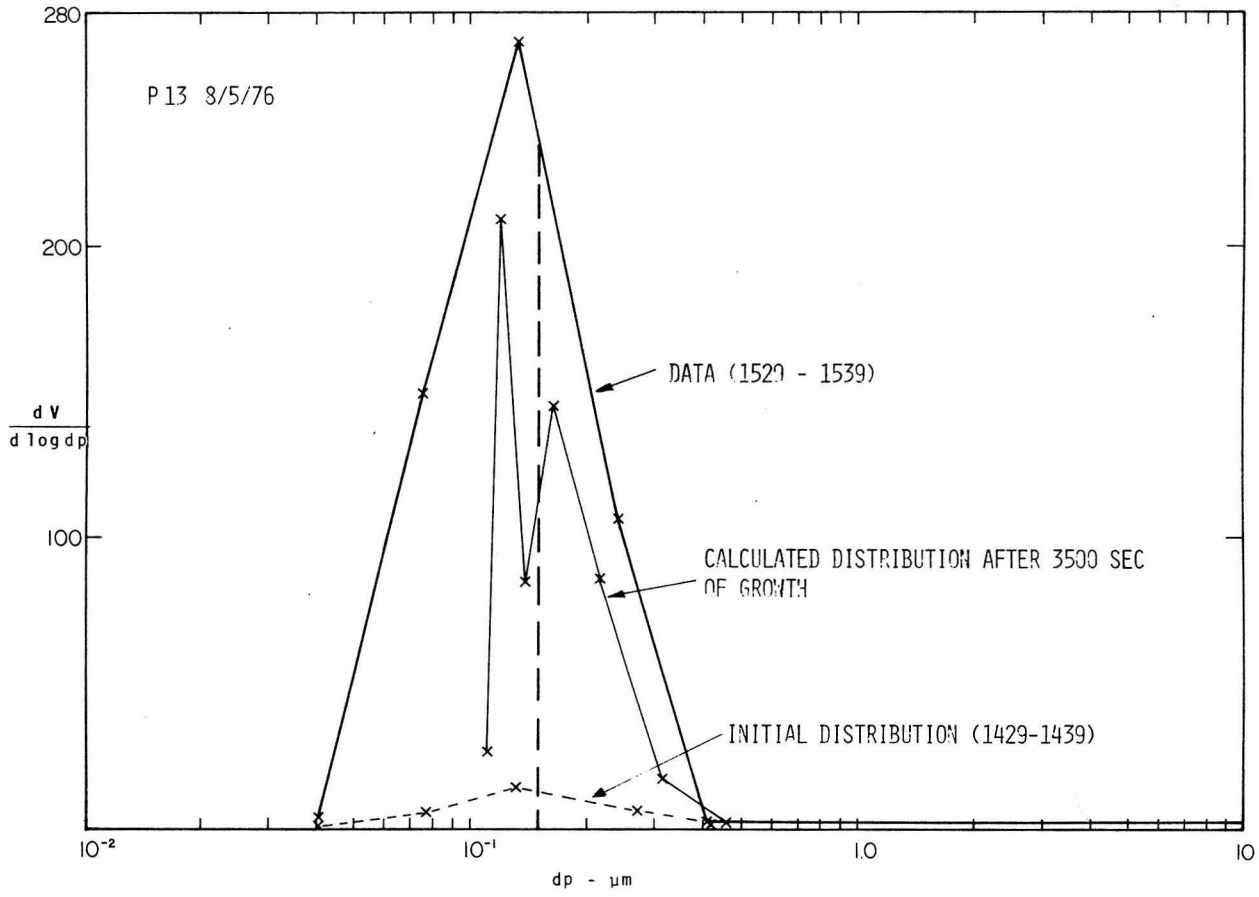

FIGURE C.3

Comparison of measured and calculated volume distributions for the growth of the preexisting aerosol in experiment P13. The calculated distribution should be compared with the data to the right of the vertical dashed line. Wall losses were taken into account when using the dynamic model discussed in Appendix A to calculate the growth of the preexisting aerosol.

the preexisting aerosol. Note that the calculated results in Figure C.1 appear to fit the data more closely than those presented in this section, although the calculated results presented in Figure C.4 agree reasonably well with the data. This is partly because the numerical technique used to solve for the evolution of the preexisting aerosol tended to overemphasize the importance of homogeneous nucleation, as was pointed out in Appendix A. Thus, the advantage of improved accuracy gained by including wall losses was lost by the need to use an approximate dynamic model. The important point of this section is that including wall losses does not change the conclusion that the growth of preexisting aerosol is consistent with a zero vapor pressure diffusion limited growth law.

APPENDIX D
EXPERIMENTAL DATA

Experimental data and basic procedures for all of the smog chamber experiments reported in this thesis are included in this appendix. Three pages are allocated for each of the SO_2-NO_x-propylene experiments.

The first page includes basic procedures such as whether or not the bag was covered while being filled, and whether or not the air was partially filtered. Also included on this page are the amount of each reactant added to the bag, and time histories of SO_2, temperature, and relative humidity during the experiment.

The second page is a plot of the time evolution of particle number concentration, total aerosol volume concentration, and aerosol surface area per volume of gas, as well as of SO_2 concentrations, the light scattering coefficient (b_{scat}), and ozone. The aerosol data was obtained by integrating over distributions measured by the electrical aerosol analyzer and the optical particle counter.

The third page contains size distribution data measured over each 10 minute interval during the experiments. Columns 2 through 12 show the number of particles per cm^3 between the diameter limits shown in column 1 for distributions measured during the experiment. Data in a given column was acquired during the time interval indicated at the top of the column. Column 3 was taken to be the initial aerosol distribution. The particle size associated with particles in a given channel was taken to be the geometric mean of the appropriate diameter limits. The gap between electrical aerosol analyzer and optical particle counter data was insignificant in comparison to other experimental uncertainties.

Also included in this appendix are data from the wall loss experiment T2, the early morning experiment RR14 discussed in Chapter 2 and experiment RR15 discussed in Chapter 3. The size distribution measured at 1338 on 8/26/76 which was used as an initial distribution for dynamic modeling in Appendix A is also included.

All of the data presented here are raw data and have not been corrected for wall losses or sample line losses.

PROCEDURE AND SO2, TEMPERATURE, AND RELATIVE HUMIDITY DATA FOR EXPERIMENT P7

THE BAG WAS FILLED FROM 12:00 TO 12:03

THE BAG WAS NOT COVERED DURING THE FILLING PROCESS

THE AIR WAS NOT FILTERED DURING THE FILLING PROCESS

REACTANTS ADDED TO THE SYSTEM:

REACTANT	AMOUNT ADDED - CM3	TIME ADDED
NO	21.50	12:51
NO2	10.40	12:53
SO2	3.25	12:55
PROPYLENE	65.00	12:56

TIME	SO2	TIME	TEMPERATURE - DEG C	RELATIVE HUMIDITY
12:02	4.75	12:02	33.	23.
12:46	4.75	12:46	40.	17.
13:05	44.19	13:05	41.	16.
13:14	46.33	13:14	41.	16.
13:25	47.04	13:43	42.	13.
13:43	46.09	13:54	41.	16.
13:54	44.67	14:08	42.	13.
14:08	43.48	14:26	40.	17.
14:26	41.58	14:38	39.	18.
14:38	40.87			

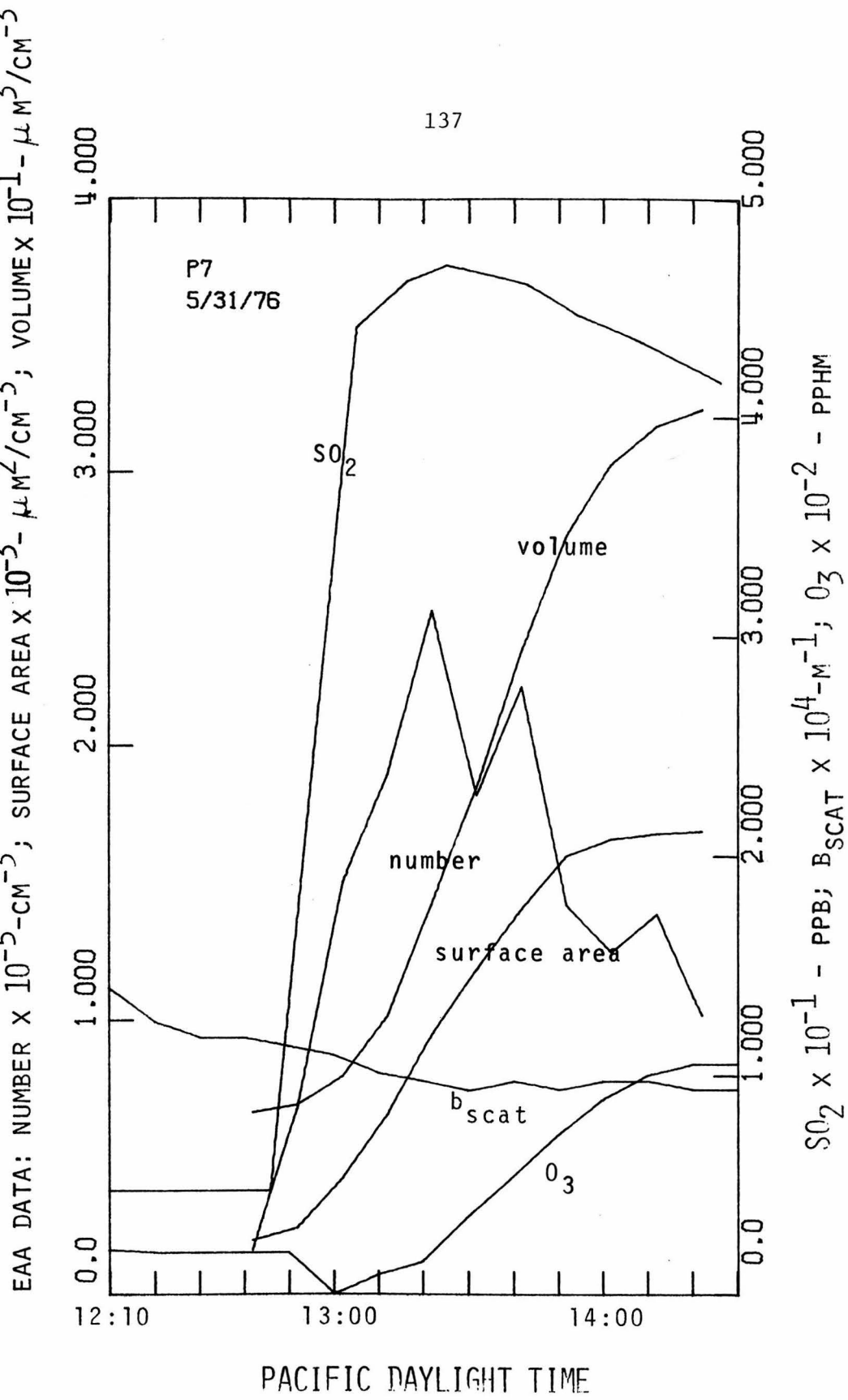
P7
5/31/76
SO2
volume
number
surface area
bscat
O3
4.000
3.000
2.000
1.000
0.0
5.000
4.000
3.000
2.000
1.000
0.0
12:10
13:00
14:00
PACIFIC DAYLIGHT TIME
EAA DATA: NUMBER X 10-5-CM-3; SURFACE AREA X 10-3- μM2/CM-3; VOLUME X 10-1- μM3/CM-3
SO2 X 10-1 - PPB; BSCAT X 10-4-M-1; O3 X 10-2 - PPHM

SIZE DISTRIBUTION DATA FROM EXPERIMENT P7

DATE 8/31/76

NUMBER PER CM3 IN EACH SIZE INCREMENT DURING INDICATED TIME INTERVAL

DIA. LIMITS	1239-1249	1249-1259	1259-1309	1309-1319	1319-1329	1329-1339	1339-1349	1349-1359	1359-1409	1409-1419	1419-1429	1429-1439
ELECTRICAL AEROSOL ANALYZER DATA												
1.000E-02	6.787E 02	1.018E 03	4.394E 04	3.580E 04	1.086E 04	4.072E 03	0.0	1.357E 03	2.715E 03	6.787E 03	2.715E 03	4.072E 03
1.780E-02	8.836E 03	8.700E 03	1.223E 04	1.053E 05	1.498E 05	1.226E 05	1.077E 05	6.362E 04	4.241E 04	2.556E 04	1.522E 04	1.305E 04
3.160E-02	2.478E 03	2.549E 03	3.080E 03	4.390E 03	2.135E 04	4.145E 04	4.347E 04	5.600E 04	5.041E 04	3.880E 04	3.342E 04	2.747E 04
5.620E-02	2.565E 03	2.746E 03	3.180E 03	3.505E 03	6.630E 03	1.765E 04	2.743E 04	3.353E 04	3.973E 04	4.659E 04	4.853E 04	4.851E 04
1.000E-01	1.383E 03	1.402E 03	1.471E 03	1.481E 03	1.530E 03	2.089E 03	3.481E 03	4.972E 03	6.325E 03	6.992E 03	7.590E 03	8.257E 03
1.780E-01	5.000E 00	5.003E 00	1.501E 01	5.504E 01	1.101E 02	1.351E 02	1.751E 02	3.152E 02	4.603E 02	5.404E 02	5.904E 02	6.054E 02
3.160E-01												
OPTICAL PARTICLE COUNTER DATA												
3.770E-01	2.601E 01	2.501E 01	2.428E 01	2.347E 01	2.330E 01	2.296E 01	2.254E 01	2.225E 01	2.106E 01	2.079E 01	1.996E 01	1.840E 01
4.670E-01	1.158E 01	1.087E 01	1.095E 01	1.042E 01	1.025E 01	1.052E 01	9.843E 00	9.977E 00	9.348E 00	9.341E 00	8.898E 00	8.223E 00
5.640E-01	4.533E 00	4.327E 00	4.033E 00	4.042E 00	4.012E 00	4.065E 00	4.137E 00	3.867E 00	3.858E 00	3.575E 00	3.553E 00	3.327E 00
6.600E-01	2.282E 00	2.150E 00	2.047E 00	1.938E 00	1.923E 00	2.008E 00	1.975E 00	1.850E 00	1.712E 00	1.707E 00	1.705E 00	1.570E 00
7.510E-01	1.187E 00	9.817E-01	9.867E-01	8.950E-01	8.283E-01	8.783E-01	8.616E-01	8.633E-01	7.553E-01	7.500E-01	7.416E-01	7.050E-01
8.190E-01	6.400E-01	5.433E-01	5.700E-01	5.200E-01	4.983E-01	5.050E-01	5.067E-01	4.817E-01	4.483E-01	4.033E-01	4.783E-01	3.867E-01
8.760E-01	4.550E-01	4.100E-01	4.067E-01	3.867E-01	3.183E-01	3.650E-01	3.017E-01	3.117E-01	3.267E-01	3.150E-01	2.767E-01	2.783E-01
9.280E-01	3.850E-01	2.933E-01	2.950E-01	2.600E-01	2.450E-01	2.350E-01	2.217E-01	2.333E-01	2.300E-01	1.833E-01	2.017E-01	2.300E-01
9.790E-01	2.967E-01	2.533E-01	2.433E-01	1.983E-01	2.317E-01	2.183E-01	2.283E-01	2.067E-01	2.033E-01	1.617E-01	1.850E-01	1.717E-01
1.040E 00	2.183E-01	2.100E-01	1.867E-01	1.800E-01	1.883E-01	1.550E-01	1.900E-01	1.300E-01	1.567E-01	9.666E-02	1.400E-01	1.367E-01
1.110E 00	2.283E-01	1.867E-01	1.833E-01	1.700E-01	1.317E-01	1.533E-01	1.150E-01	1.200E-01	1.400E-01	1.233E-01	1.400E-01	1.100E-01
1.210E 00	1.800E-01	1.400E-01	1.350E-01	1.317E-01	1.250E-01	1.150E-01	1.083E-01	1.183E-01	1.067E-01	8.500E-02	7.666E-02	8.500E-02
1.350E 00	9.667E-02	9.667E-02	7.333E-02	9.333E-02	6.000E-02	7.333E-02	7.500E-02	6.500E-02	6.333E-02	5.000E-02	6.166E-02	6.667E-02
1.480E 00												

PROCEDURE AND SO2, TEMPERATURE, AND RELATIVE HUMIDITY DATA FOR EXPERIMENT P12

THE BAG WAS FILLED FROM 14:15 TO 14:18

THE BAG WAS NOT COVERED DURING THE FILLING PROCESS

THE AIR WAS NOT FILTERED DURING THE FILLING PROCESS

REACTANTS ADDED TO THE SYSTEM:

REACTANT	AMOUNT ADDED - CM3	TIME ADDED
NO	21.50	14:15
NO2	10.40	15:20
SO2	10.40	15:20
PROPYLENE	65.00	15:20

TIME	SO2	TIME	TEMPERATURE - DEG C	RELATIVE HUMIDITY
15:24	179.80	15:24	35.	35.
15:27	183.60	16:15	34.	37.
15:31	185.00	16:51	31.	43.
15:39	187.80			
15:45	186.80			
15:59	183.30			
16:06	180.30			
16:11	178.60			
16:17	178.60			
16:20	177.20			
16:29	176.50			
16:37	175.60			
16:45	174.70			

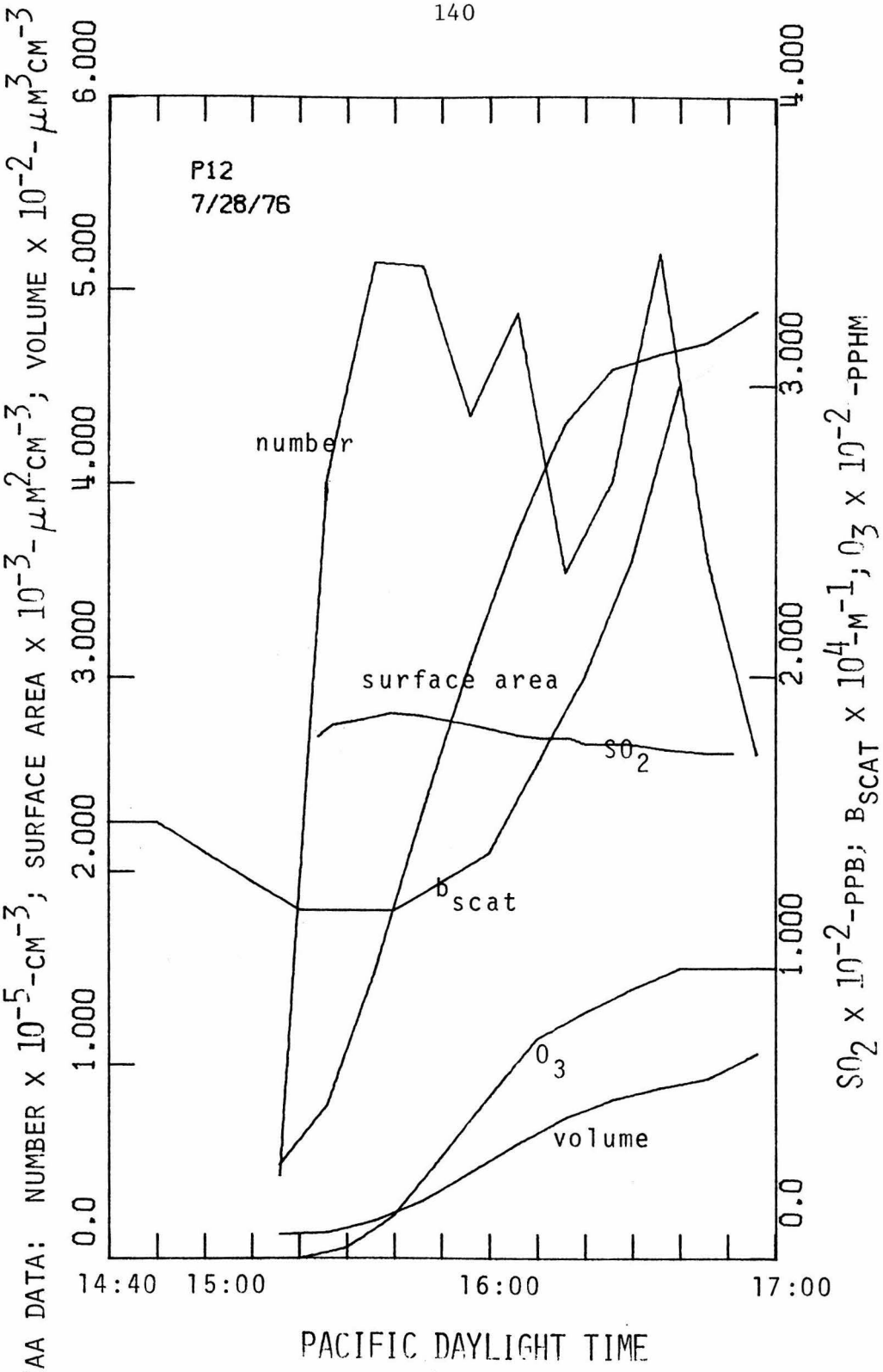
P12
7/28/76
number
surface area
SO_2
b_{scat}
O_3
volume
EAA DATA: NUMBER X 10^{-5}-CM^{-3}; SURFACE AREA X 10^{-3}-μM^{2}CM^{-3}; VOLUME X 10^{-2}-μM^{3}CM^{-3}
SO_2 X 10^{-2}-PPB; B_{SCAT} X 10^{4}-M^{-1}; O_3 X 10^{-2}-PPHM
0.0
1.000
2.000
3.000
4.000
5.000
6.000
14:40
15:00
16:00
17:00
PACIFIC DAYLIGHT TIME

SIZE DISTRIBUTION DATA FROM EXPERIMENT P12

CATE 7/28/76

NUMBER PER CM3 IN EACH SIZE INCREMENT DURING INDICATED TIME INTERVAL

DIA. LIMITS	1501-1511	1511-1521	1521-1531	1531-1541	1541-1551	1551-1601	1601-1611	1611-1621	1621-1631	1631-1641	1641-1651	1651-1701
ELECTRICAL AEROSOL ANALYZER DATA												
1.000E-02	6.872E 03	5.090E 03	2.998E 05	9.773E 04	5.904E 04	2.204E 04	2.063E 30	4.072E 03	0.0	6.108E 03	0.0	1.425E 04
1.780E-02	2.161E 04	1.988E 04	8.421E 04	3.602E 05	3.173E 05	2.006E 05	1.126E 05	5.954E 04	3.344E 04	2.039E 04	1.957E 04	4.894E 03
3.160E-02	8.071E 03	7.593E 03	9.186E 03	3.860E 04	8.581E 04	1.334E 05	1.126E 05	9.643E 04	6.797E 04	5.183E 04	4.036E 04	4.206E 04
5.620E-02	7.886E 03	7.696E 03	8.618E 03	1.474E 04	4.504E 04	6.824E 04	1.069E 05	1.278E 05	1.358E 05	1.325E 05	1.288E 05	1.186E 05
1.000E-01	2.648E 03	2.471E 03	2.618E 03	2.780E 03	5.281E 03	9.620E 03	1.309E 04	1.873E 04	2.437E 04	2.789E 04	3.041E 04	3.114E 04
1.780E-01	3.903E 02	3.602E 02	3.452E 02	4.728E 02	4.428E 02	7.055E 02	1.043E 03	1.246E 03	1.321E 03	1.509E 03	1.681E 03	2.739E 03
3.160E-01												
OPTICAL PARTICLE COUNTER DATA												
3.770E-01	2.515E 01	2.389E 01	2.252E 01	2.271E 01	2.069E 01	1.926E 01	1.834E 01	1.745E 01	1.985E 01	2.067E 01	2.222E 01	2.448E 01
4.670E-01	1.096E 01	1.053E 01	9.937E 00	1.022E 01	8.970E 00	8.898E 00	8.566E 00	7.908E 00	1.016E 01	1.098E 01	1.244E 01	1.396E 01
5.640E-01	3.555E 00	3.407E 00	3.062E 00	3.335E 00	2.872E 00	2.787E 00	2.725E 00	2.670E 00	3.757E 00	4.215E 00	4.883E 00	5.887E 00
6.600E-01	1.788E 00	1.720E 00	1.570E 00	1.823E 00	1.462E 00	1.437E 00	1.318E 00	1.308E 00	2.165E 00	2.593E 00	2.998E 00	3.960E 00
7.510E-01	7.100E-01	7.333E-01	7.083E-01	8.333E-01	6.717E-01	6.400E-01	6.016E-01	5.833E-01	1.130E 00	1.413E 00	1.682E 00	1.995E 00
8.190E-01	3.917E-01	4.000E-01	3.933E-01	4.433E-01	3.950E-01	3.167E-01	3.000E-01	3.217E-01	6.800E-01	9.333E-01	1.163E 00	1.497E 00
8.760E-01	2.450E-01	2.517E-01	2.600E-01	3.017E-01	2.033E-01	1.400E-01	1.767E-01	1.867E-01	4.533E-01	6.100E-01	7.350E-01	8.950E-01
9.280E-01	1.667E-01	1.600E-01	1.617E-01	1.650E-01	1.367E-01	1.350E-01	1.117E-01	1.183E-01	3.417E-01	4.500E-01	5.017E-01	7.250E-01
9.790E-01	1.383E-01	1.433E-01	1.117E-01	2.050E-01	1.283E-01	1.133E-01	1.067E-01	8.333E-02	2.950E-01	4.400E-01	5.150E-01	6.833E-01
1.040E 00	1.100E-01	8.833E-02	7.333E-02	1.467E-01	6.667E-02	6.000E-02	5.167E-02	5.667E-02	2.300E-01	2.917E-01	3.683E-01	4.967E-01
1.110E 00	9.333E-02	7.833E-02	5.833E-02	8.333E-02	6.000E-02	4.833E-02	4.667E-02	3.833E-02	1.683E-01	2.567E 01	2.783E-01	3.917E-01
1.210E 00	6.167E-02	5.000E-02	5.000E-02	6.500E-02	3.500E-02	5.000E-02	2.000E-02	2.833E-02	1.200E-01	1.333E-01	1.917E-01	2.367E-01
1.350E 00	4.000E-02	2.833E-02	3.167E-02	5.000E-02	2.167E-02	1.333E-02	1.667E-02	2.833E-02	5.000E-02	8.667E-02	7.500E-02	1.500E-01
1.480E 00												

PROCEDURE AND SO2, TEMPERATURE, AND RELATIVE HUMIDITY DATA FOR EXPERIMENT P13

THE BAG WAS FILLED FROM 13:30 TO 13:35

THE BAG WAS NOT COVERED DURING THE FILLING PROCESS

THE AIR WAS NOT FILTERED DURING THE FILLING PROCESS

REACTANTS ADDED TO THE SYSTEM:

REACTANT	AMOUNT ADDED - CM3	TIME ADDED
NO	21.00	13:33
NO2	10.40	14:30
SO2	15.00	14:30
PROPYLENE	65.00	14:33

TIME	SO2	TIME	TEMPERATURE - DEG C	RELATIVE HUMIDITY
14:30	14.10	14:38	36.	30.
14:38	273.40	15:06	36.	30.
14:40	276.30	15:29	35.	32.
14:45	277.50	15:44	34.	33.
14:50	277.70	15:55	33.	35.
14:54	276.30	16:12	32.	39.
15:04	270.90			
15:08	268.60			
15:14	265.00			
15:18	262.70			
15:25	259.80			
15:32	256.90			
15:44	254.60			
15:55	254.20			
16:12	253.60			
16:22	253.60			

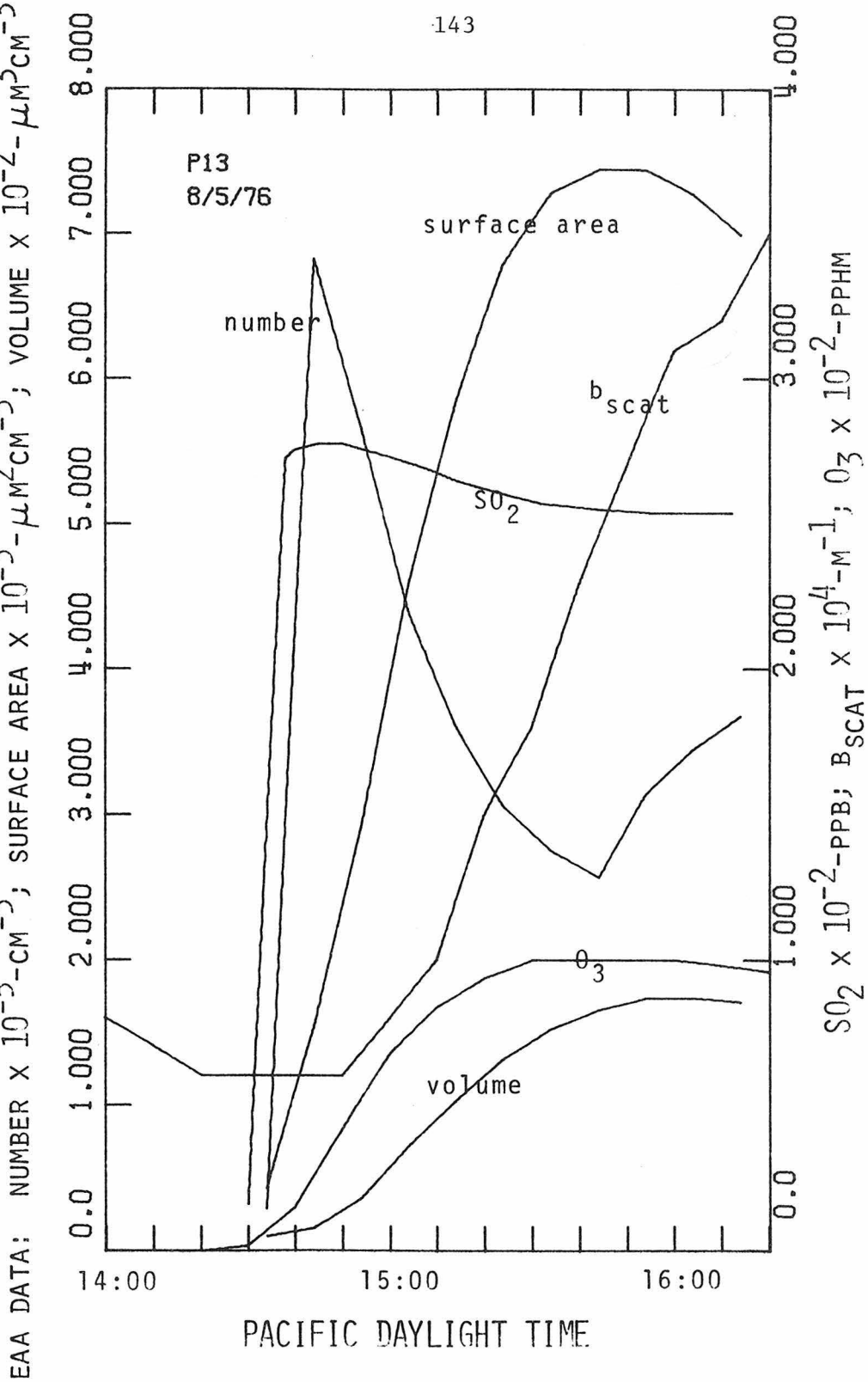
P13
8/5/76
surface area
number
b_{scat}
SO_2
O_3
volume
EAA DATA: NUMBER x 10^{-5}-CM^{-3}; SURFACE AREA x 10^{-3}-μM^{2}CM^{-3}; VOLUME x 10^{-2}-μM^{3}CM^{-3}
SO_2 x 10^{-2}-PPB; B_{SCAT} x 10^{4}-M^{-1}; O_3 x 10^{-2}-PPHM
0.0
1.000
2.000
3.000
4.000
5.000
6.000
7.000
8.000
14:00
15:00
16:00
PACIFIC DAYLIGHT TIME

SIZE DISTRIBUTION DATA FROM EXPERIMENT P13

DATE 8/5/76

NUMBER PER CM3 IN EACH SIZE INCREMENT DURING INDICATED TIME INTERVAL

DIA. LIMITS	1419-1429	1429-1439	1439-1449	1449-1459	1459-1509	1509-1519	1519-1529	1529-1539	1539-1549	1549-1559	1559-1609	1609-1619
ELECTRICAL AEROSOL ANALYZER DATA												
1.000E-02	2.036E 03	1.273E 03	1.710E 05	3.258E 04	2.036E 03	2.036E 03	6.108E 03	4.072E 03	1.832E 04	4.072E 03	1.018E 04	0.0
1.780E-02	1.305E 04	1.223E 04	4.740E 05	3.442E 05	1.411E 05	5.383E 04	1.713E 04	1.305E 04	5.709E 03	8.972E 03	3.262E 03	6.525E 03
3.160E-02	5.841E 03	5.204E 03	2.522E 04	1.202E 05	1.560E 05	1.028E 05	5.352E 04	2.846E 04	1.954E 04	1.020E 04	9.770E 03	6.797E 03
5.620E-02	7.751E 03	7.669E 03	1.065E 04	6.133E 04	1.204E 05	1.728E 05	1.808E 05	1.711E 05	1.466E 05	1.262E 05	1.099E 05	9.713E 04
1.000E-01	3.148E 03	2.971E 03	3.207E 03	7.252E 03	1.693E 04	2.757E 04	4.526E 04	5.463E 04	6.199E 04	6.627E 04	6.705E 04	6.614E 04
1.780E-01	2.777E 02	2.477E 02	3.077E 02	4.503E 02	1.373E 03	2.086E 03	2.702E 03	3.775E 03	4.616E 03	5.223E 03	5.494E 03	5.569E 03
3.160E-01												
OPTICAL PARTICLE COUNTER DATA												
3.770E-01	6.063E 00	5.732E 00	5.575E 00	4.947E 00	4.757E 00	4.472E 00	4.150E 00	3.935E 00	3.697E 00	3.377E 00	3.237E 00	3.148E 00
4.670E-01	2.348E 00	2.415E 00	2.168E 00	2.068E 00	1.885E 00	1.718E 00	1.615E 00	1.433E 00	1.368E 00	1.322E 00	1.190E 00	1.102E 00
5.640E-01	9.350E-01	9.283E-01	8.366E-01	7.133E-01	7.050E-01	6.733E-01	5.833E-01	5.617E-01	4.483E-01	4.333E-01	4.283E-01	3.500E-01
6.600E-01	5.667E-01	6.417E-01	5.817E-01	5.050E-01	4.583E-01	4.450E-01	3.733E-01	3.517E-01	3.367E-01	2.433E-01	2.750E-01	2.067E-01
7.510E-01	3.633E-01	3.750E-01	3.700E-01	3.517E-01	2.667E-01	2.467E-01	2.383E-01	2.183E-01	1.983E-01	1.867E-01	1.500E-01	1.583E-01
8.190E-01	2.717E-01	2.600E-01	2.833E-01	1.983E-01	2.033E-01	1.650E-01	1.650E-01	1.300E-01	1.467E-01	1.100E-01	1.183E-01	1.000E-01
8.760E-01	1.667E-01	2.067E-01	2.250E-01	2.017E-01	1.667E-01	1.417E-01	1.633E-01	1.150E-01	1.000E-01	1.050E-01	8.500E-02	7.500E-02
9.280E-01	1.883E-01	1.800E-01	1.617E-01	1.300E-01	1.450E-01	1.000E-01	1.083E-01	8.667E-02	7.333E-02	7.333E-02	6.333E-02	7.167E-02
9.790E-01	2.150E-01	1.617E-01	1.767E-01	1.450E-01	1.367E-01	1.250E-01	9.500E-02	1.150E-01	7.667E-02	7.833E-02	7.833E-02	8.167E-02
1.040E 00	1.483E-01	1.400E-01	1.317E-01	1.167E-01	1.067E-01	9.667E-02	8.667E-02	6.667E-02	7.833E-02	8.166E-02	5.333E-02	7.167E-02
1.110E 00	1.267E-01	1.550E-01	1.317E-01	1.317E-01	1.033E-01	8.333E-02	8.167E-02	8.000E-02	5.500E-02	7.666E-02	4.167E-02	5.333E-02
1.210E 00	1.300E-01	1.333E-01	1.033E-01	1.183E-01	1.033E-01	8.167E-02	7.500E-02	6.167E-02	6.333E-02	6.000E-02	5.333E-02	3.667E-02
1.350E 00	7.667E-02	9.500E-02	6.333E-02	4.333E-02	5.000E-02	3.500E-02	5.667E-02	4.667E-02	4.000E-02	3.000E-02	1.833E-02	1.667E-02
1.480E 00												

PROCEDURE AND SO2, TEMPERATURE, AND RELATIVE HUMIDITY DATA FOR EXPERIMENT P14

THE BAG WAS FILLED FROM 09:40 TO 09:45

THE BAG WAS NOT COVERED DURING THE FILLING PROCESS

THE AIR WAS NOT FILTERED DURING THE FILLING PROCESS

REACTANTS ADDED TO THE SYSTEM:

REACTANT	AMOUNT ADDED - CM3	TIME ADDED
NO	20.40	09:44
NO2	10.50	10:49
SO2	20.00	10:49
PROPYLENE	65.00	10:51

TIME	SO2	TIME	TEMPERATURE - DEG C	RELATIVE HUMIDITY
09:50	12.72	10:35	30.	42.
10:58	348.70	11:09	34.	35.
11:02	354.60	11:35	34.	33.
11:09	355.40	11:51	35.	32.
11:16	354.60	12:14	38.	27.
11:21	352.60	12:25	38.	27.
11:26	349.90			
11:30	347.40			
11:35	343.80			
11:41	339.40			
11:46	336.20			
11:51	333.50			
11:56	330.40			
12:08	326.40			
12:14	324.20			
12:20	322.60			
12:25	321.50			

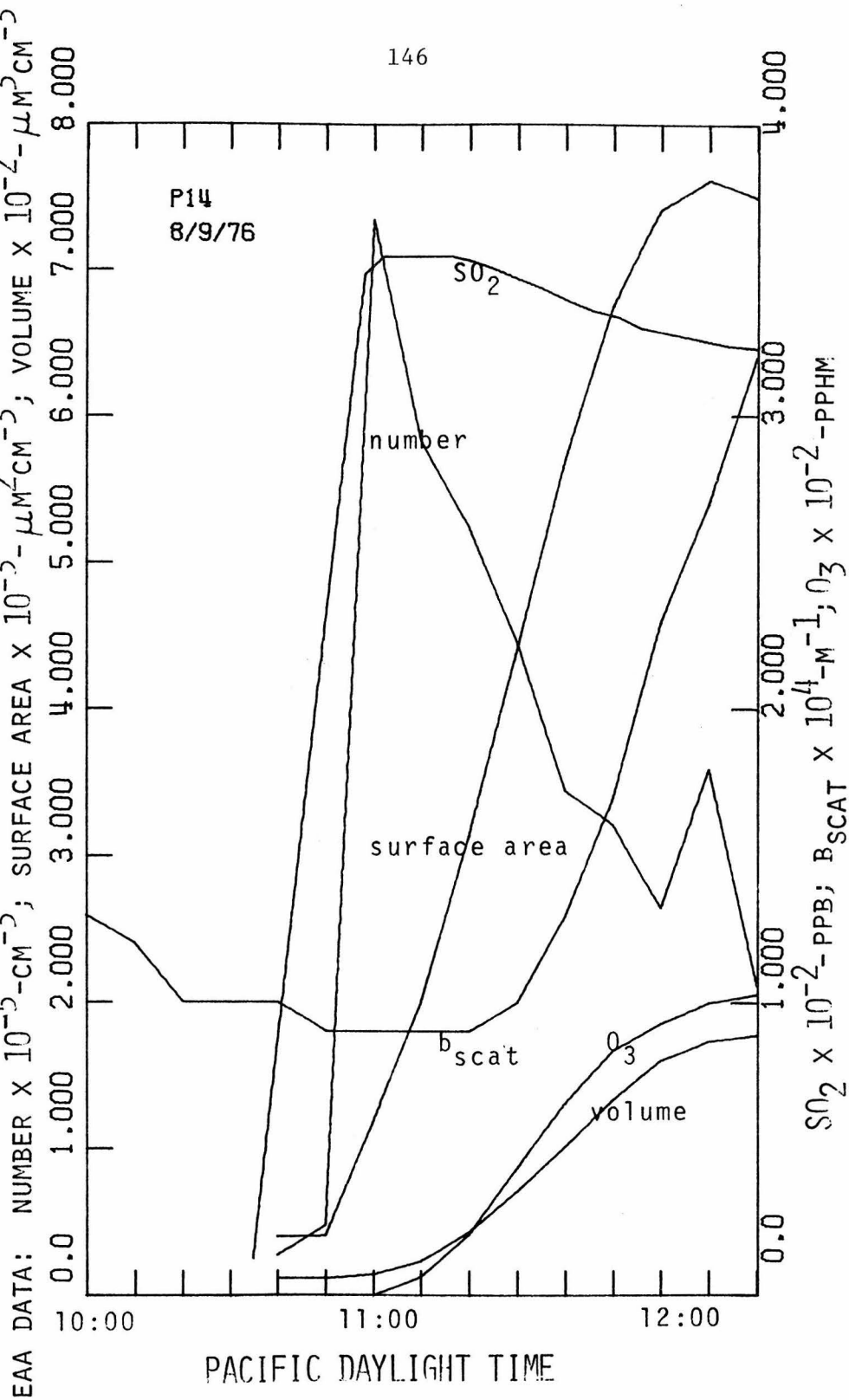
P14
8/9/76
SO_2
number
surface area
b_{scat}
O_3
volume
EAA DATA: NUMBER X 10^{-5}-CM^{-3}; SURFACE AREA X 10^{-3}-$\mu M^2 CM^{-3}$; VOLUME X 10^{-2}-$\mu M^3 CM^{-3}$
SO_2 X 10^{-2}-PPB; B_{SCAT} X 10^{4}-M^{-1}; O_3 X 10^{-2}-PPHM
0.0
1.000
2.000
3.000
4.000
5.000
6.000
7.000
8.000
10:00
11:00
12:00
PACIFIC DAYLIGHT TIME

SIZE DISTRIBUTION DATA FROM EXPERIMENT P14

DATE 8/9/76

NUMBER PER CM3 IN EACH SIZE INCREMENT DURING INDICATED TIME INTERVAL

DIA. LIMITS	1024-1035	1035-1045	1045-1055	1055-1105	1105-1115	1115-1125	1125-1135	1135-1155	1155-1155	1155-1205	1205-1215	1215-1225
ELECTRICAL AEROSOL ANALYZER DATA												
1.000E-02	3.224E 03	3.902E 03	1.306E 04	3.485E 05	8.144E 04	4.208E 04	5.429E 03	5.429E 03	0.0	6.787E 03	5.429E 03	2.715E 03
1.780E-02	1.189E 04	1.142E 04	1.128E 04	3.034E 05	3.909E 05	2.773E 05	1.365E 05	4.839E 04	1.577E 04	9.787E 03	4.894E 03	5.981E 03
3.160E-02	4.602E 03	4.283E 03	4.177E 03	1.108E 04	7.788E 04	1.272E 05	1.334E 05	9.176E 04	4.928E 04	2.464E 04	1.529E 04	1.020E 04
5.620E-02	5.637E 03	5.149E 03	5.366E 03	6.522E 03	2.878E 04	6.741E 04	1.217E 05	1.659E 05	1.766E 05	1.607E 05	1.380E 05	1.190E 05
1.000E-01	2.815E 03	2.638E 03	2.501E 03	2.726E 03	3.648E 03	9.228E 03	1.582E 04	2.922E 04	4.494E 04	5.847E 04	6.642E 04	6.863E 04
1.780E-01	4.053E 02	3.452E 02	3.602E 02	3.702E 02	3.753E 02	7.205E 02	1.431E 03	1.966E 03	3.002E 03	4.188E 03	4.958E 03	5.369E 03
3.160E-01												
OPTICAL PARTICLE COUNTER DATA												
3.770E-01	1.596E 01	1.425E 01	1.408E 01	1.259E 01	1.151E 01	1.035E 01	9.927E 00	9.267E 00	8.592E 00	8.048E 00	7.488E 00	7.383E 00
4.670E-01	5.947E 00	5.485E 00	5.290E 00	4.762E 00	4.265E 00	4.002E 00	3.592E 00	3.335E 00	3.212E 00	3.048E 00	2.778E 00	2.573E 00
5.640E-01	1.950E 00	1.723E 00	1.653E 00	1.558E 00	1.428E 00	1.337E 00	1.207E 00	1.165E 00	1.097E 00	1.073E 00	9.816E-01	9.100E-01
6.600E-01	1.103E 00	9.417E-01	1.007E 00	9.183E-01	8.300E-01	8.117E-01	8.167E-01	7.650E-01	6.633E-01	6.050E-01	5.976E-01	5.150E-01
7.510E-01	6.633E-01	5.517E-01	5.567E-01	5.333E-01	5.150E-01	4.317E-01	4.283E-01	4.667E-01	4.000E-01	3.800E-01	3.617E-01	3.700E-01
8.190E-01	4.933E-01	4.517E-01	4.000E-01	4.233E-01	3.217E-01	3.233E-01	3.100E-01	2.983E-01	2.850E-01	2.300E-01	2.333E-01	2.383E-01
8.760E-01	3.333E-01	3.283E-01	2.900E-01	2.967E-01	2.733E-01	2.483E-01	2.633E-01	2.517E-01	2.383E-01	2.067E-01	1.750E-01	1.717E-01
9.280E-01	2.850E-01	2.900E-01	2.933E-01	2.417E-01	2.417E-01	2.267E-01	1.967E-01	1.483E-01	1.500E-01	1.567E-01	1.683E-01	1.200E-01
9.790E-01	3.150E-01	3.333E-01	2.767E-01	2.450E-01	2.183E-01	2.167E-01	1.967E-01	2.083E-01	1.933E-01	1.933E-01	1.600E-01	1.417E-01
1.040E 00	2.767E-01	2.800E-01	2.283E-01	1.967E-01	2.233E-01	1.800E-01	1.783E-01	1.517E-01	1.333E-01	1.417E-01	1.150E-01	1.317E-01
1.110E 00	2.983E-01	2.750E-01	2.433E-01	2.167E-01	2.100E-01	1.483E-01	1.800E-01	1.467E-01	1.400E-01	1.033E-01	1.367E-01	1.017E-01
1.210E 00	2.383E-01	2.167E-01	1.950E-01	1.767E-01	1.883E-01	1.167E-01	1.300E-01	1.017E-01	1.183E-01	9.167E-02	7.166E-02	1.083E-01
1.350E 00	1.617E-01	1.317E-01	9.500E-02	1.200E-01	1.033E-01	9.333E-02	6.333E-02	6.833E-02	7.000E-02	4.667E-02	4.833E-02	4.667E-02
1.480E 00												

PROCEDURE AND SO2, TEMPERATURE, AND RELATIVE HUMIDITY DATA FOR EXPERIMENT P15

THE BAG WAS FILLED FROM 12:35 TO 12:40

THE BAG WAS NOT COVERED DURING THE FILLING PROCESS

THE AIR WAS NOT FILTERED DURING THE FILLING PROCESS

REACTANTS ADDED TO THE SYSTEM:

REACTANT	AMOUNT ADDED - CM3	TIME ADDED
NO	33.00	12:38
NO2	16.00	14:10
SO2	70.00	14:10
PROPYLENE	100.00	14:12

TIME	SO2	TIME	TEMPERATURE - DEG C	RELATIVE HUMIDITY
13:06	16.88	13:06	37.	24.
14:17	424.20	14:19	38.	21.
14:20	423.40	14:43	38.	21.
14:25	418.20	15:07	37.	22.
143:0	410.10			
14:37	396.90			
14:43	387.60			
14:47	382.90			
14:51	377.50			
14:55	373.60			
15:01	369.30			
15:07	366.20			
15:13	364.30			
15:21	363.40			
15:37	362.70			
16:04	360.00			
16:19	358.80			
16:31	358.40			
16:42	357.60			

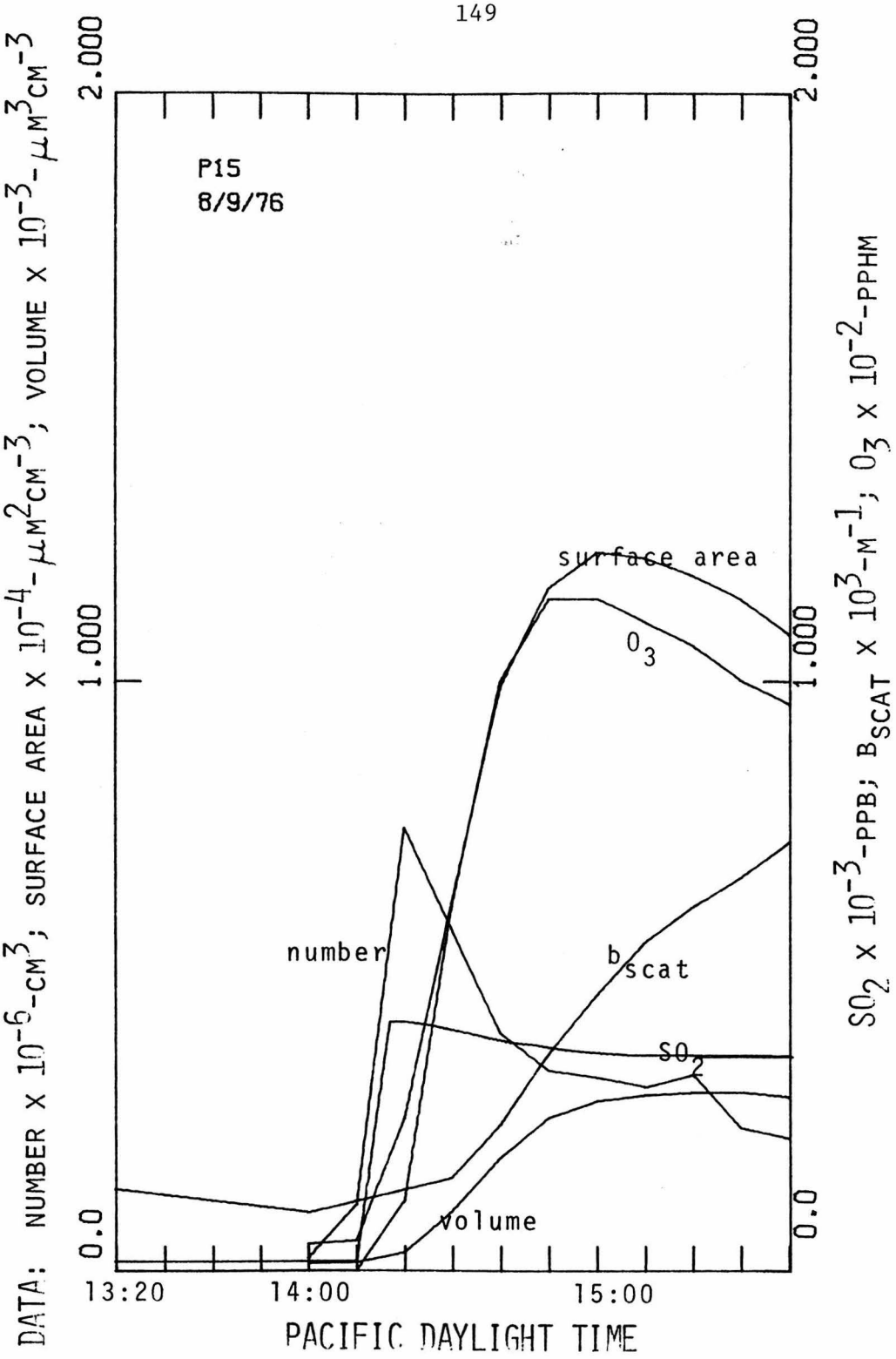
P15
8/9/76
surface area
O_3
number
b_{scat}
SO_2
volume
2.000
1.000
0.0
13:20
14:00
15:00
PACIFIC DAYLIGHT TIME
EAA DATA: NUMBER X 10^{-6}-CM^3; SURFACE AREA X 10^{-4}-μM^{2}CM^{-3}; VOLUME X 10^{-3}-μM^{3}CM^{-3}
SO_2 X 10^{-3}-PPB; B_{SCAT} X 10^3-M^{-1}; O_3 X 10^{-2}-PPHM

SIZE DISTPIBUTION DATA FROM EXPERIMENT P15

CATE 8/9/76 1

NUMBER PER CM3 IN EACH SIZE INCREMENT DURING INDICATED TIME INTERVAL

DIA. LIMITS	1345-1355	1355-1405	1405-1415	1415-1425	1425-1435	1435-1445	1445-1455	1455-1505	1505-1515	1515-1525	1525-1535	1535-5450
ELECTRICAL AEROSOL ANALYZER DATA												
1.000E-02	1.697E 03	2.375E 03	8.382E 04	6.244E 04	0.0	0.0	0.0	5.429E 03	1.222E 04	5.429E 03	4.072E 03	9.501E 03
1.780E-02	7.884E 03	7.204E 03	9.651E 03	5.630E 05	1.778E 05	0.0	0.0	1.631E 03	8.700E 03	8.700E 03	4.894E 03	4.894E 03
3.160E-02	3.929E 03	3.752E 03	3.682E 03	8.655E 04	2.093E 05	5.211E 04	0.0	5.381E 03	6.514E 03	3.682E 03	4.531E 03	3.682E 03
5.620E-02	6.070E 03	5.781E 03	5.727E 03	3.503E 04	1.688E 05	2.827E 05	2.343E 05	1.941E 05	1.578E 05	1.270E 05	1.044E 05	8.773E 04
1.000E-01	3.324E 03	3.069E 03	2.942E 03	4.835E 03	2.169E 04	6.336E 04	9.714E 04	1.127E 05	1.163E 05	1.161E 05	1.123E 05	1.073E 05
1.780E-01	5.254E 02	4.553E 02	4.753E 02	5.604E 02	2.011E 03	3.898E 03	7.159E 03	8.716E 03	9.902E 03	1.086E 04	1.163E 04	1.179E 04
3.160E-01												
OPTICAL PARTICLE COUNTER DATA												
3.770E-01	1.953E 01	1.786E 01	2.226E 01	2.435E 01	2.289E 01	2.127E 01	1.992E 01	1.847E 01	1.713E 01	1.606E 01	1.502E 01	1.372E 01
4.670E-01	6.547E 00	5.972E 00	8.810E 00	1.032E 01	9.618E 00	8.820E 00	8.162E 00	7.330E 00	6.738E 00	6.043E 00	5.588E 00	4.983E 00
5.640E-01	1.872E 00	1.758E 00	3.028E 00	3.648E 00	3.418E 00	2.975E 00	2.725E 00	2.472E 00	2.315E 00	1.953E 00	1.845E 00	1.572E 00
6.600E-01	1.067E 00	9.333E-01	1.673E 00	2.045E 00	1.927E 00	1.880E 00	1.710E 00	1.520E 00	1.315E 00	1.190E 00	1.083E 00	1.030E 00
7.510E-01	5.233E-01	5.667E-01	9.833E-01	1.145E 00	1.088E 00	9.716E-01	8.017E-01	7.667E-01	7.233E-01	6.767E-01	5.367E-01	5.083E-01
8.190E-01	4.417E-01	3.650E-01	5.883E-01	6.833E-01	6.100E-01	5.950E-01	5.550E-01	4.667E-01	4.300E-01	3.683E-01	3.783E-01	3.367E-01
8.760E-01	3.083E-01	2.600E-01	4.533E-01	4.800E-01	4.800E-01	4.050E-01	3.550E-01	3.183E-01	3.000E-01	2.567E-01	2.450E-01	2.217E-01
9.280E-01	2.533E-01	1.933E-01	3.133E-01	3.283E-01	3.217E-01	2.833E-01	2.533E-01	2.283E-01	2.067E-01	2.217E-01	1.817E-01	1.617E-01
9.790E-01	2.817E-01	2.067E-01	2.867E-01	3.083E-01	2.467E-01	2.417E-01	2.067E-01	2.000E-01	1.783E-01	1.817E-01	1.383E-01	1.217E-01
1.040E 00	2.233E-01	2.200E-01	2.683E-01	2.250E-01	2.150E-01	1.650E-01	1.833E-01	1.300E-01	1.700E-01	1.083E-01	9.333E-02	1.017E-01
1.110E 00	2.117E-01	1.833E-01	1.767E-01	1.983E-01	1.683E-01	1.333E-01	1.333E-01	1.117E-01	1.150E-01	9.500E-02	7.500E-02	9.167E-02
1.210E 00	1.683E-01	1.383E-01	1.450E-01	1.200E-01	1.250E-01	1.033E-01	8.667E-02	9.667E-02	6.833E-02	7.833E-02	7.833E-02	5.500E-02
1.350E 00	1.117E-01	9.833E-02	8.333E-02	7.500E-02	8.000E-02	7.000E-02	5.500E-02	6.333E-02	4.500E-02	4.667E-02	4.167E-02	3.667E-02
1.480E 00												

PROCEDURE AND SO2, TEMPERATURE, AND RELATIVE HUMIDITY DATA FOR EXPERIMENT P16

THE BAG WAS FILLED FROM 09:58 TO 10:03

THE BAG WAS NOT COVERED DURING THE FILLING PROCESS

THE AIR WAS NOT FILTERED DURING THE FILLING PROCESS

REACTANTS ADDED TO THE SYSTEM:

REACTANT	AMOUNT ADDED - CM3	TIME ADDED
NO	33.00	10:00
NO2	16.00	11:29
SO2	25.00	11:29
PROPYLENE	150.00	11:31

TIME	SO2	TIME	TEMPERATURE - DEG C	RELATIVE HUMIDITY
11:38	417.90	11:32	38.	28.
11:40	414.00	11:54	39.	26.
11:43	408.60	12:14	40.	25.
11:45	400.80	13:20	40.	26.
11:47	396.00			
11:49	389.10			
11:52	381.40			
11:54	375.90			
11:56	371.90			
11:58	366.60			
12:00	362.70			
12:02	359.20			
12:04	356.50			
12:07	352.60			
12:08	350.80			
12:10	348.90			
12:12	347.60			
12:14	346.30			
12:16	345.20			
12:18	344.40			
12:22	343.60			
12:25	342.60			
12:33	342.50			
12:48	342.90			

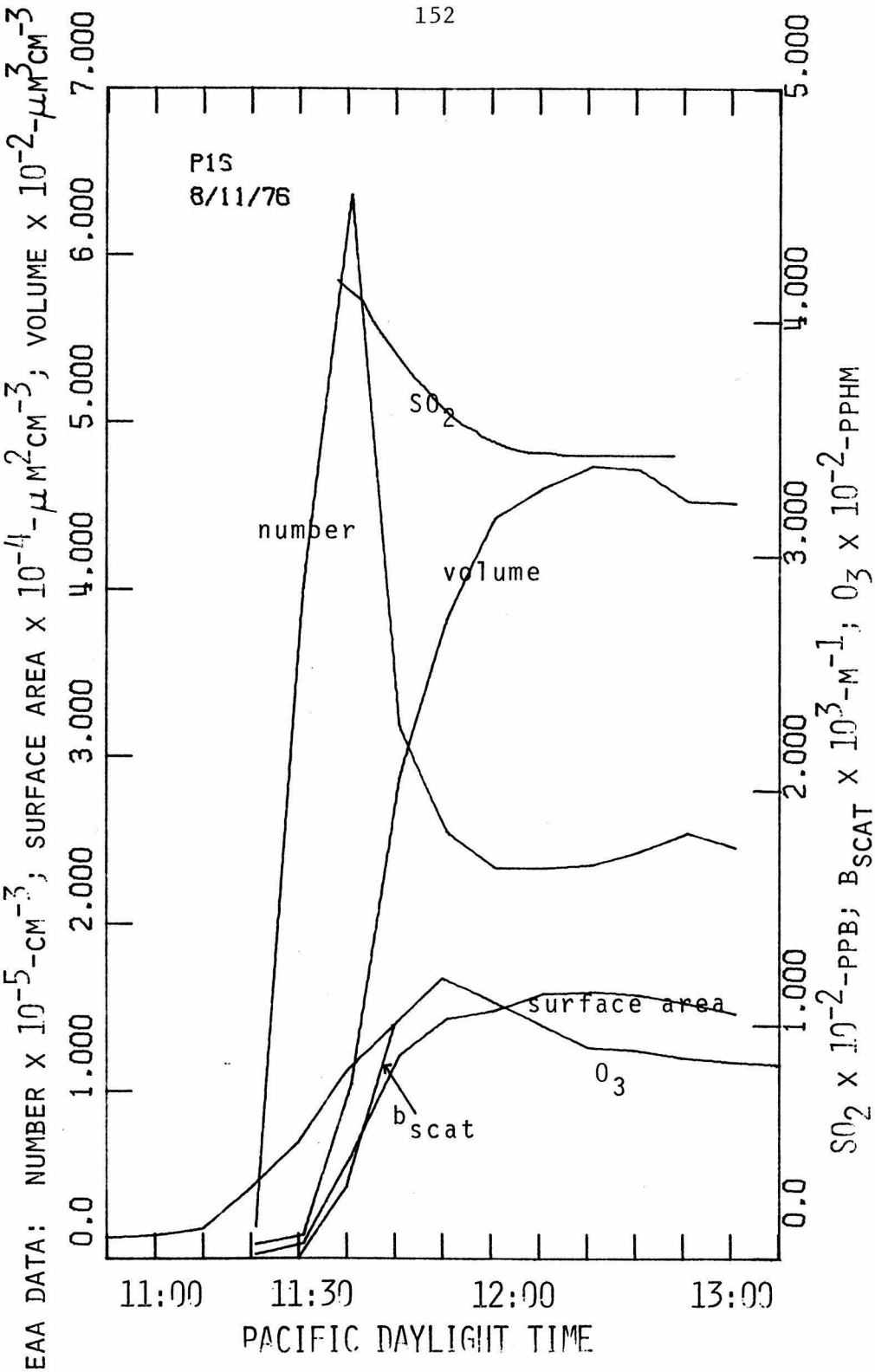
P1S
8/11/76
number
volume
surface area
SO_2
O_3
b_{scat}
EAA DATA: NUMBER X 10^{-5}-CM^{-3}; SURFACE AREA X 10^{-4}-$\mu M^2 CM^{-3}$; VOLUME X 10^{-2}-$\mu M^3 CM^{-3}$
SO_2 X 10^{-2}-PPB; B_{SCAT} X 10^{3}-M^{-1}; O_3 X 10^{-2}-PPHM
0.0
1.000
2.000
3.000
4.000
5.000
6.000
7.000
11:00
11:30
12:00
13:00
PACIFIC DAYLIGHT TIME

SIZE DISTRIBUTION DATA FROM EXPERIMENT P16

CATE 8/11/76

NUMBER PER CM3 IN EACH SIZE INCREMENT DURING INDICATED TIME INTERVAL

DIA. LIMITS	1106-1116	1116-1126	1126-1136	1136-1146	1146-1156	1156-1206	1206-1216	1216-1226	1226-1236	1236-1246	1246-1256	1256-1306
ELECTRICAL AEROSOL ANALYZER DATA												
1.000E-02	2.715E 03	2.206E 03	1.257E 05	0.0	0.0	0.0	0.0	0.0	0.0	0.0	1.222E 04	2.986E 04
1.780E-02	9.243E 03	9.379E 03	2.565E 05	2.583E 05	0.0	0.0	0.0	0.0	0.0	0.0	7.069E 03	3.806E 03
3.160E-02	2.797E 03	2.655E 03	1.260E 04	1.609E 05	0.0	0.0	0.0	0.0	0.0	0.0	1.133E 03	2.832E 03
5.620E-02	3.126E 03	3.071E 03	4.860E 03	1.929E 05	1.915E 05	6.721E 04	3.194E 04	3.859E 04	4.741E 04	6.649E 04	6.721E 04	5.290E 04
1.000E-01	1.726E 03	1.598E 03	1.873E 03	2.355E 04	1.190E 05	1.754E 05	1.847E 05	1.762E 05	1.684E 05	1.564E 05	1.461E 05	1.345E 05
1.780E-01	2.051E 02	2.101E 02	2.752E 02	1.656E 03	7.745E 03	1.219E 04	1.694E 04	1.923E 04	2.040E 04	2.116E 04	2.121E 04	2.218E 04
3.160E-01												
OPTICAL PARTICLE COUNTER DATA												
3.770E-01	2.051E 01	1.917E 01	2.242E 01	2.232E 01	2.227E 01	2.182E 01	2.048E 01	1.993E 01	3.666E 01	3.351E 01	1.809E 01	3.167E 01
4.670E-01	9.983E 00	9.326E 00	1.239E 01	1.294E 01	1.264E 01	1.197E 01	1.121E 01	1.065E 01	2.185E 01	2.007E 01	1.003E 01	1.819E 01
5.640E-01	3.605E 00	3.330E 00	5.225E 00	5.615E 00	5.275E 00	5.193E 00	4.710E 00	4.658E 00	9.811E 00	8.978E 00	4.295E 00	8.097E 00
6.600E-01	1.855E 00	1.720E 00	3.257E 00	3.427E 00	3.548E 00	3.485E 00	3.228E 00	3.170E 00	6.798E 00	6.210E 00	2.832E 00	5.607E 00
7.510E-01	8.567E-01	8.416E-01	1.712E 00	1.995E 00	2.015E 00	1.947E 00	1.878E 00	1.822E 00	4.007E 00	3.710E 00	1.672E 00	3.390E 00
8.190E-01	5.333E-01	5.483E-01	1.112E 00	1.380E 00	1.287E 00	1.237E 00	1.198E 00	1.173E 00	2.615E 00	2.518E 00	1.052E 00	2.168E 00
8.760E-01	3.400E-01	3.150E-01	7.533E-01	8.767E-01	8.833E-01	8.683E-01	8.567E-01	8.450E-01	1.890E 00	1.657E 00	7.633E-01	1.498E 00
9.280E-01	2.500E-01	2.250E-01	5.783E-01	6.767E-01	7.367E-01	6.117E-01	6.183E-01	6.083E-01	1.435E 00	1.333E 00	5.767E-01	1.200E 00
9.790E-01	2.483E-01	2.417E-01	4.983E-01	5.467E-01	5.300E-01	4.817E-01	5.367E-01	4.350E-01	1.242E 00	1.218E 00	4.350E-01	1.040E 00
1.040E 00	1.867E-01	1.600E-01	2.817E 00	3.600E-01	3.683E-01	3.450E-01	3.233E-01	3.100E-01	9.033E-01	9.550E-01	3.100E-01	7.817E-01
1.110E 00	1.683E-01	1.233E-01	2.200E-01	2.467E-01	2.467E-01	2.267E-01	2.617E-01	2.117E-01	7.450E-01	7.833E-01	1.817E-01	6.617E-01
1.210E 00	1.600E-01	1.317E-01	1.900E-01	1.900E-01	1.267E-01	1.517E-01	1.550E-01	1.517E-01	5.333E-01	4.500E-01	1.483E-01	3.850E-01
1.350E 00	7.333E-02	5.000E-02	6.000E-02	7.667E-02	5.000E-02	7.500E-02	6.000E-02	7.000E-02	2.850E-01	2.317E-01	6.833E-02	2.333E-01
1.480E 00												

PROCEDURE AND SO2, TEMPERATURE, AND RELATIVE HUMIDITY DATA FOR EXPERIMENT P17

THE BAG WAS FILLED FROM 13:45 TO 13:50

THE BAG WAS NOT COVERED DURING THE FILLING PROCESS

THE AIR WAS NOT FILTERED DURING THE FILLING PROCESS

REACTANTS ADDED TO THE SYSTEM:

REACTANT	AMOUNT ADDED - CM3	TIME ADDED
NO	20.40	13:47
NO2	10.40	14:46
SO2	3.25	14:48
PROPYLENE	50.00	14:49

TIME	SO2	TIME	TEMPERATURE - DEG C	RELATIVE HUMIDITY
14:20	15.19	14:20	36.	36.
14:52	81.05	14:52	37.	34.
14:58	81.05	15:11	37.	34.
15:11	79.58	15:24	37.	34.
15:19	78.34	16:03	37.	34.
15:24	77.10			
15:34	75.32			
15:40	74.50			
15:45	73.69			
15:59	72.53			
16:03	72.14			
16:19	71.60			
16:25	71.44			

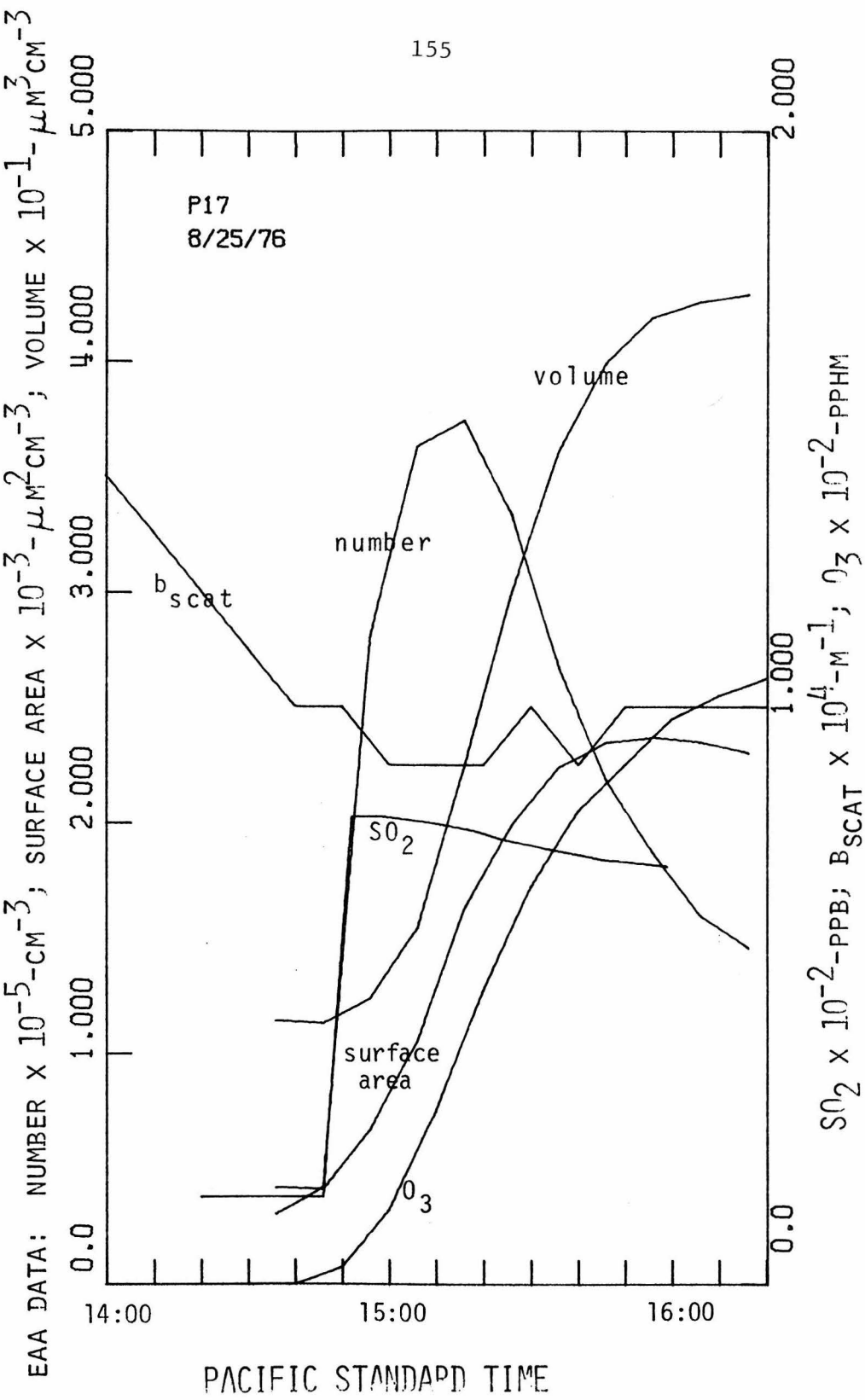
P17
8/25/76
volume
number
b_{scat}
SO_2
surface area
O_3
14:00
15:00
16:00
PACIFIC STANDARD TIME
EAA DATA: NUMBER X 10^{-5}-CM^{-3}; SURFACE AREA X 10^{-3}-μM^{2}CM^{-3}; VOLUME X 10^{-1}-μM^{3}CM^{-3}
SO_2 X 10^{-2}-PPB; B_{SCAT} X 10^{4}-M^{-1}; O_3 X 10^{-2}-PPHM
0.0
1.000
2.000
3.000
4.000
5.000
0.0
1.000
2.000

SIZE DISTRIBUTION DATA FROM EXPERIMENT P17

DATE 8/25/76

NUMBER PER CM3 IN EACH SIZE INCREMENT DURING INDICATED TIME INTERVAL

DIA. LIMITS	1421-1431	1431-1441	1441-1451	1451-1501	1501-1511	1511-1521	1521-1531	1531-1541	1541-1551	1551-1601	1601-1611	1611-1621
ELECTRICAL AEROSOL ANALYZER DATA												
1.000E-02	3.733E 03	2.545E 03	8.144E 03	1.853E 05	9.094E 04	5.972E 04	2.850E 04	1.222E 04	6.787E 03	6.787E 03	5.429E 03	5.429E 03
1.780E-02	1.400E 04	1.332E 04	1.251E 04	7.837E 04	2.362E 05	2.273E 05	1.838E 05	1.126E 05	7.069E 04	4.730E 04	2.882E 04	2.284E 04
3.160E-02	5.699E 03	5.345E 03	5.558E 03	6.797E 03	2.202E 04	5.441E 04	7.278E 04	8.269E 04	7.052E 04	5.749E 04	4.984E 04	4.078E 04
5.620E-02	6.594E 03	6.378E 03	6.522E 03	7.443E 03	1.050E 04	2.770E 04	4.023E 04	5.001E 04	5.924E 04	6.412E 04	6.415E 04	6.280E 04
1.000E-01	2.697E 03	2.550E 03	2.511E 03	2.765E 03	3.197E 03	4.217E 03	6.590E 03	8.493E 03	9.532E 03	1.022E 04	1.096E 04	1.167E 04
1.780E-01	3.502E 02	3.002E 02	2.752E 02	2.902E 02	3.402E 02	4.203E 02	5.454E 02	7.255E 02	8.406E 02	9.106E 02	9.406E 02	9.556E 02
3.160E-01												
OPTICAL PARTICLE COUNTER DATA												
3.770E-01	2.172E 01	1.927E 01	1.831E 01	1.711E 01	1.598E 01	1.484E 01	1.435E 01	1.354E 01	1.288E 01	1.194E 01	1.109E 01	1.061E 01
4.670E-01	8.588E 00	7.753E 00	7.427E 00	6.860E 00	6.390E 00	5.782E 00	5.670E 00	5.130E 00	4.947E 00	4.610E 00	4.333E 00	3.930E 00
5.640E-01	2.658E 00	2.680E 00	2.627E 00	2.380E 00	2.077E 00	1.778E 00	1.747E 00	1.583E 00	1.567E 00	1.380E 00	1.318E 00	1.153E 00
6.600E-01	1.462E 00	1.363E 00	1.523E 00	1.265E 00	1.133E 00	1.008E 00	9.233E-01	8.133E-01	7.033E-01	7.700E-01	6.550E-01	5.750E-01
7.510E-01	7.416E-01	6.667E-01	8.017E-01	7.133E-01	5.767E-01	5.550E-01	4.483E-01	4.467E-01	3.617E-01	3.700E-01	2.917E-01	3.133E-01
8.190E-01	4.450E-01	4.317E-01	5.617E-01	4.433E-01	3.867E-01	3.033E-01	3.117E-01	2.650E-01	2.367E-01	2.350E-01	1.667E-01	1.733E-01
8.760E-01	3.200E-01	2.783E-01	3.533E-01	3.067E-01	2.567E-01	2.383E-01	2.083E-01	1.900E-01	1.400E-01	1.200E-01	1.317E-01	1.350E-01
9.280E-01	2.533E-01	2.033E-01	2.533E-01	2.333E-01	1.867E-01	1.833E-01	1.600E-01	1.100E-01	1.100E-01	1.017E-01	1.000E-01	9.833E-02
9.790E-01	2.117E-01	1.850E-01	2.433E-01	1.967E-01	1.633E-01	1.483E-01	1.383E-01	9.833E-02	1.167E-01	9.500E-02	8.167E-02	6.833E-02
1.040E 00	1.650E-01	1.817E-01	1.800E-01	1.650E-01	1.433E-01	1.033E-01	9.000E-02	7.666E-02	1.067E-01	7.333E-02	6.500E-02	4.833E-02
1.110E 00	1.717E-01	1.517E-01	1.783E-01	1.583E-01	1.300E-01	1.117E-01	7.167E-02	8.166E-02	7.000E-02	4.167E-02	7.500E-02	4.333E-02
1.210E 00	1.400E-01	9.500E-02	1.483E-01	1.000E-01	1.167E-01	8.002E-02	8.000E-02	8.166E-02	7.167E-02	5.167E-02	4.500E-02	4.167E-02
1.350E 00	8.666E-02	6.000E-02	8.000E-02	9.167E-02	7.333E-02	6.333E-02	4.833E-02	4.500E-02	2.833E-02	4.333E-02	1.833E-02	3.167E-02
1.480E 00												

PROCEDURE AND SO2, TEMPERATURE, AND RELATIVE HUMIDITY DATA FOR EXPERIMENT P19

THE BAG WAS FILLED FROM 14:30 TO 14:35

THE BAG WAS NOT COVERED DURING THE FILLING PROCESS

THE AIR WAS NOT FILTERED DURING THE FILLING PROCESS

REACTANTS ADDED TO THE SYSTEM:

REACTANT	AMOUNT ADDED - CM3	TIME ADDED
NO	20.00	14:33
NO2	10.00	14:55
SO2	3.25	14:55
PROPYLENE	30.00	14:58

TIME	SO2	TIME	TEMPERATURE - DEG C	RELATIVE HUMIDITY
14:55	15.11	15:05	37.	39.
15:05	74.31	16:58	33.	47.
15:09	73.30			
15:12	72.99			
15:19	72.76			
15:35	72.37			
15:39	72.06			
15:48	71.68			
16:02	70.67			
16:08	70.36			
16:12	70.20			
16:19	69.89			
16:28	69.58			
16:32	69.35			
16:42	68.89			
16:58	68.58			

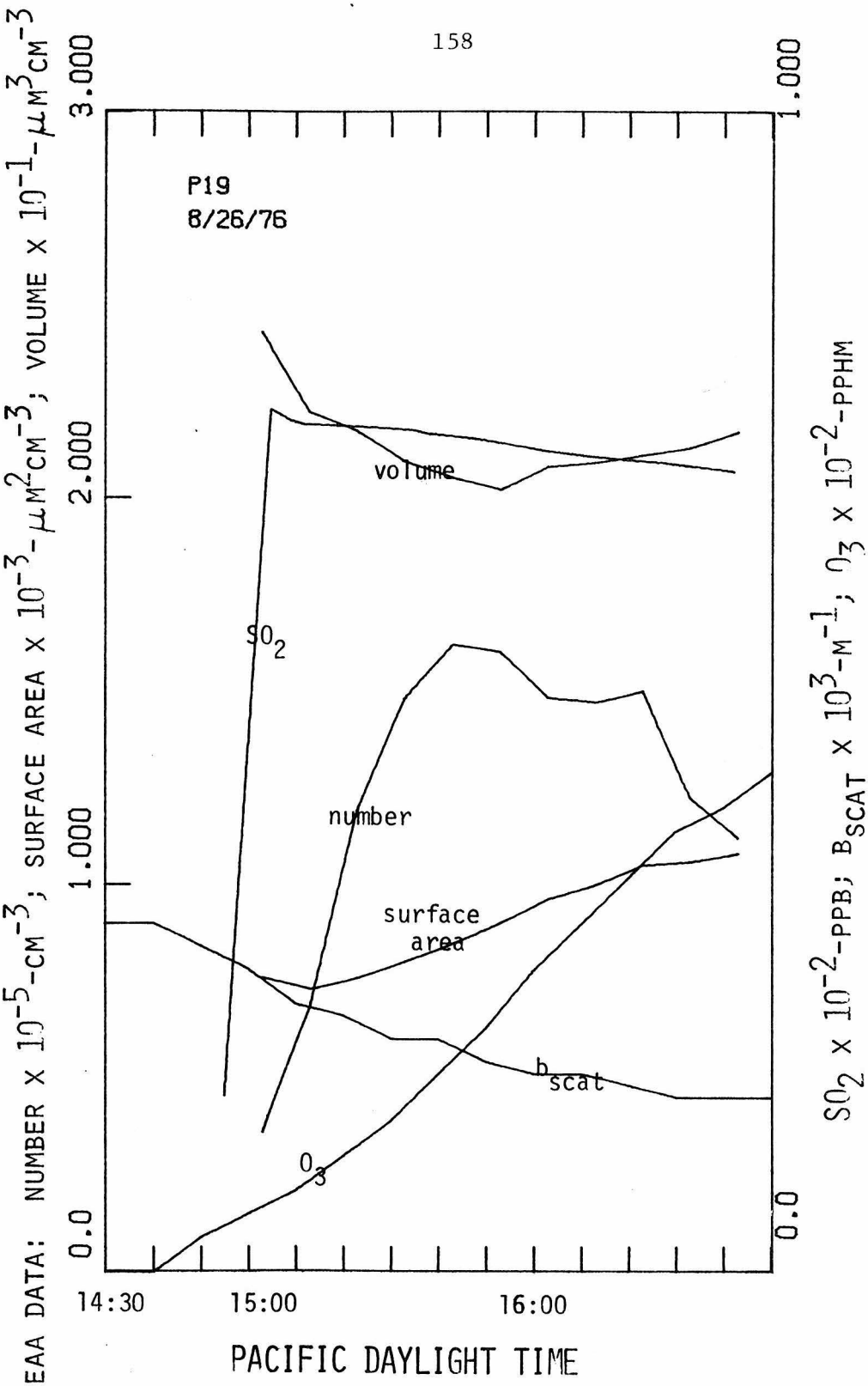
P19
8/26/76
volume
SO_2
number
surface area
b_{scat}
O_3
3.000
2.000
1.000
0.0
1.000
0.0
14:30
15:00
16:00
PACIFIC DAYLIGHT TIME
EAA DATA: NUMBER X 10^{-5}-CM^{-3}; SURFACE AREA X 10^{-3}-μM^{2}CM^{-3}; VOLUME X 10^{-1}-μM^{3}CM^{-3}
SO_2 X 10^{-2}-PPB; B_{SCAT} X 10^3-M^{-1}; O_3 X 10^{-2}-PPHM

SIZE DISTRIBUTION DATA FROM EXPERIMENT P19

DATE 8/26/76

NUMBER PER CM3 IN EACH SIZE INCREMENT DURING INDICATED TIME INTERVAL

DIA. LIMITS	1448-1458	1458-1508	1508-1518	1518-1528	1528-1538	1538-1548	1548-1558	1558-1608	1608-1618	1618-1628	1628-1638	1638-1648
ELECTRICAL AEROSOL ANALYZER DATA												
1.000E-02	5.429E 03	3.733E 03	3.597E 04	6.617E 04	5.616E 04	4.225E 04	3.393E 04	1.765E 04	1.900E 04	2.850E 04	9.501E 03	6.787E 03
1.780E-02	1.502E 04	1.305E 04	1.373E 04	3.439E 04	7.293E 04	9.549E 04	9.114E 04	8.958E 04	8.251E 04	7.014E 04	5.580E 04	4.608E 04
3.160E-02	5.381E 03	5.735E 03	5.487E 03	5.735E 03	6.514E 03	1.122E 04	2.018E 04	2.290E 04	2.418E 04	2.889E 04	3.260E 04	3.299E 04
5.620E-02	8.401E 03	7.714E 03	7.462E 03	7.443E 03	7.606E 03	8.040E 03	1.006E 04	1.375E 04	1.646E 04	1.787E 04	1.917E 04	2.079E 04
1.000E-01	5.453E 03	4.913E 03	4.531E 03	4.335E 03	4.109E 03	3.972E 03	3.883E 03	3.883E 03	4.080E 03	4.295E 03	4.482E 03	4.746E 03
1.780E-01	8.906E 02	7.955E 02	7.305E 02	7.005E 02	6.654E 02	6.354E 02	5.954E 02	5.904E 02	5.604E 02	5.454E 02	5.354E 02	5.354E 02
3.160E-01												
OPTICAL PARTICLE COUNTER DATA												
3.770E-01	5.561E 01	5.088E 01	4.725E 01	4.417E 01	4.054E 01	3.859E 01	3.571E 01	3.363E 01	3.072E 01	2.910E 01	2.642E 01	2.458E 01
4.670E-01	2.537E 01	2.320E 01	2.180E 01	2.064E 01	1.923E 01	1.790E 01	1.652E 01	1.546E 01	1.453E 01	1.344E 01	1.264E 01	1.178E 01
5.640E-01	8.250E 00	7.468E 00	6.860E 00	6.468E 00	6.167E 00	5.718E 00	5.265E 00	5.043E 00	4.678E 00	4.358E 00	4.017E 00	3.748E 00
6.600E-01	3.647E 00	3.307E 00	3.148E 00	2.970E 00	2.663E 00	2.475E 00	2.389E 00	2.215E 00	1.995E 00	1.975E 00	1.727E 00	1.590E 00
7.510E-01	1.538E 00	1.467E 00	1.245E 00	1.157E 00	1.105E 00	1.065E 00	8.816E-01	9.217E-01	8.817E-01	7.633E-01	7.033E-01	6.466E-01
8.190E-01	8.183E-01	7.000E-01	7.000E-01	6.616E-01	5.067E-01	5.933E-01	4.900E-01	4.917E-01	4.517E-01	3.733E-01	3.717E-01	3.350E-01
8.760E-01	5.117E-01	4.783E-01	4.417E-01	3.600E-01	3.517E-01	3.217E-01	2.900E-01	2.800E-01	2.483E-01	2.533E-01	1.750E-01	2.000E-01
9.280E-01	3.633E-01	2.733E-01	2.400E-01	2.383E-01	2.300E-01	2.300E-01	2.100E-01	1.867E-01	1.567E-01	1.583E-01	1.533E-01	1.283E-01
9.790E-01	2.917E-01	2.833E-01	2.467E-01	2.333E-01	2.183E-01	2.050E-01	1.717E-01	1.083E-01	1.000E-01	1.217E-01	1.183E-01	1.317E-01
1.040E 00	2.133E-01	2.100E-01	1.833E-01	1.650E-01	1.450E-01	1.250E-01	1.183E-01	1.250E-01	9.833E-02	9.500E-02	8.500E-02	9.166E-02
1.110E 00	1.850E-01	1.850E-01	1.317E-01	1.183E-01	1.150E-01	1.083E-01	1.167E-01	1.050E-01	7.000E-02	8.000E-02	7.167E-02	4.667E-02
1.210E 00	1.467E-01	1.200E-01	1.133E-01	9.000E-02	8.833E-02	8.667E-02	5.667E-02	6.833E-02	6.167E-02	4.333E-02	4.500E-02	4.000E-02
1.350E 00	9.333E-02	7.666E-02	6.000E-02	6.166E-02	6.667E-02	5.167E-02	4.000E-02	4.667E-02	4.167E-02	2.167E-02	3.333E-02	3.167E-02
1.480E 00												

PROCEDURE AND SO2, TEMPERATURE, AND RELATIVE HUMIDITY DATA FOR EXPERIMENT P21

THE BAG WAS FILLED FROM 13:00 TO 14:00

THE BAG WAS COVERED DURING THE FILLING PROCESS

THE COVER WAS REMOVED AT 14:14

THE AIR WAS PARTIALLY FILTERED DURING THE FILLING PROCESS

REACTANTS ADDED TO THE SYSTEM:

REACTANT	AMOUNT ADDED - CM3	TIME ADDED
NO	20.00	13:05
NO2	10.00	14:00
SO2	3.25	14:00
PROPYLENE	40.00	14:05

TIME	SO2	TIME	TEMPERATURE - DEG C	RELATIVE HUMIDITY
14:14	91.05	14:20	38.	30.
14:20	90.74	15:22	36.	33.
14:28	88.49	15:46	35.	35.
14:32	87.72			
14:38	85.78			
14:43	84.77			
14:49	83.14			
14:53	82.76			
14:59	81.36			
15:03	80.97			
15:09	80.15			
15:15	79.89			
15:22	79.19			
15:32	78.57			
15:39	78.26			
15:46	78.03			

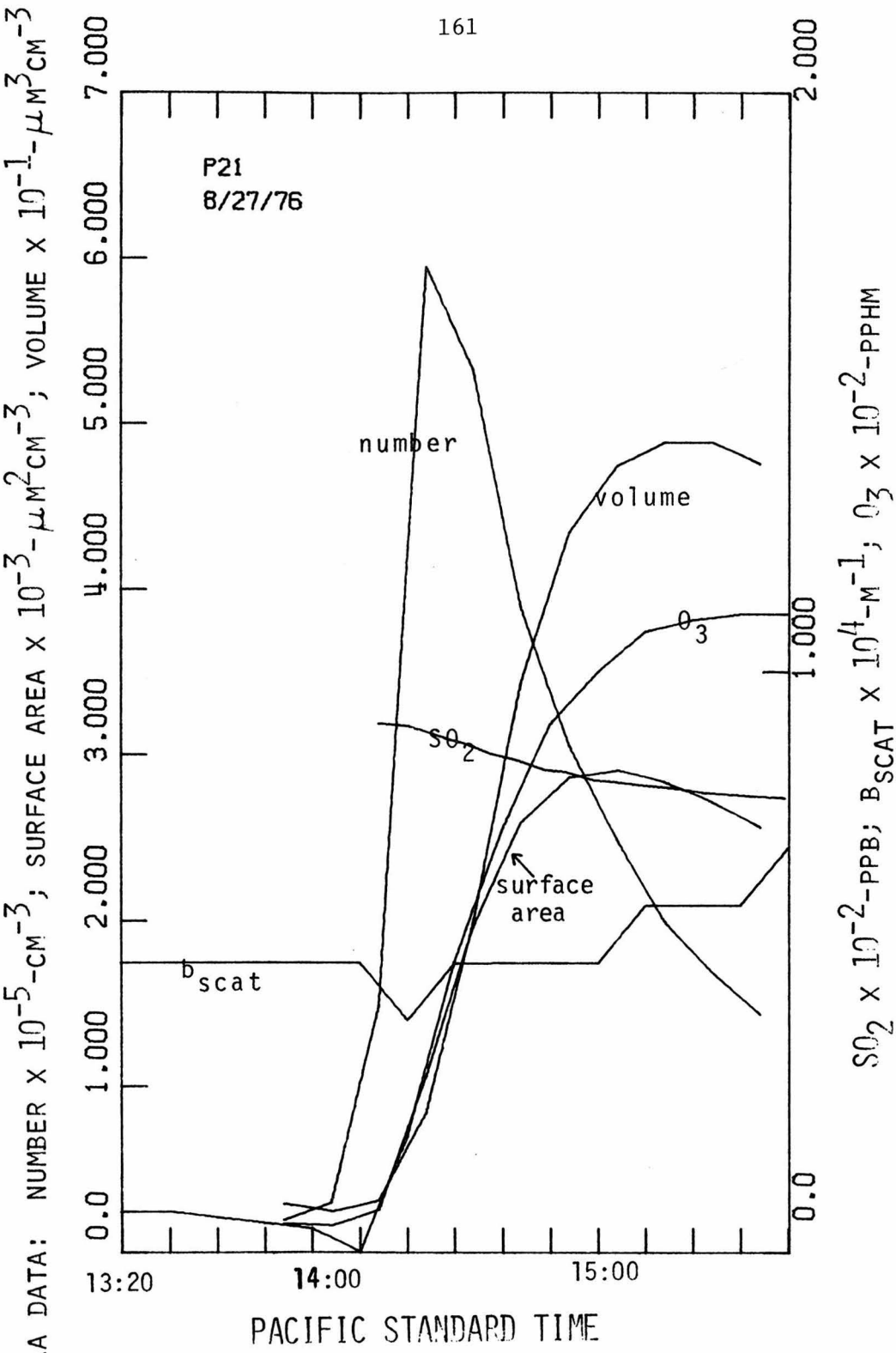
P21
8/27/76
number
volume
O_3
SO_2
surface area
b_{scat}
7.000
6.000
5.000
4.000
3.000
2.000
1.000
0.0
2.000
1.000
0.0
13:20
14:00
15:00
PACIFIC STANDARD TIME
EAA DATA: NUMBER X 10^{-5}-CM^{-3}; SURFACE AREA X 10^{-3}-μM^{2}CM^{-3}; VOLUME X 10^{-1}-μM^{3}CM^{-3}
SO_2 X 10^{-2}-PPB; B_{SCAT} X 10^{4}-M^{-1}; O_3 X 10^{-2}-PPHM

SIZE DISTRIBUTION DATA FROM EXPERIMENT P21

DATE 8/27/76

NUMBER PER CM3 IN EACH SIZE INCREMENT DURING INDICATED TIME INTERVAL

DIA. LIMITS	1339-1349	1349-1359	1359-1409	1409-1419	1419-1429	1429-1439	1439-1449	1449-1459	1459-1509	1509-1519	1519-1529	1529-1539
ELECTRICAL AEROSOL ANALYZER DATA												
1.000E-02	5.090E 03	8.483E 02	1.171E 04	8.432E 04	2.878E 05	5.022E 04	1.900E 04	1.222E 04	1.765E 04	8.144E 03	9.501E 03	5.429E 03
1.780E-02	9.651E 03	9.991E 03	9.787E 03	5.451E 04	2.685E 05	3.654E 05	1.914E 05	1.158E 05	5.818E 04	3.697E 04	2.284E 04	1.794E 04
3.160E-02	3.646E 03	4.390E 03	4.567E 03	5.168E 03	2.694E 04	7.813E 04	1.076E 05	8.581E 04	7.845E 04	6.174E 04	4.701E 04	3.597E 04
5.620E-02	3.035E 03	3.487E 03	3.306E 03	3.884E 03	1.055E 04	3.492E 04	6.291E 04	8.002E 04	8.096E 04	7.841E 04	7.416E 04	6.840E 04
1.000E-01	1.000E 03	1.020E 03	9.709E 02	1.030E 03	1.344E 03	3.648E 03	7.365E 03	1.013E 04	1.237E 04	1.395E 04	1.491E 04	1.521E 04
1.780E-01	4.003E 01	2.502E 01	0.0	1.001E 01	8.005E 01	1.601E 02	4.703E 02	7.455E 02	8.906E 02	9.606E 02	1.001E 03	1.006E 03
3.160E-01												
OPTICAL PARTICLE COUNTER DATA												
3.770E-01	4.573E 00	4.112E 00	3.328E 00	2.853E 00	2.580E 00	2.512E 00	2.257E 00	1.996E 00	1.895E 00	1.788E 00	1.617E 00	1.605E 00
4.670E-01	1.447E 00	1.278E 00	9.966E-01	9.100E-01	7.617E-01	7.350E-01	6.483E-01	5.649E-01	5.583E-01	5.217E-01	3.850E-01	4.883E-01
5.640E-01	2.933E-01	2.983E-01	2.333E-01	2.400E-01	1.833E-01	1.600E-01	1.517E-01	1.066E-01	1.433E-01	1.117E-01	6.333E-02	8.333E-02
6.600E-01	1.450E-01	1.033E-01	1.067E-01	9.333E-02	6.500E-02	6.333E-02	5.500E-02	4.499E-02	5.000E-02	4.167E-02	4.667E-02	2.167E-02
7.510E-01	4.166E-02	3.000E-02	3.000E-02	3.833E-02	2.333E-02	1.333E-02	3.000E-02	2.666E-02	1.667E-02	1.000E-02	1.333E-02	1.667E-02
8.190E-01	1.500E-02	6.666E-03	1.000E-02	1.000E-02	2.333E-02	1.000E-02	1.000E-02	9.998E-03	1.167E-02	1.167E-02	5.000E-03	1.000E-02
8.760E-01	1.167E-02	1.167E-02	1.000E-02	1.667E-03	1.000E-02	5.000E-03	5.000E-03	6.665E-03	5.000E-03	5.000E-03	1.667E-03	1.000E-02
9.280E-01	1.500E-02	5.000E-03	8.333E-03	3.333E-03	3.333E-03	3.333E-03	5.000E-03	1.666E-03	5.000E-03	5.000E-03	3.333E-03	3.333E-03
9.790E-01	9.999E-03	5.000E-03	5.000E-03	6.667E-03	3.333E-03	3.333E-03	6.667E-03	3.333E-03	1.667E-03	1.667E-03	0.0	1.667E-03
1.040E 00	1.667E-03	5.000E-03	1.667E-03	3.333E-03	6.667E-03	1.667E-03	5.000E-03	1.666E-03	0.0	3.333E-03	1.667E-03	3.333E-03
1.110E 00	0.0	5.000E-03	5.000E-03	1.667E-03	3.333E-03	0.0	3.333E-03	4.999E-03	3.333E-03	1.667E-03	0.0	5.000E-03
1.210E 00	1.667E-03	1.667E-03	5.000E-03	0.0	1.667E-03	1.667E-03	1.000E-02	1.666E-03	1.667E-03	3.333E-03	1.667E-03	1.667E-03
1.350E 00	5.000E-03	3.333E-03	0.0	1.667E-03	1.667E-03	1.667E-03	0.0	3.333E-03	3.333E-03	0.0	0.0	3.333E-03
1.480E 00												

PROCEDURE AND SO2, TEMPERATURE, AND RELATIVE HUMIDITY DATA FOR EXPERIMENT P22

THE BAG WAS FILLED FROM 09:00 TO 10:00

THE BAG WAS COVERED DURING THE FILLING PROCESS

THE COVER WAS REMOVED AT 11:03

THE AIR WAS PARTIALLY FILTERED DURING THE FILLING PROCESS

REACTANTS ADDED TO THE SYSTEM:

REACTANT	AMOUNT ADDED - CM3	TIME ADDED
NO	20.00	09:30
NO2	10.00	12:45
SO2	1.50	12:45
PROPYLENE	30.00	12:48

TIME	SO2	TIME	TEMPERATURE - DEG C	RELATIVE HUMIDITY
10:40	68.29	10:40	38.	36.
11:03	66.56	11:07	38.	36.
11:07	67.15	12:22	42.	29.
11:12	61.91			
11:16	61.76			
11:19	61.68			
11:22	61.37			
11:26	61.14			
11:31	60.75			
11:35	60.52			
11:39	60.06			
11:47	59.28			
11:52	58.66			
11:58	57.96			
12:05	56.88			
12:12	56.26			
12:18	55.64			
12:22	55.41			
12:29	54.79			
12:35	54.32			
12:43	54.01			

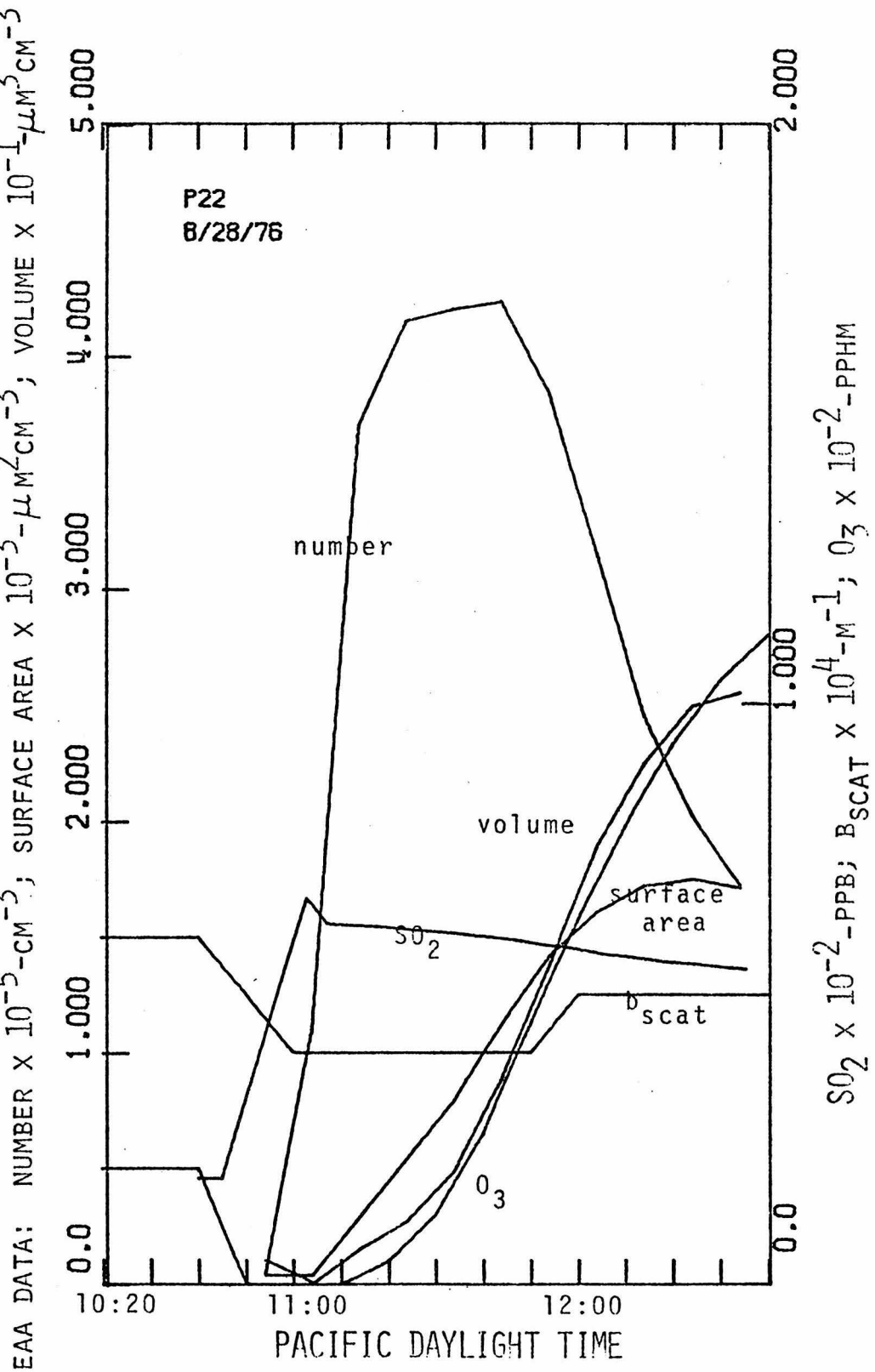
P22
8/28/76
number
volume
surface area
SO_2
b_{scat}
O_3
5.000
4.000
3.000
2.000
1.000
0.0
2.000
1.000
0.0
10:20
11:00
12:00
PACIFIC DAYLIGHT TIME
EAA DATA: NUMBER X 10^{-5}-CM^{-3}; SURFACE AREA X 10^{-3}-μM^{2}CM^{-3}; VOLUME X 10^{-1}-μM^{3}CM^{-3}
SO_2 X 10^{-2}-PPB; B_{SCAT} X 10^{4}-M^{-1}; O_3 X 10^{-2}-PPHM

SIZE DISTRIBUTION DATA FROM EXPERIMENT P22

DATE 8/28/76

NUMBER PER CM3 IN EACH SIZE INCREMENT DURING INDICATED TIME INTERVAL

DIA. LIMITS	1039-1049	1049-1059	1059-1109	1109-1119	1119-1129	1129-1139	1139-1150	1150-1200	1200-1210	1210-1220	1220-1230	1230-1240
ELECTRICAL AEROSOL ANALYZER DATA												
1.000E-02	1.697E 03	1.866E 03	6.787E 03	3.224E 05	1.973E 05	1.289E 05	1.032E 05	6.922E 04	3.665E 04	1.086E 04	9.501E 03	1.086E 04
1.780E-02	1.359E 03	1.291E 03	1.020E 03	4.629E 04	2.119E 05	2.593E 05	2.534E 05	2.186E 05	1.648E 05	1.115E 05	7.395E 04	5.057E 04
3.160E-02	4.248E 02	3.894E 02	4.602E 02	4.248E 02	4.850E 03	2.620E 04	4.899E 04	6.482E 04	7.130E 04	7.329E 04	6.514E 04	5.494E 04
5.620E-02	7.949E 02	7.227E 02	6.143E 02	7.227E 02	9.395E 02	5.583E 03	1.621E 04	2.799E 04	3.796E 04	4.354E 04	4.831E 04	4.956E 04
1.000E-01	3.923E 02	3.334E 02	2.942E 02	2.354E 02	2.550E 02	3.183E 02	9.316E 02	2.354E 03	3.599E 03	4.648E 03	5.403E 03	5.835E 03
1.780E-01	0.0	0.0	0.0	0.0	0.0	0.0	0.0	2.001E 01	1.501E 02	2.602E 02	3.552E 02	3.853E 02
3.160E-01												
OPTICAL PARTICLE COUNTER DATA												
3.770E-01	4.553E 00	4.150E 00	3.685E 00	3.153E 00	3.035E 00	2.768E 00	2.545E 00	2.335E 00	2.202E 00	2.103E 00	2.030E 00	1.780E 00
4.670E-01	1.830E 00	1.652E 00	1.457E 00	1.280E 00	1.297E 00	1.072E 00	1.095E 00	9.283E-01	8.666E-01	7.633E-01	7.733E-01	7.083E-01
5.640E-01	5.267E-01	5.267E-01	4.100E-01	3.967E-01	3.767E-01	3.450E-01	3.250E-01	2.867E-01	2.783E-01	2.250E-01	2.267E-01	2.433E-01
6.600E-01	2.033E-01	2.300E-01	1.800E-01	1.900E-01	1.517E-01	1.517E-01	1.383E-01	1.183E-01	1.283E-01	1.100E-01	1.017E-01	1.167E-01
7.510E-01	8.666E-02	9.000E-02	6.667E-02	5.333E-02	7.166E-02	5.333E-02	5.333E-02	4.167E-02	4.833E-02	4.500E-02	5.000E-02	5.833E-02
8.190E-01	3.500E-02	2.833E-02	3.500E-02	2.333E-02	3.833E-02	2.500E-02	2.333E-02	2.500E-02	4.167E-02	2.000E-02	1.833E-02	2.667E-02
8.760E-01	2.000E-02	1.833E-02	2.167E-02	2.167E-02	1.333E-02	2.000E-02	1.667E-02	8.333E-03	1.000E-02	1.833E-02	1.000E-02	1.333E-02
9.290E-01	1.667E-02	1.833E-02	1.333E-02	6.667E-03	6.666E-03	5.000E-03	1.000E-02	1.167E-02	1.167E-02	8.333E-03	1.500E-02	1.500E-02
9.790E-01	1.167E-02	8.333E-03	1.667E-02	6.667E-03	6.666E-03	6.667E-03	6.667E-03	1.333E-02	1.500E-02	1.000E-02	3.333E-03	3.333E-03
1.040E 00	0.0	8.333E-03	3.333E-03	1.667E-02	0.0	5.000E-03	0.0	3.333E-03	8.333E-03	3.333E-03	6.667E-03	6.667E-03
1.110E 00	5.000E-03	1.667E-03	1.667E-03	5.000E-03	0.0	1.667E-03	5.000E-03	1.667E-03	3.333E-03	3.333E-03	0.0	3.333E-03
1.210E 00	3.333E-03	0.0	3.333E-03	6.667E-03	0.0	3.333E-03	0.0	5.000E-03	3.333E-03	5.000E-03	1.667E-03	0.0
1.350E 00	3.333E-03	0.0	1.667E-03	1.667E-03	3.333E-03	0.0	0.0	3.333E-03	1.667E-03	0.0	0.0	3.333E-03
1.480E 00												

PROCEDURE AND SO2, TEMPERATURE, AND RELATIVE HUMIDITY DATA FOR EXPERIMENT P23

THE BAG WAS FILLED FROM 13:00 TO 14:00

THE BAG WAS COVERED DURING THE FILLING PROCESS

THE COVER WAS REMOVED AT 14:43

THE AIR WAS PARTIALLY FILTERED DURING THE FILLING PROCESS

REACTANTS ADDED TO THE SYSTEM:

REACTANT	AMOUNT ADDED - CM3	TIME ADDED
NO	37.00	13:05
NO2	0.0	14:25
SO2	1.00	14:25
PROPYLENE	20.00	14:25

TIME	SO2	TIME	TEMPERATURE - DEG C	RELATIVE HUMIDITY
13:28	13.86	14:23	46.	27.
14:23	14.65	14:31	45.	29.
14:42	43.32	15:26	40.	37.
14:48	43.40			
14:55	43.32			
15:02	43.16			
15:11	42.93			
15:16	42.70			
15:20	42.47			
15:26	42.39			
15:33	42.08			
15:41	41.62			
15:48	41.31			
15:57	40.84			
16:03	40.69			
16:22	40.14			
16:43	39.45			

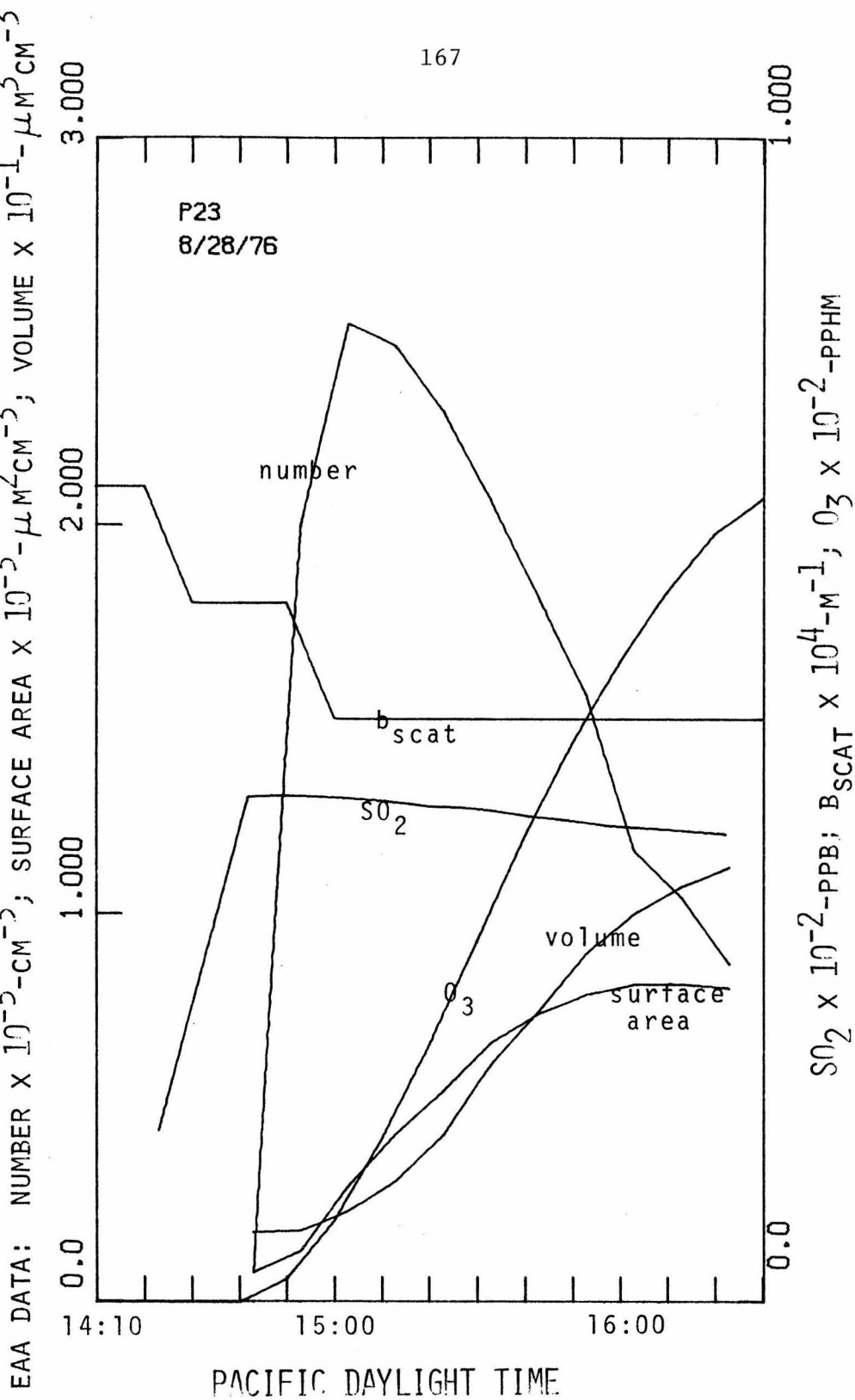
P23
8/28/76
number
b_{scat}
SO_2
volume
O_3
surface area
3.000
2.000
1.000
0.0
1.000
0.0
14:10
15:00
16:00
PACIFIC DAYLIGHT TIME
EAA DATA: NUMBER X 10^{-5}-CM^{-3}; SURFACE AREA X 10^{-3}-μM^{2}CM^{-3}; VOLUME X 10^{-1}-μM^{3}CM^{-3}
SO_2 X 10^{-2}-PPB; B_{SCAT} X 10^{4}-M^{-1}; O_3 X 10^{-2}-PPHM

SIZE DISTRIBUTION DATA FROM EXPERIMENT P23

DATE 8/28/76

NUMBER PER CM3 IN EACH SIZE INCREMENT DURING INDICATED TIME INTERVAL

DIA. LIMITS	1428-1438	1438-1448	1448-1458	1458-1508	1508-1518	1518-1528	1528-1538	1538-1548	1548-1558	1558-1608	1608-1618	1618-1628
ELECTRICAL AEROSOL ANALYZER DATA												
1.000E-02	1.018E 03	2.036E 03	9.128E 04	1.800E 05	8.178E 04	4.615E 04	2.850E 04	2.036E 04	1.222E 04	9.501E 03	5.429E 03	1.035E 04
1.780E-02	2.243E 03	2.379E 03	4.350E 03	6.824E 04	1.555E 05	1.582E 05	1.357E 05	1.095E 05	8.965E 04	6.871E 04	5.206E 04	3.643E 04
3.160E-02	1.204E 03	1.133E 03	1.274E 03	1.381E 03	5.699E 03	1.876E 04	3.041E 04	3.490E 04	3.441E 04	3.621E 04	3.597E 04	3.430E 04
5.620E-02	1.463E 03	1.427E 03	1.554E 03	1.716E 03	2.060E 03	4.986E 03	1.021E 04	1.474E 04	1.783E 04	1.930E 04	1.998E 04	2.038E 04
1.000E-01	6.865E 02	5.884E 02	5.786E 02	5.982E 02	6.767E 02	7.355E 02	9.512E 02	1.442E 03	1.912E 03	2.334E 03	2.569E 03	2.648E 03
1.780E-01	1.001E 01	0.0	0.0	0.0	0.0	0.0	1.501E 01	0.0	3.502E 01	6.004E 01	9.006E 01	1.351E 02
3.160E-01												
OPTICAL PARTICLE COUNTER DATA												
3.770E-01	7.458E 00	6.588E 00	5.503E 00	4.503E 00	3.958E 00	3.670E 00	3.322E 00	2.973E 00	2.755E 00	2.663E 00	2.440E 00	2.232E 00
4.670E-01	2.877E 00	2.365E 00	2.085E 00	1.763E 00	1.450E 00	1.345E 00	1.202E 00	1.080E 00	9.733E-01	8.717E-01	7.383E-01	7.433E-01
5.640E-01	8.367E-01	7.700E-01	6.067E-01	5.067E-01	4.400E-01	3.900E-01	3.150E-01	2.683E-01	2.567E-01	2.517E-01	1.983E-01	1.917E-01
6.600E-01	3.850E-01	3.900E-01	2.933E-01	2.350E-01	2.233E-01	2.083E-01	1.600E-01	1.433E-01	1.233E-01	1.550E-01	1.067E-01	8.500E-02
7.510E-01	1.633E-01	1.533E-01	1.200E-01	9.500E-02	8.833E-02	6.667E-02	6.500E-02	6.166E-02	6.500E-02	3.833E-02	4.167E-02	3.000E-02
8.190E-01	8.167E-02	6.333E-02	5.000E-02	4.167E-02	4.000E-02	3.667E-02	2.667E-02	3.000E-02	2.000E-02	1.500E-02	1.333E-02	1.667E-02
8.760E-01	4.500E-02	3.167E-02	2.167E-02	1.333E-02	2.000E-02	2.667E-02	1.500E-02	1.500E-02	1.667E-02	5.000E-03	5.000E-03	1.667E-03
9.280E-01	3.000E-02	1.833E-02	1.167E-02	1.333E-02	2.500E-02	1.000E-02	3.333E-03	1.167E-02	1.000E-02	1.500E-02	1.667E-03	1.367E-03
9.790E-01	3.333E-03	8.333E-02	6.667E-03	6.667E-03	5.000E-03	1.000E-02	6.667E-03	1.000E-02	6.667E-03	3.333E-03	5.000E-03	5.000E-03
1.040E 00	8.333E-03	1.667E-03	1.667E-03	1.667E-03	3.333E-03	3.333E-03	3.333E-03	5.000E-03	0.0	3.333E-03	0.0	1.667E-03
1.110E 00	3.333E-03	3.333E-03	0.0	1.667E-03	5.000E-03	1.667E-03	1.667E-03	0.0	1.667E-03	1.667E-03	0.0	3.333E-03
1.210E 00	3.333E-03	0.0	1.667E-03	0.0	0.0	0.0	1.667E-03	0.0	0.0	1.667E-03	0.0	0.0
1.350E 00	0.0	3.333E-03	0.0	1.667E-03	0.0	1.667E-03	1.667E-03	0.0	0.0	1.667E-03	0.0	0.0
1.480E 00												

PROCEDURE AND SO2, TEMPERATURE, AND RELATIVE HUMIDITY DATA FOR EXPERIMENT P26

THE BAG WAS FILLED FROM 08:35 TO 09:35

THE BAG WAS COVERED DURING THE FILLING PROCESS

THE COVER WAS REMOVED AT 10:18

THE AIR WAS PARTIALLY FILTERED DURING THE FILLING PROCESS

REACTANTS ADDED TO THE SYSTEM:

REACTANT	AMOUNT ADDED - CM3	TIME ADDED
NO	20.00	08:40
NO2	10.00	09:59
SO2	10.00	09:59
PROPYLENE	30.00	10:00

TIME	SO2	TIME	TEMPERATURE - DEG C	RELATIVE HUMIDITY
09:42	10.55	09:42	37.	48.
10:18	204.50	10:18	40.	44.
10:23	203.31	11:24	44.	40.
10:28	202.90			
10:33	202.50			
10:38	201.80			
10:43	201.50			
10:47	200.90			
10:51	200.60			
10:57	200.00			
11:05	199.10			
11:11	197.50			
11:18	196.30			
11:24	195.20			
11:33	192.70			

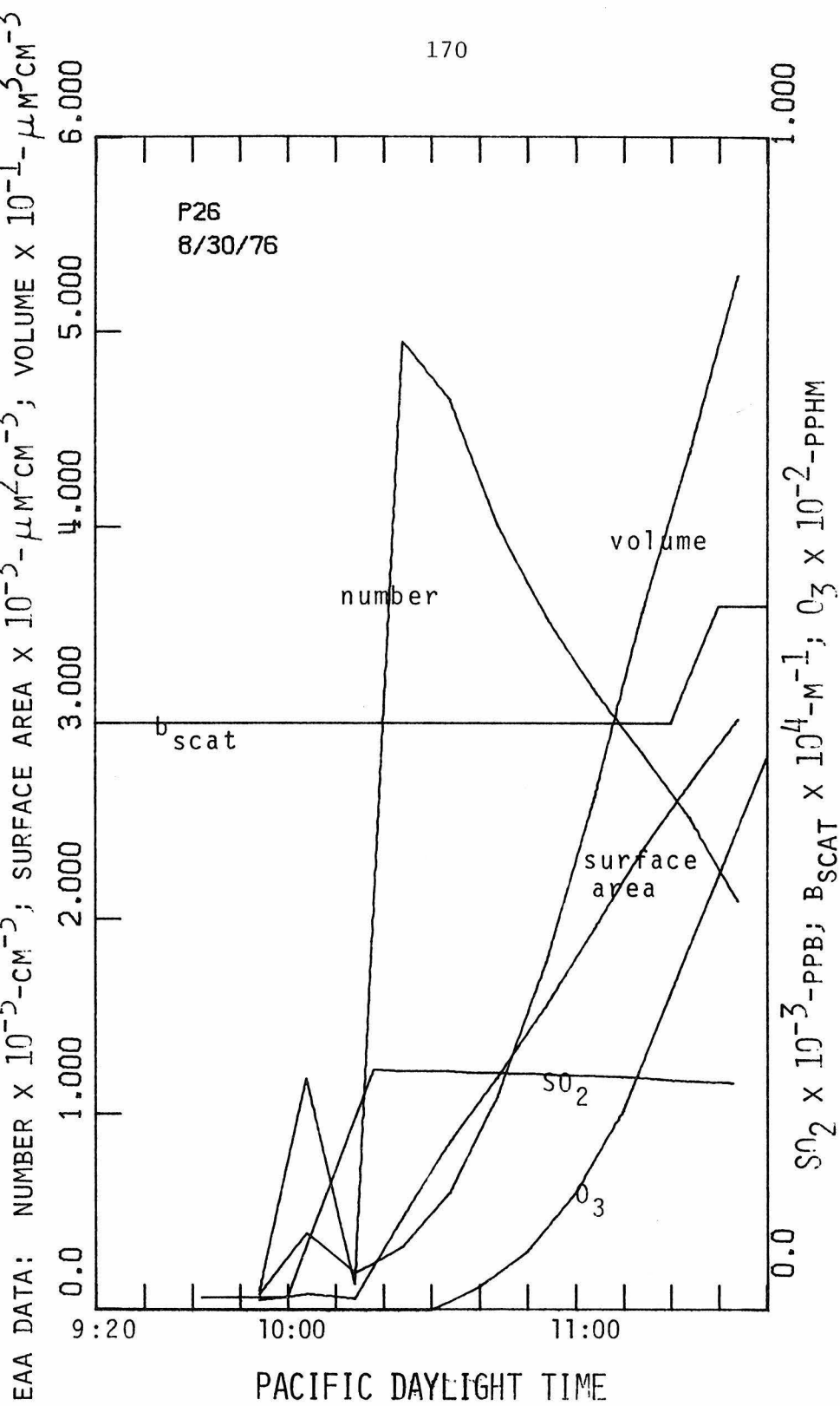
P26
8/30/76
number
volume
surface area
b_{scat}
SO_2
O_3
9:20
10:00
11:00
PACIFIC DAYLIGHT TIME
EAA DATA: NUMBER X 10^{-5}-CM^{-3}; SURFACE AREA X 10^{-3}-μM^{2}CM^{-3}; VOLUME X 10^{-1}-μM^{3}CM^{-3}
SO_2 X 10^{-3}-PPB; B_{SCAT} X 10^{4}-M^{-1}; O_3 X 10^{-2}-PPHM
0.0
1.000
2.000
3.000
4.000
5.000
6.000
1.000
0.0

SIZE DISTRIBUTION DATA FROM EXPERIMENT P26

CATE 8/30/76

NUMBER PER CM3 IN EACH SIZE INCREMENT DURING INDICATED TIME INTERVAL

DIA. LIMITS	939- 949	949- 959	959-1009	1009-1019	1019-1029	1029-1039	1039-1049	1049-1059	1059-1109	1109-1119	1119-1129	1129-1139
ELECTRICAL AERCSOL ANALYZER DATA												
1.000E-02	2.206E 03	2.206E 03	1.680E 04	3.733E 03	3.762E 05	1.357E 05	7.737E 04	6.515E 04	5.158E 04	3.665E 04	2.715E 04	8.144E 03
1.780E-02	4.962E 03	4.894E 03	6.457E 03	6.457E 03	1.147E 05	3.016E 05	2.513E 05	1.822E 05	1.381E 05	1.049E 05	7.721E 04	5.981E 04
3.160E-02	1.310E 03	1.310E 03	1.168E 03	1.239E 03	2.549E 03	2.227E 04	5.243E 04	6.917E 04	7.023E 04	6.853E 04	5.777E 04	4.305E 04
5.620E-02	9.756E 02	8.853E 02	9.214E 02	9.214E 02	1.319E 03	5.312E 03	1.837E 04	3.442E 04	5.073E 04	6.425E 04	7.519E 04	8.078E 04
1.000E-01	2.746E 02	2.256E 02	2.157E 02	1.569E 02	2.354E 02	3.923E 02	1.294E 03	3.079E 03	5.403E 03	8.571E 03	1.253E 04	1.649E 04
1.780E-01	0.0	0.0	0.0	0.0	0.0	0.0	0.0	9.506E 01	2.852E 02	5.254E 02	7.455E 02	9.656E 02
3.160E-01												
OPTICAL PARTICLE COUNTER DATA												
3.770E-01	2.663E 00	2.297E 00	4.372E 00	2.362E 00	2.228E 00	2.083E 00	2.103E 00	2.183E 00	2.052E 00	1.910E 00	1.840E 00	1.797E 00
4.670E-01	8.300E-01	6.533E-01	3.527E 00	1.463E 00	1.358E 00	1.345E 00	1.318E 00	1.222E 00	1.228E 00	1.197E 00	1.187E 00	1.112E 00
5.640E-01	1.967E-01	1.933E-01	2.005E 00	8.400E-01	7.433E-01	7.466E-01	7.383E-01	7.850E-01	7.200E-01	8.050E-01	6.866E-01	6.133E-01
6.600E-01	7.666E-02	6.833E-02	1.777E 00	6.433E-01	6.067E-01	6.533E-01	6.433E-01	5.983E-01	6.300E-01	5.433E-01	4.900E-01	4.983E-01
7.510E-01	3.000E-02	4.500E-02	1.192E 00	5.217E-01	4.533E-01	4.333E-01	4.650E-01	5.033E-01	4.183E-01	4.500E-01	3.800E-01	3.533E-01
8.190E-01	1.333E-02	2.500E-02	9.050E-01	3.867E-01	3.633E-01	3.583E-01	3.750E-01	3.500E-01	3.217E-01	3.583E-01	2.950E-01	3.267E-01
8.760E-01	8.333E-03	6.667E-03	6.450E-01	2.533E-01	2.967E-01	2.883E-01	3.200E-01	2.417E-01	2.950E-01	2.267E-01	2.333E-01	1.733E-01
9.280E-01	5.000E-03	1.000E-02	5.300E-01	2.200E-01	2.533E-01	2.367E-01	2.600E-01	2.333E-01	1.833E-01	2.217E-01	1.917E-01	2.067E-01
9.790E-01	1.667E-03	6.667E-03	5.667E-01	2.217E-01	2.533E-01	2.483E-01	2.483E-01	2.117E-01	2.333E-01	2.250E-01	1.767E-01	1.800E-01
1.040E 00	3.333E-03	1.167E-02	4.150E-01	1.783E-01	1.717E-01	1.483E-01	1.850E-01	1.517E-01	1.200E-01	1.267E-01	1.083E-01	1.350E-01
1.110E 00	1.667E-03	1.667E-02	3.417E-01	1.317E-01	1.100E-01	2.833E-02	9.833E-02	1.000E-01	8.166E-02	6.666E-02	4.833E-02	6.667E-02
1.210E 00	1.667E-03	5.000E-03	2.067E-01	7.833E-02	5.500E-02	5.833E-02	5.500E-02	4.167E-02	3.500E-02	4.333E-02	4.000E-02	2.333E-02
1.350E 00	0.0	1.667E-03	1.117E-01	4.167E-02	3.667E-02	1.833E-02	2.500E-02	1.000E-02	1.000E-02	2.833E-02	1.500E-02	2.000E-02
1.480E 00												

PROCEDURE AND SO2, TEMPERATURE, AND RELATIVE HUMIDITY DATA FOR EXPERIMENT P27

THE BAG WAS FILLED FROM 12:05 TO 12:10

THE BAG WAS NOT COVERED DURING THE FILLING PROCESS

THE AIR WAS NOT FILTERED DURING THE FILLING PROCESS

REACTANTS ADDED TO THE SYSTEM:

REACTANT	AMOUNT ADDED - CM3	TIME ADDED
NO	20.00	12:07
NO2	10.00	12:26
SO2	0.0	
PROPYLENE	30.00	12:28

TIME	SO2	TIME	TEMPERATURE - DEG C	RELATIVE HUMIDITY
12:35	10.16	12:26	49.	28.
12:47	10.16	12:47	48.	29.
12:52	10.08	13:14	46.	32.
13:03	10.00	14:35	44.	36.
13:14	9.93			
13:20	9.85			
13:33	9.77			
13:45	9.69			
14:11	9.54			
14:24	9.38			
14:35	9.38			
14:46	9.31			

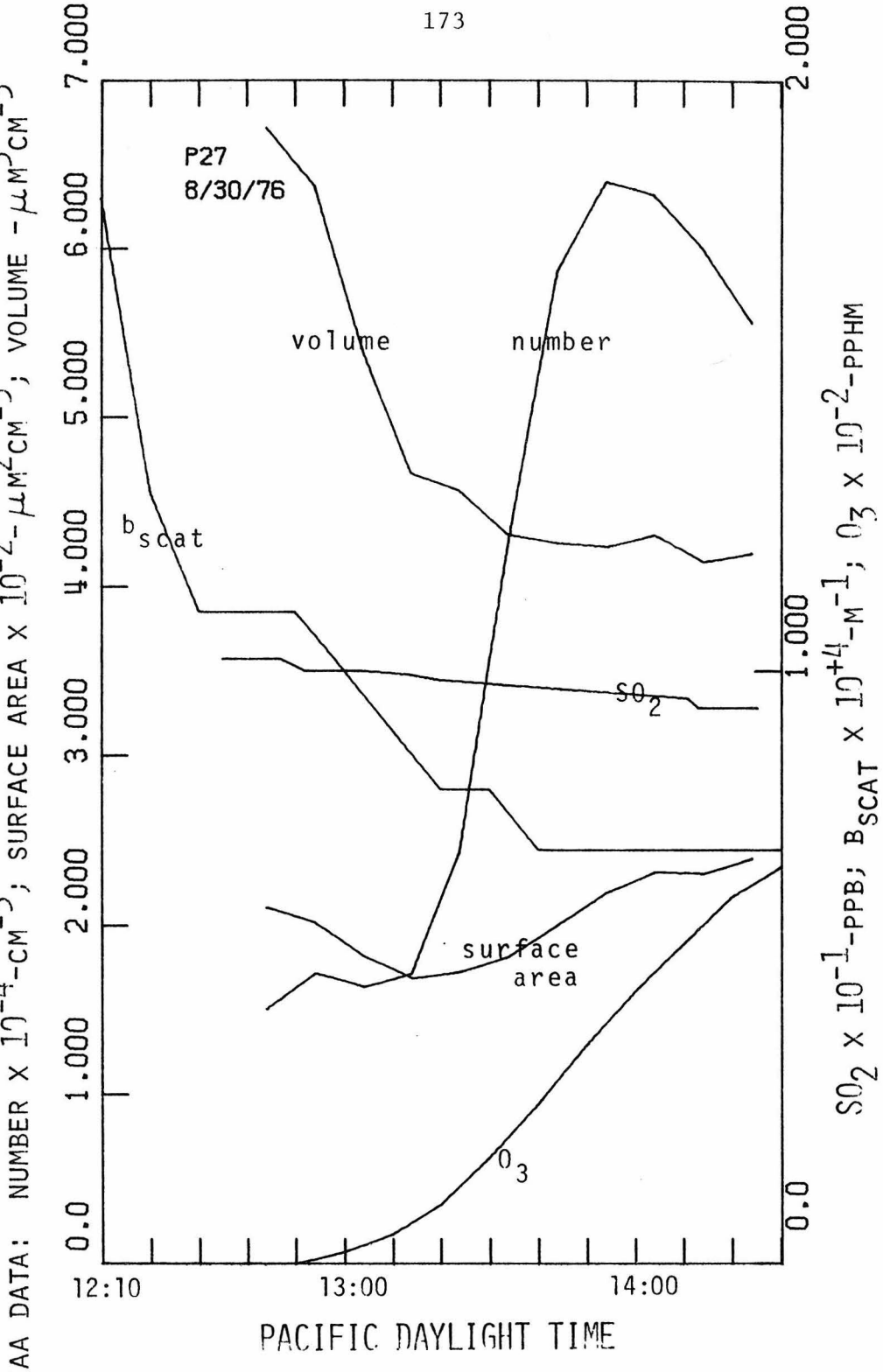
P27
8/30/76
volume
number
surface
area
b_{scat}
SO_2
O_3
EAA DATA: NUMBER X 10^{-4}-CM^{-3}; SURFACE AREA X 10^{-2}-μM^{2}CM^{-3}; VOLUME -μM^{3}CM^{-3}
SO_2 X 10^{-1}-PPB; B_{SCAT} X 10^{+4}-M^{-1}; O_3 X 10^{-2}-PPHM
0.0
1.000
2.000
3.000
4.000
5.000
6.000
7.000
12:10
13:00
14:00
PACIFIC DAYLIGHT TIME

SIZE DISTRIBUTION DATA FROM EXPERIMENT P27

DATE 8/30/76

NUMBER PER CM3 IN EACH SIZE INCREMENT DURING INDICATED TIME INTERVAL

DIA. LIMITS	1229-1239	1239-1249	1249-1259	1259-1309	1309-1319	1319-1329	1329-1339	1339-1349	1349-1359	1359-1409	1409-1420	1420-1430
ELECTRICAL AEROSOL ANALYZER DATA												
1.000E-02	5.599E 03	2.375E 03	4.411E 03	3.224E 03	3.733E 03	1.086E 04	2.800E 04	3.867E 04	3.275E 04	2.375E 04	1.612E 04	1.069E 04
1.780E-02	7.680E 03	7.408E 03	7.544E 03	7.884E 03	8.224E 03	8.020E 03	8.700E 03	1.387E 04	2.474E 04	3.249E 04	3.616E 04	3.704E 04
3.160E-02	1.770E 03	1.699E 03	1.805E 03	2.018E 03	1.947E 03	2.195E 03	2.336E 03	2.549E 03	2.726E 03	3.080E 03	3.292E 03	3.717E 03
5.620E-02	1.969E 03	1.933E 03	1.933E 03	1.987E 03	2.023E 00	2.078E 03	2.240E 03	2.349E 03	2.529E 03	2.584E 03	2.674E 03	2.836E 03
1.000E-01	1.344E 03	1.422E 03	1.304E 03	1.167E 03	1.157E 03	1.098E 03	1.128E 03	1.128E 03	1.177E 03	1.196E 03	1.236E 03	1.216E 03
1.780E-01	2.051E 02	1.851E 02	1.751E 02	1.351E 02	9.506E 01	1.051E 02	8.506E 01	9.006E 01	8.005E 01	8.506E 01	7.005E 01	8.005E 01
3.160E-01												
OPTICAL PARTICLE COUNTER DATA												
3.770E-01	1.717E 01	1.652E 01	1.525E 01	1.333E 01	1.147E 01	9.982E 00	9.143E 00	8.123E 00	7.381E 00	6.962E 00	6.503E 00	6.072E 00
4.670E-01	6.587E 00	6.242E 00	5.912E 00	5.032E 00	4.230E 00	3.655E 00	3.313E 00	2.960E 00	2.795E 00	2.495E 00	2.337E 00	2.225E 00
5.640E-01	2.083E 00	1.960E 00	1.908E 00	1.533E 00	1.370E 00	1.215E 00	1.157E 00	9.400E-01	9.116E-01	7.400E-01	6.783E-01	6.483E-01
6.600E-01	1.188E 00	1.050E 00	9.883E-01	9.233E-01	7.450E-01	6.500E-01	5.700E-01	5.183E-01	4.667E-01	3.917E-01	4.050E-01	3.233E-01
7.510E-01	5.667E-01	5.850E-01	5.350E-01	4.183E-01	4.133E-01	2.983E-01	2.733E-01	2.333E-01	2.333E-01	2.100E-01	1.733E-01	1.733E-01
8.190E-01	3.650E-01	3.450E-01	3.383E-01	2.633E-01	2.367E-01	2.000E-01	1.850E-01	1.717E-01	1.417E-01	1.117E-01	1.250E-01	6.667E-02
8.760E-01	2.317E-01	2.017E-01	2.000E-01	1.767E-01	1.433E-01	1.317E-01	1.017E-01	8.667E-02	9.000E-02	9.833E-02	6.333E-02	5.167E-02
9.280E-01	1.800E-01	1.383E-01	1.555E-01	1.150E-01	9.167E-02	1.017E-01	9.166E-02	7.500E-02	5.667E-02	6.833E-02	4.000E-02	4.667E-02
9.790E-01	1.317E-01	1.350E-01	1.300E-01	1.017E-01	8.667E-02	7.667E-02	7.833E-02	3.333E-02	4.500E-02	5.667E-02	3.833E-02	3.000E-02
1.040E 00	9.333E-02	8.500E-02	1.067E-01	6.500E-02	6.000E-02	4.167E-02	5.000E-02	4.333E-02	5.333E-02	2.000E-02	2.000E-02	2.000E-02
1.110E 00	8.667E-02	7.833E-02	8.500E-02	5.833E-02	4.833E-02	5.167E-02	4.000E-02	4.000E-02	2.667E-02	2.833E-02	2.833E-02	1.000E-02
1.210E 00	6.167E-02	6.667E-02	4.833E-02	4.333E-02	3.333E-02	4.000E-02	3.667E-02	1.833E-02	1.500E-02	1.500E-02	1.667E-02	1.167E-02
1.350E 00	4.500E-02	2.500E-02	3.000E-02	2.333E-02	2.500E-02	2.667E-02	2.000E-02	8.333E-03	8.333E-03	1.167E-02	1.167E-02	6.667E-03
1.480E 00												

PROCEDURE AND SO2, TEMPERATURE, AND RELATIVE HUMIDITY DATA FOR EXPERIMENT P28

THE BAG WAS FILLED FROM 08:35 TO 09:35

THE BAG WAS COVERED DURING THE FILLING PROCESS

THE COVER WAS REMOVED AT 10:34

THE AIR WAS PARTIALLY FILTERED DURING THE FILLING PROCESS

REACTANTS ADDED TO THE SYSTEM:

REACTANT	AMOUNT ADDED - CM3	TIME ADDED
NO	20.00	08:40
NO2	10.00	10:14
SO2	20.00	10:14
PROPYLENE	60.00	10:16

TIME	SO2	TIME	TEMPERATURE - DEG C	RELATIVE HUMIDITY
10:43	511.30	10:31	39.	27.
10:45	510.50	11:03	38.	28.
10:48	509.70	11:44	41.	24.
10:52	507.80			
10:55	506.60			
10:58	505.10			
11:01	503.20			
11:03	501.60			
11:07	497.30			
11:11	493.10			
11:15	486.90			
11:20	479.90			
11:23	474.50			
11:26	466.40			
11:32	460.50			
11:38	454.30			
11:44	448.50			
11:19	444.60			
12:00	439.20			
12:07	436.10			

PROCEDURE AND SO2, TEMPERATURE, AND RELATIVE HUMIDITY DATA FOR EXPERIMENT P28

THE BAG WAS FILLED FROM 08:35 TO 09:35

THE BAG WAS COVERED DURING THE FILLING PROCESS

THE COVER WAS REMOVED AT 10:34

THE AIR WAS PARTIALLY FILTERED DURING THE FILLING PROCESS

REACTANTS ADDED TO THE SYSTEM:

REACTANT	AMOUNT ADDED - CM3	TIME ADDED
NO	20.00	08:40
NO2	10.00	10:14
SO2	20.00	10:14
PROPYLENE	60.00	10:16

TIME	SO2	TIME	TEMPERATURE - DEG C	RELATIVE HUMIDITY
10:43	511.30	10:31	39.	27.
10:45	510.50	11:03	38.	28.
10:48	509.70	11:44	41.	24.
10:52	507.80			
10:55	506.60			
10:58	505.10			
11:01	503.20			
11:03	501.60			
11:07	497.30			
11:11	493.10			
11:15	486.90			
11:20	479.90			
11:23	474.50			
11:26	466.40			
11:32	460.50			
11:38	454.30			
11:44	448.50			
11:19	444.60			
12:00	439.20			
12:07	436.10			

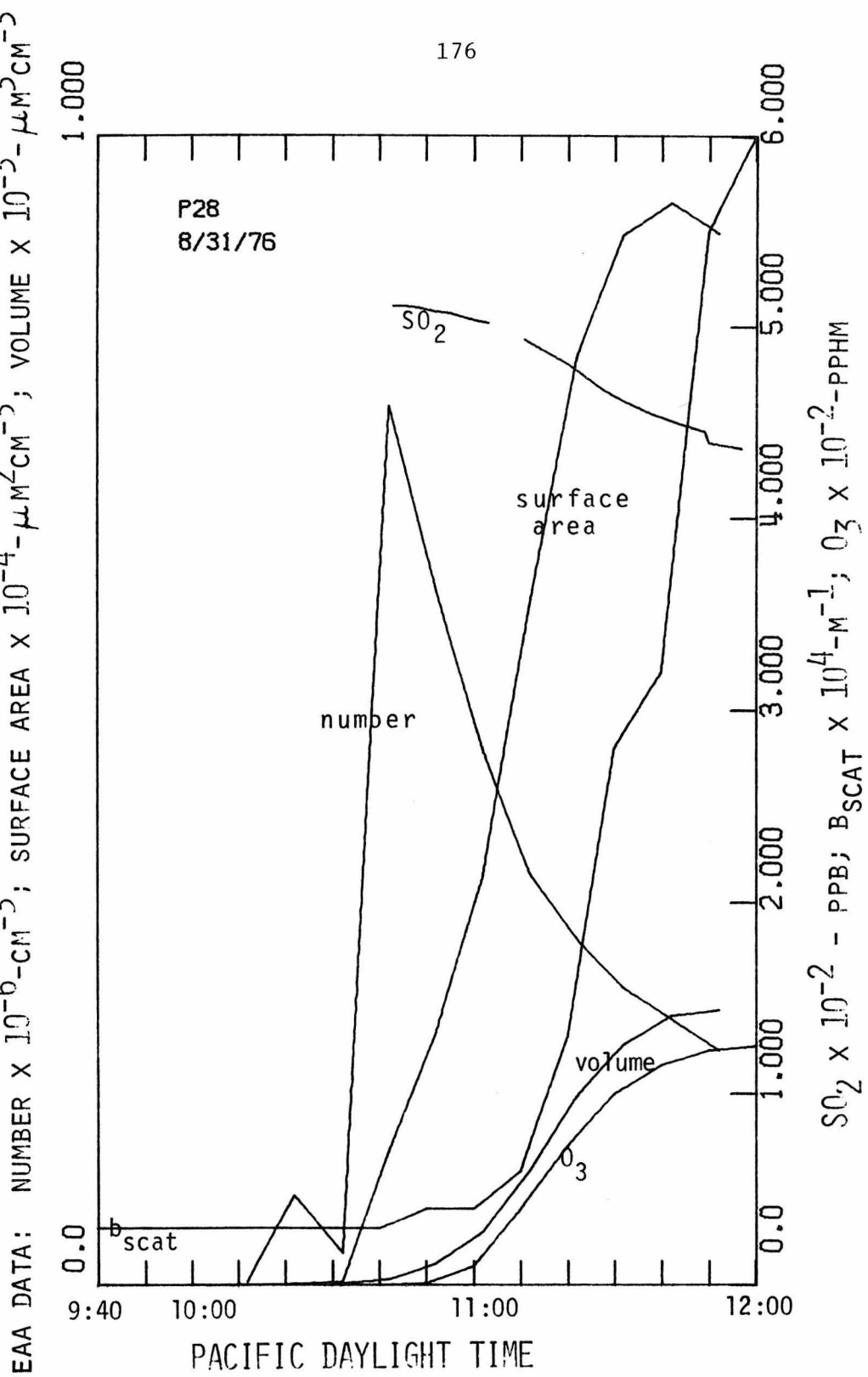
P28
8/31/76
SO_2
surface area
number
volume
O_3
b_{scat}
1.000
0.0
6.000
5.000
4.000
3.000
2.000
1.000
0.0
9:40
10:00
11:00
12:00
PACIFIC DAYLIGHT TIME
EAA DATA: NUMBER X 10^{-6}-cm^{-3}; SURFACE AREA X 10^{-4}-$\mu m^2 cm^{-3}$; VOLUME X 10^{-3}-$\mu m^3 cm^{-3}$
SO_2 X 10^{-2} - PPB; B_{SCAT} X 10^4-m^{-1}; O_3 X 10^{-2}-PPHM

SIZE DISTRIBUTION DATA FROM EXPERIMENT P28

CATE 8/31/76

NUMBER PER CM3 IN EACH SIZE INCREMENT DURING INCICATED TIME INTERVAL

DIA. LIMITS	957-1007	1007-1017	1017-1027	1027-1037	1037-1047	1047-1057	1057-1107	1107-1117	1117-1127	1127-1137	1137-1147	1147-1157
ELECTRICAL AEROSOL ANALYZER DATA												
1.000E-02	1.697E 03	1.018E 03	5.599E 03	1.323E 04	2.945E 05	6.379E 04	1.222E 04	0.0	4.072E 03	1.357E 03	8.144E 03	1.222E 04
1.780E-02	1.631E 03	1.767E 03	3.194E 03	1.026E 04	4.421E 05	3.920E 05	1.979E 05	5.383E 04	1.087E 04	5.437E 03	5.981E 03	3.262E 03
3.160E-02	3.186E 02	1.770E 02	7.080E 01	3.540E 02	2.474E 04	1.079E 05	1.487E 05	8.779E 04	2.917E 04	9.629E 03	5.381E 03	3.682E 03
5.620E-02	1.807E 01	0.0	0.0	1.807E 01	4.065E 03	4.067E 04	9.626E 04	1.855E 05	1.902E 05	1.486E 05	1.081E 05	8.296E 04
1.000E-01	0.0	0.0	0.0	0.0	2.942E 01	2.383E 03	9.238E 03	2.942E 04	6.312E 04	8.734E 04	9.548E 04	9.319E 04
1.780E-01	0.0	0.0	0.0	0.0	0.0	5.003E 00	5.804E 02	1.536E 03	3.667E 03	5.749E 03	7.750E 03	8.896E 03
3.160E-01												
OPTICAL PARTICLE COUNTER DATA												
3.770E-01	8.183E-01	7.600E-01	7.566E-01	6.467E-01	6.500E-01	6.283E-01	6.017E-01	5.417E-01	6.100E-01	5.467E-01	5.950E-01	6.233E-01
4.670E-01	2.833E-01	2.133E-01	1.950E-01	1.883E-01	1.933E-01	1.717E-01	1.417E-01	1.467E-01	1.650E-01	1.733E-01	1.683E-01	1.850E-01
5.640E-01	8.500E-02	6.500E-02	6.000E-02	6.000E-02	6.833E-02	3.833E-02	4.000E-02	4.000E-02	3.000E-02	6.167E-02	4.667E-02	2.000E-02
6.600E-01	2.667E-02	2.333E-02	3.167E-02	2.167E-02	1.333E-02	2.667E-02	1.833E-02	1.833E-02	1.333E-02	1.333E-02	1.333E-02	2.333E-02
7.510E-01	1.167E-02	1.167E-02	3.333E-03	1.167E-02	1.167E-02	3.333E-03	3.333E-03	0.0	5.000E-03	1.000E-02	6.666E-03	5.000E-03
8.190E-01	5.000E-03	1.667E-03	5.000E-03	1.667E-03	1.667E-03	3.333E-03	3.333E-03	3.333E-03	3.333E-03	3.333E-03	1.667E-03	1.667E-03
8.760E-01	1.667E-03	1.667E-03	0.0	1.667E-03	0.0	5.000E-03	3.333E-03	0.0	3.333E-03	0.0	0.0	0.0
9.280E-01	1.667E-03	1.667E-03	3.333E-03	0.0	1.667E-03	0.0	1.667E-03	0.0	5.000E-03	0.0	5.000E-03	0.0
9.790E-01	1.667E-03	0.0	1.667E-03	1.667E-03	0.0	1.667E-03	0.0	0.0	0.0	1.667E-03	1.667E-03	0.0
1.040E 00	0.0	3.333E-03	0.0	5.000E-03	0.0	0.0	0.0	1.667E-03	1.667E-03	1.667E-03	0.0	0.0
1.110E 00	1.667E-03	1.667E-03	0.0	1.667E-03	1.667E-03	1.667E-03	0.0	0.0	1.667E-03	1.667E-03	0.0	0.0
1.210E 00	3.333E-03	0.0	0.0	0.0	1.667E-03	0.0	0.0	0.0	0.0	0.0	1.667E-03	1.667E-03
1.350E 00	0.0	0.0	0.0	0.0	0.0	0.0	0.0	0.0	1.667E-03	0.0	0.0	1.667E-03
1.480E 00												

PROCEDURE AND SO2, TEMPEPATURE, AND RELATIVE HUMIDITY DATA FOR EXPERIMENT P29

THE BAG WAS FILLED FROM 12:25 TO 12:30

THE BAG WAS COVERED DURING THE FILLING PROCESS

THE COVER WAS REMOVED AT 13:00
THE AIR WAS NOT FILTERED DURING THE FILLING PROCESS

REACTANTS ADDED TO THE SYSTEM:

REACTANT	AMOUNT ADDED - CM3	TIME ADDED
NO	20.00	12:27
NO2	10.00	12:45
SO2	0.0	
PROPYLENE	60.00	12:47

TIME	SO2	TIME	TEMPERATURE - DEG C	RELATIVE HUMIDITY
13:04	10.24	13:04	43.	29.
13:13	10.16	13:44	42.	31.
13:21	10.00	15:18	42.	31.
13:28	9.85			
13:36	9.69			
13:44	9.54			
13:56	9.31			
14:02	9.23			
14:10	9.15			
14:15	9.07			
14:24	9.07			
14:35	9.07			
14:45	9.07			

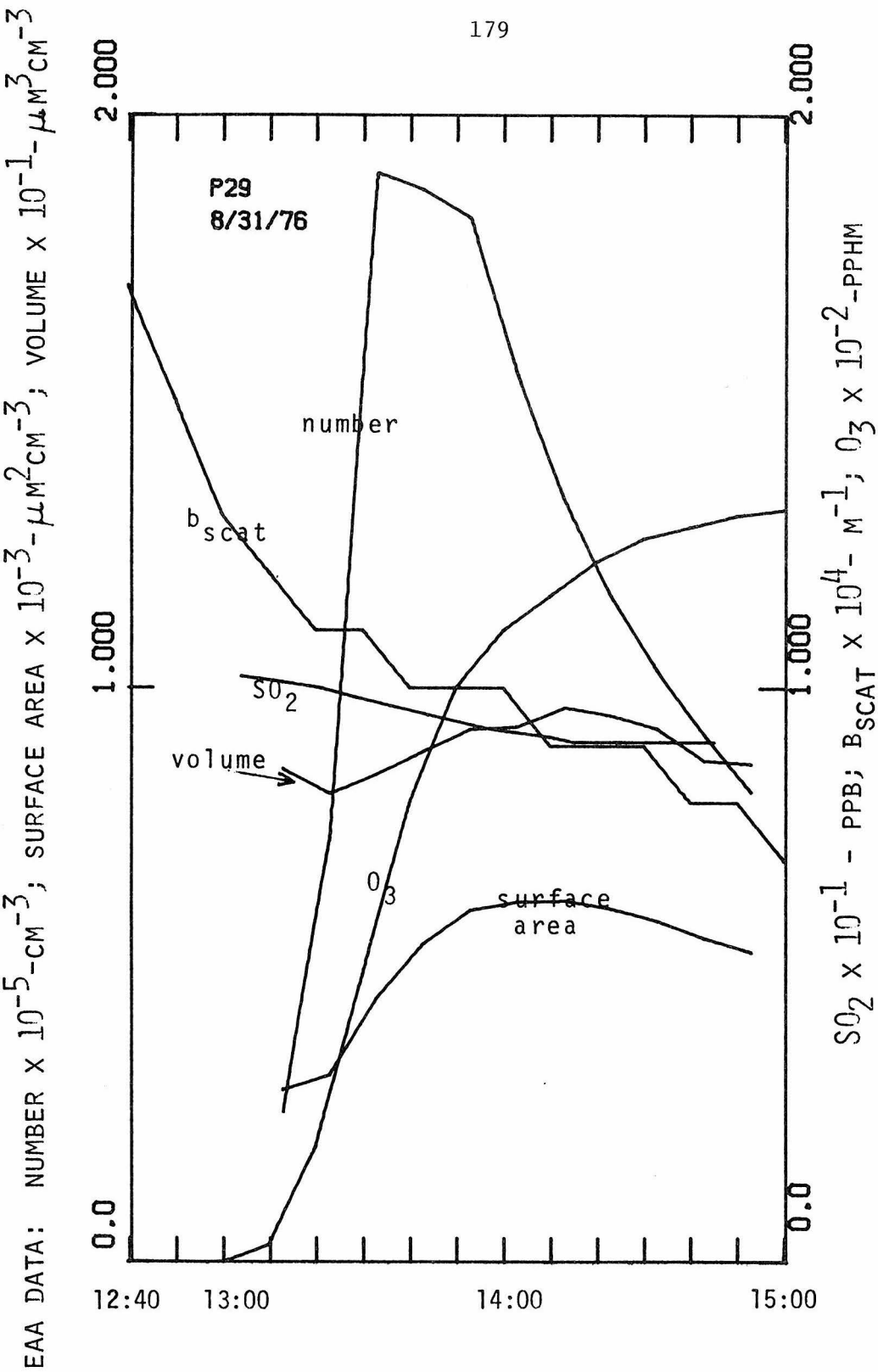
EAA DATA: NUMBER X 10^{-5}-CM^{-3}; SURFACE AREA X 10^{-3}-μM^{2}CM^{-3}; VOLUME X 10^{-1}-μM^{3}CM^{-3}
SO_2 X 10^{-1} - PPB; B_{SCAT} X 10^{4}- M^{-1}; O_3 X 10^{-2}-PPHM
P29
8/31/76
number
b_{scat}
SO_2
volume
O_3
surface area
2.000
1.000
0.0
12:40
13:00
14:00
15:00

SIZE DISTRIBUTION DATA FROM EXPERIMENT P29

DATE 8/31/76

NUMBER PER CM3 IN EACH SIZE INCREMENT DURING INDICATED TIME INTERVAL

DIA. LIMITS	1258-1308	1308-1318	1318-1328	1328-1338	1338-1348	1348-1358	1358-1408	1408-1418	1418-1428	1428-1438	1438-1448	1448-1458
ELECTRICAL AEROSOL ANALYZER DATA												
1.000E-02	4.411E 03	3.563E 03	4.937E 04	1.194E 05	5.260E 04	3.546E 04	1.832E 04	1.103E 04	7.605E 03	6.956E 03	6.278E 03	6.108E 03
1.780E-02	1.285E 04	1.271E 04	1.366E 04	5.804E 04	1.185E 05	1.236E 05	1.063E 05	8.883E 04	7.442E 04	6.239E 04	5.281E 04	4.459E 04
3.160E-02	3.788E 03	4.000E 03	4.460E 03	5.345E 03	7.682E 03	1.420E 04	1.915E 04	2.082E 04	2.096E 04	2.046E 04	1.940E 04	1.809E 04
5.620E-02	3.740E 03	3.920E 03	4.300E 03	4.950E 03	5.673E 03	6.938E 03	8.798E 03	1.010E 04	1.086E 04	1.113E 04	1.107E 04	1.097E 04
1.000E-01	1.775E 03	1.795E 03	1.726E 03	1.765E 03	1.853E 03	1.922E 03	2.040E 03	2.020E 03	2.079E 03	2.118E 03	2.216E 03	2.118E 03
1.780E-01	2.352E 02	2.051E 02	1.851E 02	1.801E 02	1.751E 02	1.701E 02	1.351E 02	1.551E 02	1.451E 02	1.351E 02	8.506E 01	1.251E 02
3.160E-01												
OPTICAL PARTICLE COUNTER DATA												
3.770E-01	2.192E 01	2.073E 01	1.876E 01	1.682E 01	1.563E 01	1.433E 01	1.302E 01	1.191E 01	1.110E 01	1.031E 01	9.188E 00	8.682E 00
4.670E-01	8.893E 00	8.423E 00	7.558E 00	6.778E 00	6.313E 00	5.653E 00	5.265E 00	4.765E 00	4.283E 00	3.933E 00	3.680E 00	3.293E 00
5.640E-01	2.787E 00	2.722E 00	2.393E 00	2.227E 00	1.978E 00	1.902E 00	1.665E 00	1.615E 00	1.373E 00	1.272E 00	1.213E 00	1.067E 00
6.600E-01	1.508E 00	1.377E 00	1.283E 00	1.160E 00	1.012E 00	9.533E-01	9.533E-01	7.733E-01	6.767E-01	6.433E-01	6.733E-01	5.717E-01
7.510E-01	8.383E-01	7.233E-01	6.100E-01	5.983E-01	4.767E-01	4.717E-01	4.083E-01	4.000E-01	3.533E-01	3.150E-01	2.683E-01	2.650E-01
8.190E-01	4.283E-01	3.683E-01	3.650E-01	3.433E-01	2.900E-01	2.517E-01	2.333E-01	2.033E-01	2.150E-01	1.883E-01	1.633E-01	1.933E-01
8.760E-01	2.667E-01	2.783E-01	2.183E-01	2.283E-01	1.883E-01	1.567E-01	1.500E-01	1.550E-01	1.233E-01	1.183E-01	9.000E-02	8.500E-02
9.280E-01	1.917E-01	1.900E-01	1.683E-01	1.483E-01	1.133E-01	1.117E-01	1.050E-01	1.017E-01	8.000E-02	8.500E-02	6.500E-02	8.167E-02
9.790E-01	1.767E-01	1.450E-01	1.433E-01	1.267E-01	1.267E-01	9.166E-02	9.000E-02	1.083E-01	9.833E-02	7.167E-02	5.333E-02	4.333E-02
1.040E 00	1.133E-01	1.150E-01	1.017E-01	1.050E-01	7.500E-02	7.333E-02	5.667E-02	6.833E-02	5.833E-02	6.333E-02	4.000E-02	5.167E-02
1.110E 00	1.200E-01	7.500E-02	1.033E-01	6.833E-02	5.500E-02	5.667E-02	5.000E-02	5.333E-02	5.500E-02	4.667E-02	2.667E-02	2.333E-02
1.210E 00	7.167E-02	5.500E-02	4.500E-02	5.167E-02	4.667E-02	3.833E-02	4.333E-02	3.167E-02	4.333E-02	2.000E-02	2.333E-02	1.333E-02
1.350E 00	5.333E-02	4.167E-02	3.667E-02	2.500E-02	3.000E-02	2.167E-02	1.667E-02	2.667E-02	1.000E-02	2.333E-02	1.000E-02	1.667E-02
1.480E 00												

SIZE DISTRIBUTION DATA FROM EXPERIMENT T2

DATE 6/22/76

NUMBER PER CM3 IN EACH SIZE INCREMENT DURING INDICATED TIME INTERVAL

DIA. LIMITS	1359-1409	1409-1419	1419-1429	1429-1439	1439-1449	1449-1459	1459-1509	1509-1519	1519-1529	1529-1539	1539-1549	1549-1559
ELECTRICAL AEROSOL ANALYZER DATA												
1.000E-02	2.454E 03	1.866E 03	8.483E 02	1.866E 03	1.357E 03	1.188E 03	1.866E 03	1.018E 03	1.357E 03	8.483E 02	1.357E 03	0.0
1.780E-02	1.257E 04	1.101E 04	1.155E 04	1.033E 04	9.311E 03	8.700E 03	7.001E 03	1.006E 04	7.816E 03	5.505E 03	5.369E 03	5.030E 03
3.160E-02	5.098E 03	5.098E 03	4.814E 03	4.531E 03	5.133E 03	4.319E 03	4.885E 03	3.363E 03	3.752E 03	4.213E 03	3.859E 03	3.894E 03
5.620E-02	8.184E 03	7.498E 03	6.956E 03	6.775E 03	6.356E 03	6.468E 03	6.233E 03	5.944E 03	5.998E 03	6.070E 03	7.353E 03	5.691E 03
1.000E-01	4.511E 03	4.168E 03	3.854E 03	3.472E 03	3.246E 03	3.030E 03	2.795E 03	2.687E 03	2.618E 03	2.471E 03	1.824E 03	2.422E 03
1.780E-01	6.905E 02	6.204E 02	5.454E 02	5.103E 02	4.853E 02	4.053E 02	4.003E 02	3.452E 02	3.202E 02	3.052E 02	1.851E 02	2.652E 02
3.160E-01												
OPTICAL PARTICLE COUNTER DATA												
3.770E-01	1.316E 01	1.214E 01	1.068E 01	9.856E 00	8.745E 00	7.983E 00	7.233E 00	6.517E 00	6.085E 00	5.358E 00	4.793E 00	4.248E 00
4.670E-01	5.115E 00	4.578E 00	4.222E 00	3.927E 00	3.453E 00	3.225E 00	2.910E 00	2.798E 00	2.480E 00	2.228E 00	1.925E 00	1.785E 00
5.640E-01	2.123E 00	1.925E 00	1.852E 00	1.718E 00	1.468E 00	1.417E 00	1.227E 00	1.200E 00	1.162E 00	9.667E-01	8.000E-01	7.767E-01
6.600E-01	1.535E 00	1.383E 00	1.292E 00	1.210E 00	1.032E 00	9.583E-01	8.683E-01	7.817E-01	7.883E-01	7.450E-01	6.467E-01	5.550E-01
7.510E-01	1.090E 00	9.100E-01	8.817E-01	8.133E-01	7.767E-01	6.883E-01	6.183E-01	5.317E-01	4.550E-01	4.367E-01	3.817E-01	4.467E-01
8.190E-01	6.916E-01	6.666E-01	6.483E-01	5.550E-01	4.983E-01	5.283E-01	4.967E-01	4.517E-01	3.267E-01	3.567E-01	3.083E-01	2.417E-01
8.760E-01	6.333E-01	5.500E-01	4.850E-01	4.400E-01	4.317E-01	3.750E-01	3.983E-01	3.133E-01	3.033E-01	2.833E-01	2.783E-01	2.300E-01
9.280E-01	5.516E-01	5.100E-01	4.300E-01	4.267E-01	3.683E-01	3.683E-01	2.850E-01	2.733E-01	2.483E-01	2.267E-01	2.250E-01	1.833E-01
9.790E-01	6.166E-01	6.050E-01	4.917E-01	4.433E-01	4.250E-01	3.717E-01	3.150E-01	2.950E-01	3.100E-01	2.533E-01	2.367E-01	2.033E-01
1.040E 00	4.833E-01	4.283E-01	3.917E-01	3.867E-01	3.117E-01	2.567E-01	2.417E-01	2.400E-01	2.167E-01	1.950E-01	1.917E-01	1.617E-01
1.110E 00	5.333E-01	4.030E-01	3.783E-01	3.367E-01	3.350E-01	2.950E-01	2.667E-01	2.300E-01	1.817E-01	2.150E-01	1.883E-01	1.483E-01
1.210E 00	3.866E-01	3.733E-01	3.383E-01	2.433E-01	2.267E-01	2.050E-01	2.067E-01	1.683E-01	1.367E-01	1.400E-01	1.333E-01	9.833E-02
1.350E 00	2.650E-01	2.150E-01	2.083E-01	1.350E-01	1.450E-01	1.267E-01	1.150E-01	1.017E-01	1.267E-01	6.167E-02	6.500E-02	5.167E-02
1.480E 00												

SIZE DISTRIBUTION DATA FROM EXPERIMENT RR14

DATE 11/9/76

NUMBER PER CM3 IN EACH SIZE INCREMENT DURING INDICATED TIME INTERVAL

DIA. LIMITS	636- 646	646- 656	656- 706	706- 716	716- 726	726- 736	736- 746	746- 756	756- 806	806- 816	816- 826	826- 836
ELECTRICAL AEROSOL ANALYZER DATA												
1.000E-02	1.120E 04	8.653E 03	7.126E 03	8.144E 03	5.599E 03	6.617E 03	7.126E 03	5.090E 03	4.581E 03	4.072E 03	4.072E 03	3.563E 03
1.780E-02	1.407E 04	1.631E 04	1.611E 04	1.529E 04	1.509E 04	1.448E 04	1.407E 04	1.346E 04	1.285E 04	1.264E 04	1.203E 04	1.244E 04
3.160E-02	2.655E 03	3.398E 03	2.867E 03	2.974E 03	2.867E 03	2.549E 03	2.549E 03	2.655E 03	2.549E 03	2.974E 03	2.761E 03	2.124E 03
5.620E-02	2.493E 03	2.385E 03	2.547E 03	2.439E 03	2.276E 03	2.385E 03	2.168E 03	2.060E 03	2.114E 03	1.843E 03	2.060E 03	2.005E 03
1.000E-01	7.355E 02	1.000E 03	9.414E 02	8.532E 02	7.355E 02	6.472E 02	6.472E 02	6.178E 02	5.590E 02	5.296E 02	3.530E 02	3.530E 02
1.780E-01	0.0	0.0	0.0	0.0	0.0	0.0	0.0	0.0	0.0	0.0	0.0	0.0
3.160E-01												

SIZE DISTRIBUTION DATA FROM EXPERIMENT RR14 CONTINUED

DATE 11/9/76

NUMBER PER CM3 IN EACH SIZE INCREMENT DURING INDICATED TIME INTERVAL

DIA. LIMITS	836- 846	846- 856	856- 906	906- 916	916- 926	926- 936	936- 946	946- 956	956-1006	1006-1016	1016-1026	1026-1036
ELECTRICAL AEROSOL ANALYZER DATA												
1.000E-02	2.036E 03	3.563E 03	2.036E 03	3.054E 03	5.090E 02	0.0	5.090E 02	2.545E 03	2.036E 03	1.527E 03	4.581E 03	4.581E 03
1.780E-02	1.142E 04	1.060E 04	1.162E 04	9.991E 03	1.121E 04	1.020E 04	1.040E 04	9.379E 03	8.564E 03	8.156E 03	8.360E 03	7.952E 03
3.160E-02	2.655E 03	2.761E 03	2.443E 03	2.974E 03	2.336E 03	2.443E 03	2.655E 03	2.443E 03	2.655E 03	2.655E 03	2.336E 03	2.655E 03
5.620E-02	1.843E 03	1.789E 03	1.897E 03	1.789E 03	1.843E 03	1.951E 03	1.518E 03	1.789E 03	1.734E 03	1.789E 03	1.734E 03	1.626E 03
1.000E-01	3.53CE 02	2.942E 02	2.354E 02	2.354E 02	2.059E 02	8.826E 01	1.765E 02	8.826E 01	8.826E 01	5.884E 01	5.884E 01	5.884E 01
1.780E-01	0.0	0.0	0.0	0.0	0.0	0.0	0.0	0.0	0.0	0.0	0.0	0.0
3.160E-01												

SIZE DISTRIBUTION DATA FROM EXPERIMENT RR14 CONTINUED

DATE 11/9/76

NUMBER PER CM3 IN EACH SIZE INCREMENT DURING INDICATED TIME INTERVAL

DIA. LIMITS	1036-1046	1046-1056	1056-1106	1106-1116	1116-1126	1126-1136	1136-1146	1146-1156	1156-1206	1206-1216	1216-1226	1226-1236
ELECTRICAL AEROSOL ANALYZER DATA												
1.000E-02	5.090E 03	6.617E 03	8.144E 03	7.635E 03	9.671E 03	8.144E 03	8.144E 03	9.671E 03	9.671E 03	8.653E 03	7.126E 03	7.635E 03
1.780E-02	7.952E 03	7.340E 03	6.729E 03	6.525E 03	6.729E 03	6.525E 03	6.933E 03	7.340E 03	8.156E 03	7.748E 03	8.972E 03	8.972E 03
3.160E-02	2.336E 03	2.974E 03	2.549E 03	2.867E 03	2.549E 03	2.761E 03	2.549E 03	2.655E 03	2.018E 03	2.549E 03	2.443E 03	2.124E 03
5.620E-02	1.734E 03	1.463E 03	1.626E 03	1.518E 03	1.463E 03	1.409E 03	1.518E 03	1.463E 03	1.518E 03	1.518E 03	1.301E 03	1.518E 03
1.000E-01	0.0	2.942E 01	0.0	0.0	0.0	0.0	0.0	0.0	0.0	0.0	0.0	0.0
1.780E-01	0.0	0.0	0.0	0.0	0.0	0.0	0.0	0.0	0.0	0.0	0.0	0.0
3.160E-01												

SIZE DISTRIBUTION DATA FROM EXPERIMENT RR14 CONTINUED

DATE 11/9/76

NUMBER PER CM3 IN EACH SIZE INCREMENT DURING INDICATED TIME INTERVAL

DIA. LIMITS	1236-1236	1236-1246
ELECTRICAL AEROSOL ANALYZER DATA		
1.000E-02	7.635E 03	6.617E 03
1.780E-02	8.564E 03	8.360E 03
3.160E-02	2.336E 03	2.443E 03
5.620E-02	1.301E 03	1.301E 03
1.000E-01	0.0	0.0
1.780E-01	0.0	0.0
3.160E-01		

SIZE DISTRIBUTION DATA FROM EXPERIMENT RR15

DATE 03/22/77

NUMBER PER CM3 IN EACH SIZE INCREMENT. MEASUREMENT STARTED AT INDICATED TIME

DIA. LIMITS	900	910	920	930	940	953	1000	1011	1020	1030	1041	1051
ELECTRICAL AEROSOL ANALYZER DATA												
1.000E-02	0.0	0.0	3.410E 04	7.330E 04	7.075E 04	4.683E 04	4.072E 04	2.647E 04	2.240E 04	1.425E 04	9.671E 03	9.162E 03
1.780E-02	0.0	0.0	0.0	7.544E 03	2.223E 04	3.752E 04	4.180E 04	4.680E 04	4.629E 04	4.547E 04	4.221E 04	3.874E 04
3.160E-02	0.0	4.248E 02	2.124E 02	0.0	0.0	0.0	4.248E 02	1.381E 03	2.549E 03	3.823E 03	4.460E 03	4.991E 03
5.620E-02	0.0	0.0	0.0	0.0	0.0	0.0	0.0	0.0	0.0	2.168E 02	4.878E 02	6.504E 02
1.000E-01	0.0	0.0	0.0	0.0	0.0	0.0	0.0	0.0	1.177E 02	0.0	0.0	0.0
1.780E-01	0.0	0.0	0.0	0.0	0.0	0.0	0.0	0.0	0.0	0.0	0.0	0.0
3.160E-01												

DIA. LIMITS	1102
1.000E-02	5.090E 03
1.780E-02	3.548E 04
3.160E-02	5.522E 03
5.620E-02	1.084E 03
1.000E-01	0.0
1.780E-01	0.0
3.160E-01	

SIZE DISTRIBUTION DATA FROM 8/26/76

Number per cm^3 in each size increment during indicated time interval

Electrical Aerosol Analyzer Data

Dia. Limits 1333-1343

1.00E-2

5.938E 3

1.78E-2

1.597E 4

3.16E-2

6.018E 3

5.62E-2

9.557E 3

1.00E-1

6.374E 3

1.78E-1

1.181E 3

3.16E-1

Optical Particle Counter Data

Dia. Limits

3.77E-1

5.330E 1

4.67E-1

2.440E 1

5.64E-1

8.130E 0

6.60E-1

3.940E 0

7.51E-1

1.698E 0

8.19E-1

8.600E-1

8.76E-1

4.950E-1

9.28E-1

3.467E-1

9.79E-1

3.117E-1

1.04E-0

2.067E-1

1.11E-0

2.133E-1

1.21E-0

1.467E-1

1.35E-0

1.217E-1

1.48E-0